RADAR
Research Archive and Digital Asset Repository

OXFORD BROOKES UNIVERSITY

Exploring the combined use of electrical and hemodynamic brain activity to investigate brain function

Anique J E Driessen (2014)

https://radar.brookes.ac.uk/radar/items/d5e7c357-e312-4fba-8cc5-774eff36180e/1/

Copyright © and Moral Rights for this thesis are retained by the author and/or other copyright owners. A copy can be downloaded for personal non-commercial research or study, without prior permission or charge. This thesis cannot be reproduced or quoted extensively from without first obtaining permission in writing from the copyright holder(s). The content must not be changed in any way or sold commercially in any format or medium without the formal permission of the copyright holders.

When referring to this work, the full bibliographic details must be given as follows:

Driessen, A J E (2014) *Exploring the combined use of electrical and hemodynamic brain activity to investigate brain function* PhD, Oxford Brookes University

Removed fig. 1.1, p.5 and fig. 1.7, p.20

WWW.BROOKES.AC.UK/GO/RADAR

Exploring the combined use of electrical and hemodynamic brain activity to investigate brain function

Anique Johanna Eduarda Driessen

A thesis submitted in partial fulfilment of the requirements of Oxford Brookes University for the award of Doctor of Philosophy

February 2014

Abstract

This thesis explored the relationship between electrical and metabolic aspects of brain functioning in health and disease, measured with QEEG and NIRS, in order to evaluate its clinical potential. First the limitations of NIRS were investigated, depicting its susceptibility to different types of motion artefacts and the inability of the CBSI-method to remove them from resting state data. Furthermore, the quality of the NIRS signals was poor in a significant portion of the investigated sample, reducing clinical potential.

Different analysis methods were used to explore both EEG and NIRS, and their coupling in an eyes open eyes closed paradigm in healthy participants. It could be reproduced that during eyes closed blocks less HbO_2 (p = 0.000), more Hbb (p = 0.008), and more alpha activity (p = 0.000) was present compared to eyes open blocks. Furthermore, dynamic cross correlation analysis reproduced a positive correlation between alpha and Hbb (r: 0.457 and 0.337) and a negative correlation between alpha and HbO_2 (r: -0.380 and -0.366) with a delayed hemodynamic response (7 to 8s). This was only possible when removing all questionable and physiological illogical data, suggesting that an 8s hemodynamic delay might not be the golden standard. Also the inability of the cross correlation to take non-linear relationships into account may distort outcomes.

Therefore, In chapter 5 non-linear aspects of the relationship were evaluated by introducing the measure of relative cross mutual information. A newly suggested approach and the most valuable contribution of the thesis since it broadens knowledge in the fields of EEG, NIRS and general time series analysis.

Data of two stroke patients then showed differences from the healthy group between the coupling of EEG and NIRS. The differences in long range temporal correlations (p= 0.000 for both cases), entropy (p< 0.040 and p =0.000), and relative cross mutual information (p < 0.003 and p < 0.013) provide the proof of principle that these measures may have clinical utility. Even though more research is necessary before widespread clinical use becomes possible.

Acknowledgements

First of all I would like to thank BrainMarker B.V. for granting me the opportunity both financially and time wise to carry out the research needed to complete my thesis. In particular I would like to thank Björn Crüts for allowing me to make use of his valuable network as well as taking the time to share interesting insights and discussions that led me to just step out of my comfort zone every time, allowing me to grow as a scientist. I would also like to thank my friend and colleague Anica Eurelings. Without your help and support on so many levels I think I would have lost my mind along the way.

Furthermore, a sincere thank you goes out to my supervising team: Helen Dawes, Paul Borm, Mojtaba Zarei and Ken Howells. A special thanks I have reserved for Helen Dawes. Your guidance in this process has been of exceptional value to me. You gave me the space, trust, and insights that I needed to develop, as well as the occasional push to make things happen. For that I cannot thank you enough. I would also like to thank Ken Howells for his role as a sounding board to me and my supervisors.

I am grateful to all participants that selflessly offered me their time and a look into their brains. Of course I am also more than grateful to the Biometrical Centre in Gulpen that allowed me to use their anonymous patient data. Without all of you this research would not have succeeded.

All colleagues at Oxford Brookes who took the time to talk to me about aspects of the thesis I would like to thank as well; Hooshang Izadi, Tjeerd Olde-Scheper and Henk Smit in particular. Of course also the members of the Movement Science Group who have ever been so kind to me during my visits to Oxford and shared their research and knowledge with me.

From Imperial College London I would like to thank Henrik Jeldthoft Jensen and Fatimah Abdul Razak for their assistance in determining the number of bins for the analyses that are derived from the information theoretic framework.

Then I would like to take a moment to thank my colleagues at BrainMarker who have been occupied with implementing analysis techniques into software. Paul Perreijn, your skills have made my life easier. Aloys Sipers, your explanations are vivid and most importantly understandable. And our intern Koen Duijsengs deserves acknowledgement for his assistance in programming the entropy calculation.

Last but not least, I would like to express my gratitude to my parents Jan and Hanneke Driessen, who always stood by my side and raised me to believe that anything is achievable. Also I would like to thank my fiancée Sven Goumans for putting up with me during the years I was occupied with this work and supporting me unconditionally. Also, thanks for not proposing until the finish was within sight.

To each and everyone: Thank you, Bedankt!

Table of contents

List of Abbreviations

ADHD: Attention Deficit Hyperactivity Disorder

AMI: Auto Mutual Information

APF: Alpha Peak Frequency

BCI: Brain- Computer Interface

BOLD: Blood Oxygenation Level Dependent

BSI: Brain Symmetry Index

CBF: Cerebral Blood Flow

CBSI: Correlation Based Signal Improvement

CBV: Cerebral Blood Volume

CCF: Cross Correlation Function

CMI: Cross Mutual Information

CMI_{rel}: Relative Cross Mutual Information

CNR: Contrast-to-Noise Ratio

CVA: Cerebro Vascular Accident

CW: Continuous Wave

dB: Decibel

DPF: Differential Path length Factor

EC: Eyes Closed

EEG: Electro Encephalography

EO: Eyes Open

ERD: Event Related Desynchronisation

ERP: Event Related Potential

ERS: Event Related Synchronisation

FFT: Fast Fourier Transform

fMRI: Functional Magnetic Resonance Imaging

GP: General Practitioner

Hbb: Deoxygenated haemoglobin

HbO_2: Oxygenated haemoglobin

HRV: Heart Rate Variability

Hz: Hertz

ICF: International Classification of Functioning, disability and health

LED: Light Emitting Diode

LFO: Low Frequency Oscillation

LORETA: Low Resolution Electrical Tomography

LRTC: Long Range Temporal Correlation

MEG: Magnetic Encephalography

MI: Mutual Information

MIME: Mutual Information from Mixed Embedding

MI_{rel}: Relative Mutual Information

mV: Milli Volt

NIRS: Near Infrared Spectroscopy

PCA: Principal Component Analysis

PET: Positron Emission Tomography

PMS: Phase Modulation Spectroscopy

PPF: Partial Path length Factor

QEEG: Quantitative Electro Encephalography

RC: Running Correlation

RSN: Resting State Network

rTMS: Repetitive Transcranial Magnetic Stimulation

SD: Standard Deviation

SNR: Signal-to-noise ratio

SOC: Self Organised Critical / Self Organised Criticallity

SOP: Standard Operating Protocol

SPECT: Single Photon Emission Computed Tomography

SRS: Spatially Resolved Spectroscopy

SSRI: Selective Serotonin Reuptake Inhibitor

STFT: Short-Time Fourier Transform

TE: Transfer Entropy

TRS: Time-Resolved Spectroscopy

µV: Micro Volt

VLFO: Very Low Frequency Oscillation

WHO: World Health Organization

List of Figures

List of Tables

Relevant publications and presentations

Papers in preparation:

Driessen A., Crüts B., Borm P., Zarei M., Howells K., Dawes H. "Exploring brain activity of the visual cortex with simultaneous EEG and NIRS measurements" (in preparation)

Driessen A., Crüts B., Borm P., Zarei M., Howells K., Dawes H. "Analyzing the dependency between EEG alpha activity and NIRS with relative cross mutual information in health and after stroke" (in preparation)

Abstracts and Presentations:

Driessen A. (2012) "Activity of the brain at rest, exploring the relationship between EEG and NIRS" Department meeting Sport and Health Sciences, Oxford Brookes University, Oxford, England (Oral presentation)

Driessen A., Crüts B., Howells K., Borm P., Zarei M., Dawes H. (2012) "Simultaneous QEEG and NIRS measurements during resting state conditions in healthy volunteers" 2nd fNIRS Conference, fNIRS organization, University College London, England (Poster presentation)

Driessen A., Crüts B., Sipers A., Borm P., Zarei M., Collett J., Howells K., Dawes H. (2011) "Cerebral NIRS for investigating fatigue in neurological disorders: ready for use?" Joint Summer Meeting of the British Society of Rehabilitation Medicine & The Society for Research in Rehabilitation, University of Keele, Newcastle-under-Lyme, Staffordshire, England (Poster presentation)

Driessen A. (2010) "Why is the resting brain so active? Diagnosis of Psychopathologies at resting brain state: use of NIRS and QEEG" Research student forum, Oxford Brookes University, Oxford, England (Oral presentation)

Driessen A., Zarei M., Borm P., Dawes H. (2009) "NIRS in neurological rehabilitation, ready for use? Preliminary results" 8th Conference on Cognitive Neuropsychiatry, Bremen, Germany (Poster presentation)

Driessen A., Zarei M., Borm P., Dawes H. (2009) “The clinical value of NIRS: potential robustness to artefacts” 3rd Oxford-Heerlen Imagery & Neurological Rehabilitation Conference. Zuyd University, Heerlen, the Netherlands (Poster presentation)

Driessen A. (2008) “The added value of using NIRS in investigating mental imagery” 2nd Oxford-Heerlen Imagery & Neurological Rehabilitation Conference. Zuyd University, Heerlen, the Netherlands (Oral presentation)

Chapter 1: Introduction

In the introduction of this thesis the framework is laid out of the principles that will be used to investigate the relationship between brain activity on a electrophysiological level and its vascular metabolic aspects. Hereto a short introduction is given to the fields of (quantitative) EEG, near-infrared spectroscopy, and their combined use. An understanding of the basics of these fields is necessary in the upcoming chapters in which cortical oxygenation modulation, the modulation of electrical oscillations and how they influence each other will be explored. At first this is done in a sample of healthy volunteers. After that the results obtained in the healthy sample will be compared to results of two stroke patients. As stroke is caused by a disruption of the blood flow, changes in brain activity as well as changes in the influence of the electrical activity upon oxygenation parameters and vice versa are expected.

1.1 Introduction and rationale

It has been established that worldwide, over one third of all people will meet the criteria for a psychopathology once in their lifetime (Organization, 2000). The largest share of psychopathologies are accounted for by anxiety disorders followed by mood disorders (Demyttenaere et al., 2013). However, 4 out of 5 people suffering from psychopathologies are not provided with the appropriate healthcare (Demyttenaere et al., 2013).

The advances in neuroscience over the last few decades have pointed towards the finding that psychopathologies are often accompanied by changes in brain function (e.g (Miguel-Hidalgo, 2013, Whitfield-Gabrieli and Ford, 2012)). Different disorders represent themselves as different patterns of brain activity and biomarkers based on brain activity are currently being researched for a variety of psychopathologies (Domínguez et al., 2013, Tregellas et al., 2014, Yener and Başar, 2012). However, despite the increased knowledge on the relationship between changes in brain function and mental disorders the use of measures of brain activity in general healthcare is still very limited.

Measurements of brain are usually only performed in case of evident brain trauma for example in head injury or stroke (Fazekas et al., 2009). Although measurements of brain activity that are well performed, together with behavioural measurements will create better insight into the mechanisms underpinning neuropsychological diseases (Buckholtz and Meyer-Lindenberg, 2012, Kloppel et al., 2012, Coburn et al., 2006), and make it easier for a clinician to unravel and categorize the problems that need to be addressed. The right use of brain measurements can not only aid in the diagnoses of a variety of neuropsychological disorders, it can also be used to design more targeted and effective forms of therapy (Howland et al., 2011). These therapies could alter brain activity in order to treat complaints on the behavioural level at the source and would therefore offer more long-lasting solutions than interventions that only target the behavioural level (Bersani et al., 2013, Egner et al., 2004, Howland et al., 2011). Furthermore, the periodic use of brain measurements could shed light on the progress a patient is making and therefore provide guidelines for when to change interventions.

In order for these advances in neuroscience to become available to the broad public, brain measurements should be implemented in early lines of health care. For instance in the general practitioner's (GP) office and with psychologists. In doing so, it is of extreme importance that measurement methods are used which are easily implemented in everyday clinical use and are relatively low-cost. Furthermore, measurement paradigms should be used that are easily implemented with all patients and data processing and analysis should be automated to ensure fast and reliable outcomes.

In this chapter two methods will be introduced that could offer such a clinical advantage. The first one, electroencephalography is able to measure brain activity on an electrophysiological level (Teplan, 2002) and the second, near infrared spectroscopy provides information on a vascular metabolic level (Obrig and Villringer, 2003). Both measurements separately are able to give information on brain functioning. However, multimodal use of the two could reveal the symbioses between neural and metabolic aspects of brain functioning which might increase the ability of differentiating between different disorders. Furthermore it could provide great insight into brain functioning in general.

Therefore the goal of this thesis is to explore the relationship between electrical and metabolic aspects of brain functioning in order to reveal its exiting opportunities in understanding brain functioning in health and disease. Before this link can be made, a basic understanding of these methods and their limitations as well as an introduction to the limited amount of multimodal studies that have been carried out so far is essential.

1.2 Measuring brain activity

In order to disentangle the relationship between brain and behaviour an initial exploration of current ways of measuring brain activity is required. And even though it is not the scope of this thesis to give a detailed explanation of brain anatomy, it is important to know what is being measured. The brain is considered to be the conductor of the body's orchestra and the behaviour it performs. Scientific research has linked different brain areas to different behaviours and tasks and it is mainly the neocortex, the outer shell of the brain that has evolved last in the evolution of man, that holds the code to behaviour (Rakic, 2009). For example the occipital cortex processes visual information and the central cortex is responsible for movement and bodily sensation (Bear et al., 2007). The neocortex is made up out of billions of neurons, arranged in layers and columns that hold the neural code (Rakic, 2009). Whereas previously it was thought that the brain operated in a fashion in which areas were isolated to a specific task, more recent research indicates that behaviour is an interplay of different neural networks that are active during information processing of specific tasks but these networks also display activity during rest (Raichle et al., 2001, Beckmann et al., 2005, Buckner, 2012). To date different methods of measuring brain activity have contributed to our understanding of human behaviour but also to the neurobiological substrates of many brain disorders (Irani et al., 2007). All methods have different advantages and limitations. In general, two groups can be distinguished, direct and indirect measurements (Bear et al., 2007).

1.2.1 Direct measurements

Direct measurements measure directly the summation of neural function, for example magnetic encephalography (MEG) (Hari and Salmelin, 2012), electro encephalography (EEG) (Teplan, 2002) and event related potentials (ERP) (Tzovara et al., 2012). These methods measure the electromagnetic activity of the brain in

milliseconds with a high temporal resolution. However, due to the spatial smearing caused by the skull and the difficulty of localizing activated sources because of multiple dipole fitting solutions the spatial resolution of these methods is limited (Bear et al., 2007, Irani et al., 2007).

1.2.2 Indirect measurements

Indirect brain imaging methods measure the hemodynamic and metabolic changes associated with the neuronal activity. Examples of indirect measurements are positron emission tomography (PET) (Portnow et al., 2013), single photon emission computed tomography (SPECT) (Warwick, 2004), functional magnetic resonance imaging (fMRI) (Chen and Li, 2012) and near infrared spectroscopy (NIRS) (Obrig and Villringer, 2003). In general indirect measures have a high spatial resolution but limited temporal resolution. Further limitations of indirect measures are that the measurements are associated with neuronal activity through a poorly understood neurovascular coupling function (Bear et al., 2007, Irani et al., 2007). Furthermore, PET and SPECT cannot perform continuous or repeated measures because of the radioactive isotopes that are necessary to perform the measurements. The use of radioactive isotopes also limits the use of PET and SPECT in children (Irani et al., 2007).

1.2.3 Multimodal imaging

Simultaneous use of methods from both direct and indirect measurements would help to obtain a clearer picture of brain functioning since in one measurement information from electrical aspects of brain functioning can be linked to metabolic aspects. In the literature this is referred to as multimodal imaging. In deciding what measurements are suitable for combined use several aspects have to be taken into account. For instance, technological aspects like the amount of noise that one measurement adds to the other and if it is possible to place the equipment of two devices on one subject without inducing too much discomfort. The combination of any direct measurement together with fMRI is challenging because no metals can be used around the fMRI scanner (Irani et al., 2007). Furthermore, in investigating neuropsychological disorders it is desirable to use modalities which can be easily implemented in the clinic and therefore need to be portable and low-cost. Measurements that could meet these needs are EEG and NIRS (Arenth et al., 2007, Irani et al., 2007). Both NIRS and EEG are non-invasive,

safe, portable and low cost methods which can be integrated with other technologies (Arenth et al., 2007, Irani et al., 2007).

1.3 The principles of (Q)EEG

EEG is the classical method of recording brain rhythms. The earliest work on EEG was performed by the English physiologist Richard Caton in 1875 when he made electrical recordings of canine and rabbit brains (Caton, 1875). The first human EEG was described by the Austrian psychiatrist Hans Berger in 1929. Between 1929 and 1938 he published fourteen reports on human EEG and its relation to cognition and neurological disturbances (Berger, 1969 a-n). To date a multitude of available EEG devices exists. For several examples see figure 1.1.

Figure 1.1 Examples of EEG devices and electrodes. A broad variety of EEG device exists ranging in size and number of possible measurement channels as depicted in the upper row of the figure. Also the way electrodes are configured on the head varies greatly. In the lower row depicted from left to right a high density 128 channel configuration, a s19 channel cap, a rigid helmet like structure as well as the use of loose electrodes over areas of interest is shown.

1.3.1 Neuronal activity

Billions of neurons make up the human cortex. All neurons have a membrane around them which has a resting potential because of the ions that are present within and outside the neuron. In its resting state more Na^+ and Cl^- ions are outside the neuron than inside and more K^+ ions and negatively charged protein ions are inside the neuron than outside. This creates a steady resting potential of about -70 millivolts (mV) (Pinel, 2003). Neurons communicate with each other by firing. When firing occurs, neurotransmitters are released into the synaptic clefts and react with the receptors present on surrounding neurons. They can either depolarize the receptive membrane, in which the resting potential is decreased, or hyperpolarize it, in which the potential is increased. As the neurotransmitters cause the membrane of surrounding neurons to reach a potential of about -65 mV an action potential is generated. An action potential is a short shift in membrane potential from -70 mV to +50 mV which causes the neuron to fire an electrical signal along its dendrite, which causes the surrounding neurons to secrete neurotransmitters and fire as well or stop to fire (Pinel, 2003). Because of the cooperation of electrical spikes and the chemical neurotransmitters neural activity is an electrochemical process (Gazzaniga et al., 2002). There are a number of neurotransmitters, of which GABA and glutamate are part of fast reacting transmitting systems and acetylcholine, dopamine and, serotonin are examples of more slow reacting neurotransmitters (McCormick et al., 1993). The interplay between the different neurotransmitters determines the amplitude and the duration of the postsynaptic potentials as well as it regulates the spatial and temporal pattern of activation (McCormick et al., 1993). However, it is not the purpose of this thesis to establish the electrochemical interplay of neurons. Although, it is essential to the knowledge of the registration of EEG that the summation of electrical changes within and outside large groups of neurons makes up the EEG recorded at the scalp (Buzsáki et al., 2012).

1.3.2 EEG

Originally it was thought that the changes in voltage that were measured with EEG originated from the currents that flow during synaptic excitations of the dendrites of many pyramidal neurons in the cerebral cortex (Teplan, 2002). A plausible explanation, considering the pyramidal neurons make up 80 % of the brain's mass and are perpendicular aligned to the pia mater, directly below the skull, where

the electric potential is passed on to the scalp where it can be measured (Bear et al., 2007, Kaiser, 2005). However, more recent EEG research in which also measurements directly from the cortex as well as from within the brain have been taken into account, has shown that electric currents from all excitable membranes contribute to the extracellular voltage that is picked up with EEG (Buzsáki et al., 2012). The largest contribution is made by synaptic activity, but also action potentials, after potentials, fluctuations in glia, Ca^{2+} spikes, and intrinsic cellular changes in voltage contribute to the extracellular voltage. It depends on the spatial alignment of neurons and the temporal synchrony whether extracellular fields are picked up (Buzsáki et al., 2012). The influence of the activity of only one neuron on the extracellular voltage is so faint that after passing through several layers of tissue including the meninges, spinal fluid, bones of the skull and skin, it cannot be detected by the electrodes anymore (Bear et al., 2007, Kaiser, 2005). In the cortex however, the dendrites of the neurons lie parallel to each other and the incoming input is perpendicularly aligned to the dendrites which creates the right prerequisites for the synchronous electrical activity to be superpositioned, leading to large electrical fields in the cortex (Buzsáki et al., 2012).

Furthermore, the detection of the signal strongly depends on the synchronicity of the firing neurons. Synchrony is often brought about through network oscillation (Buzsáki et al., 2012). The more synchronized the neurons fire, the higher the amplitude of the waves in the EEG signal are and the more rhythmic the EEG signal appears (Bear et al., 2007). The synchronous firing of different neural networks explains why different brain states are associated with very different patterns and magnitudes of extracellular voltages (Buzsáki et al., 2012). Negative and positive potentials cancel each other out so that we only detect the difference in valance (Kaiser, 2005).

In general EEG is only able to register cortical activity (Kaiser, 2005). And due to the spatial smearing of the electrical current by brain tissue and the fluids, meninges, skull and skin surrounding the brain, also known as volume conduction, the activity picked up by an electrode never represents the activity directly under that electrode (Buzsáki et al., 2012). Although, in the beginning of the 90's developments in signal analysis have made it possible to deduce from multichannel measurements where oscillations originate, which also allows the

targeting of deeper lying structures, and has resulted in the method called low resolution electrical tomography (LORETA) (Pascual-Marqui et al., 1994). LORETA uses the cortical registrations from all electrodes used during the measurement to generate a linear solution to the inverse problem which is plotted on a structural MRI brain image. The method was further developed over the next decade into standardized or sLORETA which claims to have zero localisation error (Pascual-Marqui et al., 2002) and has been used quite often in psychological research to link behaviour to brain areas (Saletu et al., 2010, Broyd et al., 2011). However, a potential drawback of sLORETA and therefore a need of caution in its use is that the algorithm source localization is inconsistent with smaller waves and can therefore generate very misleading results (Kobayashi et al., 2005). Throughout this thesis LORETA will not be used as it is not the source localization of brain activity that is of interest here, rather the dynamic interplay between electrical and metabolic activity.

For regular, cortical EEG measurements, at least two electrodes are needed because a change in voltage corresponding to the difference in potential between the recording and the reference electrode is measured (Gazzaniga et al., 2002). The electrodes are placed on the scalp with conductive paste to ensure a low resistance connection. Different regions of the brain can be assessed by choosing appropriate electrode sites (Bear et al., 2007). An international system for electrode placement is developed by Jasper (1958) which is called the 10-20 system and makes it possible for researchers to know underlying brain areas (figure 1.2). The 10-20 system uses relative distances to ensure correct placement in all head sizes.

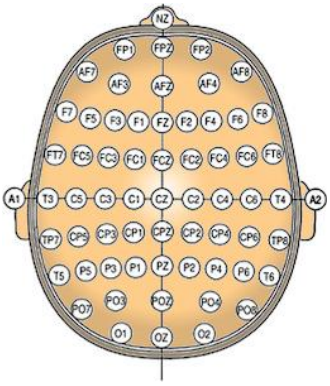

Figure 1.2 The electrode positions of the 10-20 system as developed by Jasper.

1.3.3 From EEG to QEEG

In classical EEG, as developed by Berger, the EEG signal is analyzed qualitatively. Qualitative analysis entails the characterizing of the EEG signal in a general way in which parts of the trace are divided into categories. This is still common in neurology and in sleep studies (Kaiser, 2005). This visual analysis of the ink written EEG by a qualified electroencephalographer remains the gold standard and is the first step in any quantitative EEG (QEEG) analysis (Coburn et al., 2006). In quantitative analysis mathematical and statistical analyses are performed on the EEG to quantify its features. These outcomes are more commonly used in psychological research. The EEG is evaluated in terms of period, amplitude, phase relations, morphology (waveform), topology, abundance, reactivity and variability of these parameters (Kaiser, 2005). The best known method to quantify the EEG is by means of a Fast Fourier Transform (Coburn et al., 2006).

1.3.4 Fast Fourier Transform

The quantitative analysis of EEG started in 1932 when the researcher Dietsch applied Fourier analysis to seven records of EEG (Dietsch, 1932). A Fast Fourier Transform (FFT) converts the time domain EEG record, in which voltage is plotted against time, into a frequency domain, in which magnitude or power is plotted against frequency (Coburn et al., 2006). The height or intensity of a waveform, its magnitude, is computed in micro Volts (μV) for each frequency. Frequency analysis, like FFT, involves the selection of elementary shapes or frequencies (waveforms) which are added together like weights on a scale until their total matches the patterns under investigation (see figure 1.3) (Kaiser, 2005). Since the 1960's the FFT has been used widely by researchers but it is only recently that the FFT is also employed by clinical EEG laboratories (Coburn et al., 2006). Because of its accuracy the FFT is the most used analysis technique in QEEG to date (Kaiser, 2005). Unlike with other methods, formula's for computing spectral analysis with FFT are rarely reported. However, the algorithms can be found in the original research article of Cooley and Tukey (1965).

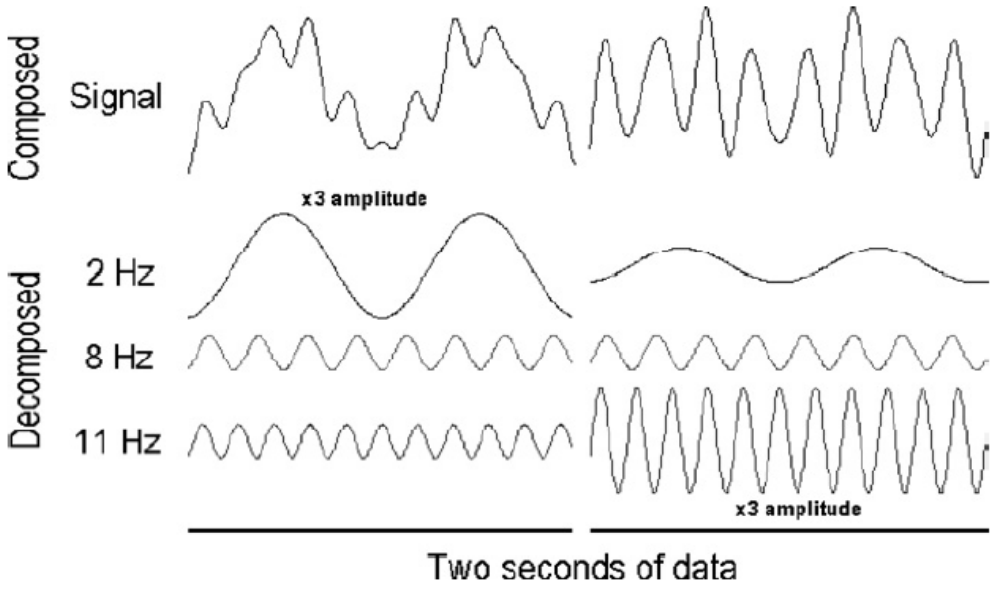

Figure 1.3 Fast Fourier Transform decomposing principle. Decomposing two seconds of impure (multiple frequency) wave form that consists of the same three frequencies. The only difference between segments is the magnitude of the 2 and 11 Hz contributions (Kaiser, 2005).

1.3.5 QEEG bands

The separate frequencies obtained in the spectral analysis are accumulated into frequency bands to correspond to the visual rhythms that are categorized by their frequency range. The EEG is generally divided into five frequency bands which are named after a Greek letter: delta, theta, alpha, beta and gamma (Stern, 2001). Different waves and waveforms are analyzed by the accumulation of narrow or wider frequency bands (Kaiser, 2005).

Delta activity oscillates between 0.5 and 4 Hz[1]. In healthy people delta activity is mostly seen during deep sleep, called slow wave sleep (Iber, 2007). When neuronal damage has occurred, often delta activity is displayed over the damaged area as seen in stroke (Finnigan et al., 2004) or with brain tumours (Selvam and Shenbagadevi, 2011). It is also known that delta activity is the predominant activity of babies in their first two years of life (Stern, 2001). Often delta waves are displayed in large amplitudes (Bear et al., 2007).

[1] The different frequency ranges adopted in this paragraph are those reported in Stern (2001). In the EEG literature these ranges are not absolute and the exact boundaries vary slightly.

Activity between 4 and 8 Hz is called theta activity. It is related to hypnagogic imagery and REM sleep (Bodizs et al., 2008), problem solving (She et al., 2012), attention and then namely a drop of attention during mental fatigue (Wascher et al., 2013) and occurs during mind wandering (Braboszcz and Delorme, 2011). The fact that sometimes the increase in theta activity is seen during heightened cognitive demands (She et al., 2012) and other times during decreased attention and mind wandering (Wascher et al., 2013, Braboszcz and Delorme, 2011) leads researchers to believe that the very same frequency range can express two types of processes (Stern, 2001).

Alpha waves are brain waves in the 8 to 12 Hz frequency and represent the idling state of the brain (Kaiser, 2005). This relates them to relaxation and the absence of cognitive processing (Stern, 2001). However, it has also proven to be related to active inhibition of other brain areas (Klimesch et al., 2007). Berger was the first one to describe the phenomenon “alpha blocking”, an abrupt suspension of alpha activity when an individual opens his or her eyes (Berger, 1969). This blocking also occurs when people are asked to perform a cognitive assignment, or pay attention to objects in the environment (Stern, 2001, Kaiser, 2005). The alpha blocking phenomenon has been referred to in the literature as event related desynchronisation (ERD) (Pfurtscheller et al., 1994). Similarly the occurrence of alpha over the occipital cortex upon closing the eyes has been referred to as event related synchronisation (ERS) (Pfurtscheller, 1992).

Brain waves in the 18-30 Hz frequency range are called beta waves. The waves are high in frequency and low in amplitude. Beta waves are visible in the EEG when a person is alert (Stern, 2001). The beta waves often are subdivided into low beta-wave activity or beta 1 activity, ranging from 12-20 Hz, and high beta-wave activity or beta 2, ranging from 20-32 Hz. It is believed that the beta1 activity could be the idling state of the motor control system (Engel and Fries, 2010). The reason for suggesting beta1 activity as idling rhythm for the motor system is the occurrence of this frequency during rest and its ERD when movement is initiated together with an increase when doing steady state contractions (Engel and Fries, 2010). Beta activity is also found to increase generally when top down cognitive information processing is warranted and therefore thought to be related to the

focussing on a task which enables someone to ignore task irrelevant stimuli (Okazaki et al., 2008, Iversen et al., 2009).

Gamma waves oscillate between 30 and 70 Hz and are related to the brain's ability to put a variety of stimuli in a coherent whole (the so called binding problem (Rolls and Deco, 2006, Body and De Rosa, 2007, Colzato et al., 2007)) but there is a lot of uncertainty still regarding this frequency waves (Cotillon-Williams and Edeline, 2004, Palanca and DeAngelis, 2005, Rauschenberger and Yantis, 2006). Fries (2009) argues that gamma synchronization is needed whenever cortical computation occurs. In line with that Merker (2013) suggests that no typical functional role should be dedicated to gamma activity, but that it should be regarded as a state of physiological activation. A summary of the categorized brain waves is given in table 1.1.

Brainwave	**Frequency range**	**Function**
Delta	0,5 - 4 Hz	Deep sleep, brain lesion, babies
Theta	4 – 8 Hz	REM sleep, problem solving, drop of attention, mind wandering
Alpha	8 – 12 Hz	Idling state, absence of cognition, active inhibition
Beta	18 – 30 Hz	Idling state motor system, top down cognitive processing, attention focus
Gamma	30 – 70 Hz	Binding problem, physiological activation

Table 1.1 The different frequency bands with their range and function.

1.3.6 Advantages and limitations

The normal or healthy (Q)EEG profiles are well established and consistent among individuals. Furthermore, (Q)EEG test-retest stability is remarkably high, even over longer time periods (Gudmundsson et al., 2007, Salinsky et al., 1991, Kondacs and Szabo, 1999). Therefore (Q)EEG can also aid in detecting abnormalities, and assist a physician in making a diagnosis (Gazzaniga et al., 2002, Coburn et al., 2006). This makes it likely that QEEG will emerge as a mainstay of neurology, sleep medicine, as well as psychiatry and psychology (Kaiser, 2005). Additional advantages of QEEG are the direct quality of the measurement, the high temporal resolution in

the millisecond range which is comparable to cortical and thalamic cell firing rates, and the painless and non-invasive use (Kaiser, 2005, Coburn et al., 2006). Also, the method relatively inexpensive and portable, all advantageous for clinical use (Coburn et al., 2006).

A disadvantage of (Q)EEG is that it needs to measure a tiny bodily signal that travels through different layers of tissue before it is picked up. This makes it necessary to ensure a good signal-to-noise ratio. Furthermore, one needs to be aware of the possible noise that is easily induced upon the signal. These features are well studied and documented (for an example see (Krauss et al., 2006)). Also, EEG has low spatial resolution due to the smearing of the signal caused by the skull. However, with the expanding number of electrodes available (up to 512) the spatial resolution has improved remarkably (Coburn et al., 2006).

1.4 The principles of NIRS

The methodology of NIRS embarks upon the optical properties of brain tissue and is therefore an optical imaging method (Boas et al., 2004). It was first described by Jöbsis (1977) who used light in the near infrared range to monitor in vivo the redox behaviour of cytochrome c oxidase. This led to the finding that skin and bone is translucent to light in the near-infrared range and that it is possible to reach brain tissue noninvasively.

The functional state of tissue can influence its optical properties. Other factors that influence tissue's optical properties are changes in blood level as well as electrochemical activity (Irani et al., 2007). These changes in optical properties can then be used to measure physiological changes with near-infrared light (Jobsis, 1977).

1.4.1 Neurovascular coupling

In order to comprehend the principles of NIRS it is necessary to understand the principles of neurovascular coupling which are schematically represented in figure 1.5 to some extent. Neuronal activity is fuelled by glucose metabolism and oxygen (Cauli and Hamel, 2010). For these sources to arrive at the neurons the cerebral blood stream is used (figure 1.4). The blood supply to the brain comes from two

pairs of cranial arteries that branch out at the base of the brain to form separate circles for the forebrain and the hindbrain, connected by the circle of Willis as safety net whenever blockage in one of the two circles occurs (Bear et al., 2007). The posterior and anterior circulation branch into smaller pial arteries and arterioles that branch out over the surface of the brain. These give rise to arterioles that reach the neurons and glial cells and subdivide into an extensive and distributed network of capillaries that provide the neural system with oxygen and glucose (Ward, 2013).

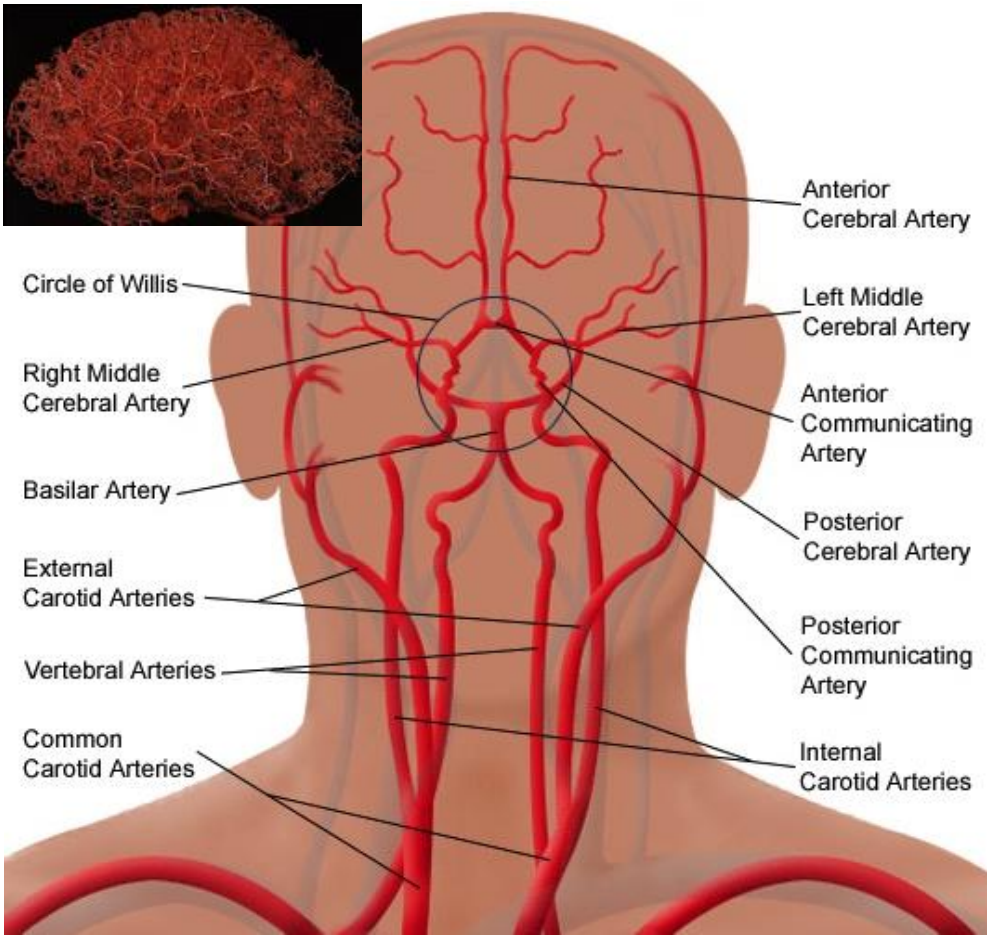

Figure 1.4 The cerebral vascular network. The lower panel shows the major arteries that are responsible for the blood supply to the brain. The upper panel shows a model of all cerebral arteries, demonstrating its density.

This cerebral vascular network uses control mechanisms to match the cerebral blood flow (CBF) with the local energy demands. In short, regulatory processes arise through the interactions between neurons, glia, and vascular cells (Ward, 2013). When neuronal activity increases, the glucose and oxygen consumption

from the local capillary bed increases as well. Because of the increased consumption, the amount of glucose and oxygen in the capillary bed decreases which stimulates the brain to increase local vasodilation. This increases local CBF and cerebral blood volume (CBV) (Irani et al., 2007). A process which is termed functional hyperaemia and is one of the key roles of neurovascular coupling (Ward, 2013, Cauli and Hamel, 2010). On the other hand is this control mechanism also capable of inducing vasoconstriction, which reduces CBF. Together, the vasodilaton and –constriction are responsible for generating the appropriate blood flow conditions that are required for optimal metabolic functioning of the neural networks (Ward, 2013). This makes sure that autoregulation is provided. The second key role of neurovascular coupling is to support the brain's ability to maintain the necessary homeostatic blood pressure during periods of changing blood flow (Ward, 2013).

This allows the assessment of two physiological responses using optical imaging techniques. The first being a slow response occurring over several seconds when the increased CBF carries both glucose and oxygen bound to haemoglobin (Hb) to the active brain area. The increased oxygen that is carried to the area exceeds the rate at which the oxygen is used by the neurons, resulting in elevated blood oxygenation in the active area. The second is a fast response that occurs when the initial increase in neural activity results in an increase of blood deoxygenation. This happens when the neurons use the present oxygen to metabolize glucose before the bloodstream is able to increase the amount of oxygen delivered to the brain area which takes several seconds (Irani et al., 2007). Because oxygenated haemoglobin (HbO_2) and deoxygenated haemoglobin (HHb) have characteristic optical properties in the near-infrared light range, it is possible to measure their concentration changes with optical imaging methods like NIRS (Boas et al., 2004, Irani et al., 2007).

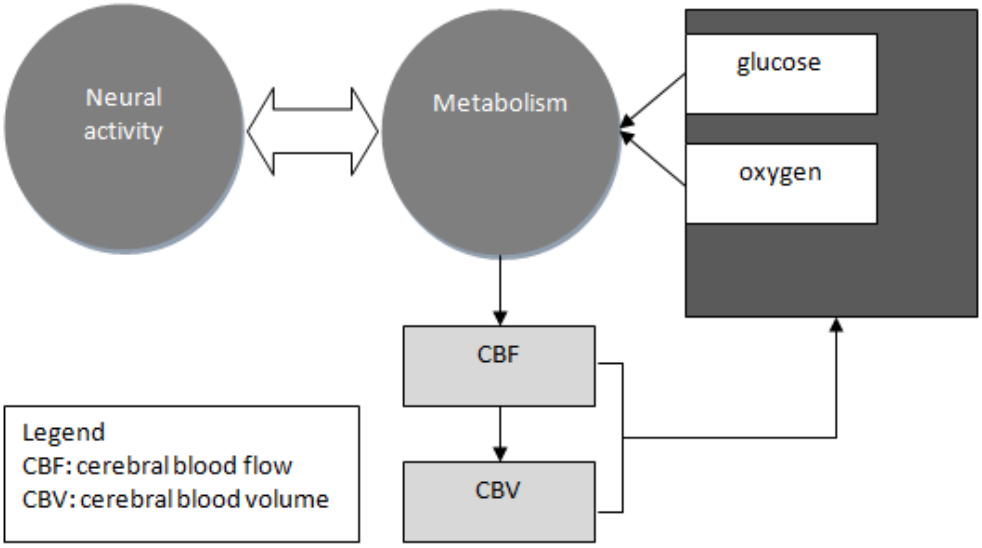

Figure. 1.5 Schematic representation of neurovascular coupling.

However, this depiction may be somewhat simplistic. The mechanisms underlying neurovascular coupling have been studied for over a century, and multiple factors have show to play a role in this intricate process (Girouard and Iadecola, 2006). And although intuitively appealing, a direct link between energy state and blood flow is not universally accepted, which leaves the physiological basis for neurovascular coupling uncertain (Cauli and Hamel, 2010). Neither the acute demand for glucose, nor the demand for oxygen primarily, fully justifies the hemodynamic response (Girouard and Iadecola, 2006, Cauli and Hamel, 2010). For a recent review on advances in neurovascular coupling research see (Howarth, 2014). Despite these limitations, fMRI, PET and NIRS research embarks upon changes in hemodynamic signals and uses it to infer claims about neural activity in various pathologies ((Chen and Li, 2012, Girouard and Iadecola, 2006, Portnow et al., 2013, Obrig and Villringer, 2003). A point which will be addressed further in paragraph 1.5.

1.4.2 NIRS

To measure the concentration changes in HbO_2 and HHb, NIRS uses near-infrared light in the range between 700-1000 nm. Most biological tissue is transparent to light at these wavelengths because a relatively small amount of this light is absorbed by Hb and water (Irani et al., 2007). The chromophores HbO_2 and HHb which are present in the blood reflect specific and different wavelengths in this range. The spectral band at which HbO_2 and HHb reflect near-infrared light is

called the optical window and is visualized in figure 1.6 (Jobsis, 1977).

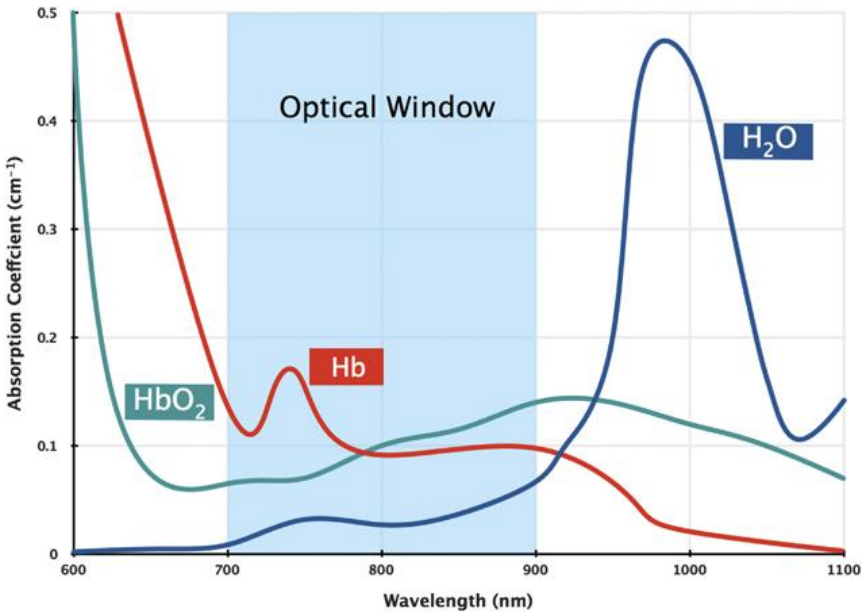

Figure 1.6 (adopted from Phan & Bullen (2010)) The optical window into the human body. At frequencies between 700 and 900 nm (near infrared range) the chromophores oxygenated haemoglobin (HbO_2) and deoxygenated haemoglobin (HHb) reflect specific and different wavelengths. Furthermore, the reflection of water (H_2O) is minimal in this range, causing little distortion.

During a NIRS measurement near-infrared light, either through light emitting diodes (LEDs) or through fibre optical bundles, is shone upon the head by means of a transmitter called an optode (Irani et al., 2007). The photons that are leaving the optode pass through the skin, skull and several cm of brain tissue where they are either absorbed, reflected or scattered by the HbO_2 and HHb chromophores (Ferrari et al., 2004). Because the quantity of photons that leave the optode is relatively predictable and the photons follow a banana-shaped path back to the surface of the skull, they can be measured by the use of photo detectors placed alongside the transmitter (Ferrari et al., 2004, Irani et al., 2007). Due to the scattering a photo detector placed 2-7 cm away from the optode can collect light after it has passed through the tissue (Irani et al., 2007). The dept that is reached by the light is approximately half the source-detector distance (Strangman et al., 2002). Changes in the chromophore concentrations cause changes in the reflected light intensity and are quantified using the modified Beer-Lambert law (Delpy et al., 1988).

1.4.3 The Beer-Lambert law

The Beer-Lambert law relates the absorption of light to the properties of the material through which the light is travelling. When the change in absorption is global throughout a medium, then the modified Beer-Lambert law is written as:

$$OD(\lambda) = \mu_a(\lambda)\, L\, \ell_{DPF}(\lambda)$$
$$= \left[\varepsilon_{HbO_2}(\lambda) \quad [HbO_2] + \varepsilon_{Hbb}(\lambda) \quad [HHb]\right] L\, \ell_{DPF}(\lambda)$$

In this equation $OD(\lambda)$ is the change in optical density measured at a given wavelength, $\mu_a(\lambda)$ is the corresponding change in tissue absorption, L is the separation between the source and the detector, and ℓ_{DPF} is the differential path length factor (DPF) (Delpy et al., 1988). The differential path length factor corrects for the increased distance that the light travels from the transmitter to the detector because of scattering and absorption. The change in absorption is related to the changes in chromophore concentrations of oxygenated haemoglobin $\Delta[HbO_2]$ and deoxygenated haemoglobin $\Delta[HHb]$ by the wavelength dependent extinction coefficients $\varepsilon_{HbO_2}(\lambda)$ and $\varepsilon_{HHb}(\lambda)$.

From measurements of $OD(\lambda)$ at two wavelengths, the concentration changes are given by:

$$[HHb] = \frac{\varepsilon_{HbO_2}(\lambda_2)\Delta\mu_a(\lambda_1) - \varepsilon_{HbO_2}(\lambda_1)\Delta\mu_a(\lambda_2)}{\varepsilon_{Hbb}(\lambda_1)\varepsilon_{HbO_2}(\lambda_2) - \varepsilon_{HbO_2}(\lambda_1)\varepsilon_{HHb}(\lambda_2)}$$
$$[HbO_2] = \frac{\varepsilon_{HHb}(\lambda_1)\Delta\mu_a(\lambda_2) - \varepsilon_{HHb}(\lambda_2)\Delta\mu_a(\lambda_1)}{\varepsilon_{Hbb}(\lambda_1)\varepsilon_{HbO_2}(\lambda_2) - \varepsilon_{HbO_2}(\lambda_1)\varepsilon_{HHb}(\lambda_2)}$$

When the change in absorption is not global, the modified Beer-Lambert law can be rewritten as:

$$OD(\lambda) = L\sum_{i=1}^{N} \Delta\mu_{a,i}(\lambda)\, \ell_{PPF,i}(\lambda)$$
$$= L\sum_{i=1}^{N} \left[\varepsilon_{HbO_2}(\lambda) \quad [HbO_2] + \varepsilon_{Hbb}(\lambda) \quad [HHb]\right] \ell_{PPF,i}(\lambda)$$

Where $\ell_{PPF,i}(\lambda)$ is the partial path length factor (PPF) through a region of uniform absorption change. A sum is made over N regions of uniform absorption change. In the case of brain activation the measured change in optical density is best

analysed with a PPF, because of the focal nature of the brain activation. However, accurate estimation of the PPF is not feasible because it requires knowledge of the position and spatial extent of the local absorption change as well as the optical properties of the surrounding tissue. Therefore, the DPF is used in most analyses (Strangman et al., 2003). The DPF is however thought to vary with age and therefore it is recommended to measure it in every subject before commencing the measurement if possible (Duncan et al., 1996, Bonnéry et al., 2012). Erroneous choice of DPF can result in errors in the estimated concentration changes influencing research outcomes which is referred to as crosstalk (Strangman et al., 2003, Umeyama and Yamada, 2009).

1.4.4 Equipment

In order to calculate the concentration changes in HbO_2 and HHb the NIRS equipment has to measure the change in optical density at, at least, two wavelengths. To do so, different types of NIRS equipment and devices are commercially available (for a recent overview see (Ferrari and Quaresima, 2012)). An overview of several commercially available devices is shown in figure 1.7. Each device has different characteristics which can be divided into three groups: photometers, oximeters and imagers. All photometers use single distance continuous waves (CW) (Ferrari et al., 2004). CW systems apply light at a constant amplitude and are only capable of measuring changes in the HbO_2 and HHb when a known DPF is included to calculate the path length of the travelled light (Ferrari et al., 2004, Irani et al., 2007, Ghosh et al., 2012). Photometers measure the changes in HbO_2 and HHb very accurately but they cannot measure tissue HbO_2 saturation due to the fact that no absolute values of HbO_2 and HHb can be given (Ferrari et al., 2004).

Spatially resolved spectroscopy (SRS), time-resolved spectroscopy (TRS) and phase modulation spectroscopy (PMS) can calculate tissue HbO_2 saturation. The SRS technique is used often in oximeters, however not all commercially available devices disclose the algorithms used to derive haemoglobin concentrations (Ghosh et al., 2012). Occasionally the techniques of PMS and TRS are used in oximeters as well but it is more common for TRS and PMS to be seen in imagers (Ferrari et al., 2004). With PMS and TRS it is possible to calculate optical absorption and scattering (Ghosh et al., 2012). Imagers use multiple channels to

perform the measurement. This allows the generation of images of a larger brain area with a higher temporal resolution (up to 10 Hz) (Ferrari et al., 2004). The results from this type of device however, are still under dispute, since the lack of path length determination limits the accuracy of the results (Ferrari et al., 2004). The different devices vary in technological complexity and therefore also costs starting with CW-technology and then proceeding to SRS and further to TRS and PMS technology (Ferrari and Quaresima, 2012). The device used by the Oxford Brookes research group and throughout this thesis is a single distance, continuous wave photometer, OXYMON Mk III (Artinis Medical Systems, Zetten, the Netherlands).

Figure 1.7 Examples of NIRS devices and sensors. Also for NIRS different sized devices are available ranging from large, whole headed devices as shown on the right bottom, to more easily transportable devices with less channels as shown on the left, to small sized devices that can be carried in a backpack and used for motion studies as shown in the middle. Also sensor configurations come in a broad variety. The top panel shows from right to left the configuration of separate optodes in a headband, the use of optodes prefixed in a headband, an optode cap, and a helmet configured with spring loaded optodes with integrated EEG sensors.

1.4.5 Advantages and limitations

Besides the afore mentioned trouble in estimating DPF and related crosstalk issues that cause the HbO_2 concentration to be mistaken for Hbb and vice versa (Strangman et al., 2003, Umeyama and Yamada, 2009), there are some limitations to the use of NIRS. Compared to other indirect measurements NIRS has a fairly limited spatial resolution. This limitation exists because the near-infrared light only penetrates the brain tissue to the extent of a few cm. Therefore only cortical activation can be measured and no deeper lying structures are reached (Arenth et al., 2007). Since the light has to penetrate the skin skull and several layers of extra cerebral matter before it reaches the region of interest, attenuation of the light occurs which makes the measurement less accurate (Boas et al., 2004). Other limitations arise in the use of cranial reference points. Since NIRS is a fairly young technique no standard has been developed in its application. Often the 10-20 system used in EEG is also used in NIRS to determine the location on the head (Irani et al., 2007).

Additional to the lack of standardization in optode placement, no consensus is reached about standardizing NIRS analysis. This leads to different streams in NIRS research in which both techniques seen in EEG as well as techniques seen in fMRI analysis are explored. Furthermore, it is hard to compare NIRS data between studies because of the use of different systems, different cranial reference points and even different wavelengths to measure the concentration changes in HbO_2 and HHb. Also the signal to noise ratio decreases among different subjects because of skin and hair pigmentation and it is difficult to obtain absolute baseline concentrations of HbO_2 and HHb (Arenth et al., 2007). As such, the technology is still in its infancy compared to more established techniques such as fMRI (Irani et al., 2007). However, there are also advantages in NIRS which make it more attractive for clinical use than other methodologies.

NIRS makes use of non-ionizing light sources, which do not build up more energy in the brain than happens on a sunny day (Arenth et al., 2007). Unlike PET and SPECT measurements, NIRS is not harmful to tissue and it is non-invasive (Boas et al., 2004). Therefore, it is also safe to use repeated measures designs.

Furthermore, unlike fMRI, it is safe to use NIRS with patients that have plates, pins or other metallic implants (Arenth et al., 2007) which is impossible in fMRI. Because of the simplicity of the equipment the manufacturing costs are not as high as they are for other imaging equipment, which makes it more appealing to use more often in the same patient. In line with that, the small size of the equipment allows the NIRS system to be used at a doctor's office, at bedside and even at home as a monitoring device (Ferrari et al., 2004). Also the size and configuration makes a NIRS device more patient friendly and less intimidating as for example a fMRI scanner. In a fMRI scanner another drawback are the loud noises and the inability to move. NIRS systems are quiet and are robust to movement which makes it very appropriate to use during "real life" tasks (Arenth et al., 2007).

1.5 Multimodal use of QEEG and NIRS

From the preceding paragraphs we have learned that (Q)EEG and NIRS measure very different modalities of brain functioning. Whereas EEG is able to measure global patterns of electrical brain activity linked to the activation of neuronal networks NIRS provides information on local changes in cortical oxygenation. In paragraph 1.4.1 it was already mentioned that the process of neurovascular coupling is not fully unravelled yet and that a direct link between energy state and blood flow is not universally accepted, which leaves the physiological basis for neurovascular coupling uncertain (Cauli and Hamel, 2010). Therefore, when NIRS is used as a single research modality it is possible that faulty inferences are made about brain functioning. However, despite the fact that we do not fully understand this neurovascular coupling, gathering information on both an electrical as well as an hemodynamic parameter in a clinical setting will provide us with more information about brain functioning, and could therefore aid in differentiating different pathologies better than the use of one modality can. It is not only the use of two separate modalities that can be of interest here but it is also its shared information content that as a separate variable could increase sensitivity and specificity in differentiating clinically relevant brain states.

The number of studies combining both measurement modalities in the investigation of human brain functioning has increased over the last decade,

affirming its feasibility. Although, the number of studies that actually aim at linking parameters from both modalities is still limited.

One of the research areas that has been using simultaneous monitoring, is the surgical field (Toet et al., 2005, Moritz et al., 2007), as well as neonatology (for a review see (Toet and Lemmers, 2009)). By monitoring both electrical as well as hemodynamic parameters during for instance cardiac surgery, or in premature infants, one is able to detect problems in blood supply to the brain and possible neurological distress instantly. These studies, however, as vital as they are when brain monitoring under critical care is investigated, use the measurement modalities separately and do not investigate an underlying coupling.

Another aspect that has been studied since concomitant application became available is brain oxygenation during seizures and epileptiform discharges. Results in this area suggest that this approach can detect changes during absences or seizures (Buchheim et al., 2004, Machado et al., 2011), predict when an absence or seizure occurs (Roche-Labarbe et al., 2008, 2010), and predict the response to anti-epileptic medication (Arca Diaz et al., 2006). However, electrical changes seen during seizures and absences are many times larger than the changes seen in the EEG during rest or any task for that matter. Therefore findings in epilepsy research may be very different from non-epileptic brains.

Studies that do try to link parameters from the electrical field to parameters in the hemodynamic field vary greatly in the subject of interest. They range from investigating sustained attention (Butti et al., 2006) to the effects of mental stress and relaxation (Ishii et al., 2008) to the mechanisms of sensory gating (Ehlis et al., 2009). Brummer et al. (2011) as well as Smith et al. (2013) even investigated what happens to brain activity measured with combined EEG and NIRS when changes in gravity are involved. It has to be said though that results of the gravity studies are not conclusive yet as the induction of hypergravity by a human centrifuge or the induction of weightlessness during a parabolic flight brings about technological challenges in the actual measurements.

An area of study which deserves special attention from a clinical point of view is brain-computer interface (BCI) research. A BCI correlates brain activity with

external devices in order to communicate or gain control over them (Pfurtscheller et al., 2010, Khan et al., 2014). Due to the intended clinical use the set-ups need to be low cost, quick, and accurate and are therefore often realized with limited sensors (Pfurtscheller et al., 2010). Recently the field has moved towards the use of hybrid BCI's in which more than one input is used simultaneously in order to enhance system performance or to be able to increase the number of commands (Pfurtscheller et al., 2010). The combination of EEG and NIRS in hybrid BCIs is made more often now. For example, Fazli et al. (2012) showed in a motor paradigm that adding NIRS measurements to an EEG based BCI improved classification in over 90% of the measurements and enhanced performance by 5%. Another method that is used in hybrid BCI research is the use of the NIRS signals as a switch in order to investigate whether movement or movement imagery is present. When the switch indicates the presence of movement related activity, the EEG signals over the motor cortex classify the type of activity which was demonstrated to be useful also in self paced as opposed to cued paradigms (Koo et al., 2014). Khan et al. (2014) used additional NIRS measurements over the prefrontal cortex to increase the number of classifiers with two in addition to the two classifiers that were generated from motor areas with EEG. Which is a different desired goal to be obtained by the use of hybrid interfaces. Besides motor paradigms, visual paradigms are also often investigated in BCI research. Tomita et al. (2014) used visual evoked potentials as classifiers. A downside in using visual evoked potentials is that during periods of rest often send out signals that the user did not intend to convey (called false positives). By using NIRS signals over the visual cortex to determine whether a user is in a communication or rest mode reduced the number of false positives ranging from 53% to 85%. The improvements listed above obtained by the use of a multimodal system with limited sensors in generating accurate predictions about states of brain activity is especially promising in clinical use. Not only for communication but also for classifying different pathologies.

The aforementioned studies illustrate the diversity of options that can be explored with multimodal brain measurements. As an additional research area the investigation of the symbioses between electrical and metabolic parameters during a resting state should be mentioned. Roche-Labarbe et al. (2007) investigated whether changes in the concentration of cerebral HbO_2, HHb and

total Hb were related to the occurrence of spontaneous bursts of electrical activity in premature infants. There seemed to be a relationship that was different for the 6 healthy babies than was found for the 4 neurologically distressed babies that were investigated. However, it is not established yet if relationships that occur in premature infants can be extrapolated to an adult human brain.

Moosmann et al. (2003) were one of the first to investigate the relationship between the occurrence of alpha wave activity and Hbb in the occipital cortex of healthy adults in an eyes open, eyes closed paradigm. They report a positive cross-correlation between alpha wave activity and Hbb in which the hemodynamic parameter has a delay of approximately 8 seconds. Koch et al. (2008) investigated a special feature within the alpha band, the alpha peak frequency. They reported that in individuals who display an alpha peak that is higher in frequency, a smaller alpha magnitude is found and a smaller response in oxygenation is seen than is in subjects that show an alpha peak lower in frequency. In this research a paradigm with visual stimulation was used. As indicated in paragraph 1.3.5 the phenomenon of alpha blocking upon opening the eyes, also known as ERD is a well know response that is found in all people and is strongest over the occipital cortex (Pfurtscheller et al., 1994). Therefore this basic brain response is an viable paradigm for investigating the difference between two different brain states. Furthermore, the ease with which the two different brain states can be summoned creates great prerequisites for use with broad patient populations including children and cognitively challenged patients. However the exact functioning in healthy people should be established first.

1.6 Conclusion

To sum up the rationale laid out in this first chapter it can be said that psychopathologies are common in more than one in every three people. Of all people experiencing a psychopathology worldwide four out of five people do not receive appropriate health care. Since it is known that different (psycho)pathologies display different patterns of brain activity, the embedding of brain measurements in early lines of healthcare could reduce this number. People could be diagnosed better and faster, and brain measurements could be used to evaluate treatment options and treatment outcomes. In order to be able to

embed brain measurements in these early lines of healthcare easy to apply, low cost methods should be used of which EEG and NIRS seem to meet these criteria. The use of these methods would create insight in the electrical brain activity as well as the hemodynamic activity. Furthermore, the synchronous, multimodal use of the two might provide additional information that increases sensitivity and specificity in detecting different patterns of brain activity.

Multimodal research, especially the BCI research has shown that the use of both EEG and NIRS increases the accuracy of identifying brain states with limited sensor set-up which may apply to the classification of pathology related brain states as well. In order to investigate this potential further, the exploration of resting state parameters seems extremely valuable for clinical use. Especially the difference between eyes open and eyes closed states over the occipital cortex and its related ERD in the alpha band would be a good starting point due to the ease with which it can be induced in a broad patient spectrum.

The goal of this thesis is to explore the relationship between electrical and metabolic aspects of brain functioning with EEG and NIRS in order to reveal its exiting opportunities in understanding brain functioning in health and disease. Before this research can be started the limitations of the NIRS equipment will be explored first. This will be done in a pilot study that will address the robustness of the NIRS measurement to artefacts which will be described in chapter 2.

Before patient populations can be investigated it is important to have an understanding of the differences between resting brain states in healthy subjects. Therefore, this will be addressed first, continuing the work of Moosmann et al. (2003) with special focus on the alpha band and its relation to HbO_2 and Hbb parameters. This relationship will be investigated in a stepwise fashion, moving from the static analysis of blocks (chapter 3), towards analysis of timing aspects (chapter 4), towards the analysis of both linear and nonlinear aspects of the relationship (chapter 5).

Then a pathology is selected in which we are absolutely sure that changes are seen in both the electrical and hemodynamic domain as well as in the neurovascular coupling, stroke (Girouard and Iadecola, 2006, Blicher et al., 2012,

Ayata, 2013, Finnigan and van Putten, 2013). If no differences can be found between stroke patients as opposed towards healthy brains, the movement of the research towards the more subtle differences seen in psychopathologies might seem still far away. This will be done by describing two case studies of stroke patients in which the same eyes open eyes shut paradigm is carried out in chapter 6. The data from these measurements are analysed with the same methods as are described in chapters 3 through 5 in order to investigate differences between healthy brains and brains post stroke. In chapter 7 a general conclusion of the findings in this thesis is given. Furthermore, implications for clinical use will be raised together with the proposal of future paths of research in order to stimulate the research in this accelerating area of neuroscience.

Chapter 2: Assessment of robustness to artefacts of Near-Infrared Spectroscopy

In this chapter the robustness to artefacts in NIRS measurements will be evaluated. Hereto a paradigm is chosen in which tasks are performed that are known to induce artefacts in EEG measurements. Several methods have been proposed to eliminate artefacts. The performance of one of these methods, the correlation based signal improvement method, will be evaluated in this chapter as well.

2.1 Introduction

As introduced in the previous chapter, NIRS measurements meet several requirements that make it a good candidate for broad clinical application (Arenth et al., 2007, Irani et al., 2007). One argument that is often used to emphasize the role of NIRS in measuring real life paradigms is its robustness to motion artefacts (Arenth et al., 2007). However, motion artefacts can indeed influence NIRS signals (Izzetoglu et al., 2005, Huppert et al., 2009, Cui et al., 2010). Papers that consider artefacts in the NIRS signal often focus on physiological noise caused by the cardiac cycle and the respiratory system or on cross talk and separability (Nolte et al., 1998, Boas et al., 2004, Uludag et al., 2004b). Cross talk was briefly mentioned in chapter 1 and occurs due to erroneous choice of the DPF that is used in obtaining concentration changes of HbO_2 and Hbb by the modified Beer-Lambert law (Strangman et al., 2003). Cross talk can lead the HbO_2 signal to mimic the Hbb response and vice versa, causing the magnitude and the time course of the Hb concentration to be influenced (Uludag et al., 2004b). Separability is different from cross talk and describes the difficulty in separating HbO_2 and Hbb concentrations due to the wave lengths used and the amount of physical noise that is present in the system (Uludag et al., 2004b).

The occurrence of motion artefacts is thought to arise from a change in optical coupling of the optode and the scalp, either by a shift of detectors or by blood moving away or towards the region of interest (Izzetoglu et al., 2005, Cooper et al., 2012, Brigadoi et al., 2014). Izzetoglu et al. (2010, 2005) specifically describe

this phenomenon in head movements. However, this is not the only situation in which motion artefacts can occur. Bodily movements, eye movements or even muscle tension may distort the collected signal and all are likely to occur during testing, especially when real life paradigms or clinical populations are examined. The impact of these factors on the signal has not fully been described yet but could lead to false interpretation in a clinical setting. A substantial body of literature describes the influence of motion and muscle artefacts in the acquired signal in similar methods, such as EEG, which is also non-invasive and makes use of sensors on the head. Every EEG book is equipped with a chapter that describes pitfalls during EEG measurements and the reader is provided with a collection of signals that can help recognize typical artefacts caused by eye movements, muscle movements and motion artefacts (for an example see (Krauss et al., 2006)). Since this kind of literature is limited for NIRS measurements, the first aim of this study was investigating the effects of a variety of movements that can occur during a NIRS measurement on the acquired signal. Secondly, it would be helpful to know whether these possible motion artefacts could be removed from the data by filtering. In order to find out, one first should be aware of all types of noise NIRS measurements are susceptible to and what methods are currently used to filter these.

In general three types of noise can be distinguished in NIRS measurements: instrument noise, physiological noise, and experimental error (Huppert et al., 2009, Cui et al., 2010). Instrument noise is induced by hardware components and is usually high in frequency (Huppert et al., 2009). Different sources of physiological noise can be defined. Cardiac pulsation is a source of noise that arises around 1 Hz and is seen mainly on the arterial side (Nolte et al., 1998, Boas et al., 2004, Zhang et al., 2005, Huppert et al., 2009). Respiration also can cause slow drifting noise in NIRS measurements (Boas et al., 2004, Zhang et al., 2007a, Zhang et al., 2007b, Huppert et al., 2009). Noise caused by respiratory signals is primarily seen on the venous side, due to changes in intra-thoracic pressure, which affect the rate of venous return (Zhang et al., 2005). Blood pressure changes can cause noise in the frequency domain between 0.08 and 0.012 Hz (Boas et al., 2004, Zhang et al., 2007a, Zhang et al., 2007b, Zhang et al., 2009, Huppert et al., 2009). As with cardiac pulsations this is also primarily an arterial effect, and has different components: intrinsic blood pressure variation, variation

coupled to heart rate, Mayer waves, low frequency oscillations (LFOs), very low frequency oscillation (VLFOs), and vasomotor waves (Zhang et al., 2007a, Zhang et al., 2007b, Zhang et al., 2009, Zhang et al., 2005). Noise caused by experimental error includes motion artefacts and noise caused by non-compliance with the experimental paradigm by the subject (Huppert et al., 2009, Cui et al., 2010).

Different ways of filtering these types of noise have been described in the scientific literature. For instrument noise usually low pass filtering will suffice, since this type of noise is high in frequency and the target frequency in NIRS measurements is in the low frequency domain (Huppert et al., 2009). Physiological noise is harder to filter since it arises in the low frequency domain. This type of noise can be filtered based on the approximated frequency content, spatial covariance, or subtraction by measuring the same physiology away from the functional signal either by using an additional channel with a short source detector separation or another direct extra-cranial measurement (Huppert et al., 2009, Zhang et al., 2009). Adaptive filtering, wavelet filtering, and principal component analysis (PCA) from baseline data are methods that can also be used to filter physiological noise from NIRS measurements (Huppert et al., 2009, Zhang et al., 2007a, Zhang et al., 2007b, Zhang et al., 2009). Along with spline interpolation and Kalman filtering the same methods have been used to filter motion artefacts (Huppert et al., 2009, Scholkmann et al., 2010, Cooper et al., 2012, Brigadoi et al., 2014). However, these methods have been reported to be only partly effective in filtering motion artefacts (Huppert et al., 2009). A challenge in determining this efficacy is that often the knowledge of the true form of the original (noise-free) signal lacks which is necessary to quantify improvement (Sweeney et al., 2012).

Sweeney et al. (2012) proposed an elegant method to measure two signals with two detectors in close proximity from the same source in which only in one detector motion artefacts were induced by gently pulling the optic fibre. The occurrence of the artefact in only this detector and not in the other or in the source was monitored by means of accelerometers. In their method two signals arise; 1. a motion artefact contaminated signal and 2. a noise free “ground truth” signal. This signal pair can then be used to test the efficacy of artefact removal methods by comparing the correlation between both signals and the signal-to-

noise ratio (SNR). With this method they showed that adaptive filtering and Kalman filtering improved the correlation by 68.22% and 66.5% respectively, as well as it improved SNR by 5 dB or more in both. The overall correlation between the filtered signal and the "ground truth" signal did not exceed 0.71 for epochs with motion artefacts and 0.77 for non affected epochs (Sweeney et al., 2012).

Adaptive filtering relies on the measured signal of a second pair of optodes with has a close source-detector separation which allows the measurement of hemodynamic changes in layers more superficial than the cortex. This measurement is then used as reference channel for the adaptive filter which subtracts the reference signal from the signal of interest (Zhang et al., 2007a, Zhang et al., 2007b, Zhang et al., 2009). The other methods can be applied without the use of an additional optode pair. For example, wavelet filtering. Wavelet filtering transforms the obtained NIRS time series into the wavelet domain by use of a general discrete wavelet transformation (for an example see (Cooper et al., 2012)). The wavelet coefficients are assumed to have a Gaussian probability distribution which leads the contributions of noise to appear as outliers. These outliers are then removed and the time series are rebuilt with an inverse wavelet transformation (Cooper et al., 2012, Brigadoi et al., 2014).

Similarly, PCA relies on the different properties of the actual signal and the artefact. PCA transforms a NIRS measurement in N linearly uncorrelated components which are ordered by the amount of variance they add to the signal. It is assumed that the variance that is added by noise is greater than the amount of variance that is added by the NIRS signal. Therefore, removing these components that have the highest contribution to the variance results in the removal of the noise (Zhang et al., 2005, Cooper et al., 2012, Brigadoi et al., 2014). Depending on the type of artefact, components adding up to 80% and sometimes even 97% of the total variance are removed. By increasing this percentage one should be aware of the risk of removing the response of interest though (Brigadoi et al., 2014).

The spline interpolation method as described by Scholkman et al. (2010) first uses the motion detection algorithm available in the open source data analysis package Homer2 (Huppert et al., 2009). It then models the motion artefact and subtracts it

from the signal of interest only in the signal in which it is detected. After that, it applies a reconstruction on the signal to correct for the shift from baseline of the signal that can occur due to the artefact (Scholkmann et al., 2010). In modelling the artefact an interpolation parameter (p_Spline) of 0.99 is recommended by Scholkman et al. (2010) for removing motion artefacts.

Like the spline interpolation method, Kalman filtering, is also an approach that is used on a channel by channel basis and is described in detail by Izzetoglu et al. (2010). The procedure uses previous points measured to predict future points and their uncertainty. The newly measured point is then used to update and correct the prediction that again is used on upcoming points. A least squares method is then used to estimate the actual signal in the noisy signal (Izzetoglu et al., 2010).

Recently a new method of motion artefact reduction, the correlation based signal improvement (CBSI) method, has been proposed for NIRS experimental noise. The method suggests, as brain activation causes HbO_2 and Hbb to be negatively correlated close to -1, that an artefact will move this correlation away from -1 as changes in HbO_2 and Hbb will not be physiologically related. This finding can be used to both detect artefacts and to improve signal quality (Cui et al., 2010). A more detailed explanation is given in the method section. CBSI has been shown to be effective in improving signal quality of measurements contaminated by motion artefacts caused by head movements (Cui et al., 2010) and jaw movements due to speech (Brigadoi et al., 2014), but as yet has not been used to detect or reduce other movements and experimental noise. So second to testing the susceptibility of the NIRS measurements to a variety of movements that can occur when subjects are sitting in an upright position, this study explores whether artefacts can be detected by another, more objective method than visual inspection. Furthermore, if artefacts are found it is investigated whether these can be filtered based on the CBSI method.

2.2 Methods

2.2.1 Equipment

After giving informed consent, 5 male students (mean age: 25.6, SD: 3,5, range 21-30) participated in this study, that was approved by the University ethics

committee (070300) in accordance with the standards of the Declaration of Helsinki. For recording use was made of an OXYMON Mk III continuous wave device (Artinis B.V. Zetten, the Netherlands) (figure 2.1). The OXYMON Mk III uses two wavelengths of near infrared light that is shone through the transmitters and carried by the 315 cm long optical fibres towards the angular optode. The optodes were screwed in an optode holder. In order to ensure a good connection between the optodes and the skin, the optodes sticked out from the optode holder and the optode holder was tightly secured on the head with help of Velcro straps. The transmitters were equipped with semiconductor, pulsed laser diodes, which used nominal wavelengths of 855 and 780 nm. The detectors were avalanche photo diodes which had a special optic filter to filter out daylight. The signal from the detector was fed back to the OXYMON Mk III by optic fibres again. The signal was sampled at 25 Hz without use of any filters and then visualized with the Oxysoft software package (Artinis B.V. Zetten, the Netherlands) as relative changes in HbO_2 and Hbb concentration changes based on the modified Beer-Lambert law as described in chapter 1. A high sample frequency and no filters were chosen to allow the artefacts to be observed in their most original state.

Figure 2.1 The OXYMON Mk III and its angular optodes screwed into an optode holder. The optode holder is held in place with help of Velcro straps. The optodes slightly stick out of the holder in order to get good optical fibre-skin contact.

In order to minimize additional artefacts arising from optode placement upon hair, measurements in this chapter were performed on the left and right prefrontal cortex, locations Fp1 and Fp2 of the 10-20 system for electrode placement respectively (Jasper, 1958). On both locations one transmitter and one receiver were used for recording NIRS signals with an inter optode distance of 35 mm (figure 2.2).

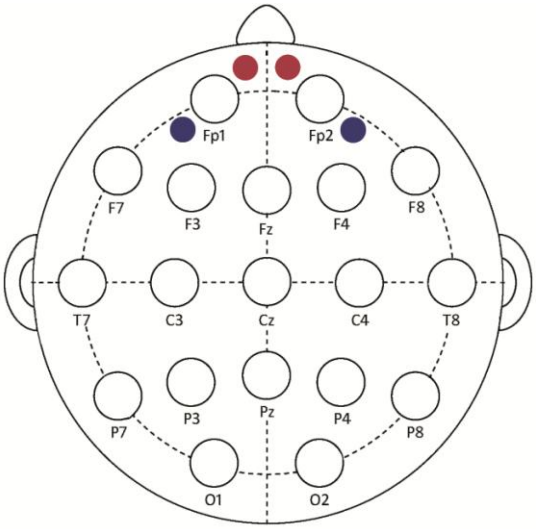

Figure 2.2. The 10-20 system for electrodes placement with in red and blue the placement of the optodes shown with respect to the left prefrontal (Fp1) and right prefrontal (Fp2) location. The transmitters are represented by the red colour, the receivers by the blue colour. In this set-up two channels are measured labelled Fp1 and Fp2.

2.2.2 Paradigm

The participants were seated in a comfortable chair facing a blank computer screen. The procedures were explained and the equipment was mounted on the head with help of optode holders and Velcro straps. The experimenter sat next to the participant to instruct him during the experiment. This included indicating when the tasks started and stopped. These time points were marked in the measurement. Furthermore, the experimenter closely observed the measurement trace as well as the participant during the data collection in order to note if the subject complied with the experimental paradigm. These notes were used to exclude tasks if they were performed incorrectly. In total sixteen tasks were performed which were divided into four categories: eye movements, muscle activation, talking & breathing, and movement (Table 2.1).

	Category	Task
1	Eye Movements	Blinking
2		Lateral eye movements (eyes open)
3		Lateral eye movements (eyes closed)
4		Vertical eye movements (eyes closed)
5	Muscle activation	Jaw clenching
6		Chewing
7		Continuous frowning
8		Intermittent frowning
9		Continuous shrug
10		Intermittent shrug
11	Talking & Breathing	Count to ten aloud
12		3x deep in- and exhale
13	Movement	Head flexion and extension
14		Lateral head movements
15		Back extension
16		Moving the cables attached to the optodes

Table 2.1. The tasks, task order, and the categories they belong to. In total 16 tasks were performed.

All tasks were chosen based on conditions that are known to induce artefacts in EEG signals (Krauss et al., 2006). The tasks are described in detail below. Each task was carried out for a block of ten seconds. Resting periods of at least ten seconds were situated between the tasks in which the subjects were required to sit still and focus on a blank computer screen to allow the NIRS signal to return to baseline. All task blocks were only performed once and every participant performed the tasks in identical order. Before the tasks started, an eyes open, resting state baseline period of 10 seconds was recorded.

2.2.2.1 Eye movements

The block of eye movement related tasks consisted of 4 tasks: blinking, lateral eye movements in an eyes open condition, lateral eye movements in an eyes closed condition, and vertical eye movements in an eyes closed condition. Participants

were instructed to execute all eye movements in a consistent and regular way at a pace that was comfortable to them. For blinking this was approximately at a rate of 2 Hz and all other eye movement tasks were carried out at a speed around 1 Hz.

2.2.2.2 Muscle activation

The following tasks made up the muscle activation category: jaw clenching, chewing, continuous frowning, intermittent frowning, continuous shrug, and intermittent shrug. For the jaw clenching task, continuous frowning, and continuous shrug, the participants had to perform the task at a strength that was consistent for 10 seconds and that avoided additional trembling or movement of the head. Chewing was performed without food or gum at a rate that was comfortable to the participant equating to approximately 1 Hz. The intermittent frowning and intermittent shrug tasks were carried out at a rate that was comfortable to the participant at the same strength at which the continuous frown and continuous shrug tasks were executed. These tasks were carried out at approximately 0.5 Hz.

2.2.2.3 Talking & breathing

In the talking and breathing block 2 tasks were performed. The first task was counting to ten aloud along with the second-hand of a watch that was displayed in front of the participant to make sure the talking task lasted for 10 seconds. During the breathing task the participants were instructed to in- and exhale 3 times slowly and deeply through the nose.

2.2.2.4 Movement

The category movement consisted of 4 tasks: head flexion and extension, lateral head movements, back extension, and moving the cables attached to the optodes. The latter task was carried out by the experimenter and the participants were instructed to sit very still. The experimenter held the 4 optic fibres in one hand approximately 50 cm away from the participant's head and moved them repeatedly 20 cm left and right from their original position. During head flexion and extension the participants were instructed to move their heads forward and backward approximately 50% of their maximum movement range at a rate that was comfortable to them but not too fast, equating to approximately 0.5 Hz. This instruction was also given in the lateral head movement task, but the participants

were required to move their heads repeatedly from left to right while they kept facing the computer screen. During the back extension task the participants had to sit up from the position they were currently sitting in.

2.2.3 Data processing

The flow of the data processing is depicted in figure 2.3. The Oxysoft software transformed the data into graphs displaying the concentration changes of HbO_2 and Hbb (Cope and Delpy, 1988; Delpy et al., 1988) and exported the unfiltered changes in HbO_2 and Hbb concentration as two separate time series per measurement.

All measurements were then split into files that just contained one task. The separate tasks were configured in 20 second files in which the first 5 seconds presented the baseline period before the task, second 5 until 15 contained the task and the last 5 seconds entailed the signal returning to baseline. These graphs were plotted for both the Fp1 and the Fp2 channel for every task.

These graphs were evaluated by means of visual inspection and by means of the running correlation. Next the data were filtered and evaluated using visual inspection and the contrast-to-noise ratio (CNR). After that the CBSI-filter was applied after which the last evaluation step was carried out. All filtering and evaluation steps are explained in detail below.

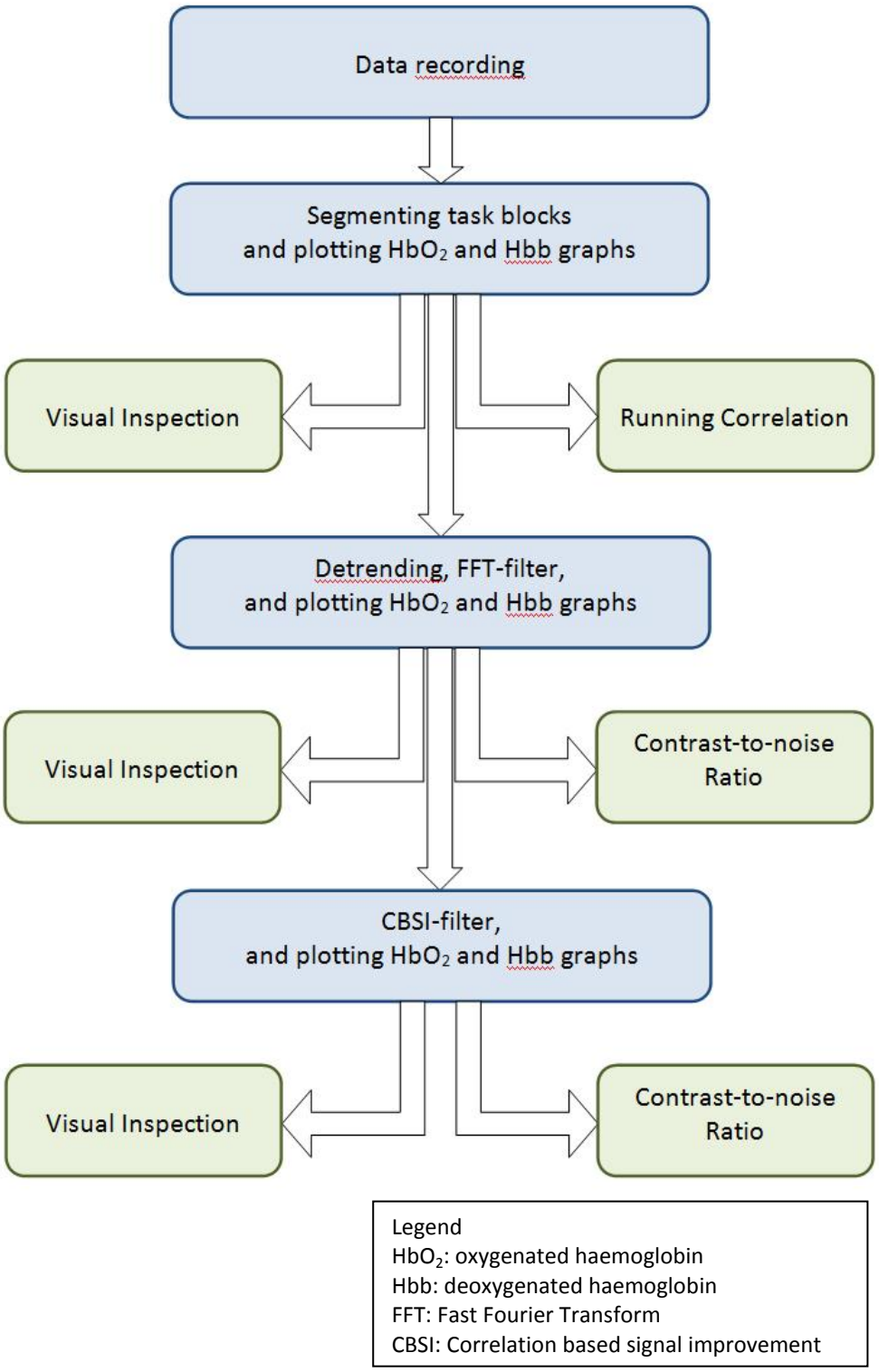

Figure 2.3. Data processing flow. The blocks displayed in blue are the steps in which the data is processed. The blocks displayed in green are the steps at which the data is evaluated.

2.2.4 Data filtering

The data were filtered in two steps. First the data were detrended and band pass filtered to remove slow drift and instrumental noise in the signal. The detrending was performed according to the following formula:

$$y(t) \coloneqq x(t) - \big(x(b) - x(a)\big) * (\frac{t}{(b-a)} - \frac{1}{2})$$

In which $y(t)$ is the detrended signal, $x(t)$ is the original signal of which the linear trend $\big(x(b) - x(a)\big) * (\frac{t}{(b-a)} - \frac{1}{2})$ is subtracted. The terms a and b specify the interval of the signal. The band pass filter was a Fourier filter (FFT-filter) with the borders set at 0.01 and 0.5 Hz. This means that from the entire signal a spectrum was obtained with an FFT. From this spectrum all frequencies below 0.01 and above 0.5 Hz were deleted and the signal was rebuilt by means of an inverse-FFT.. This filter was chosen because it produced the most stable results with no distortion of the used time series of HbO_2 and Hbb. For both the detrending as well as the FFT filtering use was made of LabVIEW analysis tools which delivered new time series after processing. The graphs of the filtered HbO_2 and Hbb traces were again plotted.

As a second step the FFT-filtered signals were then filtered according to the CBSI procedure as described by Cui et al. (2010) reprogrammed in LabVIEW and again plotted. This procedure assumes that the time series of HbO_2 (x) and Hbb (y) consist of the following parameters:

$$x = x_0 + \alpha F + Noise$$

$$y = y_0 + F + Noise$$

In these equations x_0 and y_0 are the artefact free HbO_2 and Hbb concentrations that are sought. F is the motion artefact, which has identical effects on both HbO_2 and Hbb when the weighing factor α is used for HbO_2. The $Noise$ term is the high frequency noise that is filtered by the FFT filter in the previous step. Two assumptions are posed by Cui et al. (2010). First, x_0 and y_0 are negatively correlated close to -1 and second, the true signal x_0 and the artefact term F are uncorrelated close to 0. Furthermore, the α term can be found by dividing the standard deviations of the measured x and y signals:

$$\alpha = \frac{std\ (x)}{std\ (y)}$$

By solving the following equations the artefact free HbO_2 and Hbb signal can then be recovered:

$$x_0 = \frac{1}{2}(x - \alpha y)$$

$$y_0 = -\frac{1}{\alpha} x_0$$

2.2.5 Data evaluation

At three different stages of data processing the plotted HbO_2 and Hbb graphs were evaluated. The first evaluation moment was after data collection in which the data were still unfiltered. All tasks were screened for artefacts by two methods in order to determine whether the movements chosen for the tasks resulted in artefacts in the data. The first method was visual inspection of the graphs.

During visual inspection the baseline period and task period (artefact) were compared to see if there were changes present in the task period that were not present during baseline that were larger than the changes caused by the pulsation of the heart. In doing so, the onset, duration and morphology of the artefacts could be established which then could be related to the task performed. Since the subjects were only performing the movement they were instructed to and the measurements were not taking place on the motor cortex, any change in the signal from baseline was unexpected and likely to be an artefact originating from the task performed. Measurements in which the task period was marked as being different from the baseline, but the pattern was similar to patterns seen during brain activation or deactivation were not marked as artefacts. A brain activation pattern was defined as an increase in HbO_2 together with a decrease in Hbb and a pattern of deactivation was defined as an decrease in HbO_2 combined with an increase in Hbb.

The second method was the running correlation (RC) method as described by Cui et al. (2010) which was also reprogrammed in LabVIEW. Cui et al. (2010) argue that HbO_2 and Hbb are negatively correlated during activation with a correlation value close to -1. When the data are contaminated by noise the correlation moves away from -1, becoming more positive. The RC calculates the correlation between

the HbO_2 and Hbb time series at each time point. The RC at time point *t* is defined as the correlation between segments of HbO_2 and Hbb in the time window between *t-w* and *t+w* where *w* is half the window size. Cui et al. (2010) have established *w=50,* except at the beginning and the end of the signal, where the half window size is adjusted so that the segment is symmetric around time point *t*. An example of the RC graph is given in figure 2.4.

The average RC was calculated for the baseline period and the task period for every task. Then the average RC during the baseline was subtracted from the average RC during the task. A positive outcome of this subtraction indicated an increase of the RC during the task and was therefore considered an indication of noise. Since the values of the RC can range from -1 to 1 and difference values were calculated from averages from the baseline period and the task period it was decided that an increase of 0.1 would be considered as an indication for artefacts.

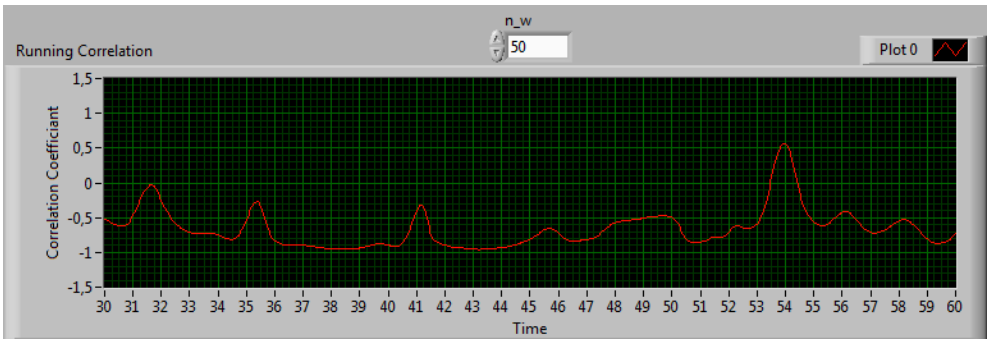

Figure 2.4. An example of the running correlation. In this example the RC is calculated between 30 seconds of the HbO_2 and Hbb time series. The y-axis represents the correlation coefficient at every given time point on the x-axis.

The second evaluation step was after FFT-filtering and the third after CBSI-filtering. Here the first method was visual inspection again which was used to determine whether the artefacts found in the unfiltered data were eliminated. To evaluate the effectiveness of the CBSI-filtering the RC could not be used because after CBSI-filtering the data have a perfect correlation of -1. Therefore, the contrast-to-noise ratio (CNR) was used in evaluation step 2 and 3 as objective method for evaluating signal improvement. The CNR can be used to quantify the signal-to-noise ratio (Zhang et al., 2005). It calculates the amplitude difference between the signal during the task and the signal during rest, divided by the

pooled standard deviation. Larger CNR indicates that the ratio of task related signal to noise is larger.

$$CNR = \frac{mean(dur) - mean(pre)}{\sqrt{var(dur) - var(pre)}}$$

In this equation dur means during the task and pre means in the rest period before the task. In this research 0-5 seconds before task onset was used as pre value and because of a possible delayed hemodynamic response, the interval 5-10 seconds after task onset was used as dur value. The difference in CNR before and after CBSI filtering was calculated in order to objectify the performance of the filter. Cui et al. (2010) reported a mean increase in CNR of 0.80 for HbO_2 signals and a mean increase of 0.89 for Hbb signals in their research that aimed at removing head movements. Therefore, increases in CNR reaching these values were considered as good signal improvement.

2.3 Results

Because one subject failed to perform the back extension task, and the other subjects showed much variability in the way the task was performed, and no subjects continued the task for 10 seconds, this task was not considered in the analyses. Furthermore, during the continuous frowning task the Fp2 channel of subject 4 had to be eliminated because the signal quality was so poor that no cardiac response could be detected. For the intermittent frowning task data from the Fp2 channel of subject 1 and both channels of subject 3 were not taken into account during the analyses because there seemed to be artefacts in the baseline period that made a correct interpretation of the artefacts during the task not possible. From the data of the lateral head movement task subject 5 was also eliminated because of artefacts in the baseline period. In the unfiltered data of the other tasks the cardiac pulsations were clearly visible in both the HbO_2 and Hbb graphs as regular, arcade shaped waves around 1 Hz. Furthermore, the visible artefacts were more pronounced in the HbO_2 trace compared to the Hbb trace. In table 2.2 the number of participants that remains for each task and channel is summarized.

	Task	N left prefrontal cortex (Fp1)	N right prefrontal cortex (Fp2)
1	Blinking	5	5
2	Lateral eye movements (eyes open)	5	5
3	Lateral eye movements (eyes closed)	5	5
4	Vertical eye movements (eyes closed)	5	5
5	Jaw clenching	5	5
6	Chewing	5	5
7	Continuous frowning	5	4
8	Intermittent frowning	4	3
9	Continuous shrug	5	5
10	Intermittent shrug	5	5
11	Count to ten aloud	5	5
12	3x deep in- and exhale	5	5
13	Head flexion and extension	5	5
14	Lateral head movements	4	4
15	Back extension	0	0
16	Moving the cables attached to the optodes	5	5

Table 2.2 Summary of the number of participants (N) for each channel in every task.

2.3.1 Task related findings –unfiltered data-

2.3.1.1 Eye Movements

Eye movements produced limited artefacts. During blinking 3 out of 5 subjects showed no artefacts in their signal. A profile that would have been seen during activation (an increase in HbO_2 and a decrease in Hbb) was apparent in 1 participant. The last participant did show an artefact during blinking that was characterized as a decrease in both HbO_2 and Hbb. The task in which lateral eye movements were made with open eyes caused artefacts in 2 out of 5 subjects and were characterized by peaks in the signal either at task onset or halfway during the task. The signals of the 3 other subjects were not influenced by the task. The lateral eye movements performed with closed eyes caused only an artefact in 1

participant in one channel and was characterized by a sudden drop in HbO_2 as well as Hbb. The signals of 3 other participants were not influenced by the task and the last subject showed a pattern of activation during the task. The other task with closed eyes, in which eye movements were made vertically, showed clear peaks in 1 participant in both HbO_2 and Hbb (figure 2.5a) and another participant only showed peaks (less obvious) in Hbb. The signals of 1 subject were not affected by this task and the 2 others showed a pattern that looked like activation.

2.3.1.2 Muscle Activation

In 2 subjects the jaw clenching task resulted in a pattern of deactivation in the form of an increase in the Hbb signal and a decrease in the HbO_2 signal, with a delayed onset in respect to the onset of the task (figure 2.5b). The other 3 subjects did not show differences between the baseline and the task. During chewing 1 participant showed an activation pattern, 2 subjects were not affected by the task and the other 2 showed artefacts. In 1 subject this artefact was characterized by a peak at the end of the task and in the other subject the artefact manifested itself as a decrease in both HbO_2 as Hbb. During the continuous frowning task as well as the intermittent frowning task the start and stop of a frown was accompanied by a sudden shift in both signals in all subjects (figure 2.5c). The magnitude of this response differed between subjects. The continuous shrug task resulted in a pattern that looked like activation in 2 participants, in a pattern that looked like deactivation in 2 other subjects (figure 2.5d) and the last participant showed a peak in both HbO_2 and Hbb at the onset of the task. The intermittent shrug task showed peak-like artefacts in 3 participants, showed an activation pattern in 1 subject and did not affect the last subject.

2.3.1.3 Talking & Breathing

The counting did not result in any artefacts in 2 out of 5 subjects. In 1 subject a pattern was seen that looked like deactivation. In 1 participant both HbO_2 and Hbb decreased in both channels during the task and in the last participant a pattern of activation was seen that ended with a large peak at the end of the task. The breathing resulted in artefacts in all participants but the artefacts were quite variable. In 3 subjects peaks were observed in one or two channels, and in one of these participants the peaks in Hbb were opposite in direction to the peaks seen in HbO_2 (figure 2.5e). In 1 subject the onset of the task was marked with an

increase in both HbO_2 and Hbb followed by a decrease in both during the task. In another subject the onset was marked with a decrease in both traces at the onset of the task followed by an increase, immediately followed by a decrease.

2.3.1.4 Movement

The head flexion and extension task resulted in peak-like artefacts in all subjects. The peaks were different in amplitude and number between subjects and in 4 subjects these peaks occurred in opposite direction for HbO_2 and Hbb on one location. The other peaks were similar in direction for HbO_2 and Hbb. During the lateral head movement task the same peak-like artefacts were observed as during the head flexion and extension task in 4 subjects. During this task the peaks were opposite in direction between HbO_2 and Hbb for one channel in 2 subjects. A typical example of the peaks observed during head movements is presented in figure 2.5f. Movement of the optode cables resulted in peaks as well as shifts in the signals, similar to the head movement artefacts and frowning artefacts respectively. A summary of the amount of artefacts that was found based on visual inspection is given in table 2.3.

A

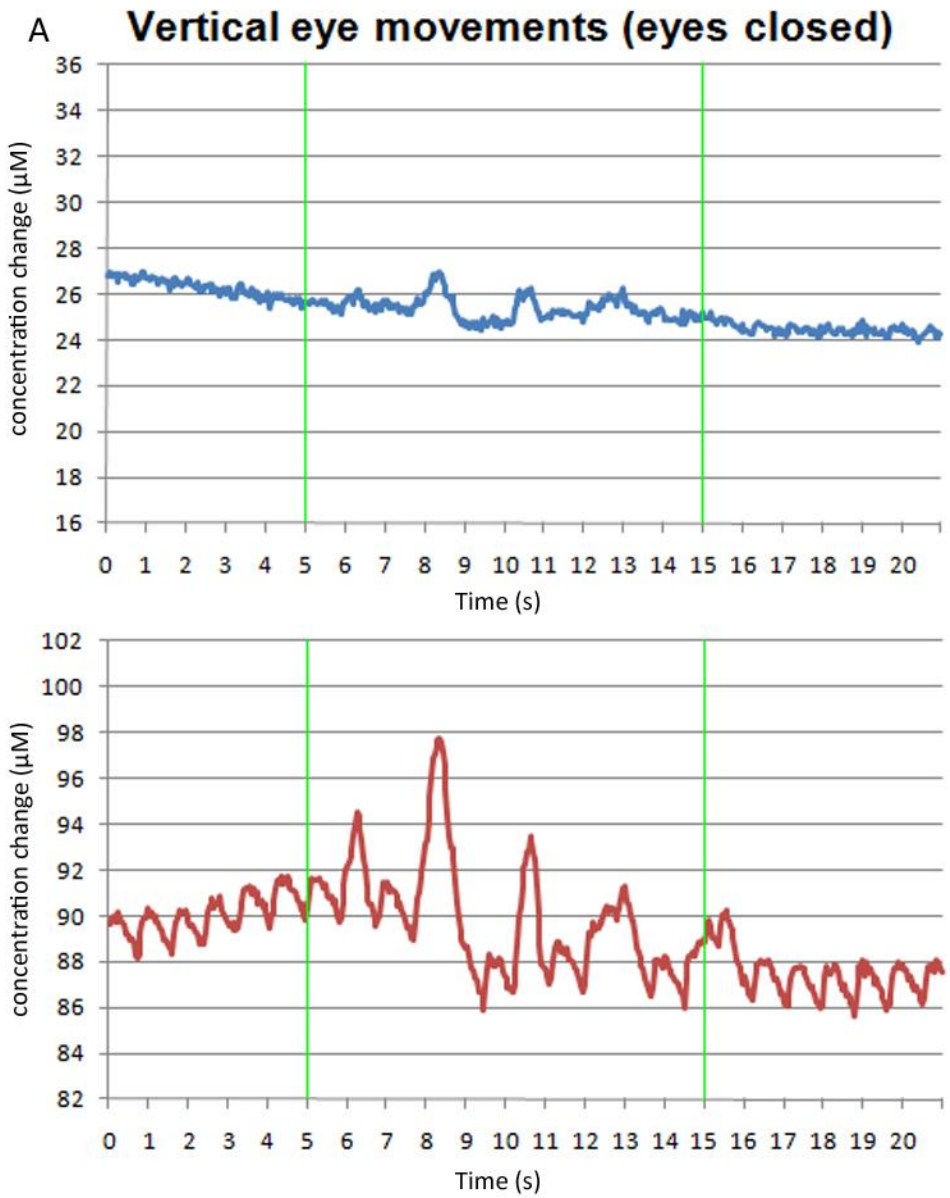
Vertical eye movements (eyes closed)
concentration change (µM)
36
34
32
30
28
26
24
22
20
18
16
0 1 2 3 4 5 6 7 8 9 10 11 12 13 14 15 16 17 18 19 20
Time (s)
concentration change (µM)
102
100
98
96
94
92
90
88
86
84
82
0 1 2 3 4 5 6 7 8 9 10 11 12 13 14 15 16 17 18 19 20
Time (s)

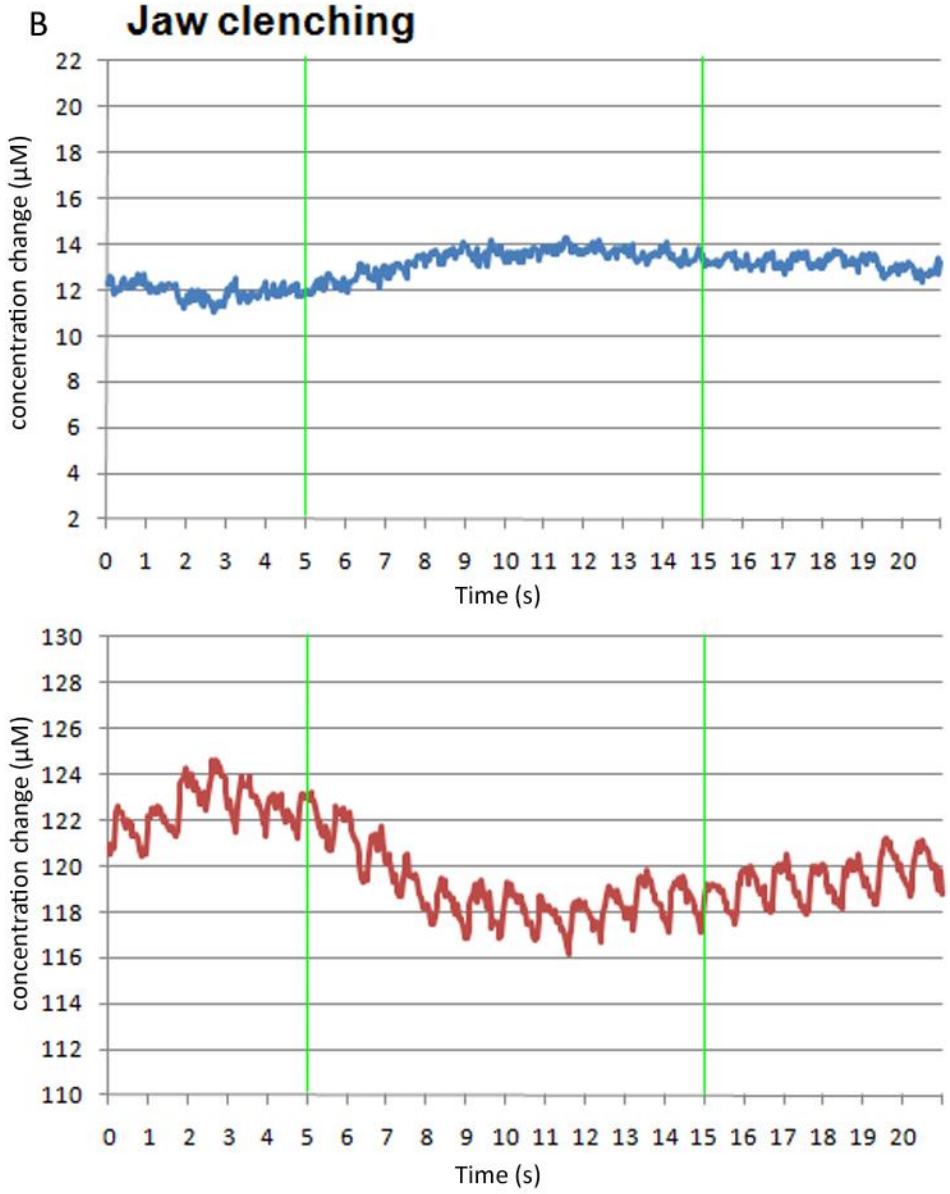
B
Jaw clenching
concentration change (µM)
22
20
18
16
14
12
10
8
6
4
2
0 1 2 3 4 5 6 7 8 9 10 11 12 13 14 15 16 17 18 19 20
Time (s)
concentration change (µM)
130
128
126
124
122
120
118
116
114
112
110
0 1 2 3 4 5 6 7 8 9 10 11 12 13 14 15 16 17 18 19 20
Time (s)

C

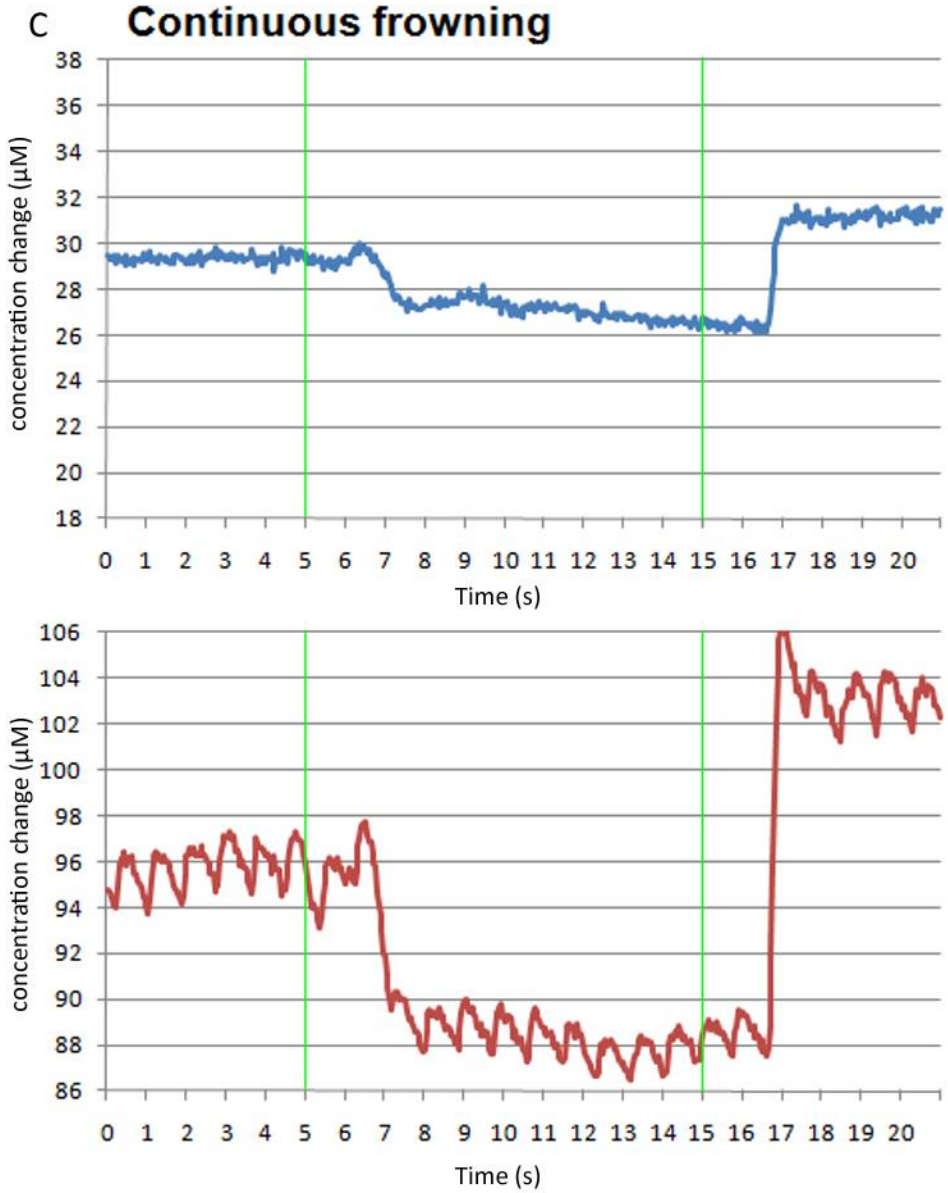
Continuous frowning
concentration change (µM)
38
36
34
32
30
28
26
24
22
20
18
0 1 2 3 4 5 6 7 8 9 10 11 12 13 14 15 16 17 18 19 20
Time (s)
concentration change (µM)
106
104
102
100
98
96
94
92
90
88
86
0 1 2 3 4 5 6 7 8 9 10 11 12 13 14 15 16 17 18 19 20
Time (s)

D

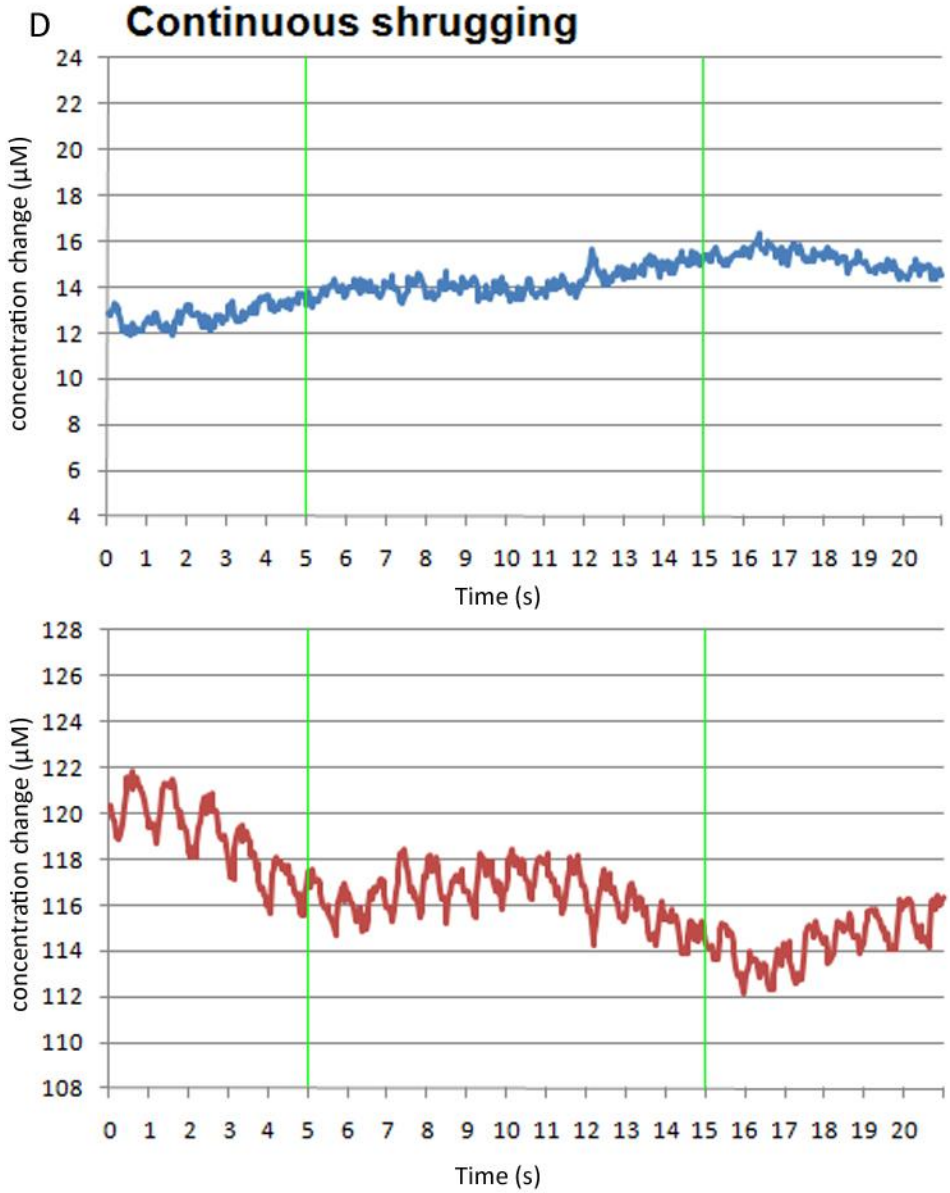
Continuous shrugging
concentration change (µM)
24
22
20
18
16
14
12
10
8
6
4
0 1 2 3 4 5 6 7 8 9 10 11 12 13 14 15 16 17 18 19 20
Time (s)
concentration change (µM)
128
126
124
122
120
118
116
114
112
110
108
0 1 2 3 4 5 6 7 8 9 10 11 12 13 14 15 16 17 18 19 20
Time (s)

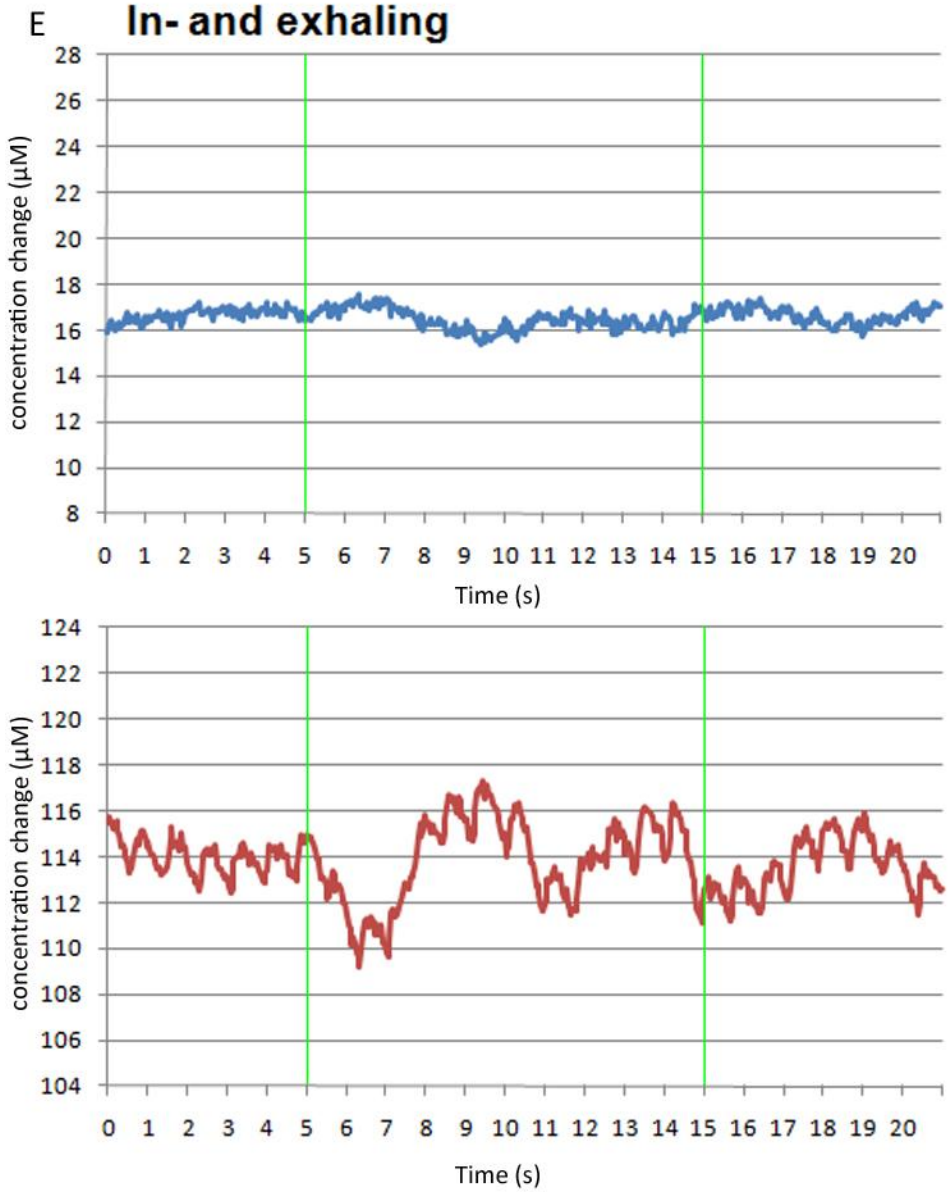
E
In- and exhaling
concentration change (µM)
28
26
24
22
20
18
16
14
12
10
8
0 1 2 3 4 5 6 7 8 9 10 11 12 13 14 15 16 17 18 19 20
Time (s)
concentration change (µM)
124
122
120
118
116
114
112
110
108
106
104
0 1 2 3 4 5 6 7 8 9 10 11 12 13 14 15 16 17 18 19 20
Time (s)

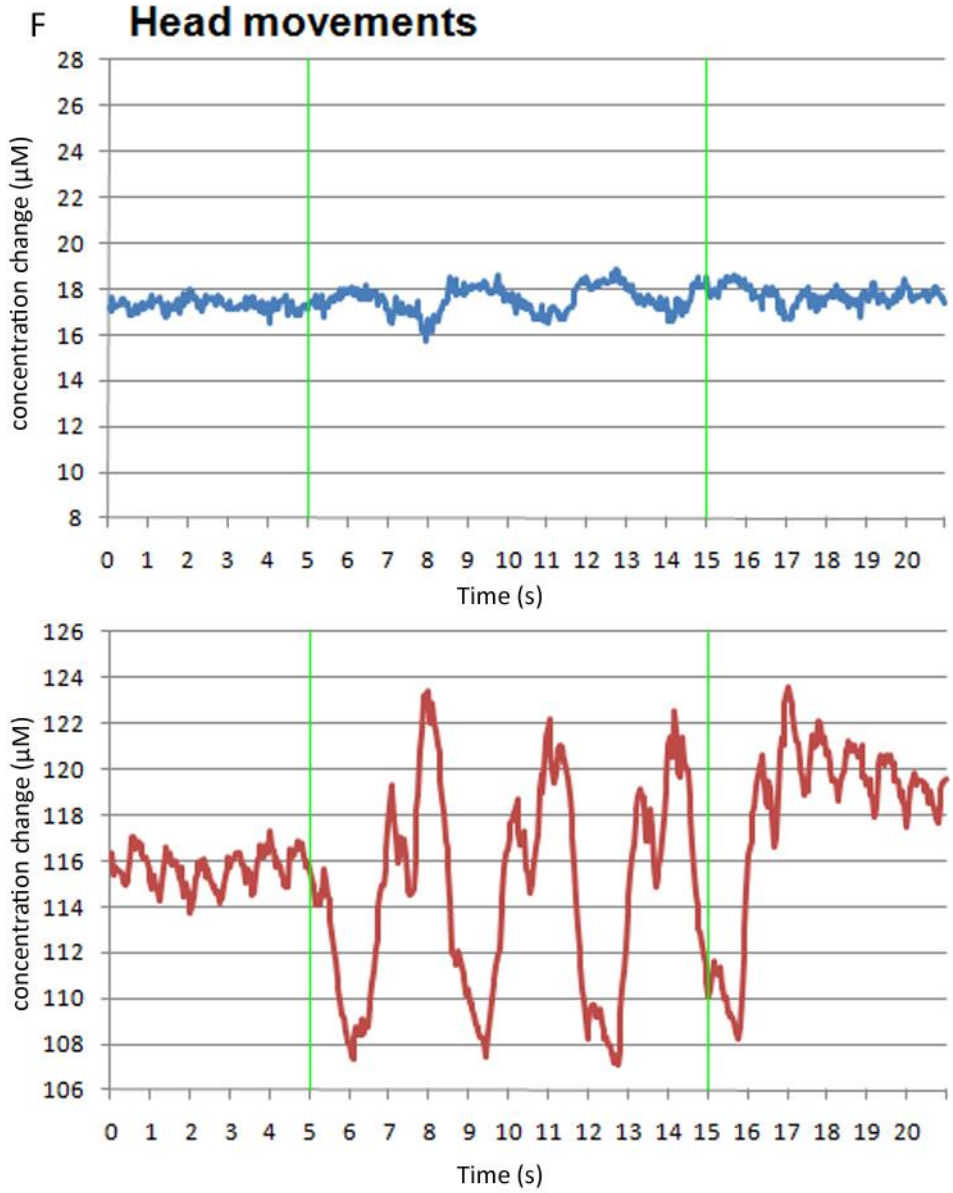

Figure 2.5a-f The most characteristic artefacts are displayed in this figure for one measurement location at a time. Panel a shows artefacts arising during vertical eye movements with closed eyes. Panel b shows artefacts that occur during jaw clenching. Panel c shows artefacts the occur during the continuous frown condition. Panel d shows the artefact occurring during the continuous shrug. Panel e shows artefacts that arise during deep in and exhaling. And panel f shows artefacts that occur during head movements. In each of the six panels a-f the deoxygenated haemoglobin (HHb) and oxygenated haemoglobin (HbO_2) signals are depicted in blue and red respectively. One unit on the x-axis represents 1 second. One unit one the y-axis represents 2 µM. The first green vertical line indicates the start of the task, the second one the end. Note the continuous pulsation artefact in each signal.

2.3.2 Running Correlation

For the eye movement category, the RC of the unfiltered data indicated that artefacts were present in 30% of the measurements. For muscle activation the RC showed that in the unfiltered data 38% of the measurements had artefacts and 62% did not. The talking and breathing tasks resulted into artefacts for 25% of the unfiltered measurements and in the movement category this percentage was 61%.

2.3.3 Visual inspection vs. Running correlation

When the percentages of measurements marked as having artefacts by visual inspection are compared with the percentage marked by the RC there is only agreement for the muscle activation category. In the eye category movement the estimated percentage of artefacts is overestimated by the RC and underestimated for the categories talking and breathing, and movement (table 2.3).

Next it was determined if visual inspection and the RC method marked the same signals as having artefacts. If patterns of activation and deactivation are not considered as artefacts there was an agreement between the visual inspection and the RC of 73% in the eye movement. In 10% of the measurements the visual inspection indicated there was an artefact present but the RC did not detect it, and in 17% of the measurements the RC detected an artefact that was not marked in visual inspection. For the muscle activation category there was an agreement between the visual inspection and the RC in 76% of cases. In 14% of the measurements the visual inspection detected an artefact where the RC did not and in 9% the detected artefact by the RC was not seen in visual inspection. The methods agree to a similar extent in the talking and breathing category, with an agreement of 75%. In the other 25% of the measurements the visual inspection method detected an artefact that was not marked as an artefact by the RC. In the last category, movement, the agreement between the two methods is lowest with an agreement of 64%. The measurements that disagree (35%) are accounted for by a detection by the visual inspection method that was not marked by the RC.

	Visual inspection	RC	Agreement between visual inspection and RC
Eye movement HbO_2	20%	30%	73%
Eye movement Hbb	20%		
Muscle activation HbO_2	40%	38.2%	76%
Muscle activation Hbb	36.4%		
Talking & breathing HbO_2	50%	25%	75%
Talking & breathing Hbb	45%		
Movement HbO_2	92.9%	60.7%	64%
Movement Hbb	89.3%		

Table 2.3 Summary of the amount of artefacts found. The amount of artefacts are expressed as percentages for the two methods visual inspection and running correlation (RC), as well as their agreement. For all tasks the amount of artefacts is given separately for the oxygenated haemoglobin (HbO_2) and deoxygenated haemoglobin (Hbb) seperately for the visual inspection method. Since the RC uses both signals to determine if there is an artefact, here only one percentage is given.

2.3.4 Signal improvement after filtering

Two filtering steps were conducted in order to improve signal quality. First the signals were detrended and band pass filtered to eliminate drift and high frequency instrument noise. The second filtering step was CBSI-filtering. It was determined visually if the artefacts that were present in the unfiltered data were eliminated by the filtering. Hereto the same visual inspection procedure was adopted as described above. The previously found amount of artefacts was set at 100% and compared to the amount of artefacts found after filtering. The effectiveness of the filtering procedure was also evaluated by the CNR. The CNR before CBSI-filtering was subtracted from the CNR after CBSI-filtering. Since an increase in CNR means the signal is less noise, a positive number is expected when the filtering is successful in increasing signal quality. An overview of these findings is presented in table 2.4.

Visual inspection indicated that only in the eye movement category filtering was beneficial for some signals. In the muscle activation and movement category even more signals seemed contaminated by artefacts after filtering. This was caused by measurements that only showed an artefact in either the HbO_2 or Hbb trace. After

CBSI filtering the artefact from the affected signal was mirrored in the other signal. In figure 2.6 an example is given, of a head motion artefact that is not filtered successfully.

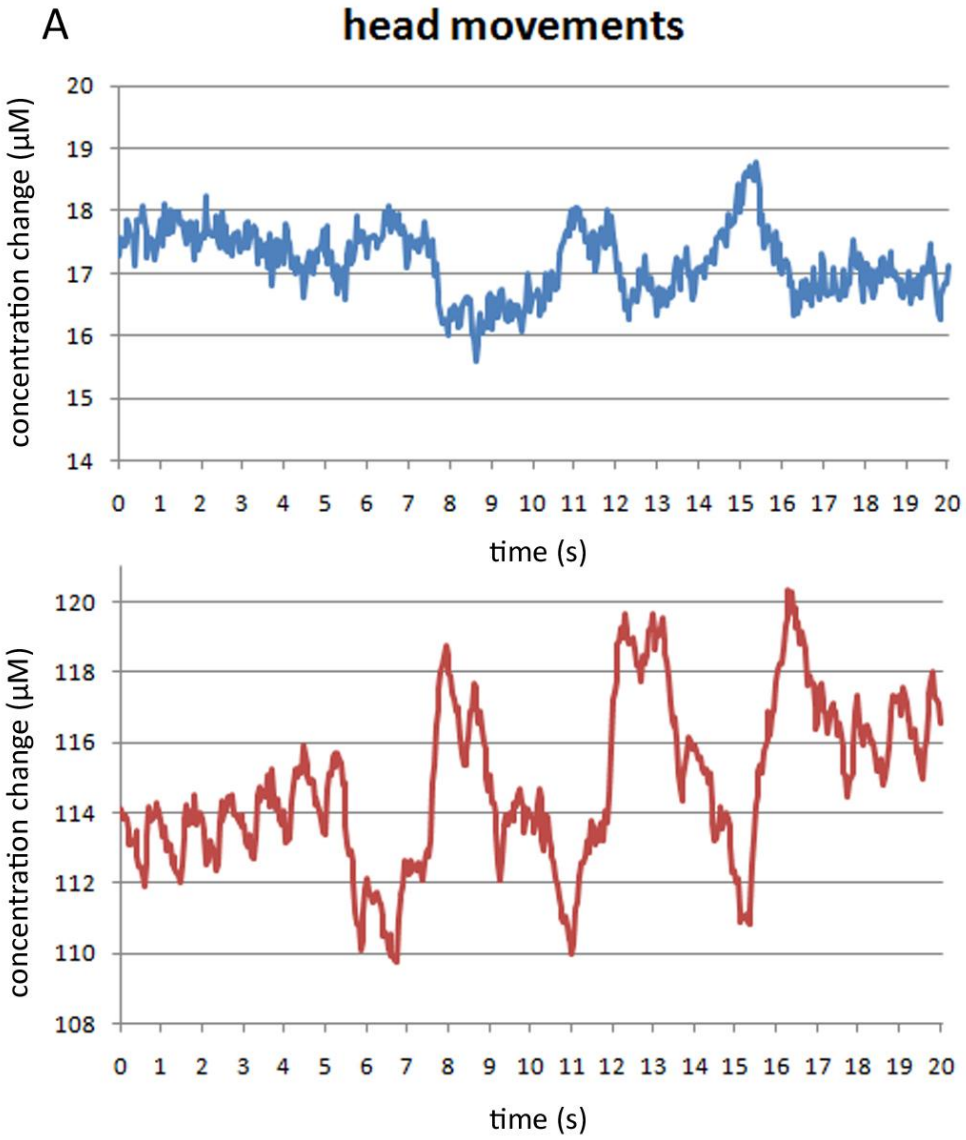

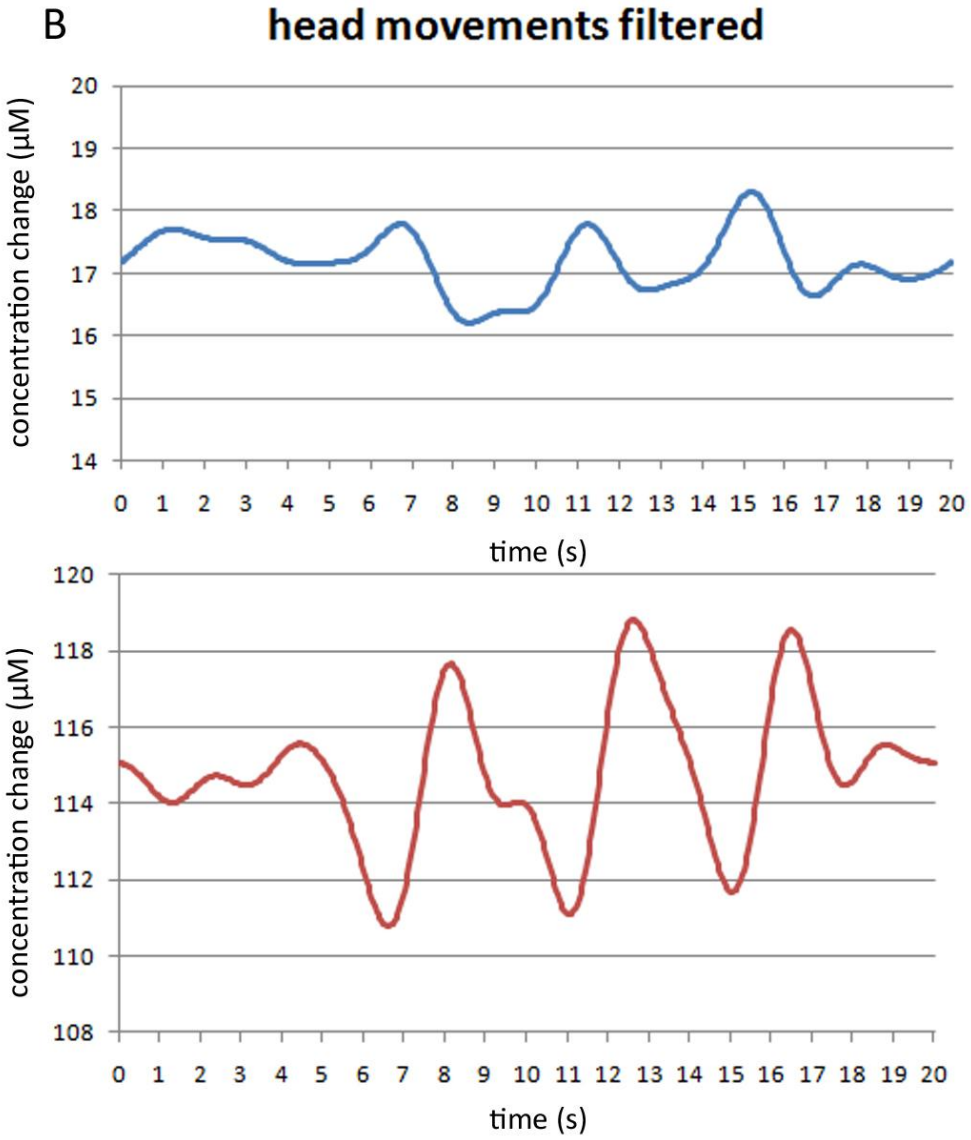
B
head movements filtered
concentration change (µM)
20
19
18
17
16
15
14
0 1 2 3 4 5 6 7 8 9 10 11 12 13 14 15 16 17 18 19 20
time (s)
concentration change (µM)
120
118
116
114
112
110
108
0 1 2 3 4 5 6 7 8 9 10 11 12 13 14 15 16 17 18 19 20
time (s)

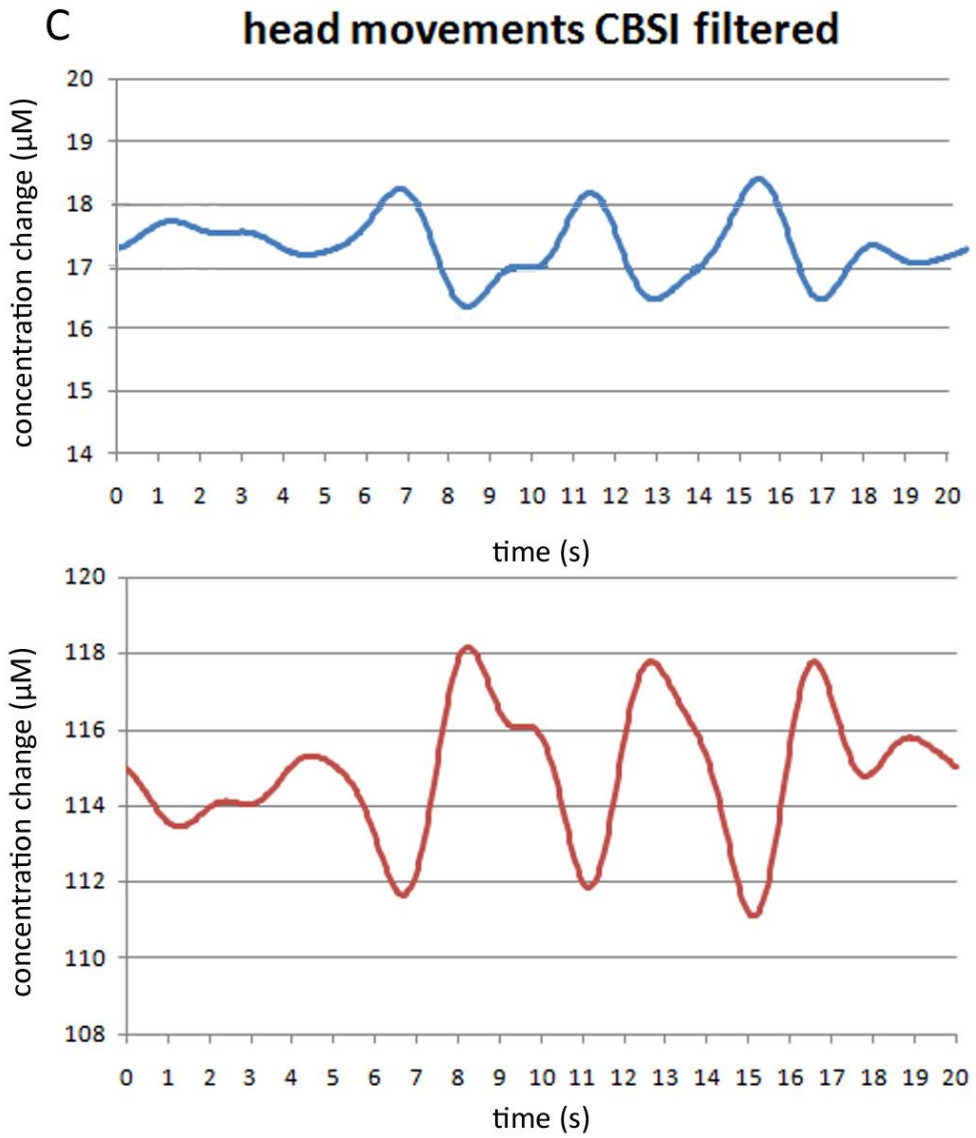

Figure 2.6. An example of ineffective filtering of a motion artefact caused by head movement. The Hbb graphs are displayed in blue and the HbO_2 graphs in red. Pane al shows the unfiltered graphs. Panel b the detrended, band pass filtered (between 0.01 and 0.5 Hz) graphs. Note that the artefact falls within the pass band. Panel c shows the correlation based signal improvement (CBSI) filtered graphs. Also after this step the peaks that appear during the task are not eliminated.

Also the CNR changes show a decrease in signal quality after filtering for 3 out of 4 conditions instead of an increase. Only in the muscle activation category was an improvement of the signal seen. If only CNR changes in signals that were affected by artefacts (since some were not) were taken into account, the signal improvement of the muscle activation category became less obvious and for all other categories the findings did not change.

Category	Artefacts after filtering (% based on visual inspection)	CNR change all signals	CNR change artefact signals
Eye movements	88.2%	-0.22 (-5.79 .. 7.14)	-0.60 (-5.79 .. 2.69)
Muscle activation	114.3%	0.45 (-7.54 .. 6.71)	0.05 (-7.54 .. 6.71)
Talking & breathing	100%	-0.42 (-8.8 .. 5.5)	-0.15 (-8.8 .. 5.5)
Movement	105.8%	-0.45 (-5.24 .. 7.34)	-0.42 (-5.24 .. 7.34)

Table 2.4: Summary of signal improvement after filtering. Signal improvement was evaluated with visual inspection and by the contrast-to-noise ratio (CNR). The percentage that is given for visual inspection is the percentage that remained after filtering compared to the amount of artefacts that was found before filtering. A percentage lower than 100% indicates an improvement, a percentage above 100% indicates a worsening. The average CNR is displayed. A positive value indicates an improvement in signal quality a negative value a decrease in quality. For the CNR the minimum and maximum value found in the sample is displayed between brackets.

2.7 Discussion

The research conducted in this chapter sought to answer two questions. Do eye movement, muscle activation, talking, breathing and head motion, that can easily occur during a measurement, cause detectable artefacts in NIRS signals? And if so, is the CBSI method effective in eliminating these artefacts? Here it was established that the investigated movements can cause artefacts in NIRS measurements. Furthermore, it appeared that using the CBSI-filter does not lead to signal improvement in the majority of the investigated artefacts in this research.

The unfiltered data were judged on morphology by visual inspection and the increase in RC was used as a more objective indication of the presence of a possible artefact. This showed that in all task categories artefacts can be an issue. Based on morphology, different types of artefacts can be distinguished, starting

with a fast response and a sudden shift. Artefacts belonging to the fast response class showed peaks in the NIRS signal that can be directly linked to the occurrence of movements made by the subject. Fast response artefacts were mainly present during the head movement tasks and the task in which the optode cables were moved. In one subject this artefact was also seen during vertical eye movements. The origin of this type of artefact is thought to be found in a change in optical coupling of the optode onto the scalp (Izzetoglu et al., 2005, Cooper et al., 2012, Brigadoi et al., 2014). If the optode is placed tightly onto the head, movement of the cables could lead to slight tilting of the optode, which causes the transmitter to illuminate a brain area adjacent to the original region of interest for a brief period of time (without the receivers collecting ambient light). Movements of the head also can lead blood to be moving away or towards the area under investigation, which causes the concentrations of Hbb and HbO_2 to change (Izzetoglu et al., 2005). A sudden shift in either the Hbb or HbO_2 signal was mainly observed in all subjects in the two frowning tasks as well as in some subjects during the task in which the optode cables were moved. This type of artefact can also originate from a change in optical coupling of the optode onto the scalp (Izzetoglu et al., 2005, Cooper et al., 2012, Brigadoi et al., 2014). Possibly the optode itself shifts either caused by the underlying muscle or the movement of the cable.

A potential third class can be distinguished based on morphology which is the slow response. Several tasks in the eye movement category, the muscle activation category and the talking and breathing category showed a pattern that looks like that seen during brain activation or during deactivation (an increase in HbO_2 accompanied by a decrease in Hbb and vice versa respectively). Often this response is delayed with respect to the onset of the task. Brigadoi et al., (2014) describe a similar kind of artefact which in their research was related to jaw movements due to speech, necessary for the task under investigation. Different from the study of Brigadoi et al. (2014), the current study lacked a tasks in which brain activation or brain deactivation is expected. Therefore this class of response needs some further attention. A possible explanation are changes in blood oxygenation of superficial muscles. This makes this type of “artefact” the most dangerous in terms of misinterpretation of data because the morphology is difficult to distinguish from an actual physiological brain response. However, since

brain activation or deactivation during the tasks cannot be excluded, these responses were not considered artefacts in this chapter. The frontal cortex could have been activated by the processing of the instructions that were given to the participant at the start of the task. Similarly, a pattern of brain deactivation could be caused by the absence of processing by the frontal cortex while participants were executing fairly boring tasks.

The final class would be the artefacts that occur due to cardio respiratory activity which have been described in the literature before (Boas et al., 2004). In this study the in- and exhaling task showed artefacts that fall within this category. Therefore, interpretation of NIRS signals during tasks in the breathing pattern of subjects is altered should be interpreted with caution.

Although the focus of this chapter is on motion artefacts, awareness needs to be raised with regards to artefacts that arise from physiology based systemic artefacts. Due to the sensitivity of NIRS to changes in the superficial layers of the head like the skin and skull, these systemic changes caused by cardiac activity, respiration, changes in blood pressure, skin conductance, body temperature or any other autonomic regulated process, contaminate NIRS results and can be mistaken for cerebral responses (Gagnon et al., 2012, Kirilina et al., 2012). Especially since autonomic changes easily occur during many research paradigms in which cognitive or emotional processing is warranted which couples the systemic artefacts to the functional evoked response (Kirilina et al., 2012). However, it is not only during tasks that this type of artefact plays a role. During resting state analysis the same autonomic changes in superficial layers can distort the signal of interest (Tong et al., 2013) This type of artefact might therefore interchangeable with the slow response class of artefacts described above which mimics brain activity but originates elsewhere.

In a multimodal NIRS and fMRI study Kirilina et al. (2012) showed that the systemic artefacts found in the NIRS signals co-localized with veins draining the scalp. They were able to filter these artefacts by using the fMRI signal as a regressor, but that is not feasible for many NIRS studies. The approach that is suggested most often is to use an optode pair with a short distance to measure the systemic artefacts in the superficial head layers and use that in order to clean

the signal from the normal distanced optode pair (Zhang et al., 2007a, Zhang et al., 2007b, Zhang et al., 2009). However, it has been reported that the systemic artefacts occur inhomogeneous across the surface of the scalp (Gagnon et al., 2012, Kirilina et al., 2012). Gagnon et al. (2012) even showed that the short separation channel must be no further away from the channel of interest as 1.5 cm in order to be able to generate improvements of practical use. Once the distance reaches 2 cm only mild or negligible improvements were found. This means that for every measurement channel a separate short distance channel is needed, which is not feasible in all research paradigms due to the limited availability of NIRS channels and the rigidity of optode configurations in some systems.

In this chapter it was evaluated whether the RC was capable of reliably detecting the presence of motion artefacts. It was shown that in approximately 75% of the measurements visual inspection and RC, methods agree whether or not an artefact is present. When only the RC is used, an overestimation on eye movement artefacts and an underestimation in talking and breathing and movement artefacts can occur. Some artefacts cause the HbO_2 and Hbb signals to move in opposite directions, pushing the correlation between them to be more negative and as such, the RC will not mark the measurement as having artefacts. Therefore an element of visual inspection of the data can never be omitted and this emphasizes the importance of guidelines for recognizing different artefacts.

Artefacts that arise from a change in optical coupling could possibly be prevented by improving this coupling. Recently, two modifications to the optodes have been proposed that aim at improving the optical coupling. The first proposal consisted of a brush-fibre optode that could be mounted on commercially available optodes (Khan et al., 2012). The brush-fibre optodes pierce through dense hair more easily, ensuring a better coupling. Furthermore, the authors established in their own research that the set-up time decreased by a factor three and the signal-to-noise ratio improved up to ten times (Khan et al., 2012). The reduction in motion artefacts was unfortunately not investigated. Yucel et al., (2014) did research the reduction in motion artefacts since they are interested in using their solution in epilepsy patients during seizures. They propose the use of a prism based fibre, which is smaller than a regular optode. The small optode can then be fixated on

the head by means of a piece of gauze soaked in collodion (a clinical adhesive used in the field of EEG). In their tests a reduction of motion artefacts of 90% was found compared to regular measurement set-ups (Yucel et al., 2014). Alongside this reduction in artefacts an increase in signal-to-noise ratio of 3 to 6 times was reported.

The second question, whether the CBSI method was effective in eliminating the observed artefacts was investigated by two methods as well. First, visual inspection was used again to decide if the artefacts had diminished, and as a more objective measure for signal quality the CNR was calculated. From visual inspection the proposed filtering method hardly seemed useful in eliminating artefacts. Artefacts that influenced the HbO_2 and Hbb signal in opposite directions were not detected by the RC and not influenced by the CBSI at all. Furthermore, artefacts that only occurred in the HbO_2 or Hbb signal were transferred to the other modality by the CBSI. Peak-like artefacts did sometimes decrease in magnitude but the most concerning aspect was that the CBSI changed the signal in terms of direction of response and timing for nearly all artefacts that were analyzed. Also, the CNR only showed a moderate improvement in signal quality for the muscle activation category. Cui et al. (2010) reported signal improvement after CBSI filtering in all measurements and improvement was largest in signals which had more artefacts. The only category that showed an increase in CNR (the muscle activation category) showed an average improvement of 0.30 which far from the average improvement of 0.85 reported by Cui et al. (2010).

A reason for the different findings in this study and the study performed by Cui et al. (2010) could be the differences in research paradigm. Cui et al. (2010) used a paradigm in which the artefacts were induced while performing a task (finger tapping) that is known to induce a brain response. The current research was conducted without an additional paradigm known to cause a response and therefore the artefacts are induced upon baseline activity. The RC and CBSI have been modelled by use of the Balloon model, which has been reported as having a good correspondence with experimental measures of HbO_2 and Hbb (Buxton et al., 1998). Furthermore, it was reported by Cui et al. (2010) that the close to -1 correlation between HbO_2 and Hbb was strongest during activation and becomes less negative during the plateau period. Since no activation paradigm was used in

this study it is likely that the RC and CBSI methods are not the optimal choice for noise reduction when trying to eliminate artefacts from baseline or resting state data.

Furthermore, the method was originally designed to filter head movements (Cui et al., 2010). As reported in this chapter and also by Brigadoi et al (2014) different types of motion artefacts exist. Their shapes, frequency content, timing and amplitude can vary greatly. Furthermore, some motion artefacts can be much harder to recognize due to a coupling with the actual hemodynamic response under investigation (Brigadoi et al., 2014). Therefore caution is warranted in the selection of methods for artefact detection and removal. Different types of artefacts might be better treated with different methods of analysis.

Brigadoi et al. (2014) investigated the CBSI method alongside other approaches in a linguistic paradigm that resulted in an artefact caused by the jaw induced by the vocal response. This caused the artefact to be coupled to the hemodynamic response under investigation. In this paradigm, where the linguistic task also caused a response, the method was capable of improving the measured signals. However, they do raise the very important issue that the CBSI method makes assumptions that are not always met. The most important assumption is that HbO_2 and Hbb are always positively correlated during an artefact, which is also contradicted by multiple examples in this chapter (e.g. see figure 2.5 and 2.6). Furthermore, it is assumed that the ratio between HbO_2 and Hbb has a constant value during both time periods with and without artefacts present. When this seems to change, it will have a tremendous effect on the results of the CBSI method, compromising interpretation. As a second drawback they emphasize the recovery of the Hbb signal from the HbO_2 signal (Brigadoi et al., 2014). In doing so, the Hbb response is not linked anymore to the acquired data and especially when studying pathologies this rigid relationship between HbO_2 and Hbb is not always maintained, leading to false interpretation again (Brigadoi et al., 2014). Brigadoi et al. (2014) report wavelet analysis to have better capability in distinguishing the actual NIRS response from noise in their paradigm. However, this again requires an actual response to be present which was not the case in this chapter.

2.8 Conclusion

This chapter demonstrates and reconfirms that motion artefacts can easily be induced in NIRS measurements. Different types of motion artefacts exist, some easier recognized than others. The RC over or underestimates motion artefacts depending on the type of artefact and should therefore never be the sole method for artefact detection. Visual inspection and knowledge about the different artefacts is essential in valid NIRS analysis, especially because some artefacts fall within the frequencies of interest. Furthermore, CBSI filtering was ineffective for filtering motion artefacts from resting state data and generated heightened conditions of false interpretation. In EEG the research in automated artefact removal has been researched for longer and is therefore better justified (Daly et al., 2013, Iriarte et al., 2003). This is not the case for NIRS. Methods that have proven ready to use in EEG are not as effective in NIRS, possibly due to multitude of factors that contribute to the artefact and the overlap with systemic physiology (Brigadoi et al., 2014, Sweeney et al., 2012).

This should be kept in mind in designing studies and clinical measurement protocols. Especially in real life studies and exercise studies, the motion artefacts as well as the artefacts caused by systemic changes will have greater influence and should be interpreted with extreme caution. Therefore, it is of great importance that researchers or clinicians working with NIRS are trained in the recognition of artefacts. Correct recognition of the artefacts is the first step in prevention and ultimately elimination of artefacts, which will lead to reliable interpretation of NIRS measurements. Before measurements are interpreted, prevention can be found in methods that enhance optode scalp coupling. Furthermore, considering the difficulty of detecting motion artefacts, it could be helpful to videotape the participant during the measurements or to monitor motion in some way. This allows for an opportunity to re-evaluate the participants' behaviour when a possible artefact is seen during offline analysis.

The occurrence of motion artefacts in NIRS as well as the occurrence of systemic physiological artefacts and the difficulties in recognizing them and filtering them may delay the introduction of NIRS as an easy to use, valid, and reliable measure

of optical brain activity in the general clinic. Hereto, more research should be devoted to overcome these issues and to generate easy to apply solutions.

Chapter 3: Exploring brain activity with simultaneous EEG and NIRS measurements in eyes open and eyes closed blocks using static analysis techniques

Resting brain activity has been found to be an important stepping stone for brain functioning in general. From a clinical perspective brain activity at rest provides great perspective for diagnostic purposes. The aim of this chapter was to investigate the feasibility of conducting measurements of both the electrical activity of the brain as well as its metabolic activity. This was done in a paradigm in which the visual cortex of healthy subjects was investigated both with eyes open and eyes closed. The electrical as well as the hemodynamic measures are explored separately as well as combined. In order to examine the interaction between electrical and hemodynamic activity this chapter is limited to the use of a static correlation analysis.

3.1 Introduction

3.1.1 Investigating resting state activity

Since 1995 a steady increase in the number of resting state functional neuroimaging studies has been witnessed (Cole et al., 2010). In classical fMRI research subjects are measured under different conditions. A baseline measurement either with open or closed eyes is carried out and subjects are required to perform a task in the scanner, or are presented with a stimulus. Subsequently, the pattern of brain activity during the baseline condition is subtracted from the pattern seen during the task, leaving a profile of regions active during and therefore involved in the execution of the task. However, this approach led researchers to bump into the phenomenon of task related decreases of activity in particular regions of the brain, indicating that the brain is more active in these regions during rest than during task performance (Raichle et al., 2001, Greicius et al., 2003). Interestingly, while different tasks cause activity in different brain areas, the areas in which decreased activity is seen during task performance appeared to be largely task independent as it was seen in a wide variety of tasks (Raichle et al., 2001). This led to the believe that the brain had a baseline mode of functioning referred to as the Default Mode Network, which was investigated by

Raichle et al. (2001) by means of the oxygen extraction factor (OEF) determined from PET measurements and showed to include among others the brain areas MPFC and the posterior cingulate and precuneus. Greicius et al. (2003) used functional connectivity analysis on resting state fMRI data in order to reveal the default mode network. Hereby they provided evidence that a cohesive, tonically active network indeed exists and showed that this default mode network was most active during rest and minimally disrupted by sensory processing tasks with limited cognitive demand. They also found evidence for an inhibitory interaction between activated regions and regions of the default mode network by establishing an inverse correlation between the default mode network and brain regions that were activated during task performance.

The idea that the brain is active during rest is not new. Already in 1929, the inventor of the EEG Hans Berger indicated that even when doing nothing the brain still showed spontaneous oscillatory activity (Berger, 1929). This notion is supported by the fact that at rest the brain consumes 20% of the bodies oxygen while only accounting for 2% of the body weight (Raichle et al., 2001, Fox and Raichle, 2007). Moreover, when performing a task, the oxygen demand of the brain does not increase by more than 5% in relation to this resting state consumption (Fox and Raichle, 2007, Raichle, 2010). So this spontaneous neural signalling during rest, that cannot be attributed to specific inputs or outputs and therefore represents neural signalling that is intrinsically generated by the brain, has to be important for brain functioning in general (Fox and Raichle, 2007).

The default mode network however, does not resemble the only brain areas that are active during resting conditions. In 1995 Biswal et al. showed that spontaneous fluctuations of the BOLD signal in the left somatomotor cortex were specifically correlated with spontaneous fluctuations in the right somatomotor cortex and with medial motor areas without overt motor behaviour being present. By means of functional connectivity analysis this finding was replicated several times and more networks were indicated. Generally it appeared that the regions that are similarly modulated by various task-paradigms are also correlated in their spontaneous BOLD activity (Fox and Raichle, 2007, Smith et al., 2009). These networks are referred to as resting state networks (RSNs) or intrinsic connectivity networks (ICNs) (Beckmann et al., 2005, Buckner, 2012). RSNs have spatially

similar characteristics between subjects and are seen in BOLD fluctuations between 0.01 and 0.1 Hz (Beckmann et al., 2005, Smith et al., 2009). Different networks that have opposing functionality also are anti-correlated in their spontaneous BOLD activity (Fox and Raichle, 2007). The notion that the spontaneous variations of BOLD activity remain present during task performance might be the explanation of the intra individual differences that are seen during event-related BOLD measurements. It might even be contributing to the inter-trial variability in human behaviour (Fox and Raichle, 2007).

This makes resting state activity a very important area of study. The relationship between brain and behaviour and especially the possible explanation of differences in behaviour could have a huge added value in the investigation of pathologies that are currently diagnosed based on behavioural criteria. This currently includes all psychopathologies that are described in the DSM-IV-TR (Association, 2000). The study of resting state activity could give insight into markers which can be an objective aid for diagnosis (Khamsi, 2012). Investigating resting state activity is also very practical. Since there is no task involved, patients that have difficulty performing certain tasks do not have to be excluded anymore. This makes it easier to study infants, children, sedated subjects or subjects with severe cognitive or physical impairments (Cole et al., 2010). Furthermore, the different networks can be assessed in one scanning session relieving the burden for the patient during testing (Smith et al., 2009). In different pathologies already disturbances in the correlation structure of the different networks have been found. These include Alzheimer's disease, multiple sclerosis, depression, schizophrenia, ADHD, autism, epilepsy, and spatial neglect following stroke (Fox and Raichle, 2007, Pievani et al., 2011, Buckner, 2012). In depression for example, a diminished connectivity between one area of the default mode network and areas that regulate emotions is found (Raichle, 2010). Besides diagnostic information it might also be possible to obtain prognostic information and obtain more insight into disease causes and treatment strategies (Raichle, 2010). However, when considering the option to implement measures of resting state brain activity in clinical practice, using fMRI might be not the most practical approach. Using a technology like near- infrared spectroscopy (NIRS) could be a preferable option since it is lightweight, portable, inexpensive to purchase and use compared to fMRI, and can be used at the bedside making it suitable for all

lines of healthcare (Lu et al., 2010, Mesquita et al., 2010). As yet, NIRS has not been used on a regular basis to investigate the brain in a resting state. Over the last 5 years a hand full of studies have been conducted in which the NIRS technology, either with or without supporting neuroimaging techniques like fMRI and EEG, has been investigated for potential use in researching RSNs (for examples see (Lu et al., 2010, Mesquita et al., 2010, Sasai et al., 2011, Sasai et al., 2012, White et al., 2009, Zhang et al., 2010). The results seem promising although more research needs to be conducted before connectivity analysis of resting state NIRS data can be implemented as a clinically valuable tool.

From that perspective one should note that it is not just connectivity that can be derived from resting state and tell something valuable about brain functioning or distinguish between pathologies. The field of quantitative EEG (QEEG), which uses profiles of frequency bands, has proven on many occasions that patterns of brain activity seen in psychopathologies can be differentiated from patterns of brain activity in healthy people (for a review see (Coburn et al., 2006). Furthermore, different patterns of brain activity are seen in different psychopathologies. In ADHD for example an increased theta/beta ratio is a marker that distinguishes children who have or do not have the disorder with a sensitivity and specificity of respectively 86% and 98% (Monastra et al., 1999). In depression the frontal alpha asymmetry in which higher amplitudes of alpha wave activity are displayed in left frontal brain areas compared to right frontal areas is the distinguishing pattern (Davidson, 1992, Davidson, 1998, Putnam and McSweeney, 2008). Findings like this make (Q)EEG suitable for investigating brain function and developing biomarkers based on brain activity.

As with NIRS, EEG (or QEEG) has the advantage of being low cost and portable makes it highly suitable for clinical use (Kaiser, 2005). Especially the combined use of EEG and NIRS in investigating brain activity at rest could create more insight in the underlying mechanism of neural activity and energy metabolism. In order to determine failing aspects in this symbioses in (psycho)pathologies, one first should have insight in the neural vs. oxygenation relationship in healthy working brains.

When resting state activity is considered, researchers adopt different protocols.

For some it is evident that resting state activity should be measured in a condition in which the eyes are closed. Others also speak of resting state activity when the subject is doing nothing with eyes open. From EEG research we know that during a resting state condition with closed eyes alpha wave activity occurs over the occipital cortex. Upon opening the eyes this alpha wave subsides due to the visual input the occipital cortex has to process (Pfurtscheller et al., 1994). Moosmann et al. (2003) investigated changes in the occipital EEG alpha rhythm upon opening and closing of the eyes together with changes in fMRI and NIRS. In their study the combination of alpha and Hbb (N=4) resulted in a strong positive correlation at a delay of about 8 seconds. As an extension of their work and in an attempt to better understand the coupling between EEG measures and oxygenation parameters during resting state, this chapter will explore the difference in resting state activity of the occipital (visual) cortex between eyes open (EO) and eyes closed (EC) in a sample of 38 healthy adults. Changes in alpha wave activity are compared to changes in HbO_2 as well as Hbb concentrations.

3.1.2 Investigating the QEEG

When investigating the brain's underlying mechanisms of functioning and possible symbioses between direct electrical activity and indirect metabolic activity, limiting the investigation to one parameter in the electrical domain, could be insufficient. As was pointed out in chapter one, quantitative EEG (QEEG) research usually investigates multiple frequency bands (Kaiser, 2005). Therefore the alpha band is not the sole band that is investigated in research regarding either EO or EC resting state activity. Changes in other bands have been reported as well. For example, Barry et al. (2007) have reported average changes in frequency bands between EO and an EC resting conditions in adults in which they found that during EC conditions delta, theta, alpha and beta activity were generally higher compared to EO conditions. The only exception here was the beta activity (which they defined between 13.5 and 25 Hz), that did show an increase upon opening the eyes in the frontal region despite the fact that the general pattern showed a decrease during EO conditions. The findings on delta, theta are perfectly in line with previous research that has coupled delta and theta activity to attention and alertness (De Gennaro et al., 2007, Braboszcz and Delorme, 2011). When a subject's attention or alertness decreases, for example when the mind wanders from a task that was assigned or because of sleepiness, the magnitude of the

delta and theta bands increases. Since the mere action of opening the eyes increases a subject's alertness, it is expected that the opening of the eyes also causes the delta and theta activity to subside. The changes in alpha activity are also straightforward. An increase in alpha wave activity has been described as the idling state of the brain (Kaiser, 2005), which would be seen upon closing the eyes. The findings of Barry et al. (2007), on the beta activity, are actually more unexpected as the beta activity of the neocortex has been related to top-down cognitive processing (Okazaki et al., 2008, Iversen et al., 2009). Therefore in this chapter it is assumed that that when the eyes are opened and the visual cortex starts to process information, the beta activity will go up instead of down. These hypotheses will be investigated in this chapter when the differences between blocks of EO and EC are compared for the delta, theta, alpha, beta1 and beta2 frequency bands.

3.1.3 The alpha peak frequency as a measure of general brain functioning

Within the alpha band a separate parameter can be found that can be important in revealing aspects of general brain functioning, the alpha peak frequency (APF). The reason why it is assumed that it gives information about general brain functioning is threefold. First, the APF increases in frequency when a brain matures. As early as the 1930s it has been described that as a person increases in age, this is accompanied by an increase in fast wave brain activity and a decrease in slow wave activity (Smith, 1938, Lindsley, 1939). Together with this increase in faster activity with age, a change in mean frequency can be observed. In adolescents and adults the brain's stationary rhythm of oscillation lies in the alpha band, usually around 10 Hz, and is visible as a distinguishing peak in the spectrum. In children this peak is slower and increases in frequency until puberty (Bazanova and Vernon, 2013). If children display a peak at a slower frequency for too long, when the dominant slow frequencies are not replaced with the faster frequencies, their EEG is characterized as having a maturational lag (Clarke et al., 2002). The maturational lag often is accompanied by difficulties in reading and writing abilities (Harmony et al., 1995, Becerra et al., 2006). This is in line with reports that couple the frequency of the APF to speed of information processing (Klimesch et al., 1996), cognitive performance (Grandy et al., 2013a), memory performance (Klimesch et al., 1993, Richard Clark et al., 2004) and even

intelligence (Grandy et al., 2013b) which all become better with higher frequency of the APF .

This link of the APF with cognitive abilities is the second clue for a role in general brain functioning. As an example Klimesch et al. (1993) have found that in an age matched sample, subjects that perform better on a memory task display an APF that is 1 Hz higher than the APF of subjects that perform less well. Along with the other evidence, this gives rise to the notion that when the APF could be influenced or trained to reach a higher frequency this would positively influence information processing speed and cognitive performance. In order to test this, Klimesch et al. (2003) stimulated the individual APF with repetitive transcranial magnetic stimulation (rTMS) during a resting condition in two groups and measured the improvement on a mental rotation task. In the first group the APF was stimulated 1Hz above the individual APF and in the control group the APF was stimulated 3 Hz under the individual APF or at 20 Hz (beta frequency). They found that only in the individual APF +1 group the accuracy of the mental rotation task increased. The very same task was used by Hanselmayr et al. (2005) however, the method chosen to influence APF was neurofeedback in which the goal was to increase upper alpha power (individual APF + 2 Hz). The control group had to decrease their theta power (individual APF -6 Hz). The subjects that were able to enhance their upper alpha during the neurofeedback sessions were the only ones who increased their performance on the mental rotation task.

The third and last reason why APF could be linked to general brain functioning can be found in the field of brain deterioration. While the APF increases when people mature, the APF is also known to drop again as we get older. Bazanova and Vernon (2013) report this drop to commence after 40 years of age. Duffy et al. (1984) report the frequency of the APF to be stable between 30 and 50 years of age and found a drop in APF in the age group between 60 and 80 years of age (Klimesch, 1999). A linear relationship between APF and age (in the 20 to 70 year old band) which can be summarized in the formula $APF = 11.95 - 0.053 \times age$ is even reported (Richard Clark et al., 2004). So despite the lack of agreement on the exact onset, research agrees that when the brain ages the APF decreases again. The decrease in APF is also seen, independent of age, when people suffer from different forms of dementia, like Alzheimer's disease (Moretti et al., 2004,

Chen et al., 2013) but also immediately after stroke (Jordan, 2004). The decline in cognitive abilities that is reported with progressing age and in the aforementioned pathologies is again a feature that is congruent with the relationship that is found between APF and cognition.

Because the APF is a key feature in the spectrum and can give us so much information on brain functioning, the APF will be explored in this chapter as well. Since the participants are healthy adults, the focus of this investigation will lie in the stability of the APF. Supposedly the APF is stable across hemispheres and between eyes open and eyes closed conditions (Grandy et al., 2013b). Therefore it is hypothesized in this chapter that no differences will be discovered between eyes open and eyes closed conditions and that no changes will be seen over the time course of the measurement conducted in this study.

3.1.4 Investigating NIRS time series

In EEG and QEEG it is very common to use spectral analysis to determine the oscillations that are present within a signal. It is the way the spectral bands described above are found and the analysis that is needed to find the APF. For EEG, Klimesch (1999) defines an oscillatory component by the presence of rhythmic activity in the EEG, which is manifested by a peak in spectral analysis. In essence spectral analysis is not limited to EEG. It can be conducted on any time series that contains oscillations. As such, it is used to break down music but also in other neuroscientific measurements like MEG spectral analysis is common (for a review see (Hari and Salmelin, 2012)). In research that investigates brain activity by NIRS, spectral analysis of the obtained time series of concentration changes, is less common. Usually the key features of interest are the concentration changes of HbO_2 and Hbb between a baseline and a task and the NIRS technique is used to obtain an image of these changes (for a review see (Obrig and Villringer, 2003)). However, spectral analysis in NIRS time series can give valuable information. It is an important tool in defining noise. As is pointed out in chapter two, instrument noise is defined as noise high in frequency whereas physiological noise like heart rate and respiration are in the low frequency domain and much more in the part of the spectrum where the changes of interest are expected (Boas et al., 2004, Huppert et al., 2009). Furthermore, resting state research has reported the occurrence of slow oscillations in fMRI BOLD as well as NIRS signals that can be

interconnected in resting state networks (Fox and Raichle, 2007, Lu et al., 2010, Sasai et al., 2011). Therefore, in this study a spectral analysis will be applied to the HbO_2 and the Hbb time series in order to determine whether oscillatory properties can be found in these signals over the O1 and O2 location. Naturally the more common concentration changes in HbO_2 and Hbb between EO and EC blocks will be investigated as well. As clarified in chapter one, an increase in neural activity is fuelled by glucose and oxygen metabolism (Irani et al., 2007). Therefore, a brain region that is more active is expected to show higher concentrations of HbO_2 and lower concentrations of Hbb. Over the visual cortex this was also found by Moosman et al. (2003) who reported an increase in HbO_2 concentrations with closed eyes and a decrease in Hbb when the eyes were open. This leads to the hypotheses for the study in this chapter that during EO blocks the concentrations of HbO_2 and Hbb are respectively higher and lower when compared to EC blocks.

3.1.5 A summary of the investigated hypotheses

In this chapter a study will be conducted in a sample of 38 healthy adults under eyes open and eyes closed conditions. Various aspects of the EEG and NIRS measurements over the occipital cortex will be explored. First, a static analysis will be performed on the EEG frequency bands delta, theta, alpha, beta 1 and beta 2 in order to determine whether there are differences between the EC and EO blocks. The hypothesis being that slower frequency bands (delta, theta and alpha) are higher during EC conditions whereas the faster bands (beta 1 and beta 2) are lower compared to EO conditions. Second, the APF will be determined and it will be investigated whether there are changes between the EC and EO blocks. Hypothesized is that this measure is stable between conditions and over time. Third, the differences between blocks in HbO_2 and Hbb concentration will be analyzed. It is expected that during EC conditions the concentration of Hbb will be higher compared to EO conditions. For HbO_2 concentrations the opposite is expected and higher HbO_2 concentrations should be found during EO blocks. Fourth, a spectral analysis will be used on the HbO_2 and Hbb time series in order to investigate potential rhythmical oscillations. No hypothesis is formulated for this exploration. Last, the changes in alpha activity will be correlated against the changes in Hbb and HbO_2 in order to reveal underlying relationships. For this

analysis it is expected that alpha activity correlates positively with Hbb concentrations and negatively with HbO_2 concentrations.

3.2 Methods

3.2.1 Subjects

In this study 38 subjects (21 female) were measured with EEG and NIRS simultaneously. In the original dataset 43 subjects were measured. However, the data of 5 subjects had to be discarded on inspection of data due to poor signals and high levels of noise. The mean age of the remaining population was 37.74 years (range 19-60). The exploratory nature of this research entailed the uncontrolled recruitment of subjects for this study, therefore no age restrictions other than over 18 years of age were applied.

Participants visited the laboratory on a single occasion. The testing procedures were explained and participants were offered the opportunity to ask questions before signing consent. The study was approved by the University ethics committee (070300) in accordance with the standards of the Declaration of Helsinki. A questionnaire was presented to the participants before testing, ruling out any neurological, psychopathological or vascular disease as well as the use of any medication that might affect the EEG or NIRS activity. After completing the questionnaire the measuring equipment was mounted on the head and participants were seated comfortably in front of a computer screen.

3.2.2 Paradigm

The testing paradigm constituted of a 5 minute measurement in which the subjects were asked to open and close their eyes and maintain this position for 30 second episodes. Two paradigms were evenly distributed between the subjects. Paradigm A started with an episode of eyes open as displayed in figure 3.1, paradigm B started with eyes closed and can therefore be seen as the reverse of paradigm A.

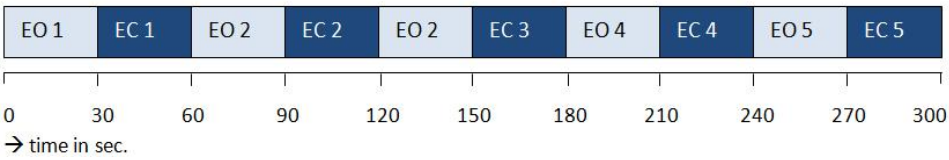

Figure 3.1 The experimental paradigm (paradigm A). Episodes with eyes open are indicated with a light blue colour and the letters EO, eyes closed episodes are indicated with the letters EC and a dark blue colour.

During the episodes in which the eyes were open subjects observed a "test screen" picture on a computer screen (figure 3.2). This picture was chosen to ensure a controlled visual stimulation task among all subjects.

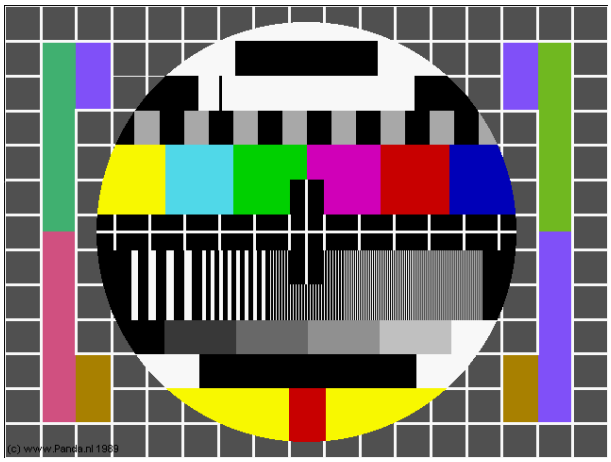

Figure 3.2 The test screen picture that was presented to the subjects on the computer screen in the eyes open blocks.

3.2.3 Equipment

EEG and NIRS measurements were performed simultaneously over the O1 and O2 location of the 10-20 EEG locations system (Jasper, 1958) as depicted in figure 3.3 with the reference electrode placed at the vertex (Cz). EEG was recorded with a BIMEC (Maastricht Instruments B.V. Maastricht, the Netherlands). The BIMEC is a universal biopotential amplifier that is able to record signals between -1000 and +1000 mV. A 20-bit AD-conversion is used to digitize the analogue input signals. In order to measure EEG a gain of 200 and a sample frequency of 250 Hz was used. The data were filtered by a 4^{th} order Butterworth high pass and low pass filter embedded in the amplifier with their cut off values set at 0.5 and 50 Hz and their roll off values being -24dB. Additionally the amplifier was equipped with a 50 Hz notch filter. Last a 7^{th} order Butterworth low pass filter with a cut off value of 32

Hz and a roll off value of -42 dB was embedded in the data acquisition software (BMC Acquisition Software, Biometrisch Centrum B.V., Gulpen) ensuring clean data between 0.5 and 32 Hz, the bandwidth of interest. The NIRS measurements were conducted with one transmitter and one receiver over both locations (OXYMON Mk III, Artinis B.V. Zetten, the Netherlands) (figure 3.3). The transmitters were equipped with semiconductor, pulsed laser diodes, which used nominal wavelengths of 855 and 780 nm. The detectors were avalanche photo diodes which had a special optic filter to filter out daylight. The signal was sampled at 25 Hz. Sampling at 25 Hz is quite high for NIRS measurements, but since multimodal measurements were conducted, sample frequencies for both modalities were chosen in a way that allows easier comparison in a later stage of data processing.

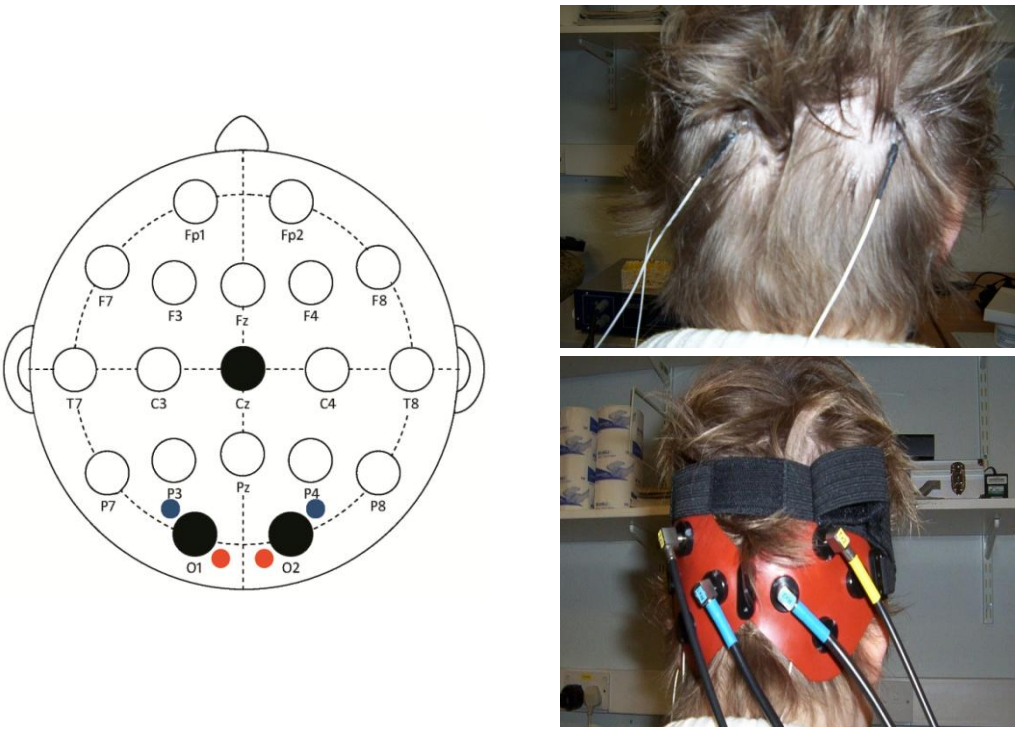

Figure 3.3 The electrode and optode positioning in the 10-20 system for electrode positioning. On the left hand side a schematic representation is shown. The electrodes are represented as black dots, whereas the transmitters and receivers are depicted in red and blue dots respectively. On the right hand side, one of the subjects demonstrates the electrode and optode positioning in which the upper picture shows the electrodes and the lower picture shows how the optode holder is placed over the electrodes and secured with a Velcro strap.

3.2.4 Experimental procedure

A schematic representation of the experimental setup is provided in figure 3.4. The participants were seated in a comfortable chair on approximately 1 m distance from a computer screen. This screen was attached to the laptop of the experimenter in order to display the test screen (figure 3.2). First the Cz, O1 and O2 positions were determined according to the 10-20 EEG locations system (Jasper, 1958) by means of a measuring tape and a dermographic pencil. The skin on these locations was gently abraded with a cotton tip soaked in NuPrep (D.O. Weaver & Co, Aurora, USA). The residual NuPrep was removed from the skin with a cotton pad and the Ag/AgCl electrodes (cable length 1 m) were attached to the scalp by means of Ten20 conductive paste (D.O. Weaver & Co, Aurora, USA). Impedances were measured and ensured to be below 10 kΩ. The EEG amplifier was attached to the laptop that also displayed the picture on the computer screen.

The optodes were then placed over the electrodes on the O1 and O2 locations (figure 3.3) by means of optode holders. The optode holders allowed the transmitter and the receiver to be securely screwed into place at an inter optode distance of 35 mm. The optode holders were fastened with help of Velcro straps after ensuring as little hair as possible was between the optode and the scalp. When necessary the hair was pushed aside with help of the back of a cotton tip. In order to reduce the amount of noise from movement the optic fibres, the 315 cm long fibres were led away from the subject by hanging them from a hat stand. From here the optic fibres were led to the OXYMON Mk III. This device was attached to a second laptop, operated by the experimenter. After checking the signal quality on both devices, the paradigm was started. The entire paradigm was measured as one measurement that lasted 5 minutes. Every switch from EO to EC and vice versa was indicated by a marker which was registered by both laptops. The experimenter was facing the subject constantly sideways in order instruct the subject and to verify compliance to the paradigm.

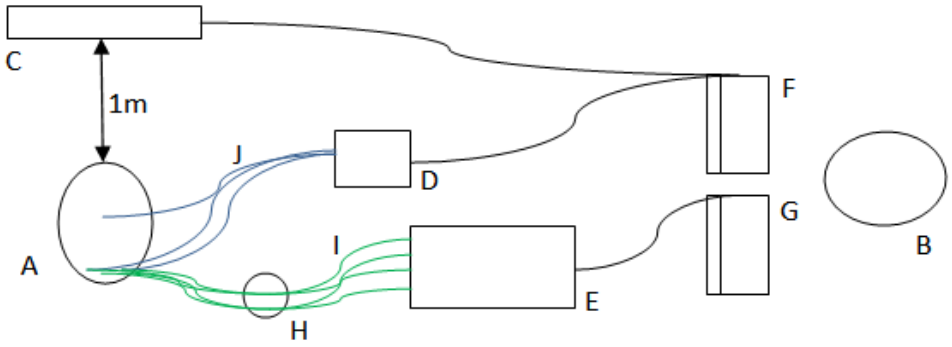

Figure 3.4 Schematic representation of the experimental setup. The participant (A) is guided by the experimenter (B) while watching the computer screen (C). The computer screen and the EEG device (D) are attached to laptop 1 (F) and the NIRS device (E) is attached to laptop 2 (G). The hat stand (H) leads the optodes (I) towards the NIRS device. The electrodes (J) are attached to the EEG device.

3.2.5 Data analysis

3.2.5.1 Spectrum content EEG

In order to calculate the shares of delta, theta, alpha, beta 1 and beta 2 activity in the EEG data, the Fourier Transform was used. The specific waves were defined in the spectrum as follows: delta 0.5-3.5 Hz, theta 3.5-7.5 Hz, alpha 7.5-12 Hz, beta1 15-20 Hz, beta2 20-32 Hz. The spectrum content was calculated over the second half of every block for both locations and every participant separately. Hereto the FFT was calculated over the entire 15 seconds of data at once, resulting in a magnitude spectrum with 0.5 Hz bins as provided by the BMC Acquisition Software that is used together with the BIMEC. Examples of spectral plots are given in figure 3.7. In order to obtain the magnitude for a given frequency band of this block of data, the magnitudes in µV of all 0.5 Hz bins falling in the range of the given frequency bands were added up. The alpha magnitude for instance was found by adding the magnitudes of the bins at 7.5, 8.0, 8.5, 9.0, 9.5, 10.0, 10.5, 11.0, 11.5 and 12.0 Hz. The second halves of the blocks were chosen because in a later phase of the data analysis the EEG data are going to be linked to the NIRS data. As the hemodynamic response that is measured by NIRS is known to have a delay (Moosmann et al., 2003), discarding the first half of every block (15s) avoids transient features in the data and it is ensured that a more representative profile of brain activity is given. The values that are analysed are absolute values from the magnitudes of the frequency bands. Absolute rather than relative EEG values are chosen because when changes in relative values are seen, it does not necessarily

mean that a change is seen in that band alone because it can also arise from a change in the other bands (Barry et al., 2007).

Comparisons between eyes open and eyes closed blocks are made by means of a repeated measures ANOVA for every frequency band separately. The analysis has two within-subject factors, the first being "block" which has 5 levels (block 1, block 2, block 3, block 4, and block 5) and the second factor being "condition" which has 2 levels (eyes open, eyes closed).

Block	**EEG O1**	**EEG O2**	**Alpha O1**	**Alpha O2**	**NIRS O1**	**NIRS O2**
EO1	-	-	-	-	2, 20, 33	26, 33
EO2	3, 20, 24, 39, 42	24	3, 20, 24, 39	24	2, 20, 33	26, 33
EO3	-	-	-	-	2, 20, 33	26, 33
EO4	-	-	-	-	2, 20, 33	26, 33
EO5	-	12	-	-	2, 20, 33	26, 33
EC1	3, 4, 12, 13, 20, 24, 37	-	37	-	2, 20, 33	26, 33
EC2	5, 12, 13, 24, 37,39	-	-	-	2, 20, 33	9, 26, 33
EC3	3, 24, 37	3, 4, 12, 13, 15, 20, 24, 25, 37, 39, 42	-	37	2, 20, 33	9, 26, 33
EC4	3, 13, 37	3	37	-	2, 20, 33	26, 33
EC5	3, 37	3, 4, 24, 37	37	4, 37	2, 20, 33	26, 33

Table 3.1 Summary of the outlying data for the EEG, the alpha band used for alpha peak frequency (APF) analysis and the NIRS measurements. For every measurement location, left visual cortex (O1) and right visual cortex (O2), the outliers were evaluated separately. The different blocks for eyes open (EO) and eyes closed (EC) are displayed in the rows. For each block the subject numbers of the participants that showed outlying data are reported in the cells.

Before statistical comparison of the blocks was initiated, the data were checked on outliers. Hereto the skewness and kurtosis of the obtained magnitudes were analysed (Howell, 2011). If the group value per frequency band did not fall within the -2 to 2 range, the histogram plot was inspected to determine the outlying subject. The EEG data of this subject were then explored in order to identify whether the signal was noisy and needed to be excluded. After exclusion the analysis cycle was repeated until skewness and kurtosis were within the accepted range. The eliminated blocks for every subject are displayed in table 3.1.

3.2.5.2 Alpha peak frequency

The APF was determined for every subject separately for both the O1 and O2 location for every second half of each block (similar to the procedure with the frequency bands). This was done by searching the interval from 7.5 to 12.0 Hz in 0.5 Hz steps for the frequency range with the highest power. From the outlier analysis it was determined which subjects showed outlying values in the alpha band due to artefacts (table 3.1). In order to avoid a distortion of the APF from these artefacts these blocks of data were also omitted in the APF analysis.

Since the APF was determined in 0.5 Hz steps, the resolution of the findings is not a continuous but an interval variable. Besides, the values that are found during a procedure like this will not have a normal distribution. Therefore, it would be inappropriate to use a repeated ANOVA analysis as was used in the frequency band analysis. To investigate whether the APF was in fact stable between measurements the nonparametric counterpart of the ANOVA analysis was chosen and performed separately on the data of the O1 and O2 location; Friedman's test. As Friedman's test tests the hypothesis that all measurements originate from the same population, all 10 blocks are tested in one analysis. In order to investigate whether there were differences between the blocks from one condition, separate Friedman tests were also performed on the 5 blocks measured with eyes open and the 5 blocks measured with eyes shut for both the O1 and the O2 location.

Next to the establishment of the APF it was investigated whether there were differences in the way the APF presented itself in the spectrum. Hereto, the width of the APF was determined by considering the first and last bins that belonged to the alpha peak and were distinctive from the background of the spectrum. For this

aspect the entire 5 min interval was evaluated separately for the O1 and O2 location.

3.2.5.3 NIRS concentration changes

The raw NIRS data were transformed into graphs displaying the concentration changes of HbO_2 and Hbb (Cope and Delpy, 1988, Delpy et al., 1988). As described in chapter 2, these time series were detrended and next band pass filtered to remove slow drift and instrumental noise in the signal. The detrending was performed according to the following formula:

$$y(t) \coloneqq x(t) - \big(x(b) - x(a)\big) * (\frac{t}{(b-a)} - \frac{1}{2})$$

In which $y(t)$ is the detrended signal, $x(t)$ is the original signal of which the linear trend $\big(x(b) - x(a)\big) * (\frac{t}{(b-a)} - \frac{1}{2})$ is subtracted. The terms a and b specify the interval of the signal. The band pass filter was a Fourier filter with the borders set at 0.01 and 0.5 Hz.

Next, the average concentration of HbO_2 as well as Hbb was calculated over the second half of every block for every participant on both locations. Only the second halves were taken into account because of the delay of the hemodynamic response, this way transient features were avoided and it was ensured that steady state values were taken into account (Uludag et al., 2004a). Then the data were checked for outliers using the same procedure as described above. Data from subjects that displayed outliers due to noise were subsequently removed before statistical analysis was undertaken (table 3.1). The statistical comparisons between eyes open and eyes closed blocks was done in a similar fashion as was done for the EEG frequency bands. A repeated measures ANOVA with two within-subject factors, “block” (5 levels) and “condition” (2 levels) was conducted separately for the HbO_2 and Hbb concentrations.

3.2.5.3 Spectrum content NIRS

Before the spectral analysis was undertaken, it was evaluated whether the HbO_2 and Hbb time series displayed good or poor signal quality. Signal quality was evaluated based on the paradigm induced response that was seen and the strength of this response. When a strong response was seen in all repeats, strong meaning a change of 2 SDs or more from baseline, the quality was marked as

"good". When the concentration change showed a response that was faint for some repeats or inconsistent, the signal was marked as "medium". When no response (under 2 SD change from baseline) or only noise was observed, the quality was marked as "bad". "Good-medium" or "medium-bad" qualifications were given to signals that fell in between two other qualifications. These qualifications were then used to divide the sample in a good-quality and a poor-quality group which were used in later stages of analysis to verify whether certain results are influenced by signal quality. All signals that were marked as "good", "good-medium", or "medium" were taken together in the good-quality group and the "medium-bad" and "bad" classifications were taken together in the poor-quality group.

In order to investigate the spectrum of the NIRS signals a Fourier analysis was applied. The spectrum that was given had a resolution of 0.05 Hz which is more precise then the previously reported EEG spectrum. This was chosen mainly because the analysis was explorative and because the range that was explored is much smaller than it is for EEG (0.01-0.5 Hz vs. 0.5-32 Hz). Peaks that occurred in this spectrum were noted down for HbO_2 and Hbb for every location (O1 and O2) separately. Then it was evaluated whether the peaks that were observed were common between subjects and whether a difference between the good-quality group and the bad-quality group was seen.

3.2.5.5 Correlating EEG and NIRS

Last a correlation analysis was performed in order to establish possible correlations between the alpha activity and HbO_2 or Hbb concentrations. For the correlation analysis, the data from the second halves of the blocks was used as well, with the outlying data removed (N=31 for O1, N=32 for O2). The data from the eyes open blocks were averaged together for every subject as well as the data from the eyes closed blocks per location before Pearson Correlations were determined.

3.3 Results

3.3.1 Spectrum content EEG

The repeated measures ANOVA's revealed that for all frequency bands, except theta, there was a significant main effect for condition on both the O1 and O2 locations. The results are summarized in table 3.2 and figure 3.5. In the EO condition there was significantly more delta activity present (O1 p=0.000, O2 p=0.000). In the EC condition the amounts of alpha (O1 p=0.000, O2 p=0.000), beta1 (O1 p=0.000, O2 p=0.000) and beta2 activity were increased compared to the eyes open condition. For the beta 2 activity additionally a significant interaction effect (Block x Condition) was observed on both the O1 (p=0.005) and O2 (p=0.023) location indicating that the difference between both conditions increases over time (Fig. 3.6).

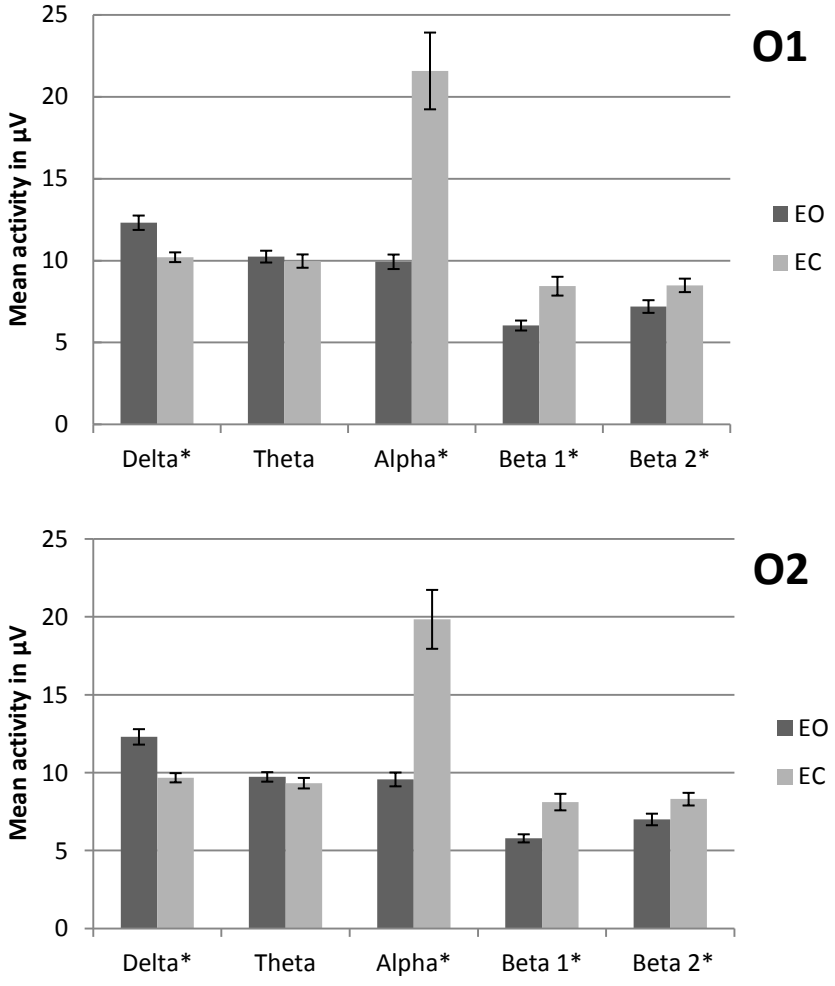

Figure 3.5 EEG frequency band results. The difference between the amount of activity in eyes open (EO) and eyes closed (EC) conditions with their standard deviations are displayed. The difference in theta activity was not significant for both the left visual cortex (O1) and right visual cortex (O2). Differences marked with an asterisk (*) indicate a significance with a p value < 0.001.

O1	**Effect**	***F* - value**	***p*-value**	**partial η^2**	**Correction**
Delta	Main, block	*(3.003, 84.094)* 0.325	0.808	0.011	yes
	Main, condition*	*(1,28)* 23.122	0.000	0.452	no
	Interaction	*(4,112)* 0.692	0.599	0.024	no
Theta	Main, block	*(2.939, 82.286)* 0.941	0.423	0.033	yes
	Main, condition	*(1,28)* 0.680	0.417	0.024	no
	Interaction	*(3.020, 84.567)* 0.898	0.446	0.031	yes
Alpha	Main, block	*(4,112)* 1.203	0.314	0.041	no
	Main, condition*	*(1,28)* 29.323	0.000	0.512	no
	Interaction	*(2.840, 79.516)* 0.240	0.858	0.009	yes
Beta 1	Main, block	*(4,112)* 0.235	0.918	0.008	no
	Main, condition*	*(1,28)* 35.761	0.000	0.561	no
	Interaction	*(4,112)* 1.007	0.407	0.035	no
Beta 2	Main, block	*(2.567, 71.867)* 1.547	0.215	0.052	yes
	Main, condition*	*(1,28)* 29.722	0.000	0.515	no
	Interaction*	*(4,112)* 3.995	0.005	0.125	no
HbO_2	Main, block	*(2.366, 80.442)* 2.576	0.073	0.070	yes
	Main, condition*	*(1,34)* 25.211	0.000	0.426	no
	Interaction	*(2.547, 86.601)* 2.474	0.076	0.068	yes
Hbb	Main, block	*(2.561, 87.070)* 0.458	0.682	0.013	yes
	Main, condition*	*(1,34)* 18.482	0.000	0.352	no
	Interaction	*(2.001, 68.025)* 1.312	0.276	0.037	yes
O2	**Effect**	***F* - value**	***p*-value**	**partial η^2**	**Correction**
Delta	Main, block	*(3.163, 85.400)* 0.520	0.679	0.019	yes
	Main, condition*	*(1,27)* 30.200	0.000	0.528	no
	Interaction	*(4,108)* 0.411	0.800	0.015	no

Theta	Main, block	*(2.840, 76.672)* 0.718	0.537	0.026	yes
	Main, condition	*(1,27)* 1.977	0.171	0.068	no
	Interaction	*(2.892, 78.080)* 1.395	0.251	0.049	yes
Alpha	Main, block	*(4,108)* 0.843	0.501	0.030	no
	Main, condition*	*(1,27)* 33.696	0.000	0.555	no
	Interaction	*(4,108)* 0.532	0.712	0.019	no
Beta 1	Main, block	*(2.880, 77.750)* 0.264	0.844	0.010	yes
	Main, condition*	*(1,27)* 30.836	0.000	0.533	no
	Interaction	*(4,108)* 0.391	0.815	0.014	no
Beta 2	Main, block	*(4,108)* 1.220	0.306	0.043	no
	Main, condition*	*(1,27)* 34.626	0.000	0.562	no
	Interaction*	*(4,108)* 2.961	0.023	0.099	no
HbO_2	Main, block	*(2.582, 87.775)* 2.563	0.069	0.070	yes
	Main, condition*	*(1,34)* 16.821	0.000	0.331	no
	Interaction	*(2.447, 83.186)* 0.689	0.533	0.020	yes
Hbb	Main, block	*(2.070, 70.392)* 1.835	0.166	0.051	yes
	Main, condition*	*(1,34)* 7.857	0.008	0.188	no
	Interaction	*(2.210, 75.140)* 0.272	0.784	0.008	yes

Table 3.2 Details of the repeated measures ANOVAs that were performed on the different frequency bands within the EEG and the oxygenated haemoglobin (HbO_2) as well as the deoxygenated haemoglobin (Hbb) concentrations from the NIRS data. The upper part of the table displays the results from the left visual cortex (O1) and the lower part the right visual cortex (O2). Effects marked with an asterisk (*) are effects that were significant.

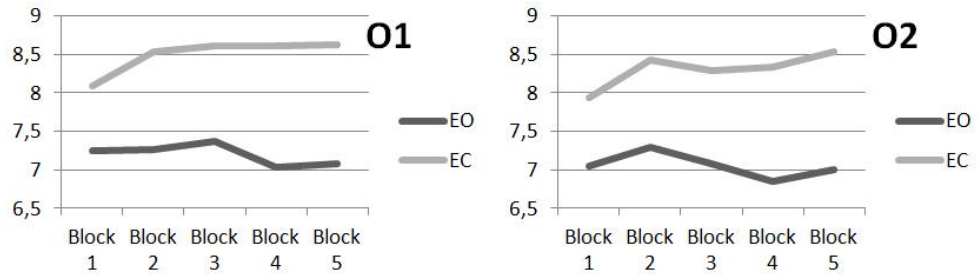

Figure 3.6 The significant interaction effect that was found for the beta 2 activity on both the left (O1) and right visual cortex (O2). The left panel displays the activity measured on the O1 location the right panel the O2 location. The dark grey line indicates the eyes open (EO) condition whereas the light grey line represents the eyes closed (EC) condition. As time increases, the lines move further apart.

3.3.2 Alpha peak frequency

Friedman's test revealed that the APF varied significantly between the different blocks when all ten blocks were taken into account; O1: $\chi^2(9, N=33) = 28.034$, $p = 0.001$, O2: $\chi^2(9, N=35) = 27.995$, $p = 0.001$. When evaluating the results within the separate conditions, eyes open and eyes closed, the overall variations seemed due to differences between the conditions rather than differences within the conditions. For the O1 location the EO blocks show variation in APF between the different blocks: $\chi^2(9, N=34) = 12.000$, $p = 0.017$. In the EC blocks however, there is no significant variation visible: $\chi^2(9, N=37) = 5.088$, $p = 0.278$. On the O2 location no significant variation is seen in either condition separately: EO: $\chi^2(4, N=37) = 9.208$, $p = 0.056$, EC; $\chi^2(4, N=36) = 2.418$, $p = 0.659$.

In order to support the claim that a significant variation is seen between the two conditions, the average APF of EO and EC was calculated per person for both O1 and O2 and a Wilcoxon signed ranks test was used to investigate differences. This also showed a significant difference for both O1 and O2 between the conditions EO and EC in which it appears that the APF is lower during the EC blocks; O1 (z = 2.622, N-Ties= 19, p = 0,009), O2 (z = 2.618, N-Ties= 22, p = 0,009). When the individual subjects are examined however, it appears that these results occur because of a limited number of subjects and that these subjects do not show a drop on every transition from EO to EC as detailed below.

For the O1 location 33 subjects remained in the sample after outlier correction,

with 10 blocks in the paradigm, 5 comparisons per subject are made, giving 165 comparisons in total. Of the 33 subjects, 18 showed no variation of the APF. In the remaining sample of 15 subjects, 3 showed a lower APF in all EC blocks and 10 others showed lower APF in some EC blocks. The remaining subjects even showed higher APF in some EC blocks. How much this change was both in positive and negative directions is summarized in table 3.3a. Out of the 165 comparisons that are made only 38 show a lower APF in an EC block is. When changes are found however, they are often 1.0 Hz in size or larger. For the O2 location the summary of results can be found in table 3.3b which are quite similar. On this location 35 subjects remained in the sample after outlier correction which leads to a total number of 175 comparisons. Out of 35 subjects, 15 showed a stable APF over all blocks. Out of the remaining 20 subjects, 2 participants showed a lower APF in all EC blocks and 14 showed a lower APF in some EC blocks. The remaining 4 participants even showed a higher APF in some EC blocks, and one of them showed this in all EC blocks. So out of 175 comparisons only 42 give rise to a lower APF in an EC block. Again, changes were often 1.0 Hz in size or larger.

A. O1	**Stable**	**0.5 Hz**	**1.0 Hz**	**1.5 Hz**	**2.0 Hz**	**Total**
Stable	118	-	-	-	-	118
EC lower	-	9	14	10	5	38
EC higher	-	2	5	1	1	9
Total	118	8	19	11	6	165

B. O2	**Stable**	**0.5 Hz**	**1.0 Hz**	**1.5 Hz**	**2.0 Hz**	**2.5 Hz**	**Total**
Stable	122	-	-	-	-	-	122
EC lower	-	11	16	9	2	4	42
EC higher	-	-	7	2	2	-	11
Total	122	11	23	11	4	4	175

Table 3.3 Results of the individual alpha peak frequency comparisons, split in 0.5Hz step changes. In total 165 comparisons are made for the location over the left visual cortex (O1) which are displayed in the upper part of the table and 175 for the location over the right visual cortex (O2) which is displayed in the lower part of the table. This difference was due to outliers.

When investigating differences in the presentation of the APF in the spectrum a distinction into four different types of peaks could be made (figure 3.7): A. a narrow base and a low magnitude peak, B. a wide base and a low magnitude peak, C. a narrow base and a high magnitude peak, and D. a wide base and a high magnitude peak. When a higher magnitude of the APF is seen the base of the peak was automatically wider.

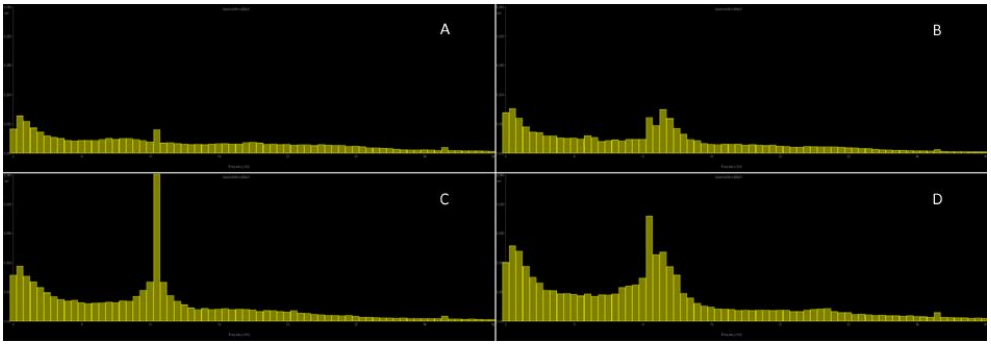

Figure 3.7. The four different types of APF. A: Narrow base, low magnitude, B: Wide base, low magnitude, C: Narrow base, high magnitude, D: Wide base, high magnitude. The x- and y-axis values of the four displayed spectra are kept constant, the horizontal axis displays the frequency from 0 on the left up until 35 on the right, the vertical axis displays the magnitude of the bins ranging from 0 µV at the base to 10 µV at the top. The bins have a resolution of 0.5 Hz, so each bin indicates an increment of 0.5 Hz on the horizontal axis.

3.3.3 NIRS concentration changes

The repeated measures ANOVAs revealed that for the HbO_2 as well as the Hbb concentrations there was a significant main effect for condition on both the O1 and O2 locations. The results are summarized in table 3.2 and figure 3.8. In the EO conditions the concentration HbO_2 was significantly higher compared to the EC conditions (O1 p=0.000, O2 p=0.000). In the EC conditions the concentration Hbb was significantly higher compared to EO conditions (O1 p=0.000, O2 p=0.008). No significant main effects were found for block, neither could significant interaction effects be found.

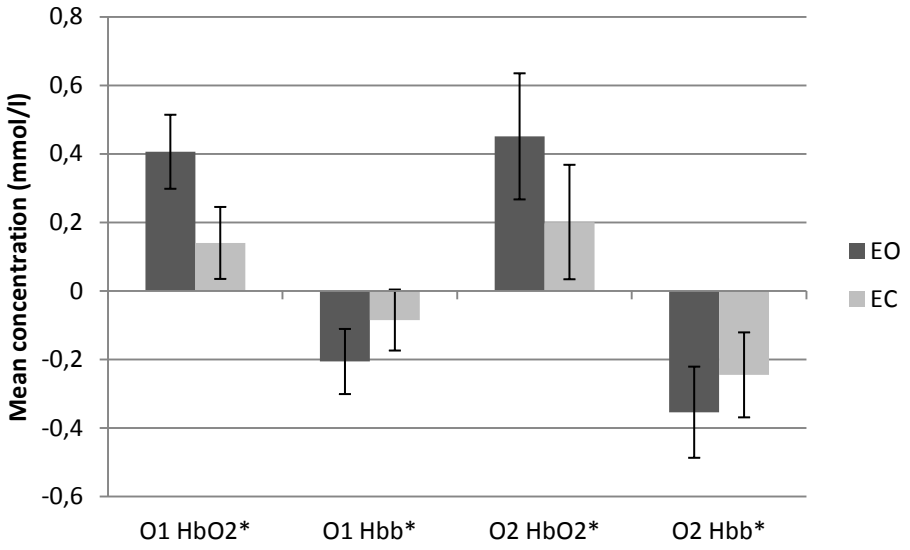

Figure 3.8 NIRS concentrations results. The differences in concentration between eyes open (EO) and eyes closed (EC) conditions with their standard deviations are displayed for the oxygenated haemoglobin (HbO_2) and deoxygenated haemoglobin (Hbb) concentration changes on both the left (O1) and right visual cortex (O2). Differences marked with an asterisk (*) indicate a significance with a p value < 0.01.

3.3.4 Spectrum content NIRS

The quality of the time series displaying the concentration changes was categorized into 5 categories: good, good-medium, medium, medium-bad and bad, as detailed in paragraph 3.2.4.3. In doing so the data of all subjects were considered, also the data that had been marked as outlier previously. These categories were then merged into two larger categories containing good-quality signals and poor-quality signals (table 3.4). This revealed that a large portion of the sample (between a half and two thirds) was classified as poor-quality data. It was seen that the signal quality obtained on O1 was slightly higher than it was on O2.

	HbO_2 O1	**Hbb O1**	**HbO_2 O2**	**Hbb O2**
N (total)	36	35	34	34
N (good-quality)	17	15	14	13
N (poor-quality)	19	20	20	21

Table 3.4 The number of subjects (N) that fall into each quality category for the time series measured over the left (O1) and right visual cortex (O2) for both the oxygenated haemoglobin (HbO_2) and deoxygenated haemoglobin (Hbb) concentration changes.

When the spectra were observed as well, it appeared that 2 subjects in the HbO_2 time series of the O1 location, 3 subjects in the Hbb time series of the O1 location and 4 subjects on both the HbO_2 and Hbb time series of the O2 location showed spectra that displayed white noise. White noise is defined as random peaks through the entire spectrum. These subjects were left out of the sample in this analysis (as is already visible in table 3.4).

An average of three peaks was seen per subject (minimum 1, maximum 5). Six separate categories of peaks could be defined with higher magnitudes seen in lower frequencies. A summary of the peaks and their occurrence is given in table 3.5, an example of a NIRS time series with the corresponding spectrum is given in figure 3.9.

Peak frequency	HbO_2 O1			Hbb O1			HbO_2 O2			Hbb O2		
	N_{total}	N_{good}	N_{poor}	N_{total}	N_{good}	N_{poor}	N_{total}	N_{good}	N_{poor}	N_{total}	N_{good}	N_{poor}
0.01-0.02	34/2	17/0	17/2	35/0	15/0	20/0	34/0	14/0	20/0	34/0	13/0	21/0
0.025-0.04	19/17	8/9	11/8	17/18	7/8	10/10	16/18	8/6	10/10	16/18	9/4	7/14
0.045-0.06	25/11	14/3	11/8	22/13	14/1	8/12	16/18	6/8	10/10	19/15	8/5	11/10
0.065-0.085	15/21	9/8	6/13	10/25	2/13	8/12	15/19	7/7	8/12	9/25	5/8	4/17
0.09-0.11	9/27	5/12	4/15	3/32	1/14	2/18	7/27	4/10	3/17	7/27	2/11	5/16
>0.11	1/35	0/17	1/18	2/33	0/15	2/18	1/33	0/14	1/19	1/33	0/13	1/20

Table 3.5. The number of subjects (N) that show peaks in various frequencies in ratios x/y, the x determining the number of subjects that do display a peak and the y determining the number of subjects that do not display it. The total N (displayed in the column Ntotal) is split up into good signal quality (displayed in the column Ngood) and poor signal quality (displayed in the column Npoor) for both the oxygenated haemoglobin concentration (HbO_2) and the deoxygenated haemoglobin concentration (Hbb) on the left (O1) and right visual cortex (O2).

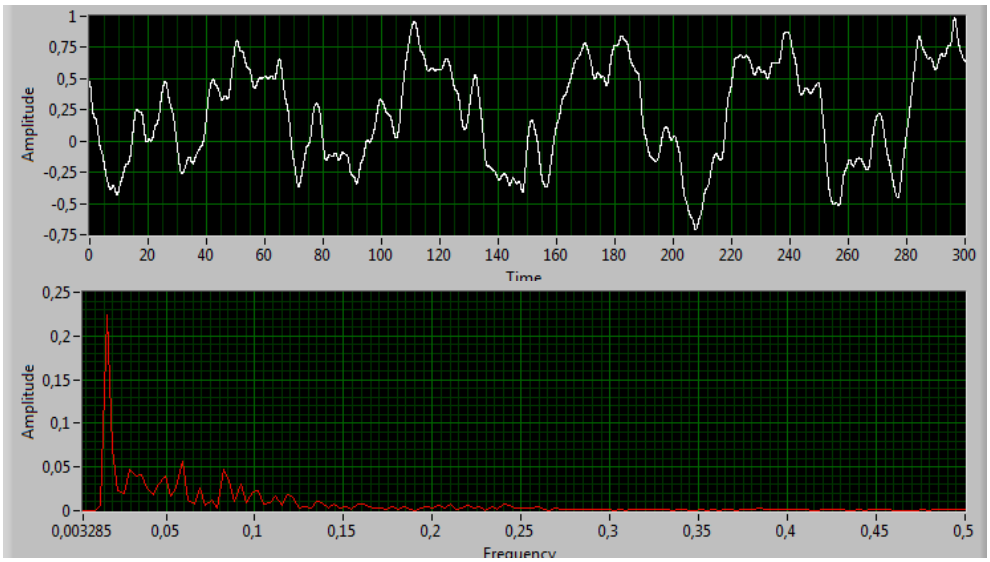

Figure 3.9 A NIRS spectrum. The 5 minute time series of the HbO_2 signal from subject 6 is shown in the upper panel. The lower panel shows the corresponding spectrum between 0.01 and 0.5 Hz. Three different peaks are seen at 0.015 Hz, 0.06 Hz and 0.08 Hz respectively.

First of all a peak in nearly all subjects was observed between 0.01-0.02 Hz. The two subjects that failed to display a peak here were both classified as having poor signal quality. Furthermore, a peak was observed between 0.025 and 0.04 Hz in nearly half of the subjects. On the O1 location a difference between the group with good and poor quality signals was not really seen whereas on the O2 location the ratios between subjects that did and did not show this peak displayed more subjects with good quality signals showing this peak.

A larger portion of subjects (nearly two third of the sample on O1 and half the sample on O2) displayed a peak in their spectrum between 0.045 and 0.06 Hz. This peak does seem to occur more often in higher quality data compared to poor-quality data.

One third of the sample displayed a peak in the spectrum between 0.065 and 0.085 Hz. Fewer peaks were seen in the 0.09-0.11 range with less than a quarter of the sample showing them. These two categories do have in common that no consistent difference was seen between the occurrence of these peaks and the quality of the obtained signals.

The last class of peaks were peaks that have a frequency larger than 0.11 Hz. This

was only seen in a limited number of subjects (3 on O1 and 1 on O2) and all subjects showed poor signal quality.

The spectral bands that were defined for the EEG signals were analyzed by means of an ANOVA for differences between the eyes open and eyes closed blocks. Since only the last 15 seconds of each block were considered in the analysis (to avoid transient features) it does not make sense to perform this analysis on the NIRS peaks that are defined here as well. The peaks indicate slow wave changes between 0.6 and 6.6 times per minute. This is too slow to base solid conclusions on when only 15 seconds of data are evaluated per block.

3.3.5 Correlating EEG and NIRS

The correlation analysis revealed no significant and only weak correlations between alpha magnitude and concentrations of either Hbb or HbO_2 (table 3.6). Generally this correlation was higher during the eyes closed blocks.

	Eyes Open		**Eyes Closed**	
	Pearson's r	*p*-value	Pearson's r	*p*-value
Alpha x HbO_2 O1	0.054	0.774	0.278	0.130
Alpha x Hbb O1	0.136	0.467	0.190	0.307
Alpha x HbO_2 O2	0.077	0.676	0.185	0.310
Alpha x Hbb O2	0.032	0.864	0.077	0.677

Table 3.6. Pearson correlations and their p-values for relationships between alpha magnitude and concentrations of oxygenated (HbO_2) and deoxygenated haemoglobin (Hbb). For measurements over the left visual cortex (O1) 31 subjects remained in the sample after outlier correction and 32 for the right visual cortex (O2). All correlation are weak and do not approach significance.

3.4 Discussion

The main goal of this chapter was investigating the possibility of simultaneously measuring neuronal (EEG) and metabolic (NIRS) resting state activity. The examination of the separate signals was highly exploratory in nature in order to determine possible parameters that can reveal the relationship between electrical and hemodynamic aspects of brain functioning. These will be addressed in

upcoming chapters. A short summary of the results will be given after which it will be discussed how these results could align with pointers for future research.

First, a static analysis was performed for the EEG frequency bands delta, theta, alpha, beta 1 and beta 2 in order to determine whether there were differences between the EC and EO blocks. It was hypothesized that slower frequency bands (delta, theta and alpha) would be higher during EC conditions whereas the faster bands (beta 1 and beta 2) would be lower compared to EO conditions. Contrary to the hypotheses, this analysis resulted in the finding that delta activity was higher during EO blocks, theta activity did not differ and alpha, beta 1 and beta 2 activity were higher in EC blocks. Furthermore, the interaction effect for the beta2 activity indicated that the difference in this band got larger over time. Second, the APF was determined and it was analyzed whether changes between the measuring conditions occurred. As it was expected that this measure would be stable, it was surprising that the analysis showed significant differences between conditions. Even though this finding was due to a relatively small portion of the sample. As expected, was the APF stable between blocks of the same condition. Third, differences in HbO_2 and Hbb concentrations between EO and EC conditions were analysed. This showed, as expected, that upon closing the eyes the HbO_2 concentration significantly diminishes and the Hbb concentration significantly heightens and vice versa. These results confirm the hypothesis that during a resting condition with closed eyes the brain activity of the occipital cortex is significantly different from a resting condition with open eyes.

Furthermore, the HbO_2 and Hbb time series were investigated by means of spectral analysis in order to reveal possible rhythmical oscillations. The first thing that was noticed was the large portion of data (over one third of the sample) that was classified as low quality data while only four subjects were classified as showing white noise. Six separate categories of peaks were defined in the low frequency part of the spectrum. Finally, in order to replicate the results found by Moosmann et al. (2003) a correlation analysis was conducted between averages of alpha wave activity and concentrations of HbO2 and Hbb. These correlations were low and did not approach significance. Possible causes for this discrepancy are mentioned below.

3.4.1 Spectrum content EEG

A significant main effect for four out of five frequency bands was found. During the EO condition more delta activity was present. During the EC condition alpha, beta 1 and beta 2 activity were higher. No significant differences were found between conditions for the theta activity. Furthermore a significant interaction effect was found for the beta 2 activity, indicating an increase of the difference between conditions over time.

As described earlier, Barry et al. (2007) found that when EO conditions are compared to EC conditions it appears that all frequency bands have higher power in the EC condition. This was not replicated in this chapter. A difference in delta activity results could be due to eye blinking. Eye blinking occurs only in EO conditions. The large potential that originates at the front of the head travels by volume conduction towards the back of the skull where the measuring electrodes are positioned. The reference electrode is placed on the Cz location and therefore this potential reaches the reference electrode sooner than the measuring electrodes, causing the common mode rejection to be unable to filter out this wave. Because of the volume conduction the potential has decreased in amplitude, causing this wave to be harder to detect while inspecting the EEG signal. However, it still heightens the delta frequency band. A filtering procedure in which these sections of data are omitted could solve this. A disadvantage of doing so will be found when the timing aspects of the EEG signal plays a role in the analysis. Furthermore, relating the origin of the enhanced delta activity in EO conditions to eye blinking in this study is speculative. The channels in which the eye blinks are most pronounced (frontal leads) are not co-registered to check for a possible mirrored artefact on occipital leads.

A reason that could lead to higher beta values during EC blocks is that drowsiness and sleepiness may have played a role. Participants often reported to be very relaxed during the paradigm and one subject admitted that he had trouble staying awake. It has been published that even in sleep stage II people can report to be awake and characteristic features in this sleep stage are beta spindles (Carskadon and Dement, 1994). This also could explain the finding that the differences between conditions got larger over time, as drowsiness increased during the paradigm and it would take less time for the beta spindles to occur (Carskadon

and Dement, 1994). For this reason there are limitations to extending resting state measures for too long, especially in a clinical setting.

For the theta band no significant difference was found. This deviation from the results indicated by Barry et al. (2007) could be due to a different methodology as their study chose to report differences in power rather than differences in magnitude as was done in this chapter. As power is the squared magnitude of a frequency band, differences that exist between conditions become more pronounced. However, as figure 3.4 shows, the small, non-significant difference that is found for theta indicates a higher magnitude in the EO condition rather than the EC condition.

As such, the question arises whether a plain analysis of frequency bands is the most appropriate analysis for QEEG profiles. From a historical perspective the QEEG bands have been defined based on waveforms that were visually recognizable (Berger, 1969a). This is the reason why the characteristic sinusoidal wave is called alpha, it was recognized first. So when an FFT is performed and an analysis is conducted that only considers values of the QEEG, it is possible that waves are defined that are not actually present. This is due to the way the FFT works; It describes the EEG time series based on sine and cosine waves, and sums as many as are needed together to obtain a resemblance of the signal (Kaiser, 2005). However, not all wave shapes are best described by a summation of different sine and cosine waves and thus this causes values to arise that are not actually present. This is a general deviation that is known to occur when the FFT is used and a reason why some researchers prefer wavelet analysis (Schwilden, 2006). Furthermore, the use of the FFT causes a correlation to arise between the different waves. Especially when the waves that occur in the EEG have a frequency that occurs on the edges of the frequency band range. A wave that has a frequency of around 7.5 Hz will influence both the height of the theta and the alpha band. For this reason it might be better to look for peaks in the entire spectrum that differentiate themselves from the background activity.

3.4.2 Alpha peak frequency

The best known peak that distinguishes itself from the background spectrum is the APF. Unexpectedly it was found that the APF differed between EO and EC

blocks, whereas it has been reported to remain stable (Grandy et al., 2013b). As pointed out in the previous paragraph, when using FFT if a wave falls in between two defined bins it will influence both. Since the spectrum was divided in 0.5 Hz bins, this is a feature that could have caused variation between the two blocks. However, this cannot explain why some subjects showed large shifts (1.5-2.5 Hz) between both conditions. Together with the striking observation that it is a relatively small subgroup of the participants that caused the results to reach significance (only 3 out of 33 subjects showed this systematically, and 10 others sometimes), an explanation might need to be sought elsewhere.

A potential explanation is an age related difference. As it is known that the APF decreases with age (Kopruner et al., 1984, Bazanova and Vernon, 2013) the difference between EO and EC conditions might be age related as well. However, even though age varied greatly in the investigated sample, subjects of different ages showed a decrease.

It has been reported in the literature that there is a small percentage of people that show an APF below the traditional alpha band (Klimesch et al., 1993, Richard Clark et al., 2004). This was not the case in this study. However, three subjects displayed a double peak of which the lower one was lying just outside the defined alpha spectrum or at the lower boundary (≤ 7.5 Hz). When the EEG signal was inspected in all three cases theta shaped waves were present together with the alpha waves. Therefore in all cases the higher peak was chosen as APF. This again illustrates the importance of checking the measured signal and having knowledge of it besides being able to handle and manipulate the data that come from the spectra.

Furthermore, the differences in width of the APF base could have played a role. Wider peaks most likely show more variation in which bin is the highest at certain time points than small peaks do. In the 4 types of APF that were found, two have a wide base. Additionally, when a higher magnitude of the APF is seen, the base of the peak is automatically wider. However, the people that displayed an APF with a wider base were not always the ones that showed a change from EO to EC. To illustrate this with an example, both subject 3 and 20 showed a wide base APF but only subject 3 showed a large shift between EO and EC while the alpha peak of

subject 20 was stable. So where the type (base and height) of the APF might play a role at some level it is not the missing link in the results that were obtained here.

Another possibility could be the methodological approach. Different approaches are described in the literature to determine APF. Lansbergen et al. (2011) report a method of defining APF in which during an EC condition a spectrum and peak are defined from which the spectrum found during the EO condition is subtracted in order to see where the largest alpha suppression is. Furthermore, when between different electrodes no differences larger than 0.5 Hz are found the electrodes of the O and P locations are pooled together. By adopting this approach differences between EC and EO are cancelled out and are unreported. From a methodological point of view it might therefore be best to not only distinct the APF based on visual inspection of the spectra and the signal, but to test statistically whether such a peak is actually different from the background of the spectrum. Hereby one should take into account the actual signal to noise ratio of the EEG itself.

Additionally there is the possibility of a functional explanation. As having a higher APF has been coupled to faster speed of information processing (Klimesch et al., 1996), better cognitive performance (Grandy et al., 2013a), better memory performance (Klimesch et al., 1993, Richard Clark et al., 2004) and higher intelligence (Grandy et al., 2013b) the toning down of the APF during EC conditions could be an indication that the brain is switching to a state in which information processing is altered to a slower level. Since cognitive performance and intelligence was not measured in the current research it is impossible to verify whether changes in these parameters between subjects caused the differences. From the point of view where the brain adapts to circumstances in which a more functional energy distribution is adopted this might make sense.

3.4.3 NIRS concentration changes

For the concentration changes in HbO_2 and Hbb between EO and EC blocks it was found that during EO blocks the HbO_2 concentration is higher and the Hbb concentration is lower. For the EC blocks these findings are reversed. These results align with reports stating that when the brain gets more active, the CBF is increased and more glucose and oxygen bound to haemoglobin is delivered to that brain area (Irani et al., 2007). The visual cortex is processing more

information in an eyes open state as opposed to an eyes closed state, after all. An increase of Hbb concentrations in EC blocks and a decrease in EO blocks was also reported by Moosmann et al. (2003). Note that the concentration changes in this chapter refer to changes in the average of the second half of every block to correct for differences in timing between EEG and NIRS parameters.

3.4.4 Spectrum content NIRS

The quality labelling of the Hbb and HbO_2 signals showed that a large portion of the NIRS data (between a half and two thirds) was labelled as poor quality data. This does not comply with the number of outliers that were found before the ANOVA analyses were conducted (3 on each location). When the entire time series are evaluated, the signal to noise component becomes more important. A possible reason could be that the sensitivity to detect hemodynamic responses is not always optimal in NIRS measurements. A recent study by Biallas et al. (2012) showed that in NIRS measurements conducted with a CW device, depending on the data cleaning algorithms chosen, the sensitivity of NIRS measurements varies between 40 and 55.2 %. This is in line with the amount of bad quality data detected here. This quality labelling also showed that that the measurements on O1 were slightly better in quality than those on O2. Possibly this is caused by the fact that the human brain is slightly rotated which causes the distance from the optode to the neocortex to be a little larger for the O2 location than for the O1 location (Toronov et al., 2007). If NIRS is going to be of any added clinical value the quality of the signals needs to increase, either by improving the optodes or optode holders or by means of signal cleaning processes.

The spectral analyses of the HbO_2 and Hbb time series showed that all oscillations that are found are within the part of the spectrum that is investigated during resting state network (RSN) analysis. Five of the six peaks that were identified fell between 0.01 and 0.11 Hz. The sixth peak was larger than 0.11 Hz but only seen in a few subjects of whom all received a bad signal quality label, which makes it likely to be related to noise.

In RSN analysis of NIRS signals often a range between 0.009 and 0.1 Hz is used (Tong and Frederick, 2010, Zhang et al., 2010, Sasai et al., 2011). This is quite a wide range when in this study 5 different peaks could be distinguished within this

range. However, the origin of the first peak (0.01-0.02 Hz) could possibly be related to the border of the Fourier filter being set at 0.01 Hz or occur because the NIRS signals have an offset. Furthermore, it is likely that the peaks seen in the second range (0.025-0.04 Hz) are related to the task, since an event occurring every 30 seconds would appear in the spectrum as a peak at 0.033 Hz.

The third category of peaks (0.045-0.06 Hz) most likely finds its origin to be coupled to heart rate variability (HRV). Whereas the exact frequency of the heart rhythm (around 1 Hz) is filtered from the signal in an early stage of signal processing, a variation in the timing from beat to beat exists for every person. The fluctuation of this HRV is also visible in the spectrum. From HRV a high frequency and a low frequency component can be derived. The centre of the low frequency component fluctuates between 0.04 and 0.13 Hz (Malliani et al., 1991). The variation of this component could be the reason why it is visible in a large portion of the subjects but not all.

The fourth (0.065-0.085 Hz) and fifth peak (0.09-0.11 Hz) are possibly caused by blood pressure changes. In chapter 2 it has already been described that blood pressure changes can cause noise in the frequency domain between 0.08 and 0.12 Hz (Boas et al., 2004, Huppert et al., 2009, Zhang et al., 2007a, 2007b, 2009). This could either be caused by intrinsic blood pressure variation, variation coupled to heart rate, Mayer waves, low frequency oscillations (LFOs), very low frequency oscillation (VLFOs), and vasomotor waves (Zhang et al., 2005, 2007a, 2007b, 2009) as well as HRV (Malliani et al., 1991).

This would lead one to argue that all peaks have a noise component in them and are therefore not related to an underlying physiological brain response. However, Pfurtscheller et al. (2012) have shown that prefrontal oscillations in NIRS measurements between 0.007 and 0.13 Hz were coupled to alpha or beta waves in the EEG and that in these cases no coupling to blood pressure existed. It might thus be too easy to dismiss the peaks found as noise. For future research it is therefore desirable to co-register variations in blood pressure and respiratory rate with an external measurement in order to entangle these noise features. Within this sample there does not seem to be an oscillation that is found in all subjects, as APF is for the EEG.

3.4.5 Correlating EEG and NIRS

No significant correlations could be found between average alpha activity and concentrations of HbO2 or Hbb over EO and EC blocks. This occurred despite the fact that the separate measurement modalities did show differences between conditions suggesting a potential positive correlation between alpha activity and Hbb and a negative correlation between alpha activity and HbO2. The correlations that were found were stronger during eyes closed though which could be due to a more stable measurement during EC conditions.

Koch et al. (2008, 2006) as well as Moosmann et al. (2003) did find an inverse relationship between alpha activity and the hemodynamic response. The most plausible explanation for this difference is a methodological one. In terms of analysis this study is limited by the static nature of all analyses performed. Since only average values of blocks are considered, nothing can be said about changes that occur over time. This could be the most important reason that the correlation analysis did not lead to significant results: only average values over all EO blocks and average values over all EC blocks were used. When entire time courses would have been considered in a cross correlation analysis like Moosmann et al. (2003) used, or use was made of the running correlation as described by Cui et al. (2010) a more adequate result could have been obtained, with additionally an indication of time lag between the investigated parameters. This approach will be adopted in follow-up research.

Another possible explanation of the lack of statistical coupling between the electrical and hemodynamic parameters may be that still a controversy exists whether optical changes due to neuronal changes that are seen in vitro and during invasive measurements can be detected non-invasively by NIRS in human adults (Steinbrink et al., 2000, Wolf et al., 2003, Franceschini and Boas, 2004, Steinbrink et al., 2005, Medvedev et al., 2008, Gratton and Fabiani, 2010, Tse et al., 2010, Biallas et al., 2012). Biallas et al. (2012) tested the sensitivity and reproducibility in 15 subjects of combined NIRS and EEG measures over the visual cortex during visual stimulation. Different from the paradigm chosen in this chapter the electrical parameter that was focused on was the visual evoked potential, which is a specific wave caused by visual stimulation as opposed to

changes in background activity. As reported in the previous paragraph the sensitivity of NIRS to detect hemodynamic changes was between 40 and 55.2 % additionally the reproducibility within a subject was low. For EEG both the sensitivity of the visual evoked potential as well as the reproducibility was higher, being 86.4 % and 57.1 %. When using the visual evoked potential no optical neural signal was detected (Biallas et al., 2012). However, the authors chose to measure NIRS over the O1 location while measuring EEG over Oz. Since NIRS measurements are very localised the measuring of two different locations may have contributed to the lack of neuronal coupling in this research. Furthermore, the choice of changes in background activity may lead to very different results which reinforces the choice of looking at changes within the alpha band.

3.4.6 Additional methodological issues

Some methodological points of this study need to be addressed. First of all, in order to investigate resting state activity this study chose to pair eyes closed resting state activity with a condition in which subjects were observing a static picture of a test screen. During other studies in which resting conditions with eyes closed and eyes open are investigated often a fixation cross is used in the eyes open condition instead of the currently used stimulus of the test screen. This might have been leaning too much towards a visual task and could have caused the differences between eyes open and eyes closed to be larger than they would have been without this stimulus. However, studies investigating eyes open versus eyes closed conditions in dark rooms in order to minimize visual stimulation during the eyes open condition have shown similar results for the alpha wave activity and Hbb responses (Moosmann et al., 2003).

Secondly, this study chose to use very few restrictions on the age of the participants. The only condition was that every participant had to be between the ages of 18 and 60. This resulted in an age range from 19-60 which is quite large. However, using a broad age range allows a study to have an exploratory nature, this was also the reason for including both male and female participants. The decision to start at 18 was that this study intended to investigate the relationship between neuronal brain activity and metabolic activity in adults. The cut-off point of 60 years of age was made based on the fact that from the 5th decade onwards the brain starts to exhibit shrinkage of the white matter volume and a significant

change of basal metabolism is found from 70 years of age onwards (Raz and Rodrigue, 2006). Ultimately, this approach led to the inclusion of 38 participants and provided the research with an ecologically valid sample to test a new paradigm which will be expanded over the upcoming chapters. Especially since a link is made to the brain during pathology in chapter 6 this ecological validity in studying healthy brains needs to be emphasized.

Furthermore, in this study a setup with two channels for EEG and two channels for NIRS was used. Using a minimal setup allows a study to test a model or hypothesis without burdening the participants greatly. When results are found in an exploratory study with a minimal setup, this model can be expanded and fine-tuned by using a more precise set-up or moving to other brain areas. Besides that, using more channels eventually also allows different types of analysis to be conducted such as connectivity analysis to investigate resting state networks.

The practical side of doing multiple channel measurements needs to be addressed though. While measuring over 40 people with use of two modalities it became apparent that getting a clear signal is not always easy. The EEG signals are not the delaying factor, although in bald people it is tough to get impedances to fall below 10 kΩ, and in people with very short hair the hair sometimes pushes the electrode away from the scalp. However, because the optode holder is secured over the electrodes, mostly this prevents shifting and it holds the electrodes nice in place as well. The NIRS measurements are more difficult. With some people it seems impossible to get a good response on both channels, which will increase when more channels are added to the experimental setup. It seems that in dark haired subjects, even though the hair often could be pushed away from to area under investigation, yield bad signals more often. A distinction between long haired and short haired subjects could not be made. The setting up of the equipment, even though small in number of electrodes and channels therefore took up the larger share of the experimental time, which bored participants. Especially when moving toward investigating subjects with any pathology one cannot expect full cooperation or attention during the following experiment which makes me reluctant to expand to more channel measurements. Only when a quicker way of setting up can be found, possibly with alterations to the optodes and preparation times can be reduced this will be feasible. The paradigm was easy to comply with

for all subjects in the age range. Therefore I would not expect difficulties with the paradigm when expanding the research group in terms of age or pathology.

3.5 Conclusion

Even though methodological issues can be raised in this study, the data that were obtained in a large and variable population in terms of age and sex were of high enough quality to establish that it is feasible to use EEG and NIRS measurements simultaneously in resting state conditions. Especially when it is kept in mind that clinical feasibility is warranted when applications are considered in which these brain measurements during resting state conditions can aid in diagnostic and prognostic procedures, although multiple channel measurements may be difficult at this stage. It was also established that the states of eyes open and eyes closed are significantly different. In terms of EEG the alpha band will remain the selected feature of which the coupling with the hemodynamic parameters will be sought. The main reason for doing so is the fact that the alpha peak is the only peak that stands out from the background spectrum. Furthermore, the variability between the APF that was found in this study will have little influence when the whole alpha band is chosen since it falls within this range. Besides that, the other frequency bands did not display changes similar to those reported before or as hypothesized.

The NIRS parameters that will be chosen will be the HbO_2 and Hbb concentrations. The spectral investigation did not reveal a feature similar to the APF which is present in all subjects. Therefore the entire range of 0.01-0.5 Hz will be analyzed in upcoming chapters. Besides that, the quality check of the NIRS data revealed a large portion of poor quality data, which is a point that needs to be addressed before the method can be transferred to the clinic. The largest methodological drawback in this exploratory chapter was the static method of analysing brain activity. Since the brain is active all the time, the aspect of time might be a missing link in unravelling the brain's symbioses between electrical and metabolic activity. Therefore, upcoming chapters will move towards dynamic analysis methods.

Chapter 4: Exploring the dynamics of EEG and NIRS signals in an eyes open- eyes closed paradigm

In the previous chapter changes in the brain's electric and hemodynamic activity over the visual cortex were investigated with static analysis in a block eyes open/eyes shut design. Subsequently, alpha magnitude was correlated against the changes in hemodynamic parameters in a static fashion. This investigation found no clear relationship in brain measures. Limiting an investigation to the use of static changes, limits understanding of the brain dynamics and the underlying mechanisms. Therefore, the aim of this chapter was to move towards a more dynamic method for analyzing brain activity.

4.1 Introduction

4.1.1 The brain as a dynamic system

The course of analysis as undertaken in chapter 3 leans entirely on finding differences between blocks. And while this is quite common in neuroscience and generates findings that lead to new, testable hypotheses, it omits the important fact that the brain is a dynamic system (McKenna et al., 1994, Fox et al., 2005). A biological dynamic system is a self organizing system that is continuously adaptive on all levels in order to maintain homeostasis despite the ever changing influences both from inside and outside (Friston, 2010). When an approach is adopted that explores changes over time, the dynamics of the brain as a biological system can be respected, and its functioning better understood.

Friston (2010) argues in his review that the free energy principle has common ground with some of the current key theories about global brain functioning since they all centre around the theme "optimization". Basically the free energy principle says that for a biological system to be able to maintain homeostasis, it needs to function within predefined physiological bounds. This can only be achieved when the element of "surprise" (an improbable outcome or state the brain is in) is avoided. The free energy element is the upper bound on surprise. Since a system does not know whether a state is surprising it does not know how to avoid it, but when free energy is minimized, the surprise element is minimized

implicitly as well. Since free energy is a function of sensory states and a recognition density (a probability distribution of the causes for these sensory states) and this is internally encoded in the brain, it is possible to evaluate the free energy. Now the system can change the free energy (and therefore limit the surprise) by either changing the sensory input by acting on the world, or by changing the recognition density, by changing the internal state. How this exactly relates to the current views on brain functioning falls beyond the scope of this chapter but can be found in the review by Friston (2010). Elements from biological, dynamic systems that do need additional attention are "scale invariance" and "self-organized criticality".

Scale-invariance or fractality is the property of many systems to display the same feature over several scales of magnification both in space and time (Bullmore et al., 2009). Scale-invariance is seen in many (biological) systems. For example, when the lungs are examined and one zooms in several times, the same tree like branching structure can be observed. This also holds true for the coastline of Norway, which shows interruptions by fjords, but at a closer look these interruptions themselves are interrupted by fjordlets (Bullmore et al., 2009). These examples illustrate fractality in space. However, when time series like for instance EEG are considered it is possible to explain fractality over time as well. When an EEG signal is considered, and a 10 second interval is observed, it is visible that the signal fluctuates around the nil-line and that it is made up of different kinds of waves (large, small, large waves with small waves on top etc.). When a 5 second interval is examined this picture does not change, and even at a smaller interval of 2.5 seconds this property will hold (figure 4.1). And it is not just within seconds that this scale-invariance is seen. In early EEG work it has been documented that rhythmical changes occur during the course of the day due to the circadian rhythm and ultradian rhythms (that represent fluctuations within the circadian rhythm) but also over seasons (Machleidt and Gutjahr, 1984).

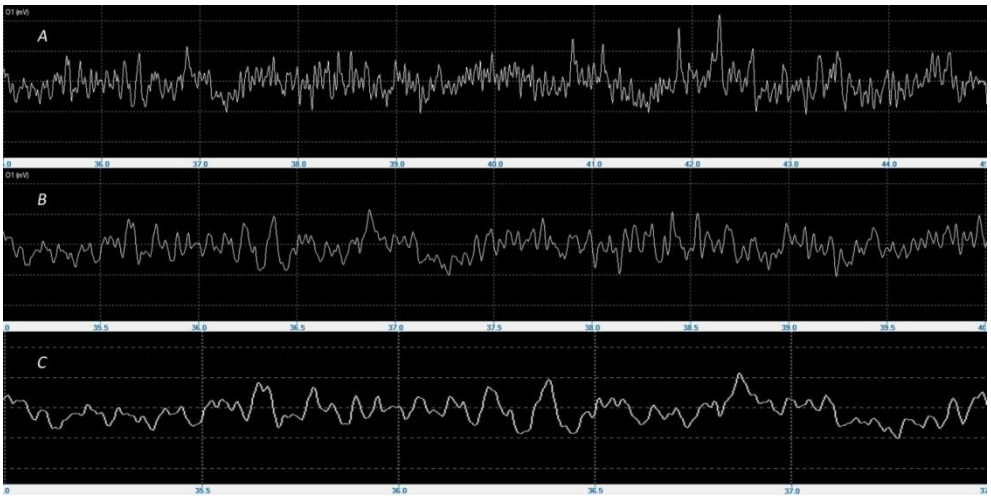

Figure 4.1 Fractality of an EEG time course. In panel A the 10 seconds of EEG is displayed. The signal varies around the nil-line and is made up out of different waveforms. In panel B the same signal is displayed, but only 5 seconds are visible and in panel C only 2.5 seconds are displayed. The properties of fluctuation around the nil-line and consisting out of different waveforms, remain unchanged despite the change in time.

The definition of Linkenkaer-Hansen et al. (2001) for scale-invariance, or scale-free behaviour as they call it, states that no characteristic scales dominate the dynamics of the underlying process. From a spectrum perspective, this would mean that no specific frequency would be visible in the spectrum. However, as was demonstrated in chapter 3, human EEG usually displays a peak frequency within the alpha range (the APF). When the specific peaks that are seen in the EEG are investigated further, it becomes clear that these separate peaks display scale-invariance (Linkenkaer-Hansen et al., 2001). The power of the alpha band varies on different time-scales in a healthy brain and this changes in pathologies such as depression (Leistedt et al., 2007) and schizophrenia (Nikulin et al., 2012). For NIRS, scale-invariant properties have not been described in the literature to date.

When a specific wave displays scale-invariance and responds in different time domains, more often than not long range correlations in space and time are observed (Bullmore et al., 2009). These long range correlations make sure that a change in a small unit of the system can be communicated quickly throughout the entire brain (Haimovici et al., 2013). The long range correlations are known to display power law behaviour. Power law behaviour occurs in many dynamic systems, for instance avalanches or forest fires, and tells us that massive forest fires occur less often than smaller ones (Bullmore et al., 2009). The relationship

between the occurrence of a forest fire and the size of it can be expressed by a straight line on a log-log scale (a power law). Power law behaviour as well as scale invariance are properties of a self organised critical (SOC) system, which is detailed below.

SOC was first explained by Per Bak and collegues (1987) and is easiest explained by their sand pile model. In this model sand grains are randomly dropped onto a grid. This causes a pile of sand with a certain slope to arise. By randomly dropping additional sand grains on the pile the pile grows and the slope changes. At a certain point the sand pile is in a critical state and when a new grain of sand is added either nothing happens or the sand starts to slide and affects a lot of neighbouring sand grains. The sand slides again display power law behaviour with regards to their magnitude. This sand pile model illustrates that a SOC system (a pile of sand in a critical state) emerges spontaneously from the random interactions between the agents in the system (the sand grains) and that changes in the system are caused by the addition of energy to the system (adding sand grains causes sand slides). SOC can also be found in the dynamic properties of electrical brain activity (Linkenkaer-Hansen et al., 2001, R Chialvo, 2004, 2006, Bullmore et al., 2009).

When it is assumed that in a resting state the brain is in a state of SOC, the alpha band also should display its markers, namely that of power law behaviour. This will be investigated in this chapter. Many forms of analyzing time series and brain dynamics exist (Cold and Cold, 2007, Michel and Murray, 2012). The analysis that will be explored here is the long range temporal correlation (LRTC) which gives a number for the slope of the straight line in the power law (Linkenkaer-Hansen et al., 2001). In EEG research the use of LRTC has revealed its value in differentiating pathology from health and is therefore an interesting approach worthy of investigation (Linkenkaer-Hansen et al., 2005, Montez et al., 2009, Nikulin et al., 2012). First it will be investigated whether a straight line (a power law) can be found for changes in the magnitude of the alpha band over time and if so what the slope of this line is. The higher the steepness of the slope, the larger the amount of energy that evaporates from the system and the shorter in time the correlations are. The less steep the slope is, the longer is the memory trail and therefore it is easier it is to determine how the system will behave. Then it will be

investigated whether this power law behaviour and its slope is specific for the alpha band by scrambling the order of the occurrence of the waves in surrogate signals. Furthermore it will be investigated whether the NIRS parameters HbO_2 and Hbb display power law behaviour. As was argued in chapter 3, the spectral analysis did not reveal individual peaks like the APF that is seen in the EEG. Therefore the whole frequency range of these parameters (0.01-0.5 Hz) will be considered.

4.1.2 Investigating dynamic relationships

In the previous chapter the correlation analysis between the electrical and hemodynamic modality, was static with block averages correlated against each other. When it is assumed that the brain operates as a dynamic system it might be more appropriate to analyse the relationship between electrical and metabolic features in a dynamic fashion a well. Several analysis techniques exist to investigate the correlation between two time series. In chapter 2 use was made of the running correlation (RC) (Cui et al., 2010) to investigate noise in the NIRS signals. It would be possible to use the RC in the current paradigm to correlate the alpha fluctuations with the HbO_2 and Hbb time series separately. Since it is suspected that the NIRS signal will correlate at a delay of around 8 seconds (Moosmann et al., 2003) the window of the RC would need to be adjusted in order to capture this. However, no matter how large the window is made, it slides as fast along signal x as it moves along signal y, so the optimal match will possibly never be made. Therefore, it would make more sense to use a correlation analysis method that uses a time lag on one signal like the cross correlation method (Box et al., 2013), which was also the analysis method of choice by Moosman et al. (2003).

To summarize, the dynamics of the alpha band will be explored in order to determine whether there is power law behaviour by means of long range temporal correlation (LRTC) analysis. NIRS time series will also be analysed to explore if these show power law behaviour too. Finally, the correlation between the fluctuations of the alpha band and fluctuations in HbO_2 and Hbb concentration over time will be investigated by means of cross correlation analysis.

4.2 Methods

4.2.1 Subjects

In this chapter the data from the same group of participants were used as in the previous chapter. This means that there were 38 subjects in the sample (21 female) and the age range was 19-60 years (mean 37.74, SD 13,30). All participants volunteered to participate in this research and signed a consent form after the testing procedures were explained to them. They also completed a questionnaire before testing procedures commenced in order to rule out neurological, psychopathological or vascular disease. Medication that could possibly affect brain activity was also an exclusion criterion.

4.2.2 Paradigm and Equipment

The paradigm used is similar as is reported in chapter 3, paragraph 3.2.2 and a schematic representation of it can be found in figure 3.1.

4.2.3 Equipment

A description of the EEG and NIRS amplifiers can be found in paragraph 3.2.3 of the previous chapter. The electrode and optode positioning is clarified and illustrated in figure 3.3.

4.2.4 Data Analysis

4.2.4.1 Fluctuation of Alpha power

In order to determine the fluctuation of the alpha power over time, the alpha envelope was calculated by performing a Short-Time Fourier Transform (STFT) over the entire 5 minute measurement. The parameters of the STFT were set to 5 data point time steps, 1000 frequency bins, a rectangular window with a length of 250 samples, and a power spectrum was used during the analysis. These parameters were chosen as they generate stable results for EEG measurements collected with a sample frequency of 250Hz (as stated in personal communication by Björn Crüts, PhD student at Imperial College London, August 14th 2012). The power (μV^2) of the 7.5 – 12 Hz alpha band was plotted and saved in a new time series with a sample frequency of 50 Hz. An example of the alpha envelope is presented in figure 4.2.

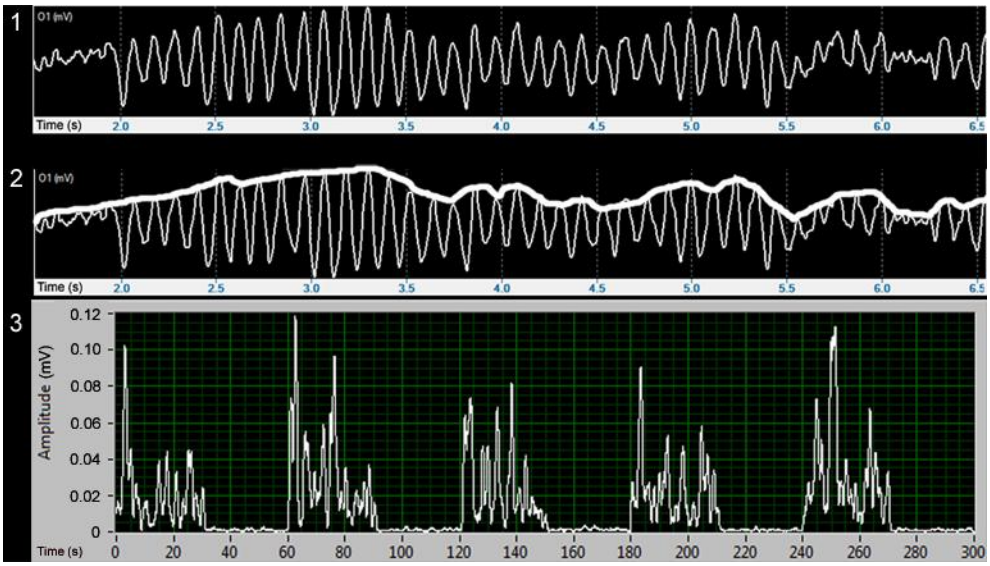

Figure 4.2 A simplified illustration of the retrieval of the alpha envelope. 1. The EEG trace from the O1 location is plotted. In this example 5 seconds of EEG is shown 2. The alpha band between 7.5 and 12 Hz is selected and it is determined what the alpha amplitude is at every time point. Shown by the bold white line. 3. The alpha amplitude at every time point is plotted in a new time series. Here shown for the entire 5 minute measurement, representing the alpha envelope. A clear distinction can be seen between blocks of eyes open and eyes closed data in which the eyes closed blocks show enhanced alpha amplitudes.

For the alpha envelope of each subject for both hemispheres it was determined whether a good or a poor response was seen in a similar fashion to the quality check that was performed on the NIRS signals in chapter 3. The quality of the response was again defined as whether a response was seen that followed the paradigm. When a strong response (2 SD or larger change from baseline) was seen in all repeats (5 out of 5), the quality was marked as “good”. When a response was faint for some repeats or inconsistent (2 or 3 out of 5), the signal was marked as “medium”. When no response (under 2 SD change from baseline) or only noise was observed, the quality was marked as “bad”. “Good-medium” or “medium-bad” qualifications were given to signals that fell in between two other qualifications. These labels were used to divide the group into a good-quality and a poor-quality group. All signals that were marked as “good”, “good-medium”, or “medium” were taken together in the good-quality group and the “medium-bad” and “bad” classifications were taken together in the poor-quality group.

4.2.4.2 LRTC analysis

A Fourier Transform was then performed on the alpha envelope, the HbO_2 time series and the Hbb time series. This FFT was plotted on a log-log scale in order to determine whether long range temporal correlations (LRTC) were found as a prerequisite of scale-invariant behaviour (figure 4.5). Hereto a rectangular window was used and the lower and upper bound of the frequency range of the log-log plot were set to 0.1 and 10 respectively. Which again were chosen because of their stability of the results (as stated in personal communication by Björn Crüts, PhD student at Imperial College London, August 14th 2012). Then it was determined whether the plot showed a straight line and if so, what the slope of this line was for both the O1 and O2 location.

Simultaneously, for each signal that was used for LRTC analysis, a surrogate signal was created in which the phases of the waves were mixed. By doing so the time series differ from the original while the spectra remain unchanged (Linkenkaer-Hansen et al., 2001). An FFT was performed on the surrogate signal and plotted on a log-log scale. This plot was evaluated for a straightness of the line and its slope is determined. Subsequently, a Wilcoxon signed ranks test was performed to investigate whether differences existed between the measured data and the surrogate data. Then this test was repeated on the good quality and poor quality data group separately to investigate possible differences between these groups.

4.2.4.3 Correlating EEG and NIRS over time

In order to investigate the coupling of the electrical brain activity and the hemodynamic response, the time series of the alpha envelope obtained for LRTC analysis was correlated against the concentration changes in the HbO_2 time series as well as the Hbb time series. Important in correlating two time series is that they move at similar time steps. The alpha envelope that was extracted from the EEG had a sample frequency of 50 Hz. Since the NIRS time series were sampled at 25 Hz, the alpha envelope had to be down sampled to 25 Hz. This was done by omitting every second data point from the alpha envelope sequence.

The two signals were then correlated against each other by means of a cross correlation function (CCF). The CCF plots a graph of the linear correlation between the two time series at different lags. Since a delay of around 8 seconds was

expected, the signals were analyzed for all lags between -10 to 10 seconds (-250 to 250 samples) in which the signal containing the hemodynamic information was the lagged time series. The height of the maximal (or minimal) correlation (or anti-correlation) and its accompanying time lag was obtained for all subjects. Then it was investigated whether signal quality influenced either correlation strength or timing by first omitting the signals that had received a bad quality label and second by also omitting physiological illogical data. Physiological illogical data were defined as data showing a negative and therefore unexpected time delay between the signals, indicating that changes in the hemodynamic parameter precede changes in electrical activity.

4.3 Results

4.3.1 Scale-invariance of Alpha power

As previously performed with the NIRS signals in chapter 3, the quality of the alpha response was evaluated. The quality labels that were used consisted out of 5 categories: good, good-medium, medium, medium-bad and bad. These categories were merged into a good-quality and a poor quality group. Table 4.1 shows the number of good-quality and poor-quality signals and shows that 26 out of 38 subjects (68,4%) had good signal quality. When the quality of a signal was good for the O1 location it was also good for the O2 location.

	Alpha O1	**Alpha O2**
N (total)	38	38
N (good-quality)	26	26
N (poor-quality)	12	12

Table 4.1. The number of subjects (N) that fall into each quality category for the alpha envelope on both the left occipital (O1) and right occipital (O2) location.

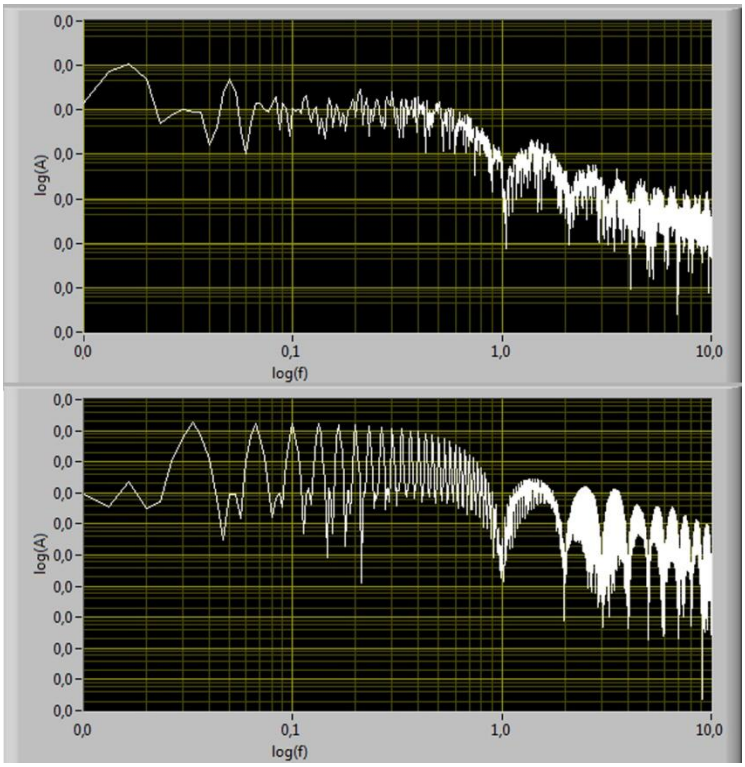

Figure 4.3. Long range temporal correlation (LRTC) slopes. The upper panel shows the LRTC graph of subject 15 in which the dip around log(f) = 1.0 is visible. The lower panel shows the LRTC graph of subject 18 who shows an artefact in every transition from EC to EO and vice versa.

Subsequently it was investigated whether the LRTC plot resulted into a straight line. A typical example of a LRTC plot in this study is illustrated in figure 4.3 (upper panel, subject 15) along with an atypical response of subject 18 who showed an artefact in the EEG every time the switch was made from eyes open to eyes closed and vice versa (lower panel). In the typical response, all subjects showed a dip in their LRTC slope at log (frequency) = 1.0. This dip can be explained by the way the paradigm was set up. Every 30 seconds the subjects change conditions (EO to EC and EC to EO) leading the amplitude of the alpha activity to be modulated, increasing when eyes were closed and decreasing when eyes were opened. This caused a slow wave at the transit phases within the alpha envelope which appears as a peak around 0.01 Hz in the spectrum that was obtained when the FFT is performed on the alpha envelope and causes the dip at 0.1 on a log scale in the otherwise straight line. Because the paradigm can explain this peak it is safe to conclude that the lines obtained for the subjects in this study are straight lines. The plots did show jitter which increases towards the end of the tail. However,

this is common in LRTC plots (Linkenkaer-Hansen et al., 2001). The lower panel of figure 4.3 shows that when large artefacts are present in the signal, the LRTC plot is also affected and will show multiple dips in the slope.

The linear slopes of the LRTC analysis were all negative and ranged from -3.18 to -1.41 for the O1 location and from -3.13 to -1.53 for the O2 location. In figure 4.4 an example of the difference between the alpha envelope and the accompanying surrogate signal is displayed. The original and surrogate signal have an identical spectrum, however these time series are created to have no temporal correlations (Linkenkaer-Hansen et al., 2001). The linear slopes of the obtained surrogate signals ranged from -2.93 to -1.35 for the O1 location and from -3.02 to -1.39 for the O2 locations. The Wilcoxon signed ranks test showed that the linear slopes of the surrogate data were significantly different from the slopes of the LRTC from the original alpha envelope data for both the O1 (z = 4.967, N-Ties = 38, p = 0.000) and the O2 (z = 4.713, N-Ties = 36, p = 0.000) location. Indicating that the original data resulted in steeper linear slopes than the surrogate data.

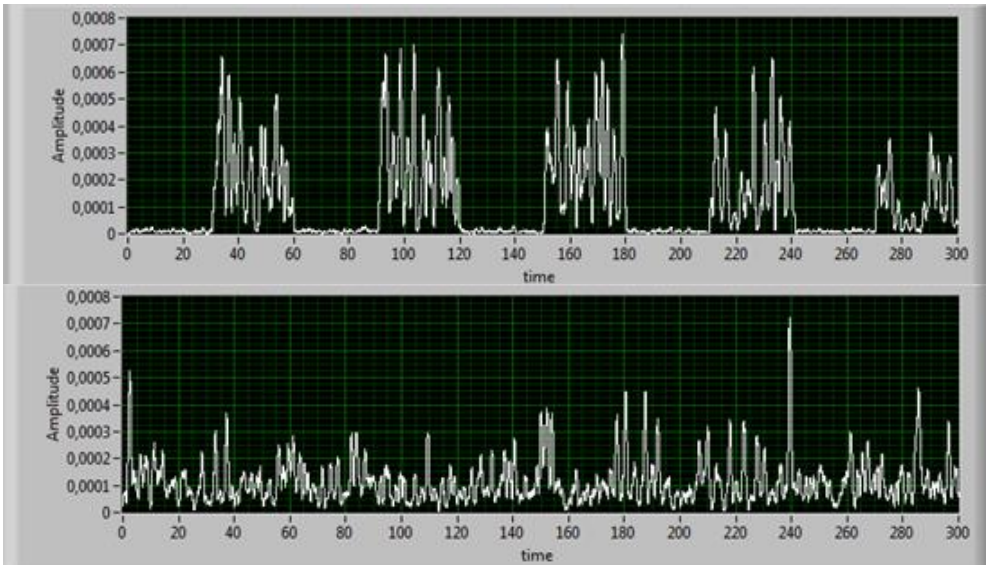

Figure 4.4. The alpha envelope and its surrogate signal. In the upper panel the original alpha envelope from the O1 location of subject 15 is displayed and in the lower panel its surrogate signal in which the phases of the waves are shuffled. A surrogate signal has a spectrum that is identical to the spectrum of the original signal but has no temporal correlations.

When the tests were repeated for the good-quality sample and the bad quality sample separately the difference between original and surrogate data remained

intact. In the good-quality group (N= 26) the slopes of the original data were steeper for the O1 (z = 4.000, N-Ties = 26, p = 0.000) and the O2 (z = 3.780, N-Ties = 25, p = 0.000) location. And in the bad-quality group (N=12) this finding was also true for both locations, O1 (z = 3.059, N-Ties = 12, p = 0.002) O2 (z = 2.845, N-Ties = 11, p = 0.000).

A difference that was found between the good-quality and the poor-quality sample was the value of the slope. The good-quality sample had an average slope for O1 of -2.60 (range –3.19 tot -1.71) and for O2 of -2.66 (range -3.13 to -1.96). Whereas the bad-quality sample has an average slope for O1 of -1.80 (range –2.30 tot -1.41) and for O2 of -1.85 (range -2.15 to -1.53). This showed that the slope becomes less steep when the data do not show the expected response upon the opening and closing of the eyes.

4.3.2 Scale-invariance of NIRS parameters

Since no distinguishing peak could be found in the spectral analysis of the NIRS time series in the previous chapter, the entire 0.01-0.5 Hz part was used for the LRTC analysis. The analysis parameters were adjusted for NIRS signals to: 5 second time steps, 1000 frequency bins, a window length of 25 samples with no predefined shape, and again a power spectrum was used. The example in figure 4.4 shows that the analysis does not yield a straight line on the log-log scale in step 5. This possibly occurs because of the large changes that are seen in the Hbb (and HbO_2) concentration due to the paradigm. As figure 4.5 shows on the right hand column, even when the phases of the signal are shifted in the surrogate signal, the slow wave underlying the paradigm remains recognizable and results in a nearly similar envelope. Since this was something that was found in both Hbb and HbO_2 time series and for all subjects it was decided not to continue the LRTC analysis for the NIRS signals.

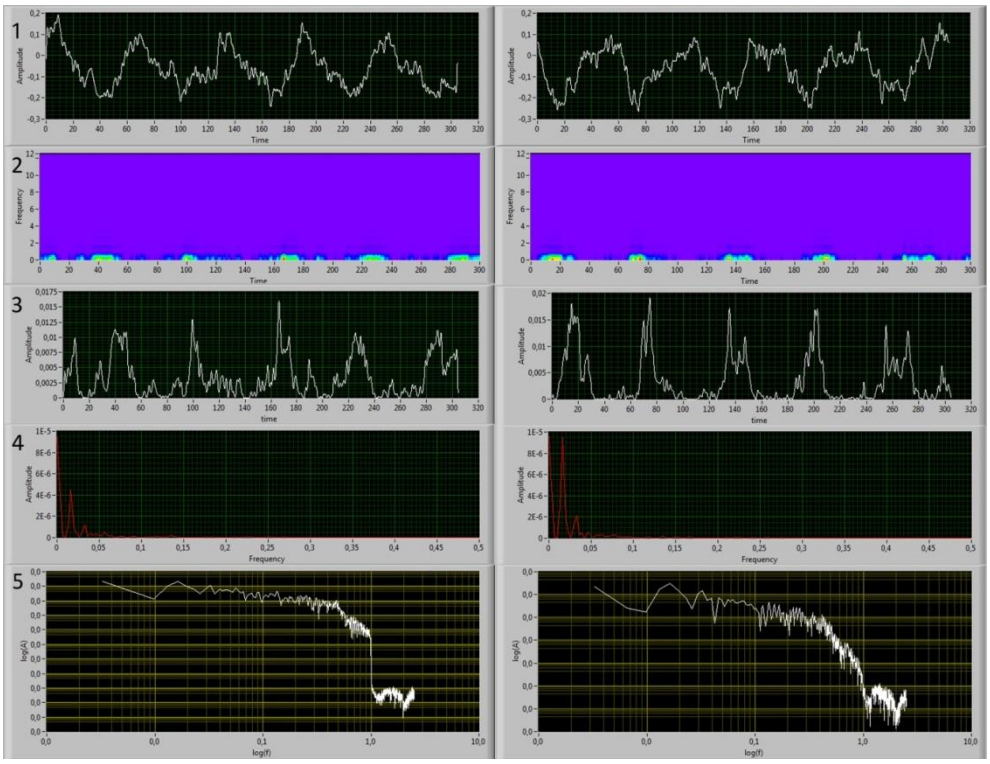

Figure 4.5. Long range temporal correlation (LRTC) analysis on a deoxygenated haemoglobin time series. The left hand column depicts all steps undertaken in the LTRC analysis: 1. The measured signal is plotted, 2. The short time Fourier transform (STFT) is depicted in colour, more red indicates a higher intensity, 3. The selected frequency band (in this case 0.01-0.5 Hz) is plotted in a new time series (the envelope), 4. A fast Fourier transform (FFT) of the envelope is made, 5. The FFT is plotted on a log-log scale. The right hand column shows the same steps for the surrogate signal.

4.3.3 Correlating EEG and NIRS over time

An example of the alpha envelope along with the obtained Hbb and HbO_2 time series is from the O1 location of subject 3 is illustrated in figure 4.6. The correlation analysis between the fluctuation of the alpha band (the alpha envelope) and the Hbb and HbO_2 fluctuations yielded the following results. When all subjects (N=38) were considered in the analysis, a negative correlation (-0.171) for the alpha envelope and the HbO_2 concentration changes was found on the O1 location with an average delay of 2.79 seconds. For the alpha envelope and the Hbb concentration changes on this location, a positive correlation (0.183) was found with an average delay of 1.94 seconds. On the O2 location a similar correlation pattern was found. Here a negative correlation (-0.120) for the alpha envelope and the HbO_2 time series and a positive correlation (0.104) for the alpha envelope and the Hbb signal was seen. The delay however was different from the

O1 location with an average delay of 0.50 seconds for the Hbb trace and a negative delay of -0.08 seconds for the HbO_2 signal. The average correlations, delays and the standard deviations are summarized in table 4.2 A.

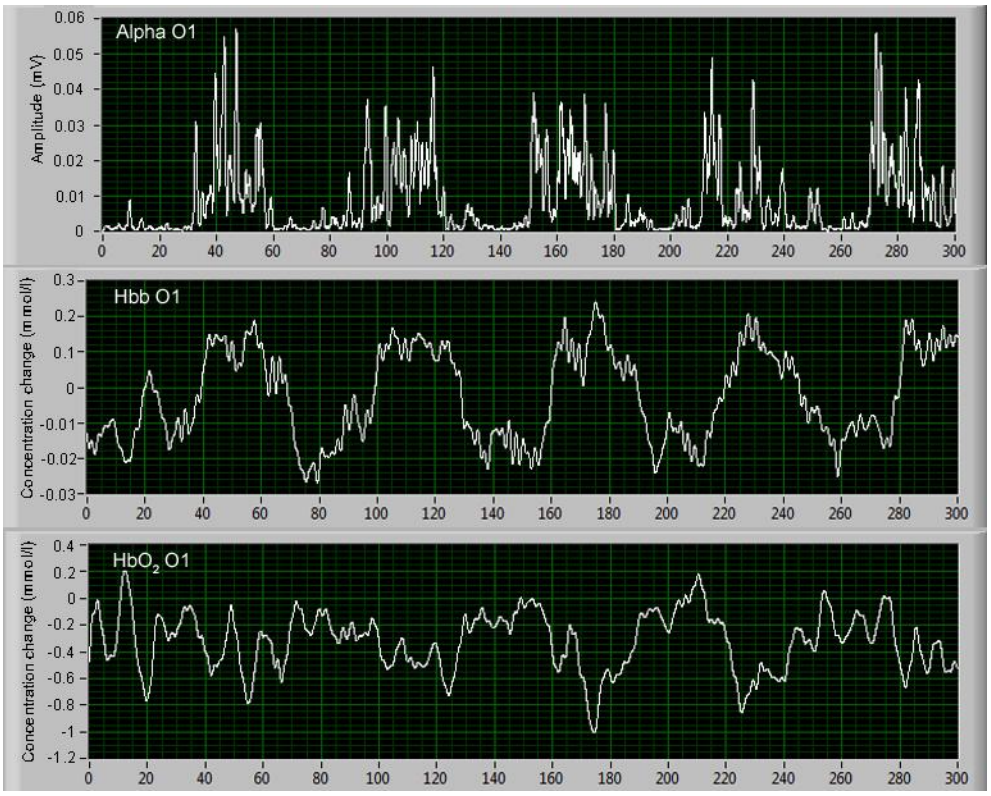

Figure 4.6. The alpha envelope with the accompanying Hbb and HbO_2 time series from subject 3 on the O1 location.

The quality labels that were given to the separate signals were then used to split the data. All data that received a "bad" quality label were excluded from the sample and the analysis was run again to investigate differences in correlation strength and timing. These results are also visible in table 4.2 (section B). After the data were cleaned, around one quarter of the sample was left. In this sample, stronger average correlations in the left hemisphere (alpha x HbO_2 = -0.276; alpha x Hbb = 0.403) were found that had a larger average delay of the hemodynamic response (HbO_2: 5.03 s, Hbb: 5.01 s). The average correlations in the right hemisphere also increased but not as much as they did in the left hemisphere (alpha x HbO_2 = -0.153; alpha x Hbb = 0.251). Furthermore, the time delay of the hemodynamic response that increased to 5 seconds in the left hemisphere was smaller in the right hemisphere (HbO_2: 0.19 s, Hbb: 3.24 s).

When the subjects were evaluated on an individual level, it became apparent that there was large inter-individual variation in the correlation data. Some subjects even showed a physiologically unexpected response, namely a negative delay value often accompanied by a change in sign of the correlation value. When these subjects were excluded from the sample as well (table 4.2 C), less subjects remained but correlation strengths increased to moderate levels (O1:alpha x HbO_2 = -0.380; alpha x Hbb = 0.457, O2: alpha x HbO_2 = -0.366; alpha x Hbb = 0.337). And the delay time varied between 7 and 8 seconds (O1: HbO_2: 8.01 s, Hbb: 7.08 s; O2: HbO_2: 7.07 s, Hbb: 7.69 s).

A	**O1 alpha x HbO_2 N=38**	**O1 alpha x Hbb N=38**	**O2 alpha x HbO_2 N=38**	**O2 alpha x Hbb N=38**
Correlation	-0.171 (0.257)	0.183 (0.324)	-0.120 (0.202)	0.104 (0.201)
Delay (s)	2.79 (6.07)	1.94 (5.72)	0.50 (7.08)	-0.08 (6.90)
B	**O1 alpha x HbO_2 N=11**	**O1 alpha x Hbb N=10**	**O2 alpha x HbO_2 N=9**	**O2 alpha x Hbb N=9**
Correlation	-0.276 (0.263)	0.403 (0.272)	-0.153 (0.293)	0.251 (0.198)
Delay (s)	5.03 (6.78)	5.01 (5.21)	0.19 (7.40)	3.24 (7.05)
C	**O1 alpha x HbO_2 N=9**	**O1 alpha x Hbb N=8**	**O2 alpha x HbO_2 N=4**	**O2 alpha x Hbb N=6**
Correlation	-0.380 (0.137)	0.457 (0.143)	-0.366 (0.140)	0.337 (0.093)
Delay (s)	8.01 (1.50)	7.08 (3.15)	7.07 (3.01)	7.69 (2.11)

Table 4.2. Group averages of the highest correlation values and their shift in time domain. The standard deviation is presented between brackets. A positive value for delay portraits the number of seconds that the hemodynamic response is slower. Section A displays the values that are obtained for the entire sample. Section B contains the values obtained after the data that was not of high enough quality was eliminated. Section C contains the results after the omission of the bad quality as well as the physiologically unexpected signals. Legend: N= number of subjects, O1= left visual cortex, O2= right visual cortex, HbO_2= oxygenated haemoglobin, Hbb= deoxygenated haemoglobin.

4.4 Discussion

In this chapter it was tested whether the alpha band as well as the HbO_2 and Hbb time series displayed features of scale-invariance indicated by power-law behaviour, both properties of SOC systems. First, the dynamics of the alpha band

was investigated with LRTC analysis and revealed that after removal of the dip caused by the paradigm, power law behaviour was present and this was statistically different for actual signals compared to surrogate signals. When the quality of the signals was taken into account it appeared that the good quality signals showed significantly steeper power law slopes. Secondly, the same analysis was performed on the time series of the HbO_2 and Hbb concentration. Here no power law could be found which was potentially due to the underlying paradigm of eyes open eyes shut that was used during data collection which caused an underlying slow oscillation to be present. Finally, the correlation between the fluctuations of the alpha band and fluctuations in HbO_2 and Hbb concentration were investigated in which the hemodynamic signal was lagged as opposed to the alpha envelope. This analysis yielded higher correlations than were found in chapter 3, especially when the data were cleaned from bad quality data and physiologically illogical data.

4.4.1 Scale invariance of alpha power

Quality labels were assigned to the responses seen in the alpha envelope. For both the O1 and O2 locations 68,4% was graded as having a good quality. Compared to the NIRS time series, described in chapter 3, the quality of the EEG signals was much better even though it is a method that is known to be prone to artefacts (for artefact examples see e.g. (Krauss et al., 2006)).

When the LRTC analysis was then performed and these data were compared to the surrogate data it appeared that the surrogate data were significantly different. This is a similar finding as was reported by Linkenkaer-Hansen et al. (2001). The finding indicates that there is a temporal effect that is caused by the sequence of the waves that are present within the alpha envelope. This sequence tells something about the scalability of the system within the, for this research, defined parameters.

This finding remained true when the sample was split up in a good-quality and a bad-quality group. A difference that did show up because of this quality division was that the steepness of the slope appeared to be higher in the good-quality sample. The higher the steepness of the LRTC slope is, the larger is the amount of energy is that evaporates from the system (Linkenkaer-Hansen et al., 2001). This

finding can be explained well by the paradigm that is used. As it is known that upon closing the eyes the amount of alpha activity increases and the alpha activity subsides when the eyes are opened and it is also known that the good-quality group is defined based on the presence of this finding, this is the subsample in this research that shows a large difference in the amount of alpha activity present every 30 seconds. Because this fluctuation is so large, it creates a slow wave, which causes a higher amplitude in the first peak of the spectrum (low frequency), which in turn causes the slope to be steeper.

4.4.2 Scale invariance of NIRS parameters

As shown in the results (figure 4.5) the attempt to analyze the entire band resulted in a plot that was so distorted by the paradigm performed, that a straight line could not be obtained. The switching form EC to OE and vice versa cause a slow wave throughout the time series. Even when the data were shuffled for the surrogate condition, this slow wave remained present, causing the data to look almost similar. The spectrum of this slow wave cause 1 large peak which transferred to an arch when plotted on a log-log scale. Therefore it was chosen not to continue this analysis on the NIRS signals in this study.

When in future studies scale-invariance of NIRS parameters will be explored one might want to choose to analyse steady measurements of eyes open and eyes closed data separately. This will allow removal of the additional wave that occurs from having a subject change conditions multiple times. From a SOC point of view one could say that every time the eyes are opened or shut energy is added to the system. Therefore, it is recommended to perform this kind of analysis on resting state data with either eyes open or eyes shut separately. When it is found that brain activity measured with EEG and metabolic activity measured with NIRS are coupled it is expected that both modalities will show SOC and power law behaviour. According to the features of SOC, a system anticipates on all levels and time scales (Bak et al., 1987). The hypothesis is that if anticipation on one of these levels is failing disease occurs. That is why these types of analysis could have a great clinical advantage and why this is an aspect that needs to be addressed in future research.

4.4.3 Correlating EEG and NIRS over time

In chapter 3 the investigation for the coupling of alpha and Hbb and HbO_2 started with a correlation analysis of block averages. This analysis led to weak, none significant results. In this chapter a more dynamic approach was adopted by performing a cross-correlation analysis in which the alpha envelope was correlated both with Hbb concentration changes and HbO_2 concentration changes. The positive correlation of alpha magnitude and Hbb concentration as well as the negative correlation of alpha magnitude and HbO_2 concentration was confirmed in this investigation. Albeit with correlations of moderate strength. The stepwise approach of using all data and eliminating first bad quality data and later on physiologically illogical or unexpected data illustrated that in a clean dataset similar results can be obtained as reported in previous research even with similar time delays for the hemodynamic signals (e.g. (Moosmann et al., 2003)).

However, the fact remains that there is a lot of inter-individual variation in the correlations and direction of correlation that is found. And while it seems physiologically illogical that a change in oxygenation would precede the occurrence of alpha waves it might not be that uncommon. Pfurtscheller et al. (2012) found in a resting state that hemodynamic signals, measured with NIRS on the frontal cortex, coupled with alpha or beta waves measured at the central cortex for periods of 100 s. In six out of nine subjects, the slow wave oscillations in HbO_2 concentration preceded the changes in EEG frequency bands by 3.7 s. The hemodynamic signal preceding the EEG signal was for some subjects the only deviant finding. Therefore, it might be worth to be more open-minded to the possibility that the coupling between electrical and hemodynamic features does not always need to mean that the hemodynamic signal is the delayed signal. Especially when resting state data are considered. In determining RSNs the primary focus lies on the LFOs and VLFOs (Beckmann et al., 2005, Smith et al., 2009). Assuming that these slow oscillations carry further than the faster changes in EEG do, it might be worth considering that it are the slow, larger waves that determine and therefore “drive” the brain state. Which would mean that the EEG can be the “follower” in this symbioses. A finding that should be further investigated.

A different possibility as to why the correlations that are found between the electrical and hemodynamic signals are only of moderate strength is that the wrong electrical parameter is being investigated. Besides correlations between hemodynamic signals and alpha waves, also correlations with beta waves have been found (Pfurtscheller et al., 2012). Furthermore, it has been assumed that possible relationships might be found between higher frequency EEG like gamma activity (60-100 Hz) and hemodynamic parameters (Koch et al., 2009). However, while other spectral peaks surely deserve attention in future research the uniqueness of the alpha peak, especially in relationship with an EO EC paradigm, cannot be dismissed with only moderate correlations.

When it is assumed that the brain as a dynamic system is a SOC system and obeys power law behaviour, it is likely that besides linear correlations, non-linear relationships exist as well. Therefore, a possible reason that the correlations found in the sample are not that strong is that the cross correlation analysis only takes into account linear correlations. In order to investigate this a method is needed that analysis both linear and non-linear correlations while taking into account the slower fluctuating oxygenation changes as opposed to the faster moving electrical brain activity responses. A method that seems to be a good candidate in doing so is Mutual Information analysis which will be explained in the next chapter.

4.5 Conclusion

In this chapter a beginning is made in the field of analysing dynamics of brain activity when both electrical and hemodynamic measurement methods are used. When the understanding of the relationship between these modalities is strived for, the movement towards dynamic analysis is a logical step. While the analysis of the separate methods that are illustrated in this chapter show that difficulties in applying dynamical analyses exist, the necessity of exploring this in future research does not diminish. The path that will be adopted in this thesis revolves around a better understanding of the relationship between the NIRS and EEG data with special focus on the alpha band, the Hbb concentration and the HbO_2 concentration that have been explored previously. Therefore, the following chapter will be centred around exploring the relationship between the signals and

will utilise Mutual Information analysis and its potential to analyse linear as well as nonlinear relationship between signals from different modalities.

Chapter 5: Introducing relative cross mutual information, a new non-linear analysis for coupling between NIRS and EEG

This chapter will focus on one type of dynamic analysis that is capable to look at relationships within one signal, between two signals but also between two signals of different modalities. Mutual information analysis. Mutual information (MI) analysis takes into account linear as well as nonlinear aspects within time series and might therefore be a perfect asset to investigate the relationship between the electrical and hemodynamic aspects of brain functioning. However, there are two challenges with MI. The first one being the selection of the appropriate bin size for the analysis and the second one being the difficulty in the interpretation of the values. Therefore, after the introduction of MI, this chapter will elaborate on how an appropriate bin size can be established. Then, relative MI will be introduced as a transformation of MI results based on the individually used data per analysis. Increasing the ease of comparing results.

5.1 Introduction

Mutual information (MI) was first introduced by Claude Shannon in 1948, an electrical engineer at Bell Telephone laboratories, as part of classical information theory (Shannon, 1948, Walters-Williams J., 2009). Shannon set out to mathematically quantify the statistical nature of "lost" information in telephone line signals. Hereby the central problem was that a message selected at one point needed to be reproduced at another and that the system would need to make a selection out of a set of possible messages (Shannon, 1948). A few of his suggested principles need clarification before MI and its implications for brain research can be addressed. The first one being entropy.

Entropy is the amount of information or uncertainty that an event (for instance values in a signal) contains and it is calculated from the probability of that event. Usually a logarithmic base is used to calculate entropy so it can be expressed in bits. The average entropy H, of an event is calculated as follows:

$$H = -K\sum_{i=1}^{n} p_i \log p_i$$

In this formula, K is a positive constant (this amounts to a choice of a unit of measure), p_i is the probability of a system being in state i of its phase space (Shannon, 1948).

Calculating the entropy of a signal can be illustrated with an example[2] in which signal X will be used (table 5.1 and figure 5.1). Signal X consist out of 8 numbers that range between 1 and 4. The average entropy of signal X, $H(X)$, can be calculated by summing the probability of occurrence of each event (value) that is in this signal. In signal X four events occur; event $x = 1$ occurs 1 out of 8 times, event $x = 2$ occurs 4 out of 8 times, event $x = 3$ occurs 1 out of 8 times, and event $x = 4$ occurs 2 out of 8 times. Filling out these probabilities in the formula leads to the following result:

$$H(X) = -\sum_{x\in\{1,2,3,4\}} p(\{x = x\}) \cdot \log_2 p(\{x = x\})$$

$$= -p(1) \cdot \log_2 p(1) - p(2) \cdot \log_2 p(2) - p(3) \cdot \log_2 p(3) - p(4) \cdot \log_2 p(4)$$

$$= -p\frac{1}{8} \cdot \log_2 p\frac{1}{8} - p\frac{4}{8} \cdot \log_2 p\frac{4}{8} - p\frac{1}{8} \cdot \log_2 p\frac{1}{8} - p\frac{2}{8} \cdot \log_2 p\frac{2}{8}$$

$$= \frac{1}{8} \cdot 3 + \frac{1}{2} \cdot 1 + \frac{1}{8} \cdot 3 + \frac{1}{4} \cdot 2$$

$$= \frac{3}{8} + \frac{1}{2} + \frac{3}{8} + \frac{1}{2}$$

$$= 1\frac{3}{4}$$

t	1	2	3	4	5	6	7	8
X	2	1	2	4	2	2	3	4

Table 5.1 Signal X. The upper row t denotes the time steps and the lower row denotes the value of signal X at that time point. This signal is used to calculate average entropy from which is done by summing the probability of occurrence of each event (value) in the signal. The values of the signal are also plotted in figure 5.1.

[2] All courtesy goes to A. Sipers (Zuyd University/ Maastricht University, department of knowledge engineering), who used this example to explain entropy more clearly to me.

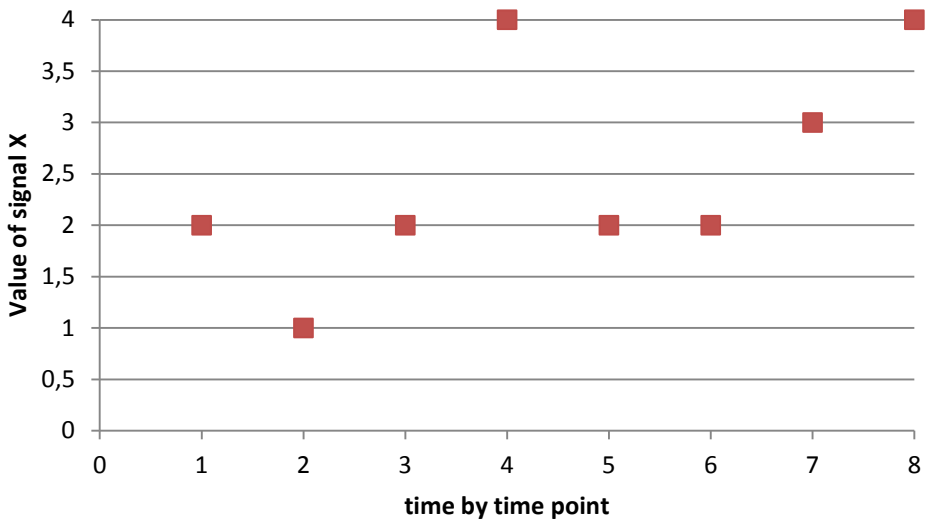

Figure 5.1 The plotted values of signal X. At every time point the value of the signal is expressed with a red square.

Entropy has a few properties that are important. First of all, it is always a positive number, unless we know what the outcome of an event will be for sure. In that case $H = 0$. Second, the maximum entropy value is reached when all probabilities of an event are equally likely to occur and this depends on the number of possibilities, n ($\max H = \log_2 n$). As a consequence this means that maximum entropy means maximum uncertainty and minimal predictability (Shannon, 1948).

As the example above shows, this formula was designed to handle one variable. When there are two events X and Y (or two signals) one can calculate separately the entropy for both signals ($H(X)$ and $H(Y)$), but it is also possible to calculate the joint entropy $H(X,Y)$.

$$H(X,Y) = -\sum_{i,j} p(i,j) \log p(i,j)$$

While filling out the probabilities in the joint entropy equation, imagine a signal like in table 5.1 that has an additional signal Y below it. The probabilities that need to be addressed are then the possible pairs of both signals (x,y) that can occur on the 8 points in time. If events x and y are totally independent their joined entropy will be equal to the sum of the individual entropies. In any other case, the joint entropy is smaller (Shannon, 1948).

The last type of entropy that needs to be addressed is called conditional entropy. Shannon defines the conditional entropy of y, $H_X(Y)$ as the average of the entropy of y for each value of x, weighted according to the probability of getting that x:

$$H_X(Y) = -\sum_{i,j} p(i,j) \log p_i(j)$$

Which can also be defined in terms of how much entropy y has remaining if the value of a second random variable x is known and be written as $H(X|Y)$ (Walters-Williams J., 2009).

Figure 5.2 explains how these three forms of entropy relate to each other and to MI. To start with, entropy the information or uncertainty within every event (or signal) is represented by a cloud for each signal $H(X)$ and $H(Y)$. When the events (or signals) are completely independent from each other the clouds are separate and MI equals 0. When signal X and Y are dependent the clouds (partly) overlap. Both clouds together define the joint entropy of the events, $H(X,Y)$. The joint entropy can also be calculated by adding the entropy of event x to the conditional entropy of y once x is known $H(X,Y) = H(X) + H(Y|X)$ (Shannon, 1948, Walters-Williams J., 2009). Similarly, conditional entropy can be found by subtracting the entropy from the known variable from the joint entropy $H(Y|X) = H(X,Y) - H(X)$ (Shannon, 1948, Walters-Williams J., 2009). The uncertainty of y is never increased by knowledge of x. It will be decreased unless x and y are independent events, in which case it is not changed (Shannon, 1948). When then the two events are believed to be signals that are communicated from a sender to a receiver, these signals can be communicated separately. By doing so the entropy or uncertainty is as large as the two separate clouds. However, when the signals are sent in pairs, the entropy of the two separate clouds decreases with the Mutual Information of the two signals $MI(X,Y)$:

$$MI(X,Y) = H(X) + H(Y) - H(X,Y)$$

The MI can also be found by deducting the conditional entropy of x once y is known from the entropy of event x, $MI(X,Y) = H(X) - H(X|Y)$, and by deducting the conditional entropy of y once x is known from the entropy of event y, $MI(X,Y) = H(Y) - H(Y|X)$ (Ramanand et al., 2010).

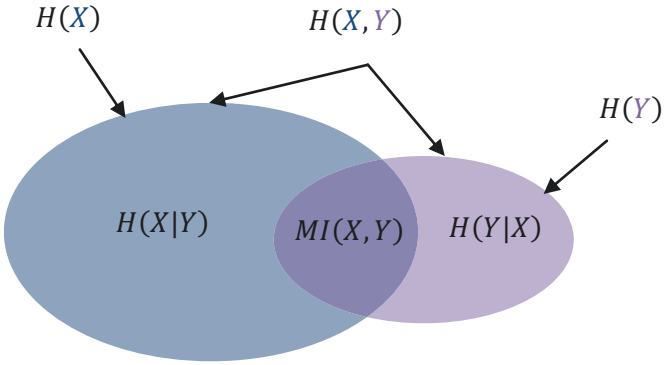

Figure 5.2 (adapted from (Harrison et al., 2006)). The relationships that exist between the different forms of entropy (entropy $H(X)$ and $H(Y)$; joint entropy $H(X,Y)$; conditional entropy $H(X|Y)$ and $H(Y|X)$) and how mutual information ($MI(X,Y)$) can be deduced from them.

In essence, MI measures the mutual dependence of two variables. It can tell how much uncertainty is lost once one variable is known, and therefore it gives an indication of how much information event y can give about event x (Walters-Williams J., 2009). Since it measures linear and non-linear dependencies between two variables, MI is often regarded as the nonlinear equivalent of the correlation function that was used in chapter 4 (Alonso et al., 2010, Ramanand et al., 2010).

MI is a symmetric function so the amount of information event y can give about event x is the same as the amount of information event x can give about event y, $MI(X,Y) = MI(Y,X)$. Furthermore, MI is always a non-negative between X and Y (the uncertainty of X cannot be increased by knowing of Y), $MI(X,Y) \geq 0$. And last, the information the variables contain about each other cannot be greater than the information the variables contain about themselves (the entropy), $MI(X,Y) \leq H(X)$ and $MI(X,Y) \leq H(Y)$ (Walters-Williams J., 2009). The higher the value of the MI, the more information the two variables contain about each other.

When the MI is applied to two different time series it is often referred to as Cross Mutual Information (CMI). Often this function is also lagged in time to be able to determine the predictability of x once y is known (Jeong et al., 2001, Ramanand et al., 2010). When the MI is applied to just one time series, that time series is also lagged in time against itself. In this circumstance it is referred to as Auto

Mutual Information (AMI) and it tells something about the predictability of the signal given past measurements (Jeong et al., 2001, Ramanand et al., 2010).

5.1.1 Mutual information in EEG research

The use of MI analysis has become an appealing tool in neuroscience. When the MI is applied to two EEG signals, it gives a quantitative measure of dynamic, functional coupling between them (Jeong et al., 2001, Alonso et al., 2010). Especially the estimation of statistical dependencies without assumptions about the distribution of the data (whether this is linear or not) is a great asset, as well as the stability of the measure with large data sets (Ramanand et al., 2010). MI has been applied to the entire EEG spectrum, but also in narrow band analysis in which one band is inspected on two locations or when one band is inspected together with another (Ramanand et al., 2010).

Jeong et al. (2001) used MI in the analysis of Alzheimer's patients to explore the information transfer across brain regions. They found that, compared to age-matched controls, Alzheimer's patients show a functional problem in long-distance connections. Recently it was also found that the inter-hemispheric and right-hemisphere MI is lowered in patients with multiple sclerosis (Lenne et al., 2013). Another neurological population that was investigated with MI analysis on EEG signals was a group of Parkinson's patients on and off L-dopa medication (Palmer et al., 2010). Also the effects on short time coupling of medicinal substances in healthy volunteers were assessed by means of MI (Alonso et al., 2010). Furthermore, MI has been used to study the EEG after sleep deprivation (Na et al., 2006) and to quantify differences in between sleep stages in both young (Xu et al., 1997) and middle-aged and elderly subjects (Ramanand et al., 2010). These examples illustrate the use of MI analysis of EEG data with clinical perspective. A flag that is raised while performing MI analysis to investigate functional coupling of neural data is that the information transfer needs to be understood in a statistical sense. The linear and non-linear coupling that might be found cannot reveal the exact mechanisms or structural pathways that underlie this statistical coupling (Jeong et al., 2001, Alonso et al., 2010).

5.1.2 Mutual information in NIRS research

To the best of my knowledge, MI analysis in research conducted with NIRS has only been carried out once. Herff et al. (2012) investigated the potential use of speech in a brain computer interface that uses NIRS measurements. Use was made of three speaking modes; audible speech, silent speech, and imagined speech, distinctive Hbb and HbO_2 responses were registered for each condition, called the training data. Subsequently, the brain computer interface used MI to classify in which class the data that were measured would fall. Differences between either task condition or pauses could be classified with an accuracy between 69 and 88%, and differences between tasks could be classified with an accuracy between 61 and 80% (Herff et al., 2012). This is a very different approach than the approaches that are described for EEG analysis and illustrates the diversity in potential use MI analysis has.

When other measures of hemodynamic activity are considered, like fMRI, MI is found to be a technique that is used more often recently, but still not as often as it is in EEG research. One of the first applications of MI in fMRI was performed by Kim et al., (1999). They propose to use MI on the slices obtained as anatomic dataset as reference to slices obtained during the task to set a threshold for motion correction. Later on the technique also proved useful for assessing the connectivity between brain regions, or clusters of brain regions during rest (Salvador et al., 2007) or during a task (Hinrichs et al., 2006). But also timing aspects of information processing in the brain have been investigated. Fuhrmann-Alpert et al. (2008) used MI to identify the latency of the BOLD response in which the highest information content for an audio-visual stimulus was seen compared to purely auditory or purely visual stimuli. And even more recently an approach of MI maps was suggested to unravel regionally specific effects in fMRI data (Gómez-Verdejo et al., 2012).

5.1.3 Mutual information in combined electrical and hemodynamic research

With the variety of possibilities the MI analysis possesses it does not come as a surprise that possibilities are sought to use it to link electrical and hemodynamic activity. Especially because it has been postulated that the more information two signals contain about each other (high MI) the higher chances are that the two signals are biologically related (Palmer et al., 2010). Since this assumption already

exists for electrical and hemodynamic activity, the MI appears an elegant method to illuminate linear and nonlinear dependencies between both modalities. Another reason for the increase in popularity of MI to analyse signals from two different modalities is that MI uses the probability distributions of the dataset rather than actual data. Therefore, it is not restricted by assumptions of the distributions of the datasets used (Ramanand et al., 2010).

Ostwald et al. (2010, 2011, 2012) have used MI analysis on simultaneously acquired EEG and fMRI signals to investigate the visual response upon checkerboard stimulation, to investigate the effects of checkerboard stimulation upon the coupling between low resolution electromagnetic tomography (LORETA) derived from EEG and fMRI, and explored how these analysis can be used to investigate the neural underpinnings of perceptual decisions. Other researchers used MI on concurrent EEG and fMRI in order to map hemodynamic changes related to interictal epileptic discharges in the EEG (Caballero-Gaudes et al., 2012).

Studies that have sought to link EEG activity with fMRI data usually model the fMRI data based on the EEG. MI analysis treats both modalities symmetrically and does not need an a priori model of the hemodynamic function). Together with its ability to assess both the linear as well as the nonlinear aspects of the dependency (Alonso et al., 2010, Ramanand et al., 2010), these are great advantages on current analysis techniques. In this chapter the first attempt will be made to use MI analysis to investigate the coupling between EEG alpha wave activity and Hbb and HbO_2concentration changes. However, two challenges in MI analysis exist. First, the probability distribution needs to be determined adequately, and second the obtained MI values need to be interpreted correctly.

5.2 Determining the number of bins

The first difficulty that arises when performing MI analysis is estimating the probability distributions needed to calculate the entropies (Ramanand et al., 2010). A method that is often used to estimate probability distributions is referred to as the histogram method, which uses bins.

In this chapter the probability distributions of NIRS and EEG time series need to be estimated. The histogram method divides the amplitude of the time series into partitions (figure 5.3) or bins. The probability distribution can then be obtained by calculating the ratio of the number of data points that fall within each bin N_i divided by the total number of samples in the time series N: $p_i = \frac{N_i}{N}$ (Thakor and Tong, 2004).

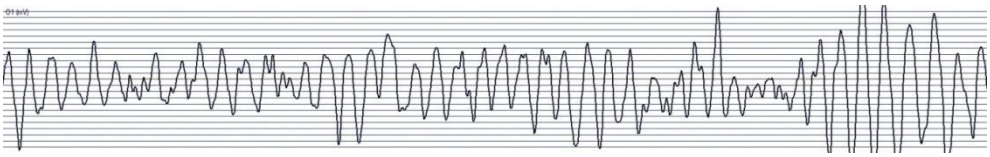

Figure 5.3 The partitioning of the amplitude of an EEG time series into bins. To illustrate the concept these 5 seconds of EEG from the left visual cortex of subject 3 (µV range + and – 50) are partitioned into 24 equal sized bins. The 0-line is indicated with a black line and also indicative of a partitioning between two bins.

The number of bins that is chosen for the analysis needs to approach the average probability adequately. When larger (and therefore fewer) bins are chosen to determine the entropy of each signal, more data points fall within each bin and the average probability per signal is more accurate. However, the estimate of the joint probability will be too flat, causing the MI to be underestimated. When smaller (more) bins are chosen, the fluctuations in the joint probability distribution over short distances are followed better, but when these fluctuations are due to a smaller sample size the MI is overestimated (Fraser and Swinney, 1986). The first objective therefore is determining an appropriate amount of bins for the current EEG-NIRS dataset. Hereto three approaches are adopted: 1. Investigate current literature, 2. Investigate the distribution of the dataset, 3. Test the analysis by use of dummy data.

5.2.1 Investigate current literature

Since MI analysis has not been conducted before to investigate concurrent EEG and NIRS data, no literature is available to illustrate the choice of the appropriate number of bins. MI analysis has only been performed once on NIRS data and this study used a kernel density estimation with Parzen window approach (for explanation see (Parzen, 1962)) to estimate the probability distribution (Herff et al., 2012). Therefore, the appropriate binning method was sought in EEG research.

The EEG literature revealed that the underlying theory of how to decide the number of bins is scarce. Some studies even fail to mention the amount of bins used (Abasolo et al., 2007, Hornero et al., 2009). Often studies only report the use of the histogram method and state how many bins were used. The most studies use 64 bins of which most (but not all) of these studies use datasets of 4096 data points (Jeong et al., 2001, Na et al., 2002, 2006, Min et al., 2003, Jin et al., 2006, Escudero et al., 2008, Lee et al., 2011). Teplan et al. (2006) use 295 bins with 87000 data points and state as a rule that the number of bins is equal to the square root of the number of data points. When this rule is applied to a dataset of 4096 data points $\left(\sqrt{4096} = 64\right)$ it is revealed that 64 bins would indeed be advised.

Another rule for calculating the amount of bins to be used is given by David et al. (2004) and states that the number of bins used to estimate the probability density is the number just below $\ln N / \ln 2$ in which N is again defined as the amount of data points in the dataset. This leads to the use of fewer bins as was shown by Abasolo et al. (2008) who adopted this approach and used 12 bins for 4096 data points. Even fewer bins, namely 8, were preferred by Alonso et al. (2007, 2010) and Luo and Sajda (2009). The latter study ranged the amount of bins from 6 to 12 but did not find much differences between the options so decided to go with 8.

A study that systematically researched different amounts of bins (8,16,32,64 and 128) with different types of signals (synthetic signals as well as surface EEG and intracranial EEG) argued that 32 bins generated the most accurate outcome for AMI analysis (Escudero et al., 2009). Other numbers that have been found in the literature were 16 bins with approximately 4000 data points (Jin et al., 2010, Ramanand et al., 2010), 50 bins with 500 data points (Lu et al., 2011), and 20 bins while investigating a motor task (number of data points unknown) (Wang et al., 2009, Palmer et al., 2010).

Due to the inconsistency that exists, the use of only the alpha band in this chapter and the additional use of NIRS data it was empirically tested in a random subject what number of bins would be most appropriate. First, 64 bins were used since most EEG studies use this number of bins. Second, the rule by Teplan et al. (2006)

was explored. When the 5 min time series are analysed by MI similarly as was done in chapter 4 with the CC analysis, all time series consist of 7500 data points. Fed into the formula this results into $\sqrt{7500} = 86{,}60$ 87 bins. As a third option the rule of David et al. (2004) was investigated: $\ln 7500/\ln 2 = 12{,}87$, which suggested to use 12 bins. The results of this test are summarized in table 5.2.

Bins	**Alpha- HbO_2 O1**	**Alpha-Hbb O1**	**Alpha- HbO_2 O2**	**Alpha-Hbb O2**
12	0.18	0.25	0.10	0.12
64	0.69	0.77	0.55	0.52
87	0.90	0.98	0.73	0.68

Table 5.2 Exploration of different bin sizes on data of subject 3. Values that are reported are the average cross mutual information (CMI) values of all values found between time shifts of -10 and +10 seconds. Legend: O1= left visual cortex, O2= right visual cortex, HbO_2= oxygenated haemoglobin, Hbb= deoxygenated haemoglobin.

The results suggest that the more bins are used, the higher the MI values get. Furthermore, when the time point at which the highest MI was found is considered as well it was found that this value was stable for 87 and 64 bins, but shifted to higher time delays with 12 bins for this subject. Whereas this shift is 0.5 seconds on the O1 location, the O2 location even shows a shift of 2.5 seconds. These results illustrate that bin size matters but are inconclusive in determining which bin size would be more adequate.

5.2.2 Investigate the distribution of the dataset

To solve the binning problem, help was sought in the department of mathematics of Imperial College London. Prof. Henrik Jeldthoft Jensen and Dr. Fatimah Abdul Razak explained a two step procedure. First, the data are normalized based on the standard score and subsequently all data is plotted in a single histogram. The number of bins that makes the histogram look smooth and normally distributed is the number that is chosen for the MI analysis. The normalizing of the data assures that the binning range is uniform. Furthermore, since the changes in amplitude of the time series are the property of interest (resulting in magnitude changes for the EEG signals and concentration changes for the NIRS signals), normalizing the data corrects for possible inherently high values.

The alpha time series as well as the $HbO_2$and Hbb time series were normalized individually for both measurement locations (O1 and O2) by subtracting the distribution's mean (μ) from every data point and dividing the outcome by the standard deviation of the distribution (σ), resulting in z-scores (Moore et al., 2012): $z = \frac{x-\mu}{\sigma}$.

The data from all participants, from both locations and from all three measurements parameters (alpha, HbO_2, and Hbb) were placed into one file and a histogram was created in SpSS with several numbers of bins (figure 5.4). The three possibilities that were suggested from the literature 64, 87 and 12 were investigated first. The different plots showed that too few bins (12) did not present a normal curve and that a larger number of bins increased the smoothness of the histogram (64). Using too many bins (87) resulted in a skewed curve. Because the 64 binned plot was a little skewed as well, lower bin numbers were investigated subsequently.

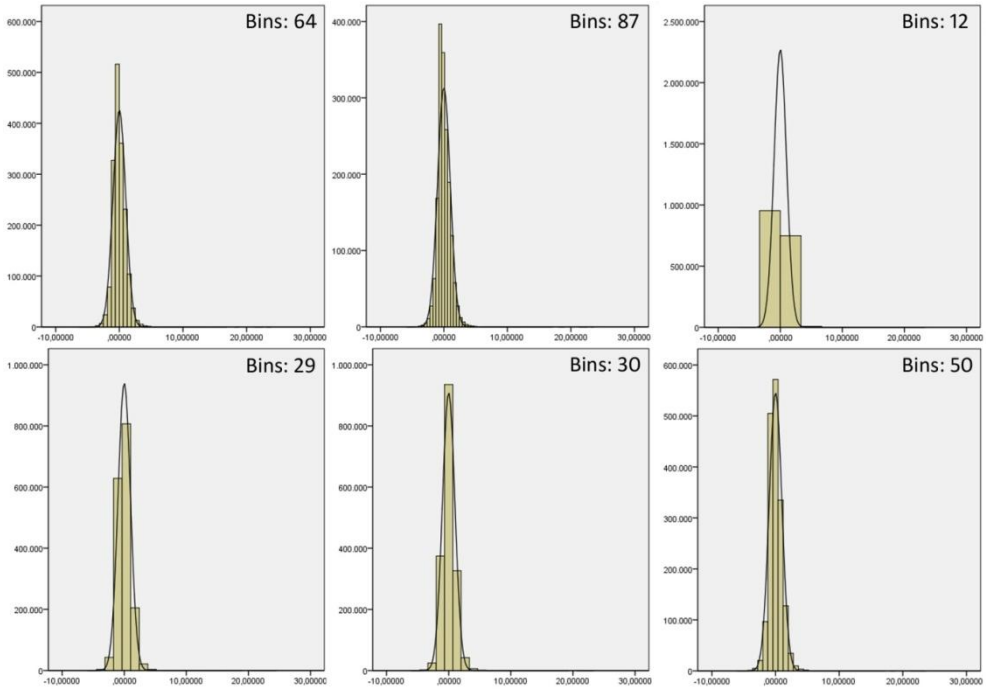

Figure 5.4 Histograms of different bin sizes. The black curve indicates the normal curve. On the x-axis the z-scores are displayed, on the y-axis the frequency a data point falls within a bin is displayed. The different pictures show that with more bins the normal curve is followed smoother, too many bins however, show a skewed peak with increased kurtosis.

Since 29.4 units were found in the data (range -5.7 to 23.7) 29 and 30 bins were also explored. As is visible in figure 5.4, 30 bins resulted in a better fit than 29 bins. Therefore, as a last step the possibilities between 30 and 64 bins were tested in increments of 2 bins to explore the best match, which was found in 50 bins. However, just like the histogram created with 64 bins, despite the increased smoothness, some skewness was detected.

5.2.3 Test the analysis by use of dummy data

Signal	**Alpha z-scored**	**HbO_2 z-scored**	**Hbb z-scored**
min	-1.8609	-4.8202	-5.7401
max	23.2967	4.6466	4.8330

Table 5.3 The ranges of the z-scores for each measure based on the experimental data of all participants. Dummy data were randomly generated within the ranges specified in the table. Legend: HbO_2= oxygenated haemoglobin, Hbb= deoxygenated haemoglobin.

In order to verify that the chosen bin number was correct, dummy data were used. Dummy data were randomly created to be independent, had similar length as the actual time series (7500 data points), and were generated within the ranges of each used parameter (table 5.3). After the time series were generated, MI analysis was performed in which bin sizes were varied for each analysis. Since the dummy data were generated to be independent, the optimal bin size would result in an MI that approaches 0 (Shannon, 1948, Walters-Williams J., 2009).

The results of the MI analysis are summarized in table 5.4. The investigation started with 64 bins as this was the number of bins that was most reported in EEG research. This was followed by the reasonably good fits of 50 bins and 30 bins from the histogram method. When these results did not lead to outcomes of zero, the smaller size of 12 was also tested. As seen in paragraph 5.2.1, the use of less bins leads to smaller numbers of MI. To test whether the results kept decreasing or whether there was an optimum all smaller bin sizes were tested as well. This showed MI values only were zero with the dummy data when 1 bin was used. With 3 or 4 bins, results in which the first three decimals were zero were obtained though.

Bins	Alpha-HbO_2 O1	Alpha-Hbb O1	Alpha-HbO_2 O2	Alpha-Hbb O2
64	0.46	0.46	0.46	0.46
50	0.26	0.26	0.26	0.26
30	0.084	0.085	0.084	0.084
12	0.011	0.011	0.011	0.011
3	0.0004	0.0004	0.0004	0.0004
1	0	0	0	0

Table 5.4 Exploration of different bin sizes in independent dummy data. Values that are reported are the average cross mutual information (CMI) values of all values found between time shifts of -10 and +10 seconds. Legend:O1= left visual cortex, O2= right visual cortex HbO_2= oxygenated haemoglobin, Hbb= deoxygenated haemoglobin.

5.2.4 Discussion on the number of bins

Fraser and Swinney already pointed out in 1986 that the number of bins that are chosen to perform MI analysis can influence the results. This was enforced by Escudero et al. (2009) for the use of MI analysis in biomedical signals. When the binning is too fine or too coarse the results are biased. In this section three methods were explored to investigate the appropriate amount of bins for the current data set. The first method was an investigation of the current literature. This search is however, impaired by the deficit of literature that is available on MI analysis in NIRS or concurrent EEG and NIRS research. In the EEG literature often 64 bins are used but the underlying theory is left unreported. The rules of thumb that are provided by David et al. (2004) and Teplan et al. (2006) were tested on a random subject and showed that the fewer bins were used, the lower MI results were. This finding was accompanied by a shift in time when maximal MI was reached when a lower bin size was used, leading to the conclusion that different bin sizes can lead to different results.

Secondly, upon advice from Dr. Fatimah Abdul Razak, the data distribution of the normalized data was inspected for various bin sizes. In this approach the optimal bin size would lead to a normally distributed histogram which is smooth as well. This approach showed that more bins leads to a more smoothly defined histogram. However, there seems to be an optimum because when the bin size is increased too far, the histogram becomes more skewed. A downside of this

method is that it is still a rather arbitrary choice to say which histogram is preferred.

As a last option, it was tried to determine the right bin size by using the properties of the analysis itself. When independent time series are analyzed MI should be zero. So independent dummy data generated within the range of the actual data were used to explore different bin sizes. Unfortunately, this did not lead to the results hoped for. When using the options suggested by the histogram method, the results did not approach zero. When much smaller bin sizes were used the results did lean towards zero. However, these were bin sizes that were smaller than the ones reported in the literature and the histogram method displayed that a small amount of bins is an inappropriate fit.

5.2.5 Conclusion on the number of bins

A choice upon a bin number needed to be made however to be able to continue the analysis. This choice was 30 bins. In this choice the normally distributed shape of the histogram was taken into account with a compromise on the smoothness. The second factor that contributed to this choice were the results from the dummy data. The MI analysis on dummy data performed with 30 bins was the only option that shows results < 0.1 while still displaying a normally distributed histogram. The fact that independent time series generate results in the MI analysis that are > 0 is a factor that will be taken into account in the interpretation of the results.

5.3 MI in an eyes open eyes closed paradigm

In this chapter MI analysis is performed as an extension of the analyses that have been performed so far on the dataset that was used in chapters 3 and 4. In order to be able to compare the results of this analysis to the cross-correlation analysis that has been performed in chapter 4, a similar approach is adopted.

A difference between MI analysis and CC analysis, other than the nonlinear relationships that can only be investigated by MI analysis, is the interpretation of the results. The results of CC analysis always range from -1 to 1, indicating anything in a range from a perfect anti-correlation to a perfect correlation

(Howell, 2011). The result obtained with MI analysis, always ranges between 0 and a positive number (Walters-Williams J., 2009). Therefore the direction of the relationship cannot be interpreted directly from the results. Furthermore, no other guidelines for interpretation are given than the higher the MI value, the higher the mutual dependence of the two signals is (Walters-Williams J., 2009). The Venn diagram displayed in figure 5.2 shows the relationships that exist between the different forms of entropy and the MI. The more radical situations of independent signals and maximal dependent signals are illustrated the Venn diagrams in figure 5.5.

The left sided Venn diagram shows that theoretically independent signals would yield an MI of 0, similar to what was reported by Shannon (1948). However, the findings in paragraph 5.2 showed that when bins are used to determine the entropies needed for MI analysis, independent signals do not yield a value of 0. The right sided Venn diagram shows that maximum dependence between two signals results in a maximum MI. And that this maximum MI is equal to the smallest entropy of the two signals that are used for analysis. Knowledge of these properties can aid in the interpretation of the results.

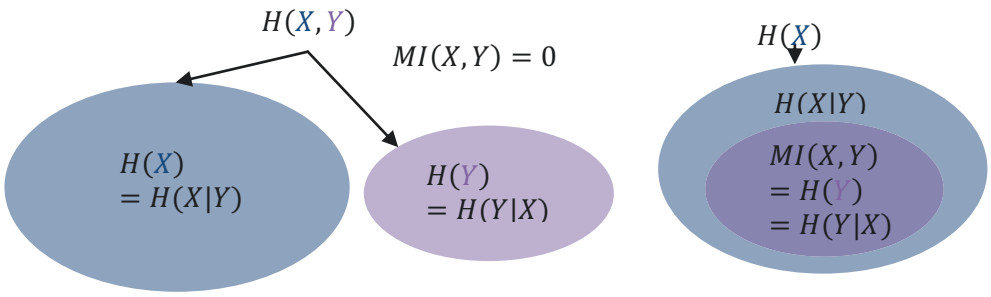

Figure 5.5 Venn diagrams for independent and maximal dependent signals. The left hand side Venn diagram displays the relationship between the different forms of entropy for a situation in which the two signals that are used are completely independent. The right hand side Venn diagram displays this relationship when maximal dependency exists between two signals. Legend: $H(X)$ *and* $H(Y)$*= entropy,* $H(X,Y)$*= joint entropy,* $H(X|Y)$ *and* $H(Y|X)$ *= conditional entropy,* $MI(X,Y)$ *= mutual information*

Here a proposition is made for a transformation of the MI values based on the properties of the signals and parameters that are used in the MI analysis. This transformation will be referred to as relative MI (MI_{rel}):

$$MI_{\mathrm{rel}} = \frac{(MI(X,Y) - MI(X_{dummy}, Y_{dummy}))}{\left(H(X\ or\ Y) - MI(X_{dummy}, Y_{dummy})\right)} \times 100$$

For each signal that is used in the MI analysis (x and y) a dummy signal is generated randomly with values that fall within the range of the actual signal (x_{dummy} and y_{dummy}). Since the dummy signals are generated randomly they will be independent. MI is then calculated over x_{dummy} and y_{dummy} ($MI(X_{dummy}, Y_{dummy})$) using the same bin size as is used to calculate $MI(X,Y)$. This creates a new 0-threshold. Then for each signal that is used in the MI analysis (x and y) the entropy is calculated ($H(X)$ and $H(Y)$). From these two entropy values it is determined which is lowest for this is the maximum value that can be reached by the MI analysis. In order to calculate MI_{rel}, the new 0-threshold is deducted from the actual MI value and from the smaller entropy. Then this new MI value is divided by the new entropy and multiplied by 100. By doing so, the initial MI value that is found can be related to the minimum and maximum possible MI, expressing the dependency of a signal in a percentage. This approach will be adopted here.

5.3.1 Methods

5.3.1.1 Subjects

Since the MI analysis is an extension of the previously performed analysis the group of participants is similar to the group described in chapters 3 and 4. The group exists out of 38 participants (21 female) with an age range of 19-60 years (mean 37.74, SD 13,30). All subjects volunteered to participate, and signed informed consent. The study was approved by the University ethics committee (070300).

5.3.1.2 Paradigm

During the experimental session of each participant concurrent EEG and NIRS measurements were taken from the visual cortex during 5 minutes. Hereto, recordings from both the left and right hemisphere were taken approximately over O1 and O2 locations of the 10-20 EEG locations system (Jasper, 1958). Subjects were asked to sit comfortably in front of a computer screen that displayed a picture of a “test screen” (figure 3.2). Every 30 seconds the participants were asked to change from eyes open to eyes shut and vice versa (a

schematic view of the paradigm is displayed in figure 3.1). Half of the participants started the measurement with closed eyes, the other half with their eyes open.

5.3.1.3 Equipment

The specifications of the EEG equipment (Bimec, Maastricht Instruments B.V. Maastricht, the Netherlands) and the NIRS equipment (OXYMON Mk III, Artinis B.V. Zetten, the Netherlands) and electrode as well as optode configurations are described in paragraph 3.2.3.

5.3.1.4 Data analysis

In chapter 4 it was shown that subject 18 showed artefacts in the alpha envelope on every transition from EC to EO and from EO to EC and that these artefacts influenced the dynamics of the signal. Therefore, it was decided to exclude subject 18 from the MI analysis, leaving 37 subjects in the sample.

For both locations (O1 and O2) the CMI was determined for the normalized 5 minute time series of the down sampled alpha envelope and the HbO_2 concentration change as well as the alpha envelope and the Hbb concentration change. As explained in chapter 4, the alpha envelope contains the changes in magnitude over time of the alpha frequency band (7.5-12 Hz). This time series is down sampled to 25 Hz in order to match the sample frequency of the HbO_2 and Hbb time series. By doing so each time series has the same number of data points and the possible time shifts of either signal in relation to the other can be observed more adequately.

CMI was calculated by means of a LabVIEW application programmed as element of the BrainMarker EXG analysis software (BrainMarker B.V., Gulpen the Netherlands). This application plots a graph of the CMI value of the chosen signals at different time lags (figure 5.6). Similar to the CCF used in chapter 4, the signals were analyzed for all lags between -10 to 10 seconds. For all signals, 30 bins were used to estimate the probability densities. From the plot it was then determined at what time shift maximum CMI was reached. Both the CMI value as well as the time shift were noted for each pair of signals. Since the calculation of CMI for time series of 7500 data points and 30 bins has a long calculation time, it was chosen

only to plot the CMI values in a resolution of 0.5 s. This decreases the accuracy of the time shift to some extent, but speeds up analysis time.

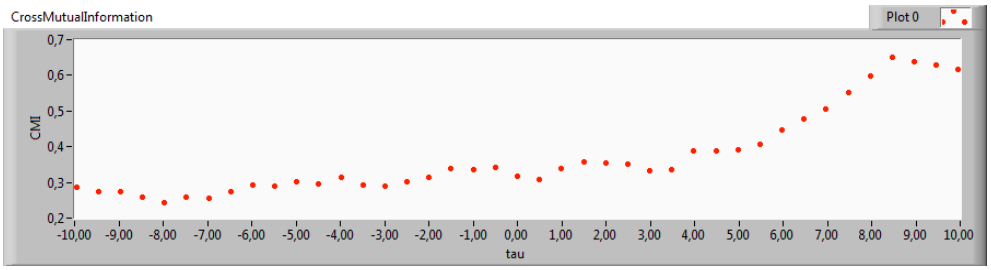

Figure 5.6 A cross mutual information (CMI) plot (subject 3, left occipital cortex, Alpha – oxygenated haemoglobin, 30 bins). On the x-axis the time steps that are analysed are displayed (tau), in this case 10 seconds back and 10 seconds ahead. This plot shows that the maximum CMI is reached at 8.5s and the CMI value is 0.65.

Then for each signal the range (min-max) was determined and a dummy signal was randomly generated within this specified range consisting out of 7500 data points. For each signal pair used in the CMI analysis the CMI analysis was repeated with the dummy counterparts. In this analysis similar settings were used. Separately, for every genuine signal the entropy was calculated according to the following formula:

$$H(X) = -\sum_{x\in\{1,2,3,\ldots,30\}} p(\{x = x\}) \cdot \log_2 p(\{x = x\})$$

Here, also 30 bins were used to bin the signal. The width of the bins is determined by the range of the signal. Here, $p(\{x = x\})$ is the probability that a data point (x) falls within a predefined bin (x). For each signal pair used in the CMI analysis it was determined which signal had the lowest entropy.

The lowest entropy, the CMI of the dummy signals and the CMI of the genuine signals were then used to calculate relative CMI for each signal pair:

$$CMI_{\text{rel}} = \frac{(CMI(X,Y) - CMI(X_{dummy}, Y_{dummy}))}{\left(H(X\ or\ Y) - CMI(X_{dummy}, Y_{dummy})\right)} \times 100$$

Once all 37 data sets were analyzed it was investigated whether the values that were found were influenced by the signal quality that was established in chapters 3 and 4. Furthermore by means of paired t-tests and Wilcoxon signed ranks tests it was evaluated whether outcomes differed between hemispheres. It was also

tested with similar tests whether the comparisons between alpha envelope and HbO_2 concentrations and alpha envelope and Hbb concentration changes were different.

5.3.2 Results

In order to calculate relative CMI the entropy of each signal used had to be calculated in order to determine which of the two signals of each pair displayed lowest entropy. The entropy on its own is an indication of the amount of information or the uncertainty that is contained in that signal (Shannon, 1948). The higher the entropy, the more uncertainty a signal contains which decreases predictability. When the entropies of the alpha envelopes and the NIRS signals were compared in this dataset it was shown that the entropy of the alpha envelope was lower than the NIRS entropies and therefore more predictable (averages displayed in table 5.5). Interestingly, the variability between subjects was larger for the alpha envelope compared to the NIRS signals as is visible in the higher SDs and ranges. No significant differences between right and left hemisphere were detected by means of a paired samples t-test for all measuring modalities. A significant difference was found though between the entropies of the HbO_2 and Hbb concentrations on the same location (O1: t=2.036, df=36, p=0.045; O2 t=3.076, df=36, p=0.004). Since higher entropy values were found for the HbO_2 concentrations, this difference indicates that the Hbb signals have higher predictability.

Entropy	**Alpha O1**	**Alpha O2**	**HbO_2 O1**	**HbO_2 O2**	**Hbb O1**	**Hbb O2**
Average	2.91	2.93	4.31	4.26	4.22	4.14
SD	0.60	0.59	0.25	0.30	0.28	0.30
Range	1.3–3.85	1.69–3.92	3.52–4.70	3.43–4.73	3.47–4.66	3.23– 4.59

Table 5.5 The average entropies for all signal modalities with their standard deviation (SD) and range. Legend: O1= left visual cortex, O2= right visual cortex, HbO_2= oxygenated haemoglobin, Hbb= deoxygenated haemoglobin.

The CMI_{rel} analysis between the alpha envelope and the HbO_2 as well as the Hbb concentration changes led to the following results, which are summarized in table 5.6A. When all subjects participate in the analysis it was found that on the O1 location on average 7.57 % dependency existed between the alpha envelope and

the HbO_2 concentration. On average this dependency was highest with a time shift of 3.03s. For the alpha envelope and the Hbb concentration the average dependency was a little higher, 8.12%, as was the time delay, 3.32s. For the O2 location, on average lower dependencies and time delays were found. Here the dependency between the alpha envelope and the HbO_2 concentration was 6.50% with a time delay of 2.05s and the dependency between alpha and the Hbb concentration was 5.83% with a time delay of 2.05s. A Wilcoxon signed ranks test revealed that this difference between the left and right hemisphere was only significant for the dependency of the alpha envelope and the Hbb concentration changes (z= 2.384, N-ties= 37, p= 0.017). Differences between dependencies on the same location were not significant.

Similar to the procedure that was adopted with the CCF analysis it was investigated whether data quality influenced the obtained results. All data that received a bad quality label in chapter 3 or 4 were excluded from the sample and the analysis was repeated (results are summarized in table 5.6B). This led to higher dependencies. On the O1 location the average dependency between the alpha envelope and the HbO_2 concentration changes was now 12.86% with an average time delay of 5.05s. The average dependency between alpha and Hbb concentration changes even reached 15.06% and had an average delay in reaching maximum CMI of 4.6s. For the O2 location the dependency values remained lower than for the O1 location. Here an average dependency of 10.32% was found for the alpha envelope and HbO_2 time series and 9.42% for the alpha envelope and the Hbb time series. Time delays were also lower compared to the O1 location, 2.78s and 1.5s respectively, with the latter one even being lower than was found when no data was excluded. Wilcoxon signed ranks tests were used to evaluate whether differences between left and right and differences between analyses over the same location were significant. It needs to be noted though that not for every subject that is left in the sample all comparisons could be performed because of missing data. Similar to the previous analysis, only the dependency of the alpha envelope and the Hbb concentration was significantly different between left and right (z= 2.028, N-ties= 7, p= 0.043).

As a last step the data showing a physiologically unexpected response (a negative delay of the hemodynamic data) were deleted from the sample. This resulted in

further increases of the dependencies between the signals as well as increases in timing of the delay (table 5.6C). In the analysis of the alpha envelope together with the HbO_2 concentration changes on the O1 location the average dependency was 14.28%, and maximum dependency was reached on average after 6.39s. When on the same location the alpha envelope was analyzed together with Hbb concentration changes a dependency of 15.51% was found and on average the maximum dependency was reached after 6.5s. For the O2 locations the average dependency values were slightly lower again (alpha envelope and HbO_2: 12.93%; alpha envelope and Hbb: 11.76%). However, the average time it takes to reach maximum dependency was longer for the O2 location (7.6s for alpha and HbO_2; and 7.0s for alpha and Hbb). Since only 3 pairs remained in the sample for statistical testing of differences between left and right these results are unreported.

A	**O1 alpha x HbO_2 N=37**	**O1 alpha x Hbb N=37**	**O2 alpha x HbO_2 N=37**	**O2 alpha x Hbb N=37**
CMI_{rel} (%)	7.57 (5.16)	8.12 (6.52)	6.50 (4.89)	5.83 (3.96)
Delay (s)	3.03 (6.15)	3.32 (5.80)	2.05 (6.30)	2.05 (6.63)
B	**O1 alpha x HbO_2 N=11**	**O1 alpha x Hbb N=10**	**O2 alpha x HbO_2 N=9**	**O2 alpha x Hbb N=9**
CMI_{rel} (%)	12.86 (5.53)	15.06 (6.60)	10.32 (6.94)	9.42 (4.99)
Delay (s)	5.05 (3.32)	4.6 (4.29)	2.78 (5.94)	1.5 (7.39)
C	**O1 alpha x HbO_2 N=9**	**O1 alpha x Hbb N=8**	**O2 alpha x HbO_2 N=5**	**O2 alpha x Hbb N=5**
CMI_{rel} (%)	14.28 (4.99)	15.51 (6.48)	12.93 (8.60)	11.76 (5.39)
Delay (s)	6.39 (1.61)	6.5 (1.73)	7.6 (2.16)	7.0 (3.82)

Table 5.6. Group averages of the highest relative cross mutual information (CMIrel expressed as a percentage) values and their shift in time domain. The standard deviation is presented between brackets. Section A displays the values that are obtained for the entire sample. Section B contains the values obtained after the data that was not of high enough quality was eliminated. Section C contains the results after the omission of the bad quality as well as the physiologically unexpected signals. Legend: N= number of subjects, O1= left visual cortex, O2= right visual cortex, HbO_2= oxygenated haemoglobin, Hbb= deoxygenated haemoglobin.

5.4 Discussion

In this chapter a method for evaluating the underlying coupling of the time series of the alpha envelope and the HbO_2 concentration changes as well as the Hbb concentration changes was presented. This method was derived from the information theoretic framework of Shannon (1948). To my knowledge, similar analyses have not been conducted on EEG and NIRS signals together yet. Two key aspects of performing this analysis in a meaningful way were highlighted in this chapter. The first one being the choice of the amount of bins to estimate the probability distributions based on the provided dataset. The second being the transformation of the obtained CMI values into relative CMI values based on the data to be analysed.

5.4.1 Choosing the appropriate bin size

Deciding upon the correct bin size when conducting analyses of measures derived from the information theoretic framework is an important first step. Lower bin numbers can lead to an underestimation of the MI, while higher bin numbers can lead to overestimation (Fraser and Swinney, 1986, Escudero et al., 2009). The differences in results were also found in this study when different bin sizes were applied to the data from the same subject, showing that the more bins were used, the higher MI values got. Furthermore, the choice of bins influenced the time point at which maximum MI was reached for this subject.

The method proposed here, first normalizes the data and then joins all data in one distribution. The number of bins that is chosen depends on whether the appearance of the distribution is normal and smooth. Simultaneously, this choice is guided by the analysis of dummy data, which are generated randomly in the same range as the experimental data so two signals are independent. The analysis of the independent data needs to approach zero. The choice in this study was 30 bins and a value of the dummy data of > 0.90.

A factor that strengthened this decision was that when the value of the dummy data was used as a threshold to determine whether two signals were independent all MI values found in the 30 bin analysis were higher than this threshold. This is expected since the EEG and NIRS data were measured over the same location

during the same paradigm and some form of coupling was determined already in chapter 4. When this was explored for the threshold of the 64 bin analyses (0.46) it was found that over half the subjects showed MI values below this threshold, suggesting that lower dependency between the EEG and NIRS data existed than it did for independent data (data unreported).

This method of deciding bin size has the advantage that it is easily understood and applied, however the choice of bin size remains somewhat arbitrary and the wrong choice leads to biased results. Other methods besides histogram binning exist for estimating the probability distributions needed for estimating MI. Among these are both parametric and non-parametric methods of estimation. The pros and cons of a number of these methods are reviewed by Walters-Williams J (2009). A further in depth discussion falls beyond the scope of this thesis but could be conducted in future research.

5.4.2 Relative Cross Mutual Information

As an extension of the exploration of the relationship between the changes in alpha magnitude and the HbO_2 and Hbb concentration changes that was carried out in chapters 3 and 4, the analysis of relative CMI was performed in this chapter. As expected, it was found that there was a mutual dependence both when alpha magnitude and HbO_2 were considered as well as when alpha magnitude and Hbb were evaluated. Similar to the findings with the CCF analysis in chapter 4, the strength of this dependency increased when bad quality data were removed, and even a further increase was seen when physiologically illogical data were removed. This was also true for the time point on which maximum CMI_{rel} was reached. For the CCF analysis this timing was between 7 and 8 seconds for all comparisons made. With the CMI_{rel} these values were a bit lower, between 6 and 7.5 seconds. In the CCF analysis the timing could be established with a resolution of 0.04 s. In order to speed up analysis time for the CMI_{rel} analysis the resolution was brought back to 0.5 s which could be an explanation for this difference. Another difference that was found between the different analyses was that not the exact same subjects that presented the physiological response in which a negative delay was seen. This finding could be due to the fact that the CMI_{rel} takes into account both linear and nonlinear relationships (Alonso et al., 2010, Ramanand et al., 2010). The additional nonlinear findings in coupling could

possibly result in a shift in time of maximum CMI_{rel}. Different from the CCF analysis it was also investigated whether there were statistical differences in the obtained CMI_{rel} values and the timing, between hemispheres as well as differences between alpha envelope and HbO_2 concentrations and alpha envelope and Hbb concentrations within the same hemisphere. When the whole sample was investigated it was shown that there was a significant difference between the left and right hemisphere for the dependency between the alpha envelope and the Hbb concentrations. Suggesting a stronger dependency in the left hemisphere. This was the only significant difference that was found. This finding remained when the bad quality data were removed from the sample. When also the physiological illogical data were removed only 3 pairs remained for statistical testing so these results were omitted. A reason for this finding was already briefly highlighted in chapter 3 when it was found that on the location measured over the right hemisphere more bad quality data was found. The human brain is positioned slightly rotated in the skull (Toronov et al., 2007). This causes the neocortex to be a little further away from the optode on the right side of the hindbrain compared to the left side of the hindbrain (for the frontal cortex this is the other way around). Since the difference between left and right remains when the bad quality data are removed another factor that possibly contributes to this difference is the amplitude of the Hbb signal. Compared to the HbO_2 signal, the Hbb signal showed smaller fluctuations in this data set. A standard feature of NIRS measurements is that during brain activation a response of two to three times the magnitude is seen in HbO_2 compared to Hbb (Ferrari et al., 2004). This smaller signal to noise ratio combined with the rotation of the brain could explain why this left-right difference is seen for the Hbb concentrations but not for the HbO_2 concentrations.

MI has been used previously to establish the dependency between EEG and fMRI data. Ostwald et al. (2010) used high and low contrast checkerboard stimulation in order to determine the dependency of the P100 peak of the visual evoked potential from a single electrode and the hemodynamic response under the area surrounding the electrode of the occipital cortex. However, the MI values that were found were low and mostly not significantly different from zero. In a follow-up study a different approach was adopted and MI was calculated over LORETA (low resolution electromagnetic tomography) and fMRI during a similar paradigm

Ostwald et al. (2011). In this study also the change in EEG alpha power to the stimulus of the checkerboard was considered. Again no dependency was found between the measurement modalities. A reason for the inconsistency with the current data, is that Ostwald et al. (2010) calculated MI over extracted features of both the EEG and fMRI data like peak amplitude and latency to a single stimulus. In doing so the time frame that is observed is small (1s for EEG and max 15s for fMRI) compared to the 5 min dataset that was analyzed in the current study. So to increase the number of data points (or time) that is used for MI analysis could have an advantage. Another advantage of simultaneously analysing NIRS and EEG data over the simultaneous analysis of fMRI and EEG data is that the EEG signal loses information due to the noise caused by the scanner and the subsequent data cleaning algorithms (Ostwald et al., 2010). The imposed noise and the necessity of cleaning the EEG time series extensively could also have confounded the information needed for the source localization algorithms. With the simultaneous use of NIRS and EEG this is less of an issue since the modalities do not impose noise onto one another.

A challenge with any MI analysis is the interpretation of the values. The higher the MI value between two signals is, the higher is their mutual dependence (Walters-Williams J., 2009). However, when the minimum and maximum possible value of the CMI are omitted this number has little meaning. Furthermore, it even becomes hard to compare results between subjects, because the maximum CMI value can have inter subject variation. In order to tackle this problem relative CMI was proposed in this chapter. The CMI_{rel} transforms the obtained CMI values to relative values based on the minimum and maximum possible values derived from the experimental data. By doing so, the obtained CMI can be expressed as a percentage. This makes sure that not only results can be compared between subjects, it allows the comparison of different brain regions, different measurement modalities, different clinical samples, and different points in time. It basically allows for the comparison of virtually anything because the values are corrected for the data that is used. This creates a great clinical advantage. The only potential drawback would be if the CMI_{rel} does not increase linearly. However, as Shannon (1948) points out in his framework of information theory, choosing a logarithmic base to compute entropy and MI causes parameters of importance to engineering, like time, bandwidth and number of relays to vary

linearly with the logarithm of the number of possibilities. Closely related to this it complies with people's intuitive feelings that two punch cards hold twice as much information as one punch card does (Shannon, 1948). Therefore, here the assumption is made that a CMI_{rel} value of 20% expresses a dependency which is twice as high as 10%. It also has to be noted that the bin size needs to be evaluated for each new dataset that is analyzed. In this study use was made of the alpha envelope only. When a broader EEG spectrum or a different frequency band is used the most appropriate bin size might be different. Therefore, clinically speaking, it would be beneficial to automate the processes described in this chapter in order to obtain a method of analysis that is less prone to arbitrary choices. In this automation process the generation of the dummy signals and thresholds for calculating CMI_{rel} should be the first step which can be performed hidden in the program before the entropy of the signals as well as the CMI_{rel} between the signals is given as a result both in number and in graph. Together with a database of representative data for healthy and pathological conditions clinicians would be able to interpret outcomes in a much more intuitive way to asses changes in the relationship between electrical and hemodynamic parameters in patients without the need to have in depth knowledge about the information theoretic framework. Furthermore, researchers from different fields could use the automated analysis in order to provide and expand the database for multimodal analysis but also for example to do connectivity analysis within one measurement modality between different brain locations.

However, something that CMI or CMI_{rel} is unable to do is to tell something about the direction of the dependency. The interpretation of the time point of when CMI_{rel} reaches a maximum when one of the signals is lagged in time is only a rough estimate. By doing so, the assumption is made that when the NIRS signal is the lagged signal and the maximum CMI_{rel} is reached after 6 to 7.5 s that this is because the hemodynamic response to neural activation takes several seconds, even though considerable variation is seen between subjects and brain regions (Handwerker et al., 2004). Based on this finding, subjects that showed a negative delay of the NIRS signal were excluded in the last step of the analysis because this indicated a physiologically illogical finding. However, as mentioned in the discussion of chapter 4 a lot of variation existed in the timing of the maximum CCF. This was also the case when the timing was considered for the CMI_{rel}. A

possibility exists that in some cases the changes in blood oxygenation parameters precede the changes in electrical activity with a physiologically sound reason. Similar to the study of Pfurtscheller et al. (2012) that indicated that in 2/3rd of the sample the slow waves seen in the HbO_2 preceded the waves in the EEG when HbO_2 at the frontal cortex and alpha and beta waves at the central cortex were found to be coupled.

There are measures derived from classical MI that are able to illuminate the direction of dependency between two parameters. Examples of these are Transfer Entropy and Mutual Information from mixed embedding. Transfer entropy (TE) measures the direction of information transfer between coupled dynamic systems and is explained in full by Schreiber (2000). Feas and Nollo (2013) however, point out in their research that TE is unable to specifically define the time lag needed in order to evaluate the timing of information transfer. They propose a modification of the TE that makes this possible (Faes and Nollo, 2013). Mutual Information from mixed embedding (MIME) and partial MIME are measures of directional coupling as well (Kugiumtzis, 2013). The exact functioning and application of these methods could be investigated further in future research on the coupling of EEG and NIRS parameters.

5.4.3 Entropy as a meaningful measure

Since the CMI_{rel} transformation corrects MI values based on the experimental data that is used, the entropy of all signals needed to be calculated. Entropy provides information on the amount of uncertainty in a signal, or in reverse, its predictability (Shannon, 1948). Higher entropy expresses higher uncertainty and therefore lower predictability. In the current dataset it was found that the alpha envelope yields smaller entropies and therefore higher predictability than either NIRS signal. The variety between subjects is larger though in the alpha entropy than it was for the NIRS entropies. Furthermore, it was established that when HbO_2 and Hbb concentrations were compared, the Hbb concentrations showed lower entropy and therefore higher predictability than the entropy of the HbO_2 concentrations. This finding is an important one when signals derived from NIRS measurements are evaluated as a whole instead of just the activation period. During an activation period it is after all assumed that the signal containing the HbO_2 changes and the signal containing the Hbb changes are anti-correlated close

to -1 (Cui et al., 2010). When this is the case, the predictability of both signals and therefore their entropy should be nearly equal. When the entire time series are considered in the analysis or during resting state, it is not only the activation period anymore that is contained in the signal. In this chapter it was shown that the information content of the HbO_2 and Hbb concentration changes are different in essence in which the Hbb signal has higher predictability This is an argument that enforces the view within the NIRS community to report both parameters in any NIRS research (as witnessed at the 2010 fNIRS conference in Boston). Furthermore, it complies with expectancy. Hbb concentration changes occur due to brain activation and are therefore quite straightforward, when neural activity increases, the Hbb concentration decreases and this decrease is tightly coupled to changes seen in the fMRI's BOLD response (Obrig and Villringer, 2003). The HbO_2 concentration changes however, are susceptible to more factors than brain activation like the regional CBF, changes in blood pressure, and increases in skin blood volume (Obrig and Villringer, 2003). Together with the two to threefold magnitude changes compared to Hbb changes (Ferrari et al., 2004) this leads to more components that influence the signal, which could increase the amount of uncertainty of the signal.

Knowing the entropy of brain activity can have a clinical advantage as well. For instance during epileptic seizures the EEG changes and displays more regular waves. Using entropy to detect changes in the EEG's predictability it was found that this measure had a sensitivity of 97% in discriminating EEG segments with and without seizures (Sakkalis et al., 2013). Gao and Hu (2013) used the measure of entropy together with several other measures to propose a real-time monitoring algorithm that is a candidate to monitor epileptic seizures in a clinical setting. However, it are not only neurological diseases that can benefit from the analysis of entropy. It has been shown that the EEG of people suffering from alcohol dependency displays, among other measures, lower entropy than the EEG of healthy people (Acharya et al., 2012). Furthermore, Takahashi et al. (2010) showed that patients suffering from schizophrenia showed less predictable EEG (estimated by entropy) in anterior brain areas compared to healthy people. When antipsychotic medication was administered, it was shown that this predictability normalized even though spectral changes could not be observed. Therefore, calculating the entropy of different signals, measurement modalities and

measurement locations, and how this entropy changes over time could potentially help to increase sensitivity and specificity of markers derived from brain activity as well as provide information about treatment effects.

5.5 Conclusion

This chapter showed that applying a method of data analysis derived from classical information theory as proposed by Shannon (1948) is feasible in analysing simultaneously acquired EEG and NIRS signals. Besides demonstrating this feasibility for the first time, the chapter illustrates how an appropriate bin size can be obtained needed for this analysis. It provides the reader with tools to transform the obtained results into CMI_{rel} values that simplify interpretation and comparison of results. Furthermore it was highlighted that besides information on the MI, calculating a quantitative measure of predictability of a signal (entropy) could have a clinical advantage as well. Future research should be directed at validating the clinical advantage in using these measures of entropy and CMI_{rel} to improve the sensitivity and specificity of diagnostics performed based on brain measurements as well as the guidance of treatment choice and treatment evaluation. In doing so providing clinicians and researchers with an automated unified analysis program would be beneficial.

Chapter 6: Simultaneous EEG and NIRS measurements explored in two cases of stroke

In the preceding chapters different forms of analysing brain activity have been explored to shed light on the information that can be extracted from individual measures of electrical and hemodynamic activity as well as the relationship between the two in a sample of healthy people. A pathology that is most likely to display a disturbance in the symbioses between electrical and hemodynamic activity is stroke. Therefore in this chapter two stroke cases will be used to illustrate possible dysfunction in this symbioses.

6.1 Introduction

The explorations that have been conducted so far in this thesis are all related to the functioning of the brain in an eyes open eyes closed paradigm in healthy people. Once a sense of a normal pattern of activation has been obtained and how the measures relate to each other, this exploration can be taken to the next step. Here it is explored how the parameters of brain activation and the dependency of electrical related parameters and hemodynamic parameters change in pathology.

As explained in chapter 1, the cerebral vascular network provides the neurons with oxygen and glucose and matches the CBF with the specific, local energy demands (Ward, 2013). The process of neurovascular coupling, in which vasoconstriction and –dilation give rise to functional hyperaemia and make sure that homeostatic blood pressure is maintained during periods of changing blood flow is a complicated one (Girouard and Iadecola, 2006, Cauli and Hamel, 2010, Ward, 2013, Howarth, 2014). Neurovascular coupling is, among other diseases, disrupted in stroke (Girouard and Iadecola, 2006, Blicher et al., 2012, Ayata, 2013). Stroke is a disruption to the cerebral blood supply and mostly occurs because of a vascular rupture or a blockage of an artery which causes the surrounding tissue or tissue that is prevented from blood to be damaged or die. According to the World Health Organisation stroke is worldwide the second

leading cause of death and the first leading cause of disability. The probability of a first stroke is 1.6 per 1000 (WHO).

Due to the disruption of the CBF the homeostasis is disrupted as well, causing a disturbance to the delivery of nutrients to the neural cells, impairing the removal of potential harmful by-products of cerebral metabolism, and potentially leading to brain dysfunction (Girouard and Iadecola, 2006). Another mechanism that could be responsible for a disruption in neurovascular coupling after stroke is caused by spreading depolarization (or spreading depression) which is common in migraine, but also visible after stroke (Ayata, 2013). Blicher et al. (2012) demonstrated that chronic stroke patients showed other changes in BOLD response compared to healthy people elicited by a motor task, ranging from positive, to negative, to absent changes in hemodynamics, while increases in CBF and CBV due to the task were present. This could be due to the fact that in stroke, baseline CBF and CBV as well as impaired vascular reserve capacity alters hemodynamic changes (Mandell et al., 2008). As a consequence of these changes in hemodynamics, neural activity is not necessarily coupled to regional CBF and CBV changes to the same degree as in healthy subjects (Blicher et al., 2012). In order to gain insight in both the neural and hemodynamic changes after stroke the multimodal approach of combining EEG and NIRS as discussed throughout this thesis would be helpful.

Since NIRS has advantages of being relatively low cost and it is capable of bedside monitoring of brain oxygenation, one would expect NIRS to have found its way into clinical neurology 35 years after its discovery by Jobsis (1977). However, possibly due to the difficulties in comparing research from different groups and the number of parameters that are suggested to hold promise in differentiating health and disease this is not quite the case (Obrig, 2013). Clinical use is made of NIRS in the operating room to monitor possible ischemia during cardiac and carotid artery surgery as well as in neonatology (Obrig and Steinbrink, 2011). However, continuous monitoring of brain oxygenation with NIRS during the subacute phase just after diagnosis and during initial treatment of stroke also has promising potential (Obrig, 2013). Monitoring of this kind could help detecting delayed ischemia in the stroke unit. Quantitative EEG possesses similar advantages in bedside monitoring and has been used more often than NIRS to show changes directly after stroke. Due to ischemic stroke a diminishing of the

beta activity can occur, followed by a slowing of the alpha peak and lastly enhanced delta activity is found (Jordan, 2004). The occurrence of this enhanced delta activity correlates with the site of the lesion and puts QEEG forward as an aid to localising the lesion (Finnigan et al., 2004). Also measures obtained from the QEEG have shown to have predictive value of the patient's outcome. Here one of the strongest predictors is the change in delta power in the (sub)acute phase which has been shown to correlate well with the National Institute of Health Stroke Scale (Finnigan et al., 2004). The reduction of delta wave activity over the site of the lesion also correlates with the amount of language recovery (Meinzer et al., 2004). For short term outcome the reactivity of the theta and alpha band can also be a good indicator when the QEEG is made within the first 24 hours (Cuspineda et al., 2007). Therefore, it has been suggested that the delta-alpha-ratio could be used as an appropriate index of outcome, since this index 48h post stroke shows significant correlations with the National Institute of Health Stroke Scale scores at 30 days as well as other functional outcome measures (Finnigan et al., 2004, Leon-Carrion et al., 2009). In addition to the delta-alpha-ratio, the brain symmetry index (BSI) in which asymmetries between homologous pairs of electrodes are computed, has also been found to correlate with stroke outcome and to have predictive value for disability (Finnigan and van Putten, 2013). In this case higher asymmetry scores indicates worse outcome. Evidence shows that recovery depends on the involvement of areas unaffected by stroke, either proximal to the damaged areas or in contra lateral homologues (Eliassen et al., 2008).

During the rehabilitation phase, possible differences in hemodynamic functioning can be investigated by assessing the responsiveness to established tasks (Obrig, 2013). This is of course also true for EEG. The eyes open, eyes shut response of the visual cortex which has been described throughout this thesis is one of these established tasks. Differences in the expected response can be observed as a primary indication of altered brain function. Besides that, also two aspects of functional reorganization can be assessed: 1) the recruitment of additional cortical areas during the task, not seen in healthy subjects, and 2) lateralization in cases where this applies (like unilateral motor control or language) (Obrig, 2013). For example, hand movement and gait studies with NIRS have shown that initially post stroke, activity is measured over both hemispheres (Kato et al., 2002), but as

rehabilitation continues this activation becomes unilateral or asymmetric (Miyai et al., 2003, Takeda et al., 2007). Furthermore, EEG signal synchrony between the medial and lateral motor areas was found to be greater in stroke patients than in healthy people but this difference diminished with recovery (Strens et al., 2004).

Other investigations could rely on findings from resting state measurements. For EEG, the parameters obtained in the (sub)acute phase, like delta power, delta-alpha ratio and BSI can be monitored in follow-up measurements to see if the patient is getting better or worse (Finnigan and van Putten, 2013). A resting state NIRS study found that the group of patients that had had a cerebral infarction at least 12 months prior to the measurements, had lower amplitudes of LFO's compared to a healthy sample, which was assumed to be related to a diminishing of the vasodilation capabilities (Li et al., 2010).

So by regularly using brain measures from diagnosis onwards throughout intervention or rehabilitation clinicians would be able to get a quality monitoring system that has the ability to assess the severity of the stroke as well as an indication of the magnitude of the recovery or possible treatment outcome. The concurrent measurement of EEG and NIRS in stroke patients has, as yet, not been described in the literature. In this chapter the brain activity of two stroke patients will be explored in order to reveal how their brain activity in the electrical and hemodynamic domain as well as the dependency between both is different from the outcomes that have been found in earlier chapters of this thesis.

6.2 Method

6.2.1 Participants and paradigm

The data for this study were provided by the Biometrical Centre in Gulpen, the Netherlands. The therapist conducting the measurements was certified according to the Dutch Ministry of Health, Welfare and Sports (BIG-registered) and its ethical terms and regulations apply. Two stroke patients came to the Biometrical Centre in order to obtain a clearer picture of their brain activity. The participants signed consent that their anonymous data could be used for scientific purposes. The patients underwent simultaneous measurements of EEG and NIRS over the O1 and the O2 locations of the visual cortex. The first patient was a female in her

early thirties. The other patient was a male is his late fifties. The Dutch version of the Barthel Index was administered prior to the measurement in order to obtain insight in the degree of normal functioning in everyday life (de Haan et al., 1993). The paradigm used was similar to the paradigm described in paragraphs 3.2.2 and 4.2.2. which meant that 5 minutes of brain activity was registered in an upright position and every 30 seconds the participants were asked to change from eyes closed to eyes open and vice versa.

6.2.2 Equipment and data analysis

The equipment used for conducting the measurements was also similar to the equipment used to measure the healthy population (a description of the EEG and NIRS amplifier can be found in paragraphs 3.2.3 and 4.2.3).

First the static measures of the frequency bands (paragraph 3.2.4.1) were investigated together with the changes in HbO_2 and Hbb concentrations (paragraph 3.2.4.3). Hereto average amounts of delta (0.5-3.5 Hz), theta (3.5-7.5 Hz), alpha (7.5-12 Hz), beta1 (15-20 Hz) and beta2 (20-32 Hz) activity as well as HbO_2 and Hbb were calculated for the last halves of every block. All obtained measures were tested for normality by means of the Kolmogorov-Smirnov test. When normality was assumed, a one-sample t-test was conducted in order to determine whether the obtained result for the stroke patient was different from the healthy sample. When the assumption of normality was violated a one-sample Wilcoxon signed ranks test was used to investigate possible differences.

Then the APF was explored for each block (paragraph 3.2.4.2) and it was determined whether a difference with the healthy sample was seen. When a structural difference in APF was found, an individual alpha band was determined with the individual APF based in the centre. All following tests were then performed on the original alpha band as well as the individual alpha band. When it was found that the faster wave activity was hardly seen anymore and the most prominent activity was seen in the delta band due to the severity of the stroke, all following analyses were also conducted on the delta frequency band (0.5-3.5 Hz).
The alpha envelope was calculated and assessed on quality (paragraph 4.2.4.1). This quality check was also performed for the HbO_2 and Hbb time series (paragraph 3.2.4.3). After that the nonlinear measurement LRTC was used on the

alpha envelope to investigate possible changes in EEG dynamics in stroke (paragraph 4.2.4.2). The LRTC value was compared to the LRTC values of the norm group as well as to a subset of surrogate data obtained from the alpha envelope of the stroke patient. When the data was found to be normally distributed a one-sample t-test was used for this comparison, otherwise the nonparametric equivalent, the one-sample Wilcoxon signed ranks, was performed.

Then the information or uncertainty in each time series for alpha, HbO_2, and Hbb was investigated by means of the entropy measure (paragraph 5.3.1.4). For the estimation of the entropies 30 bins were used. These outcomes were also compared to the outcomes obtained in the healthy sample by means of the one-sample t-test or its nonparametric equivalent.

As a last analysis the CCF (paragraph 4.2.4.3) of alpha and HbO_2 and alpha Hbb and its non-linear counterpart CMI_{rel} (30 bins) (paragraph 5.3.1.4) were explored to see whether differences in the electrical versus the hemodynamic relationship exist for stroke patients compared to healthy subjects. This was again done by means of a one-sample t-test or a one-sample Wilcoxon signed ranks.

6.3 Results

6.3.1 Case 1

The female patient described in this case suffered from a CVA in the right hemisphere when she was in her childhood. Since then she has gone through extensive rehabilitation. At the time of the measurement she was in her early thirties. The score on the Barthel Index was 20, which is the maximum score and an indication that she is able to function independently (Appendix C1).

6.3.1.1 Static EEG frequency measures

When the averages of the last half for each block were considered for every frequency band it appeared that during EC conditions each band displayed higher magnitudes compared to EO conditions. An exception to this rule was the delta activity which showed this pattern less distinctively. Another finding was that over the 5 minute measurement all values seemed to increase slightly. These findings were similar for the O1 and the O2 location (figure 6.1).

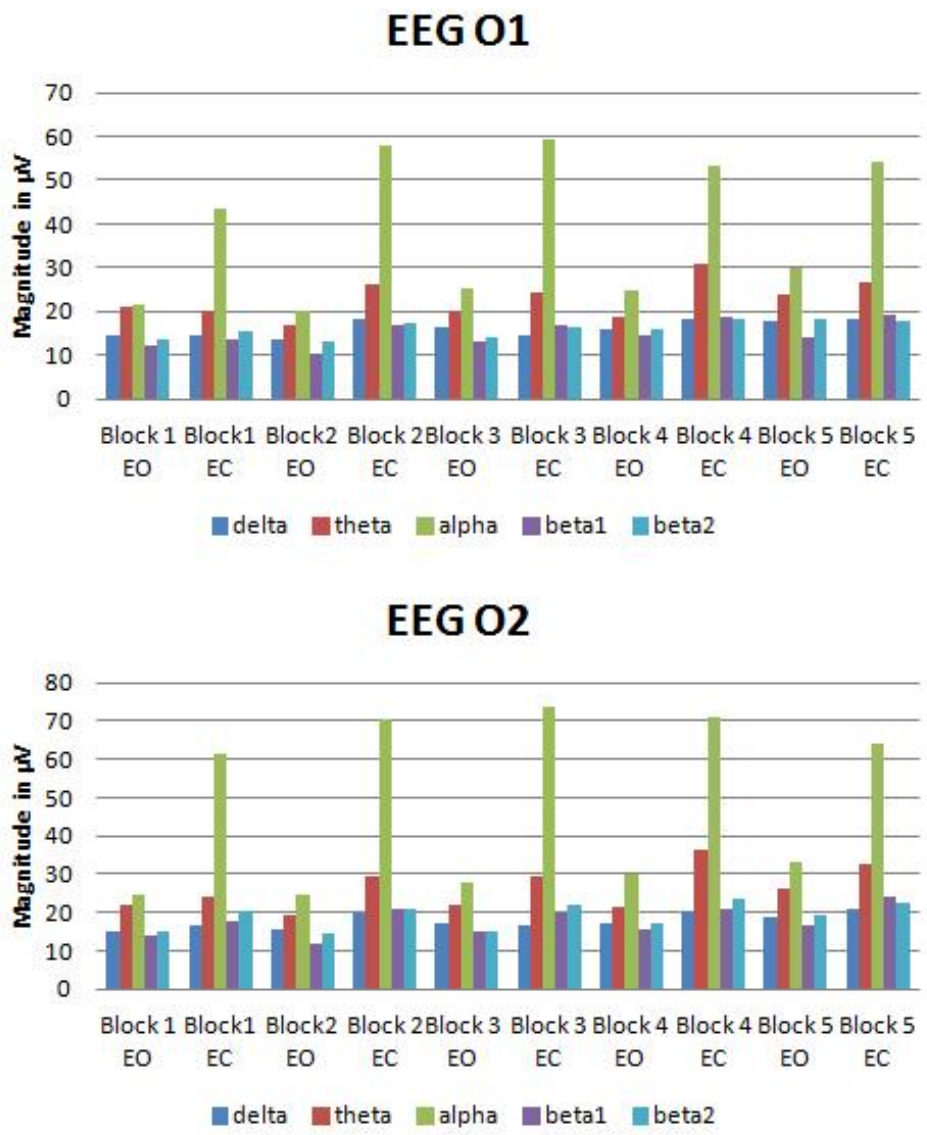

Figure 6.1 The EEG fluctuations of each frequency band for both the left occipital (O1, upper panel) and right occipital (O2, lower panel) locations. The average magnitudes per last half of the block are plotted.

In the norm group higher values during EC conditions were only found for the alpha, beta1 and beta2 bands. The difference in theta activity was not different between conditions and within the delta band higher values during EO conditions were found. The deviances from the healthy sample in direction of change were therefore mainly seen in the delta and theta band. When the obtained values were compared to values found in the norm group by means of a one sample t-test it was found that this patient showed significantly higher values in all frequency bands in every block on both measurement locations except for the

delta activity in block 2 with eyes opened on the O1 location. All p-values were highly significant (a summary of all results can be found in Appendix A).

6.3.1.2 Static NIRS measures

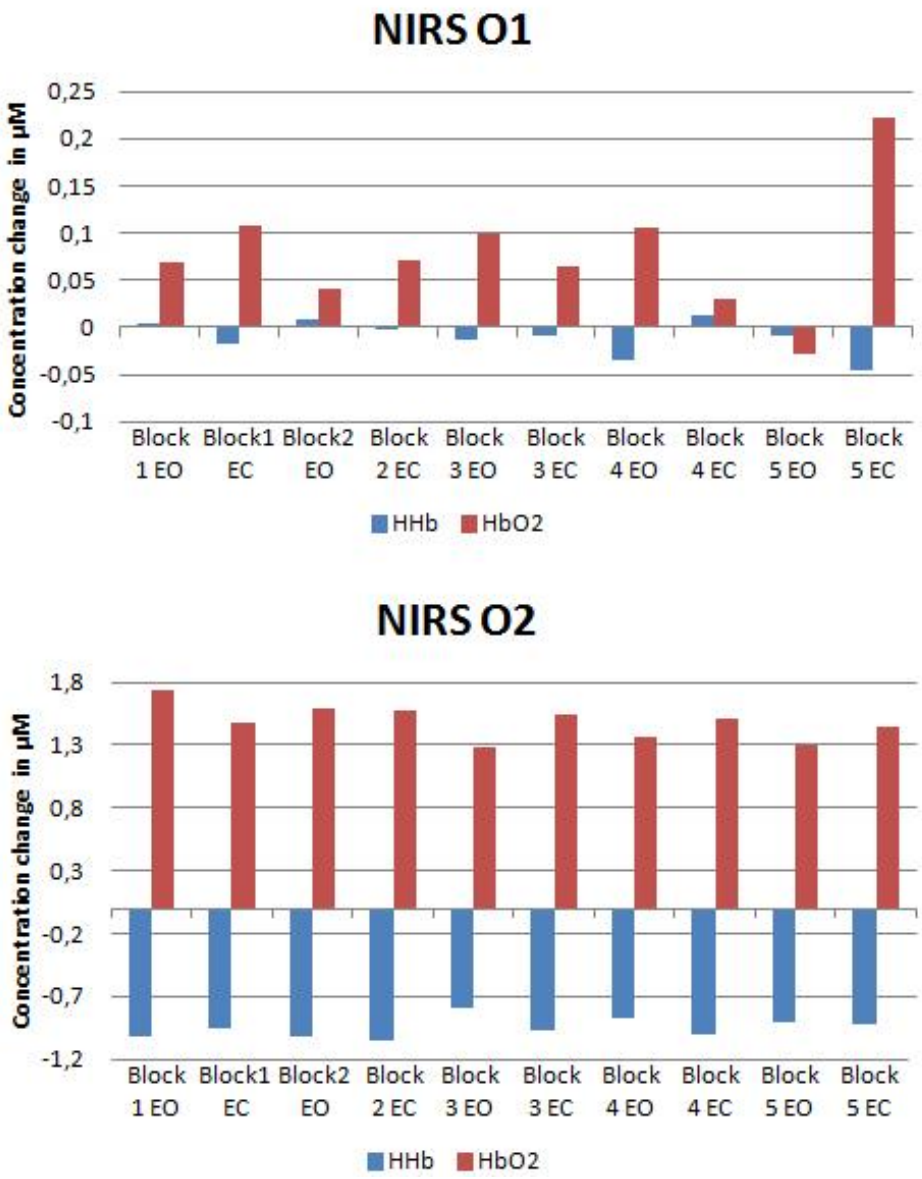

Figure 6.2 The fluctuations of oxygenated haemoglobin ($HbO_{2)}$ and deoxygenated haemoglobin (Hbb) concentrations on both the left occipital (O1, upper panel) and right occipital (O2, lower panel) locations. The average concentration changes of the last half of each block are plotted.

Whereas a pattern in which higher values of HbO_2 concentrations during EO blocks and higher values of Hbb concentration was expected, the results for this patient were more diverse and sometimes even reversed (figure 6.2). On the O1 location the first two minutes showed a reversed pattern in which the HbO_2

concentration increased upon closing the eyes and the Hbb concentration decreased upon closing the eyes and vice versa. In the third and fourth minute the pattern changed and an expected pattern was shown. The fifth minute however, showed a reversed pattern again. When the concentrations were tested against the concentrations found in the healthy population only significant differences were found during the EO blocks. The findings indicated that during blocks EO1, EO2, and EO5 (the reversed blocks) a significant lower concentration HbO_2 and a significant higher concentration Hbb was found. During the EO3 and EO4 blocks the concentration HbO_2 remained significantly lower than that of the healthy population whereas the Hbb concentration was not significantly different anymore (Appendix A, table A3).

On the O2 location it were the first two minutes that an expected response was seen for the HbO_2 concentration, for the Hbb concentration this was only the first three blocks (1.5 min). After that, the response changed to a reversed response. The one sample t-tests for the O2 location revealed that all measurements taken from this location were significantly different from the measurements in the healthy group in which in all blocks a higher concentration HbO_2 was registered and a lower Hbb concentration (Appendix A, table A4).

6.3.1.3 Alpha Peak Frequency

During the first two minutes a stable APF of 10.5 Hz was observed in every selected block on both the O1 and O2 location. In the last three minutes however, a drop in the APF was seen only in the EO conditions in which the APF ranged between 7.5 and 8.5 Hz. This was a significant drop and especially striking since the drop that was seen in a subsample of the healthy population only showed a lower APF during EC conditions.

6.3.1.4 Time series quality labels

When the quality of the alpha envelope as well as the filtered HbO_2 and Hbb time series was evaluated as was done with the healthy sample it became apparent that the alpha response was clearly visible on both locations. The response seen in both NIRS signals got a medium or a medium-bad quality label in which the O1 location showed a better response than the O2 location (the direction of the response was not evaluated here).

6.3.1.5 Long range temporal correlations

	t	df	Sig (two tailed)	Mean dif.	Tested value	Group mean
Alpha O1	4.708	37	.000*	.3743	-2.7190	-2.3446
Surrogate O1	18.106	19	.000*	.1607	-2.7190	-2.5583
Alpha O2 group	4.737	37	.000*	.3597	-2.7615	-2.4018
Surrogate O2	2.343	19	.030*	.0193	-2.7615	-2.7421

Table 6.1 The difference in long range temporal correlation (LRTC) slope. Results from the one samples t-test, testing differences between the stroke case and the healthy sample as well as it is tested against surrogate data on both the left (O1) and right (O2) occipital cortex. Significant results are indicated with an asterisk.

The LRTC of the alpha envelope was calculated for both locations and tested against the values that were found in the healthy sample as well as it was tested against 20 surrogate signals that were obtained by shifting the phases of the original alpha envelope (table 6.1). These tests showed that the alpha envelope was significantly different from the healthy sample and that it was also different from its own surrogate data. In all comparisons lower values were found which indicate a steeper slope.

6.3.1.6 Entropy

Next the entropy of the alpha envelopes, the HbO_2, and the Hbb time series were investigated. Equal to the findings in the healthy sample, lower entropy was found for the alpha envelope compared to the entropy of the NIRS signals. However, when the entropies were compared to the entropies found in the healthy sample it was found that the entropies of the alpha envelopes were significantly higher and the entropies of the HbO_2 time series were significantly lower (table 6.2). The entropy of the Hbb time series was also significantly lower on the O1 location, but did not reach significance on the O2 location.

	t	df	Sig (two tailed)	Mean dif.	Tested value	Group mean
Alpha O1	-6.278	36	.000*	-.61757	3.53	2.9124
Alpha O2	-9.945	36	.000*	-.96135	3.89	2.9286
HbO_2 O1	2.722	36	.010*	.11108	4.2	4.3111
HbO_2 O2	7.787	36	.000*	.35757	3.9	4.2576
Hbb O1	2.128	36	.040*	.09676	4.13	4.2268
Hbb O2	-1.058	36	.297	-.05162	4.19	4.1384

Table 6.2 The difference in entropy. The results from the one samples t-test, testing differences between the stroke case and the healthy sample. Significant results are indicated with an asterisk. Legend: O1= left visual cortex, O2= right visual cortex, HbO_2= oxygenated haemoglobin, Hbb= deoxygenated haemoglobin.

6.3.1.7 Correlation and dependency between modalities

First the CCF was calculated for the pairs alpha with HbO_2 and alpha with Hbb to obtain insight in the linear correlation (figure 6.3). Then the nonlinear counterpart CMI_{rel} was calculated (figure 6.4).

Despite the functions being similar on the O1 and O2 locations, the CCF analysis showed higher correlation strength on the O1 location. Here the alpha x HbO_2 had a maximum correlation value of 0.289 whereas this value only reached 0.099 on the O2 location. For the alpha x Hbb analysis a maximum correlation was found with a value of -0.358 on the O1 location and -0.207 on the O2 location. This could be due to the better signal quality that was registered for the NIRS signals on the O1 location. All correlations were above the confidence interval of 95%. The direction of the correlation is unexpected and therefore caused the results to be different from the healthy sample (an overview of these results is given in table A5 in Appendix A).

All comparisons showed a maximum correlation at a negative time lag (O1 alpha x HbO_2: lag -176 (-7.04s); alpha x Hbb: lag -175 (-7s); O2 alpha x HbO_2: lag -209 (-8.36s); alpha x Hbb: lag -188 (-7.52s)). This is an indication that the changes in the hemodynamic parameters preceded the changes in alpha response.

When the CMI_{rel} was used to analyse the time series, the difference between the O1 and O2 location was not present anymore. The maximum CMI_{rel} for the alpha x HbO_2 pair was 5.7151 on the O1 location and 6.7262 on the O2 location. For the alpha x Hbb pair the O1 location showed a maximum CMI_{rel} of 6.8215 and the O2 location 6.9890. CMI_{rel} was found to be lower than it is for the healthy sample. When this was statistically tested against the data from the healthy sample that had the bad signals removed only the comparisons obtained on the O1 side were significantly lower (table 6.3).

When the timing of the maximum CMI_{rel} value was considered it appeared that the timing was found to be different from the CCF analysis except for O1 alpha x HbO_2 (O1 alpha x HbO_2: -7.0s; alpha x Hbb: 9s; O2 alpha x HbO_2: -6s; alpha x Hbb: -1.5s). The maximum dependency value of alpha x Hbb on the O1 location had switched to a positive value which indicated that changes in the alpha signal precede the hemodynamic signal. Furthermore, the negative lags that were found on the O2 location became less negative indicating a smaller delay in responsiveness of the alpha signal to the hemodynamic signal.

	t	**df**	**Sig (two tailed)**	**Mean dif.**	**Tested value**	**Group mean**
Alpha x HbO_2 O1	4.282	10	.002*	7.14125	5.7151	12.8564
Alpha x Hbb O1	3.946	9	.003*	8.23652	6.8215	15.0580
Alpha x HbO_2 O2	1.637	9	.136	3.59178	6.7262	10.3180
Alpha x Hbb O2	1.463	8	.181	2.43548	6.98900	9.4244

Table 6.3 The difference in relative cross mutual information (CMIrel). The results from the one samples t-test of the stroke case tested against the healthy sample that has the qualitatively bad data removed. Significant results are indicated with an asterisk. Legend: O1= left visual cortex, O2= right visual cortex, HbO_2= oxygenated haemoglobin, Hbb= deoxygenated haemoglobin.

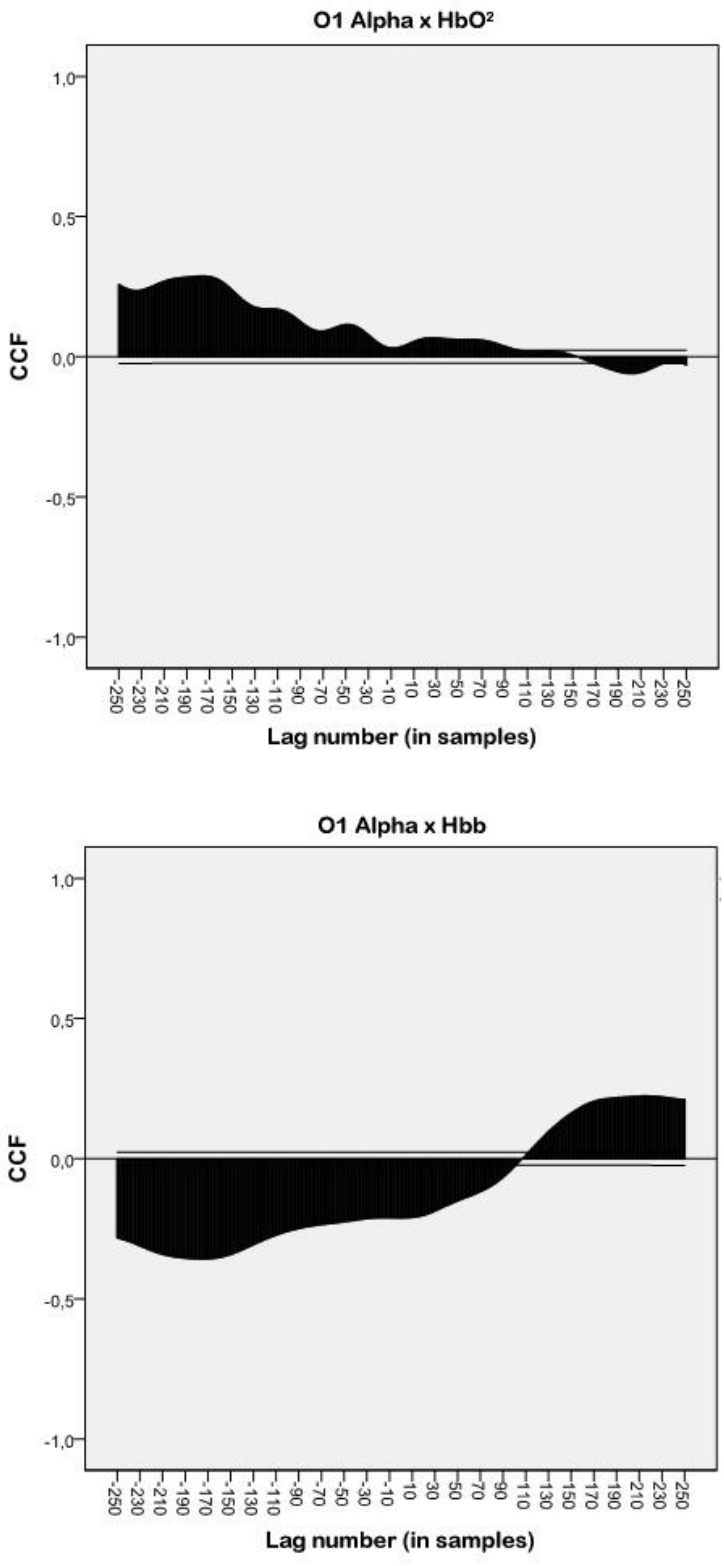

Figure 6.3a The cross correlation function (CCF) for the pairs alpha x HbO_2 (upper panel) and alpha x Hbb (lower panel) for the O1 location. The hemodynamic signal is the signal that is lagged +10 and -10 seconds. The two horizontal lines above and below the nil line indicate the 95% confidence interval. Legend: O1= left visual cortex, HbO_2= oxygenated haemoglobin, Hbb= deoxygenated haemoglobin.

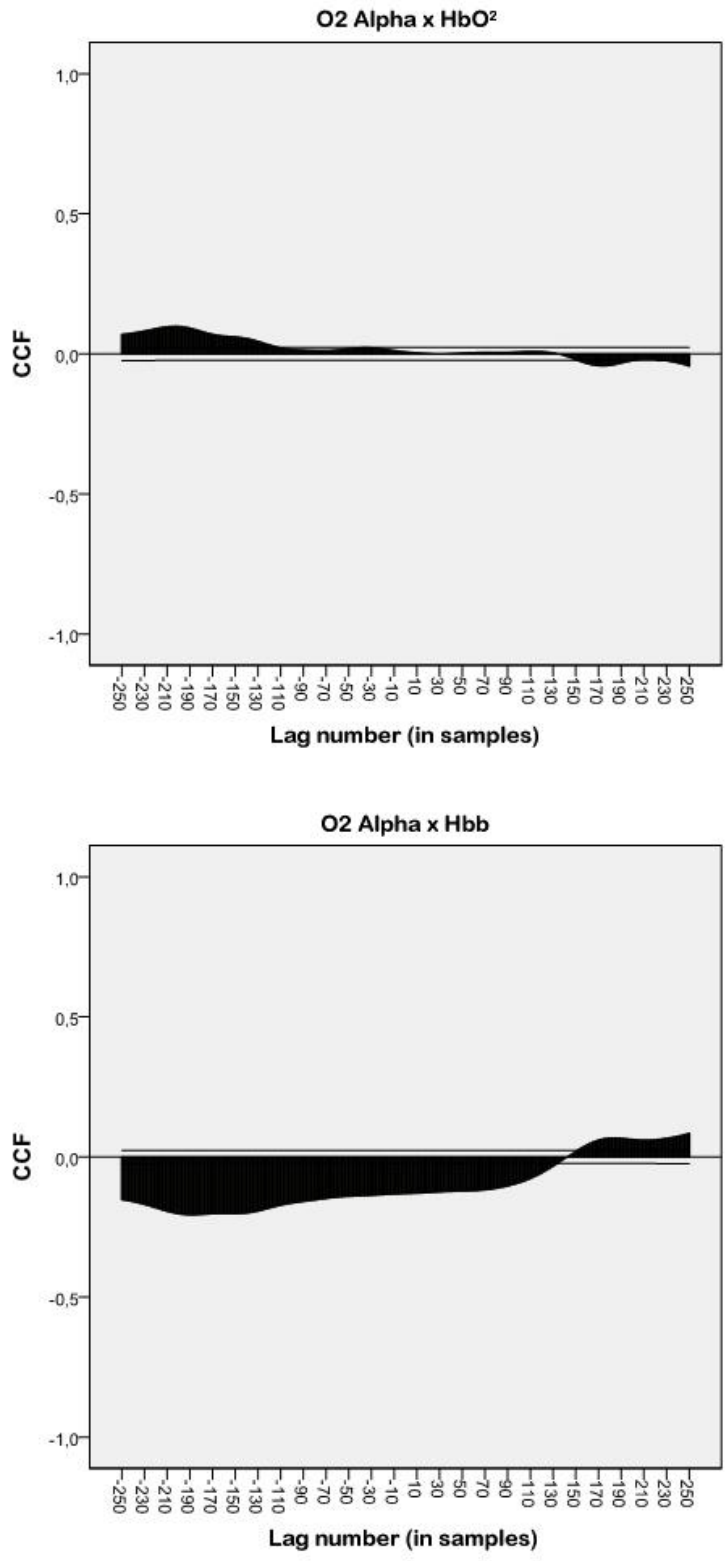

Figure 6.3b The cross correlation function (CCF) for the pairs alpha x HbO_2 (upper panel) and alpha x Hbb (lower panel) for the O2 location. The hemodynamic signal is the signal that is lagged +10 and -10 seconds. The two horizontal lines above and below the nil line indicate the 95% confidence interval. Legend: O2= right visual cortex, HbO_2= oxygenated haemoglobin, Hbb= deoxygenated haemoglobin.

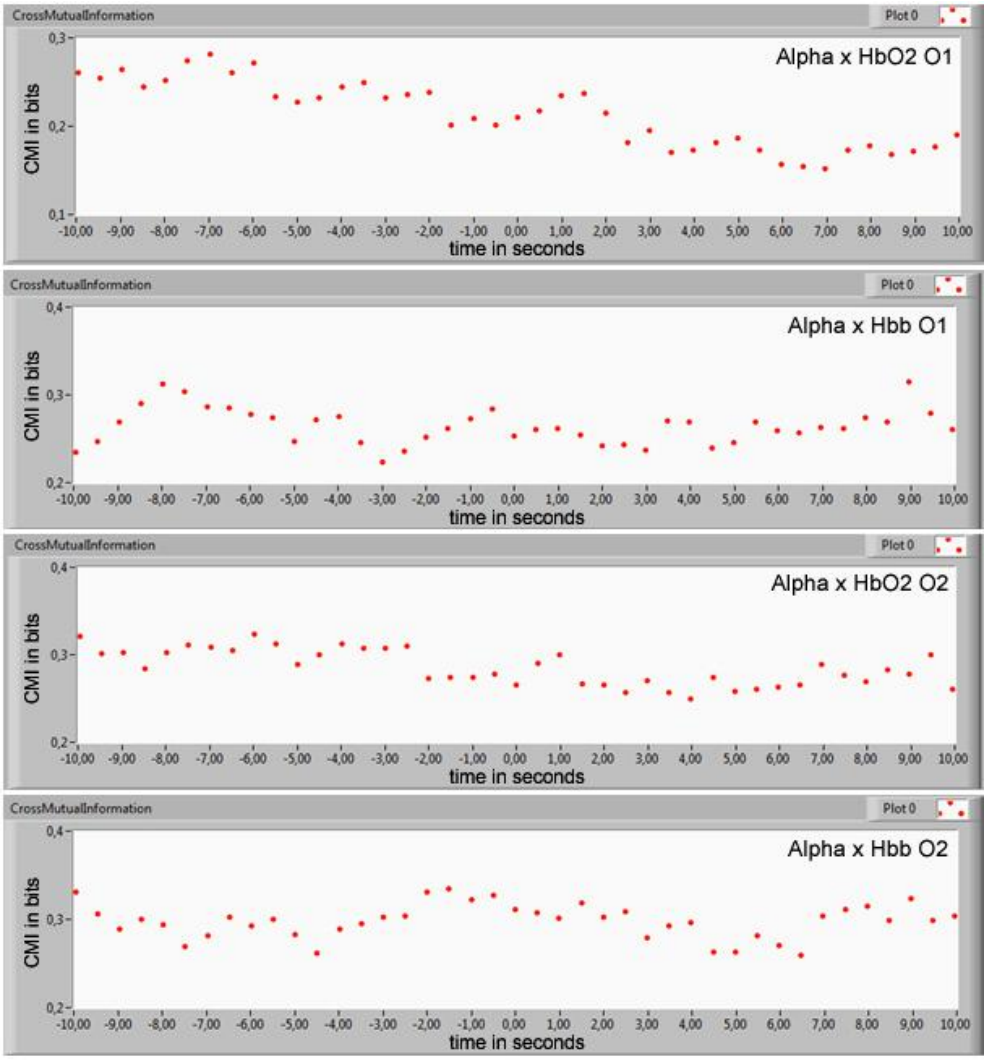

Figure 6.4 The cross mutual information (CMI) for the pairs alpha x HbO_2 and alpha x Hbb for both the O1 and O2 location. The hemodynamic signal is the signal that is lagged +10 and -10 seconds. Legend: O1= left visual cortex, O2= right visual cortex, HbO_2= oxygenated haemoglobin, Hbb= deoxygenated haemoglobin.

6.3.2 Case 2

The second patient was a male in his late fifties. This patient had suffered multiple strokes. As a consequence of the severity, vision and mobility were highly impaired as indicated by the score on the Barthel Index (Appendix C2). This score was 1, which is an indication this patient cannot function independent and is in need of help. The time between his last stroke and the measurements was >12 months.

6.3.2.1 Static EEG frequency measures

A striking observation in the EEG was that the delta band was the only band that showed a consistent change between conditions in which the magnitude was always higher in the EC condition compared to the EO condition. All other frequency bands hardly changed or showed inconsistent changes (figure 6.5). The average magnitudes for each block and frequency band were compared to the results obtained in the healthy sample by means of a one sample t-test. The results of all comparisons can be found in appendix B (table B1 and B2). Out of all 50 comparisons that were made on the O1 location a significant difference was found in 36 blocks. On the O2 location 39 blocks out of 50 showed statistically significant differences. The delta band showed lower magnitudes than it did for healthy population in the EO conditions and higher magnitude in the EC conditions. For the O1 location in the blocks EO1 and EO5 this difference failed to reach statistical significance. For the O2 location the lower delta values during EO blocks and higher delta values during EC blocks were only seen in the last three minutes of the measurement. Blocks EC1, EO2 and EC2 failed to reach statistical significance and in these EC blocks the direction of the difference was not confirmed.

The theta activity appeared to be constantly higher in this patient compared to the healthy sample on both locations with the exception of block EC2 on the O2 location. This was the only block on this location that also did not show a statistical significant difference. For the O1 location the higher theta magnitude was not significant for the blocks EC2, EC3, and EO4.

All alpha blocks showed a statistically significant difference from the healthy population which is possibly due to the lack of responsiveness of the alpha band to the paradigm. It was found that in all but one comparison (EO2 O1) the magnitude of the alpha activity was significantly higher during EO conditions and significantly lower during EC conditions. In the EO2 block on the O1 location the alpha magnitude was lower than found in the healthy sample.

For the beta 1 activity, all comparisons that were significantly different from the healthy sample showed a lower magnitude. This included all blocks on the O2 location and all but the EO1 and EO2 block on the O1 location. The differences

found in beta2 magnitude were mostly not significantly different from the healthy group. Both on the O1 and O2 locations only 3 out of 10 blocks were different. These were for the O1 location EO2, EC3, and EC4 and for the O2 location EC1, EC2, and EC4 in which during EC blocks a lower beta2 magnitude was registered and in the EO block a higher beta2 magnitude.

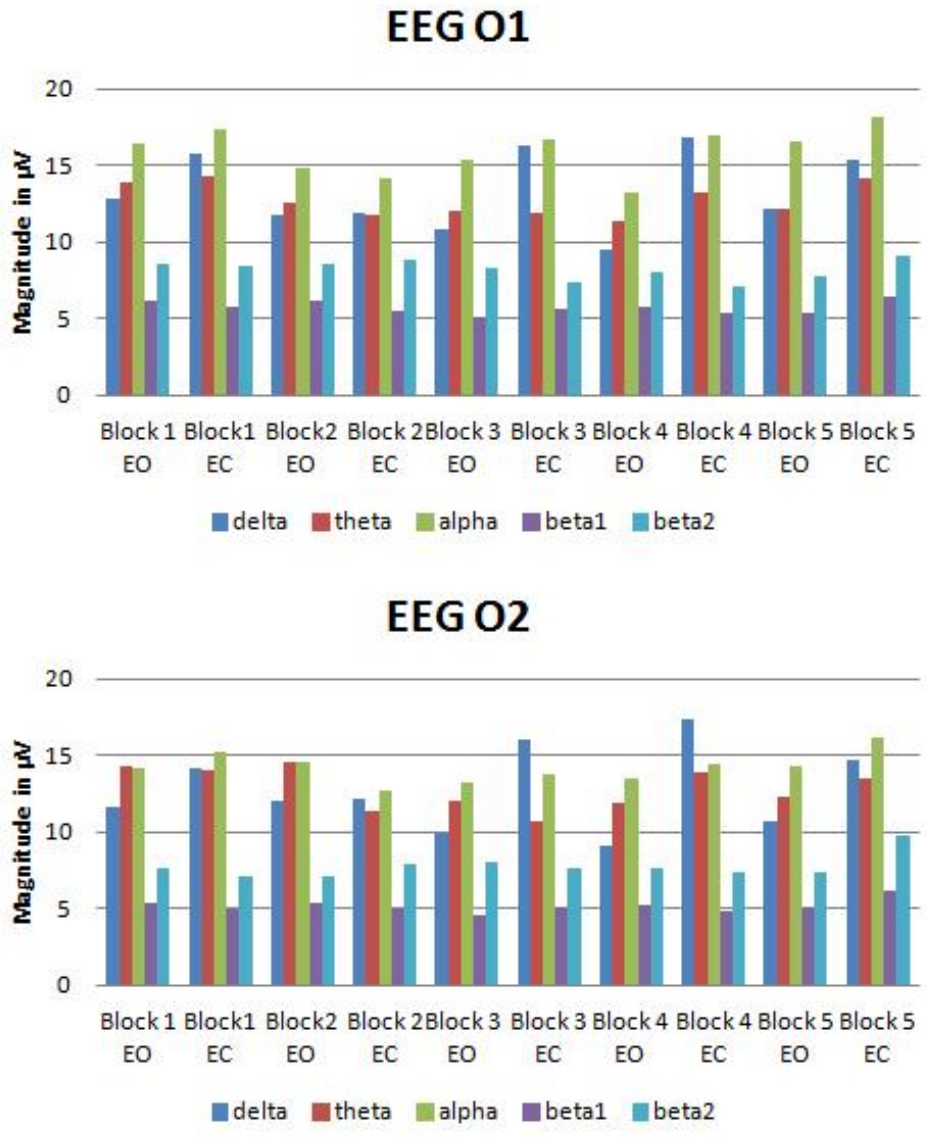

Figure 6.5 The EEG fluctuations of each separate frequency band for both the left occipital (O1, upper panel) and right occipital (O2, lower panel) locations. Only the average magnitudes per last half of the block are plotted.

6.3.2.2 Static NIRS measures

The changes in HbO_2 and Hbb concentrations differed from the expected findings as well. A visual interpretation of the findings is presented in figure 6.6. Firstly, the

signals on the O1 and the O2 location were very different from one other. The signal that showed the largest response on the O1 location was the Hbb signal whereas usually a larger response in HbO_2 is seen. This response followed the expected pattern of increase in concentration in EC blocks and decrease in EO blocks nicely. The HbO_2 response was much smaller and followed the shape of the Hbb concentration changes the first 3 minutes, while opposite changes were expected. This opposite reactivity occurred in blocks EO4, EC4 and EO5, but block EC5 showed a similar response to the HbO_2 signal again. On the O2 location an opposite reactivity between HbO_2 and Hbb was seen and as expected the HbO_2 signal showed the largest reactivity. However, in the first 5 blocks (2.5 minutes) a reversed activation response was seen, which switched to an expected response in blocks 6 through 9. The last block showed a reversed response again. The part of the measurement that showed the expected response was also the part that showed the largest differences between the sequential blocks.

When the results were compared to the healthy sample, different findings occurred on both locations. On the O1 location it was found that all but three blocks constantly displayed statistical significant differences from the healthy sample. The findings indicated lower HbO_2 concentrations and higher Hbb concentrations during both EO and EC blocks. The only blocks that failed to reach significance were the EC2, EC3 and EC4 blocks for the HbO_2 concentration. For the O2 location fewer blocks reached statistical significance, 12 out of 20 (the exceptions were: HbO_2: EC2; Hbb: EC1, EO2, EC2, EO3, EO4, EC4, EC5). The blocks that did display significant differences showed a similar pattern as was seen on the O1 location with lower HbO_2 concentrations and higher Hbb concentration in both EO and EC blocks. A summary of all comparisons and their *p*-values can be found in Appendix B (table B3 and B4).

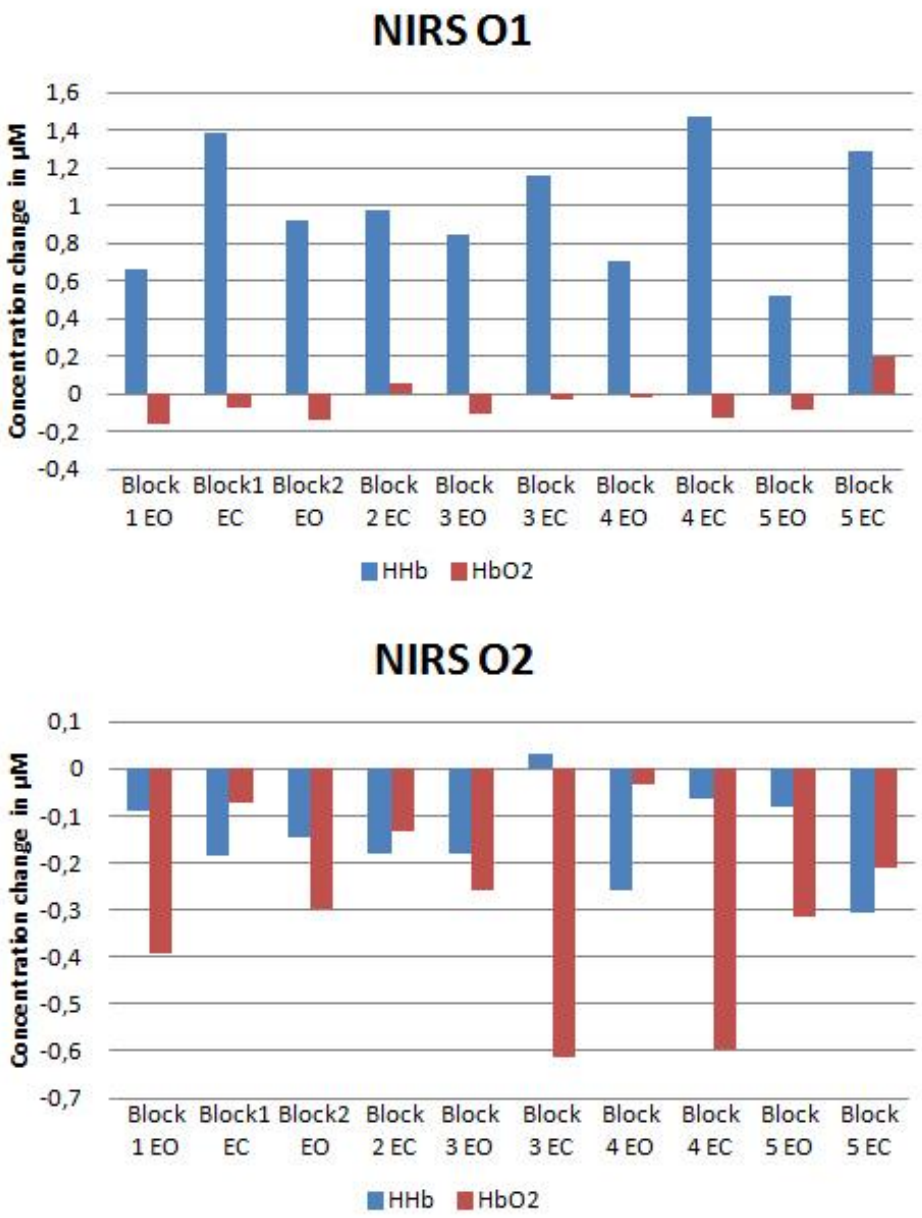

Figure 6.6 The fluctuations of oxygenated haemoglobin (HbO_2) and deoxygenated haemoglobin (Hbb) concentrations on both the left occipital (O1, left panel) and right occipital (O2, right panel) locations. Only the average concentration changes of the last half of each block are plotted.

6.3.2.3 Alpha Peak Frequency

When the spectrum of the EEG was inspected to determine the APF it appeared that in all blocks either the 7.0, 7.5, or 8.0 Hz bin showed a distinctive peak in the spectrum. The base of the APF was quite wide. Since a peak at 7.0 Hz falls just outside the alpha band it was chosen for further analyses to include an individual alpha band which was based on an APF of 7.5Hz. This individual alpha band was defined between 5 and 9.5 Hz. Since it was also noted in paragraph 6.3.2.1 that

the delta band seemed to be the only band that displayed reactivity towards the eyes open eyes shut paradigm it was decided to include the delta band in the upcoming analyses.

6.3.2.4 Time series quality labels

When the quality of the alpha envelope, the individual alpha envelope and the delta envelope as well as the filtered HbO_2 and Hbb time series was evaluated, both the alpha envelope and the individual alpha envelope showed no response. The delta envelope did display a medium response that became stronger as the protocol progressed. The NIRS signals were all qualified as medium-good with the exception of the HbO_2 time series on the O1 location which was qualified as medium-bad.

6.3.2.5 Long range temporal correlations

The LRTC of the alpha envelope, the individual alpha envelope and the delta envelope were calculated for both locations and tested against the values of the alpha envelope that were found in the healthy sample. The obtained values were also tested against 20 surrogate signals that were obtained by shifting the phases of the original signals (table 6.4). When the predefined alpha band was analysed a significant difference from the healthy sample was found on both locations indicating a slope that was less steep in the stroke case. On the O1 location this slope was not significantly different from the obtained surrogate data. When the individual alpha band was analysed, the slopes became steeper and the O1 location was no longer different from the healthy sample and is different again from its surrogate data. However, the O2 location still showed a slope that is significantly less steep than was found in healthy people and this slope was not different from its surrogate data.

The delta envelope showed a pattern that was in accordance with the alpha envelope of the healthy sample. No significant differences were found here and the slopes of the delta envelope were different from their surrogate data. The difference between the slopes of the delta envelopes and the surrogate data was that the actual slopes were found to be steeper.

	t	df	Sig (two tailed)	Mean dif.	Tested value	Group mean
AlphaO1	-4.91	37	.000*	-.3913	-1.9534	-2.3446
Surrogate O1	1.595	19	.127	.0167	-1.9534	-1.9367
AlphaO2	-7.722	37	.000*	-.5863	-1.8155	-2.4018
Surrogate O2	-8.089	19	.000*	-.0726	-1.8155	-1.8881
Individual Alpha O1	-1.463	37	.152	-.1163	-2.2283	-2.3446
Individual Surrogate O1	4.204	19	.000*	.04889	-2.2283	-2.1794
Individual Alpha O2	-2.841	37	.007*	-.2157	-2.1861	-2.4018
Individual Surrogate O2	.343	19	.735	.0044	-2.1861	-2.1816
Delta O1	0.940	37	.353	0.0748	-2.4194	-2.3446
Surrogate O1	10.027	19	.000*	0.1258	-2.4194	-2.2936
Delta O2	1.484	37	.146	0.1127	-2.5145	-2.4018
Surrogate O2	13.871	19	.000*	0.1564	-2.5145	-2.3581

Table 6.4 The difference in long range temporal correlation (LRTC) slope. Results from the one samples t-test, testing differences between the stroke case and the healthy sample as well as it is tested against surrogate data on both the left (O1) and right (O2) occipital cortex. Significant results are indicated with an asterisk.

6.3.2.6 Entropy

For the alpha envelope, the individual alpha envelope, the delta envelope and the HbO_2 time series as well as the Hbb time series the entropy was calculated and compared to the alpha, HbO_2 and Hbb entropies that were found in the healthy group. The results are summarized in table 6.5. Both the alpha envelope and the individual alpha envelope were statistically different from the healthy group. These time series showed higher entropy. When the delta envelope was compared to the alpha envelope of the healthy sample, no differences were found on the O1 location. On the O2 location the entropy was higher. For the NIRS time series only a significant difference was found on the O1 location which indicated again higher entropy than was found in the healthy group.

	t	df	Sig (two tailed)	Mean dif.	Tested value	Group mean
Alpha O1	-8.616	36	.000*	-.84757	3.76	2.9124
Alpha O2	-7.876	36	.000*	-.76135	3.69	2.9286
Individual Alpha O1	-10.344	36	.000*	-1.01757	3.93	2.9124
Individual Alpha O2	-9.635	36	.000*	-.93135	3.86	2.9286
Delta O1	.940	36	.354	.09243	2.82	2.9124
Delta O2	-4.152	36	.000*	-.40135	3.33	2.9286
HbO_2 O1	-5.364	36	.000*	-.21892	4.53	4.3111
HbO_2 O2	.818	36	.419	.03757	4.22	4.2576
Hbb O1	-3.590	36	.001*	-.16324	4.39	4.2268
Hbb O2	-.033	36	.974	-.00162	4.14	4.1384

Table 6.5 The difference in entropy. The results from the one samples t-test, testing the difference in entropy against the healthy sample. Significant results are indicated with an asterisk. Legend: O1= left visual cortex, O2= right visual cortex, HbO_2= oxygenated haemoglobin, Hbb= deoxygenated haemoglobin.

6.3.2.7 Correlation between modalities

The linear correlation between the electrical activity and the two NIRS concentration changes was investigated with the CCF analysis for the alpha signal (figure 6.7) the individual alpha signal (figure 6.8) and the delta signal (figure 6.9). The O1 and the O2 locations showed different patterns regardless of the electrical parameter that is investigated. All correlation values that were found, regardless of electrical parameter that was investigated showed values above the 95% confidence interval.

When the alpha band was correlated against the HbO_2 concentration changes a positive maximum correlation of 0.161 was found on the O1 location and a negative maximum correlation of -0.095 was found on the O2 location. For the analysis in which alpha was correlated against the Hbb concentration changes the O1 location showed a maximum negative correlation of -0.085 and the O2 a maximum positive correlation of 0.067. On the O1 location this pattern was reversed from the expected activation pattern. Significant differences from the

healthy sample were found on the O1 location due to this reversed pattern (all results are summarized in table B5 in Appendix B). When timing was considered, only for the correlation between alpha and HbO_2 on the O1 location the timing of the maximum correlation was found at a negative time lag (lag -72 (-2.88s)). The other comparisons showed a maximum value at a positive time lag (O1 alpha x Hbb: lag 118 (4.72s); O2 alpha x HbO_2: lag 45 (1.80s); alpha x Hbb: lag 42 (1.68s)). When the individual alpha band was used for the analysis the maximum correlations on the O1 location both became positive with values for individual alpha with HbO_2 of 0.081 and with Hbb of 0.099. The correlation between individual alpha and HbO_2 was again statistically different from the healthy sample due to the reversed correlation. On the O2 location individual alpha with HbO_2 showed a maximum negative correlation of -0.118 and individual alpha with Hbb a maximum positive correlation of 0.089. And even though the correlation strengths were weak, the use of the individual alpha band increased the correlations on the O2 location. In this analysis all correlations reached their maximum at a positive time lag indicating that changes in the individual alpha band preceded the changes seen in the NIRS response (O1 individual alpha x HbO_2: lag 65 (2.60s); individual alpha x Hbb: lag 153 (6.12s); O2 individual alpha x HbO_2: lag 94 (3.76s); individual alpha x Hbb: lag 108 (4.32s)).

The highest correlation values were found when the delta band was used as the electrical parameter. The direction of the correlation as well as the timing show findings in 3 out of 4 comparisons that are similar to the alpha findings in healthy brains (delta x Hbb O1: 0.266, lag 80 (3.2s); delta x HbO_2 O2: -0.191, lag 129 (5.16s); and delta x Hbb O2: 0.129, lag 126 (5,04s)). Only the correlation between delta and HbO_2 on the O1 location showed a reversed pattern in which the highest correlation was reached at a negative time lag (-207 (-8.24s)) and showed a positive correlation of 0.119. When these findings were tested against the findings in alpha correlation with the NIRS parameters in the healthy sample and all bad quality data were left in the analysis a difference was found for the correlation and timing of the delta x HbO_2 on the O1 and the O2 location as well as the timing of the highest correlation between delta and Hbb on the O2 location (see table B5 in Appendix B). However when all bad quality data were removed from the sample, the only significant differences that remained were the correlation value and timing of the delta x HbO_2 on the O1 location (table 6.6).

These results are summarized also for the other electrical parameters in Appendix B, table B6).

	t	df	Sig (two tailed)	Mean dif.	Tested value	Group mean
Delta x HbO_2 O1	-4.971	10	.001*	-.39455	0.119	-.27555
Timing Delta x HbO_2 O1	6.506	10	.000*	332.636	-207	125.64
Delta x Hbb O1	1.597	9	.145	.13740	0.266	0.403
Timing Delta x Hbb O1	1.097	9	.301	45.200	80	125.20
Delta x HbO_2 O2	.248	9	.810	.0220	-0.191	-0.169
Timing Delta x HbO_2 O2	-1.653	9	.133	-99.800	129	29.2
Delta x Hbb O2	1.847	8	.102	.12211	0.129	0.251
Timing Delta x Hbb O2	-.764	8	.467	-44.889	126	81.11

Table 6.6. Results from the one sample t-test of the cross-correlation analyses for both the correlation value and the time point at which the highest correlation was found for the delta correlated against the hemodynamic parameters compared with the alpha correlations with the hemodynamic parameters in the healthy group. Significant results are indicated with an asterisk. Legend: O1= left visual cortex, O2= right visual cortex, HbO_2= oxygenated haemoglobin, Hbb= deoxygenated haemoglobin.

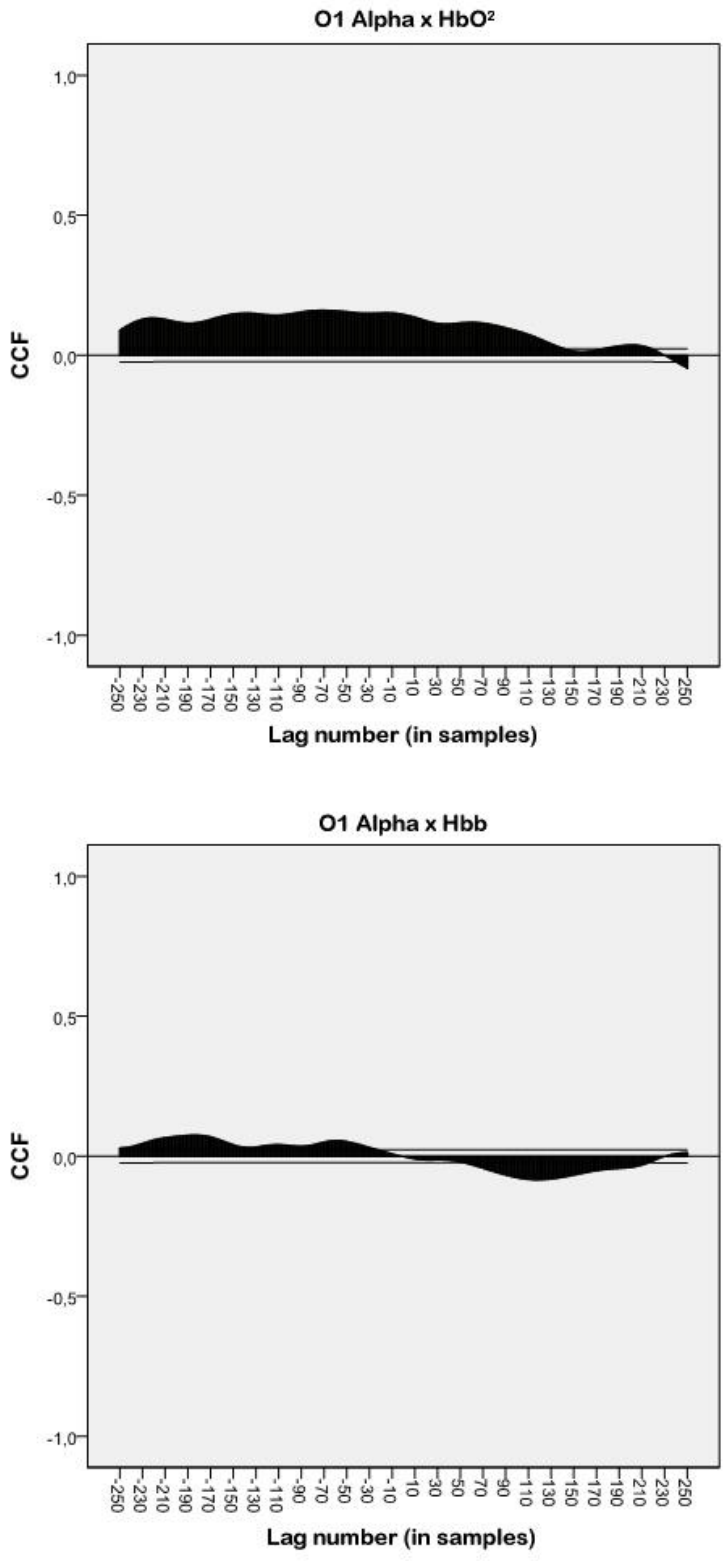

Figure 6.7a The cross correlation function (CCF) for the pairs alpha x HbO_2 (upper panel) and alpha x Hbb (lower panel) for the O1 location. The hemodynamic signal is the signal that is lagged +10 and -10 seconds. The two horizontal lines above and below the nil line indicate the 95% confidence interval. Legend: O1= left visual cortex, HbO_2= oxygenated haemoglobin, Hbb= deoxygenated haemoglobin.

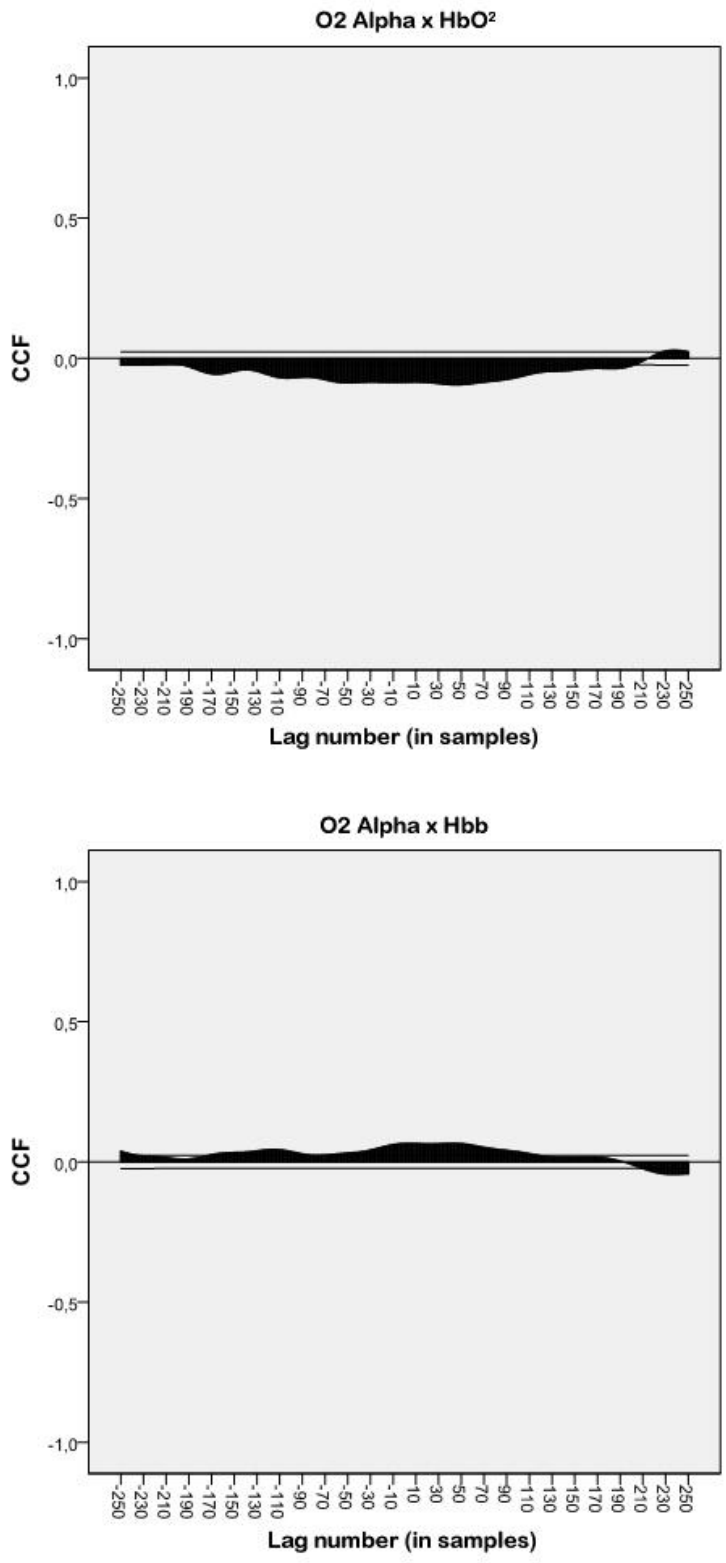

Figure 6.7b The cross correlation function (CCF) for the pairs alpha x HbO_2 (upper panel) and alpha x Hbb (lower panel) for the O2 location. The hemodynamic signal is the signal that is lagged +10 and -10 seconds. The two horizontal lines above and below the nil line indicate the 95% confidence interval. Legend: O2= right visual cortex, HbO_2= oxygenated haemoglobin, Hbb= deoxygenated haemoglobin.

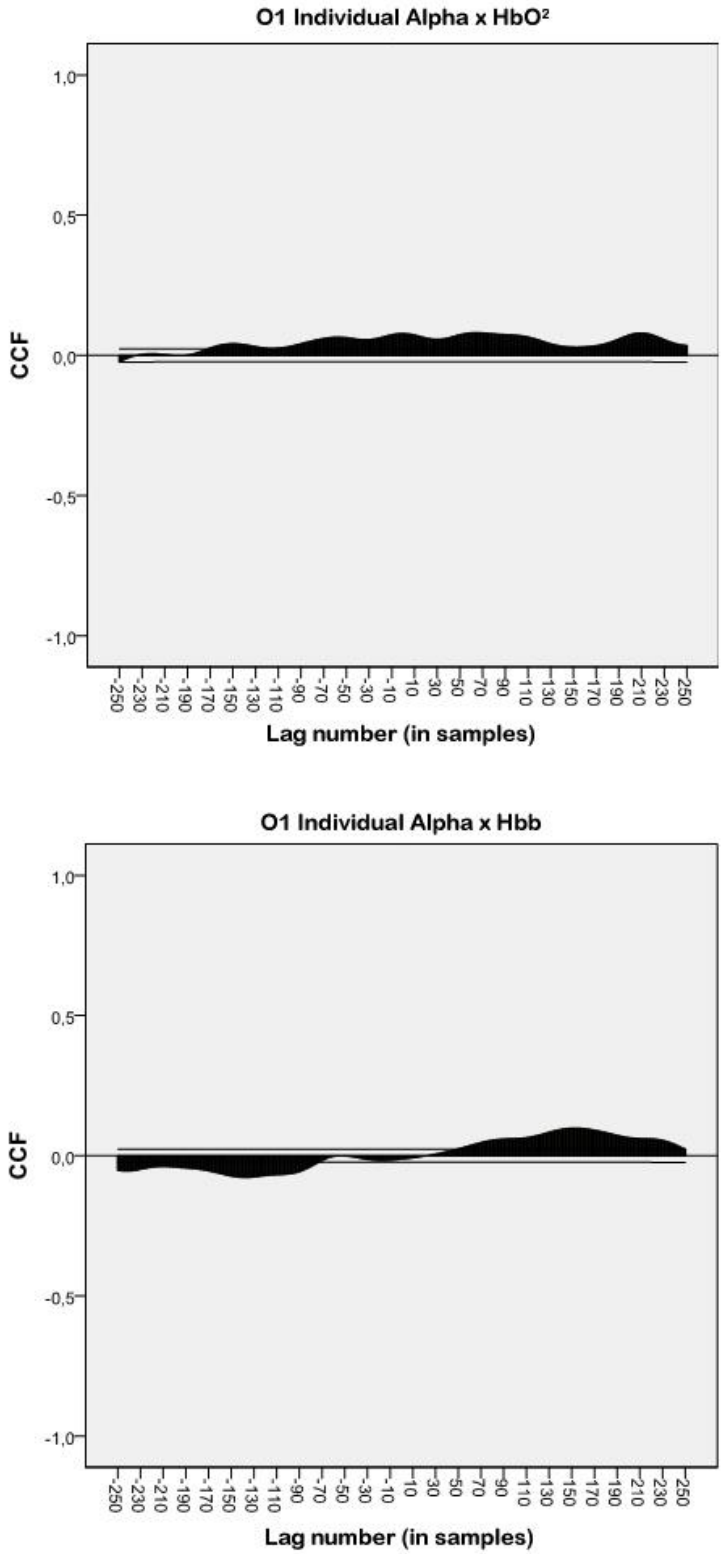

Figure 6.8a The cross correlation function (CCF) for the pairs individual alpha x HbO_2 (upper panel) and individual alpha x Hbb (lower panel) for the O1 location. The hemodynamic signal is the signal that is lagged +10 and -10 seconds. The two horizontal lines above and below the nil line indicate the 95% confidence interval. Legend: O1= left visual cortex, HbO_2= oxygenated haemoglobin, Hbb= deoxygenated haemoglobin.

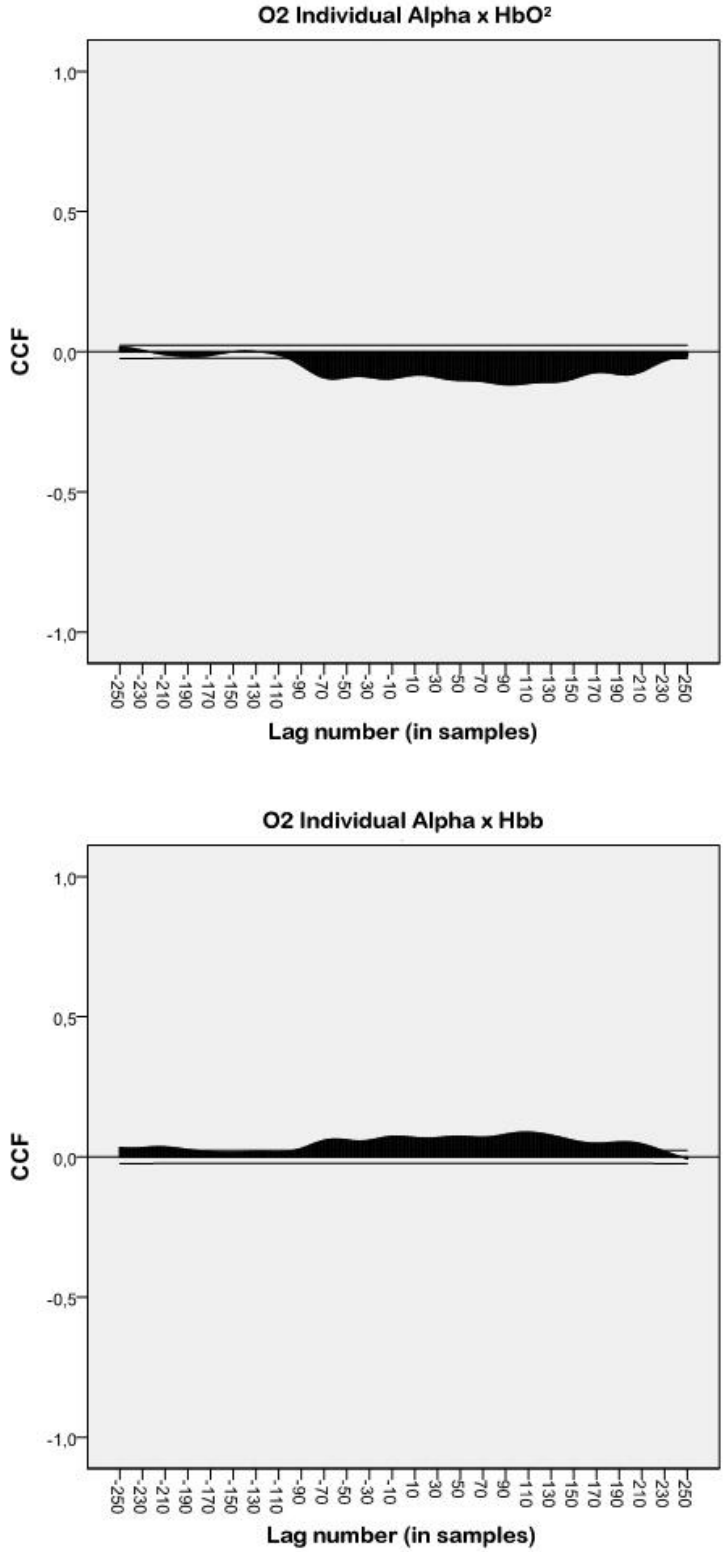

Figure 6.8b The cross correlation function (CCF) for the pairs individual alpha x HbO_2 (upper panel) and individual alpha x Hbb (lower panel) for the O2 location. The hemodynamic signal is the signal that is lagged +10 and -10 seconds. The two horizontal lines above and below the nil line indicate the 95% confidence interval. Legend: O2= right visual cortex, HbO_2= oxygenated haemoglobin, Hbb= deoxygenated haemoglobin.

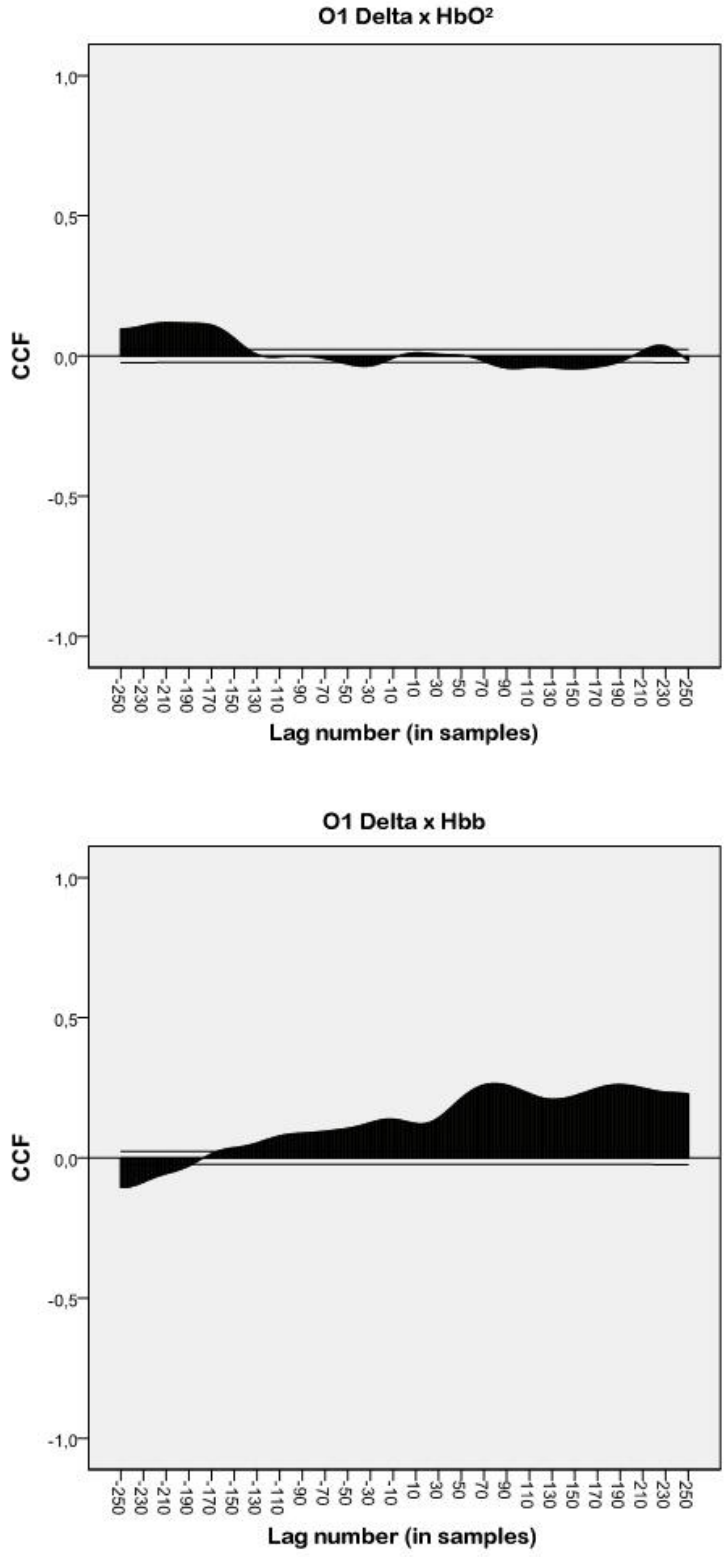

Figure 6.9a The cross correlation function (CCF) for the pairs delta x HbO_2 (upper panel) and delta x Hbb (lower panel) for the O1 location. The hemodynamic signal is the signal that is lagged +10 and -10 seconds. The two horizontal lines above and below the nil line indicate the 95% confidence interval. Legend: O1= left visual cortex, HbO_2= oxygenated haemoglobin, Hbb= deoxygenated haemoglobin.

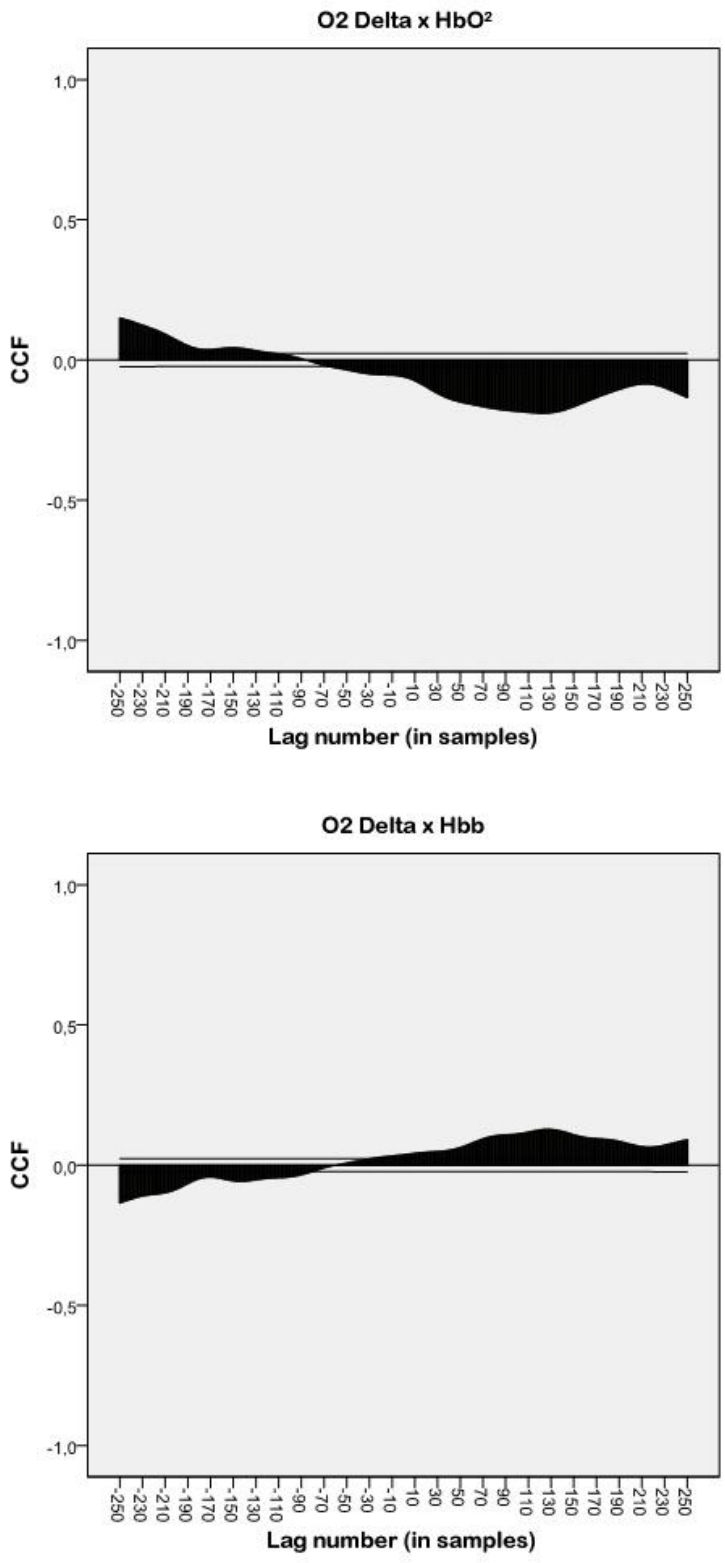

Figure 6.9b The cross correlation function (CCF) for the pairs delta x HbO_2 (upper panel) and delta x Hbb (lower panel) for the O2 location. The hemodynamic signal is the signal that is lagged +10 and -10 seconds. The two horizontal lines above and below the nil line indicate the 95% confidence interval. Legend: O2= right visual cortex, HbO_2= oxygenated haemoglobin, Hbb= deoxygenated haemoglobin.

6.3.2.8 Dependency between modalities

The nonlinear counterpart of the CCF analysis, the CMI_{rel} values were also calculated for the alpha signal paired with the NIRS concentrations (figure 6.10), the individual alpha signal paired with the NIRS concentrations (figure 6.11) and the delta signal paired with the NIRS concentrations (figure 6.12). All maximum CMI_{rel} values that were found are low. The maximum CMI_{rel} for the alpha x HbO_2 pair was 3.7520 on the O1 location and 3.4942 on the O2 location. For the alpha x Hbb pair the O1 location showed a maximum CMI_{rel} of 4.2437 and the O2 location was 3.2169. The values were found to be slightly higher for 3 pairs when the individual alpha was used (individual alpha x HbO_2: O1 4.3162; O2 4.4468 ; individual alpha x Hbb: O1 3.8212; O2 4.4215). These values increased for three pairs even further when the delta band was used as electrical parameter (delta x HbO_2: O1 6.4327; O2 5.1432 ; individual alpha x Hbb: O1 3.5088; O2 5.1140). When one sample t-tests were conducted to see whether there were differences between the patient data and the data from the healthy group which had the bad quality data removed, the patient values were all significantly lower regardless of the electrical parameter under investigation (table 6.6).

When the timing was considered, different time points were found to give a maximum CMI_{rel} value when the alpha analyses were compared to the individual alpha analyses or the delta analyses. This was also true for the comparison with the CCF timing. However, because of the oscillating nature of the CMI_{rel} graphs the timing of the maximum CMI_{rel} value seemed to occur quite randomly and possibly not too much weight should be allocated to it.

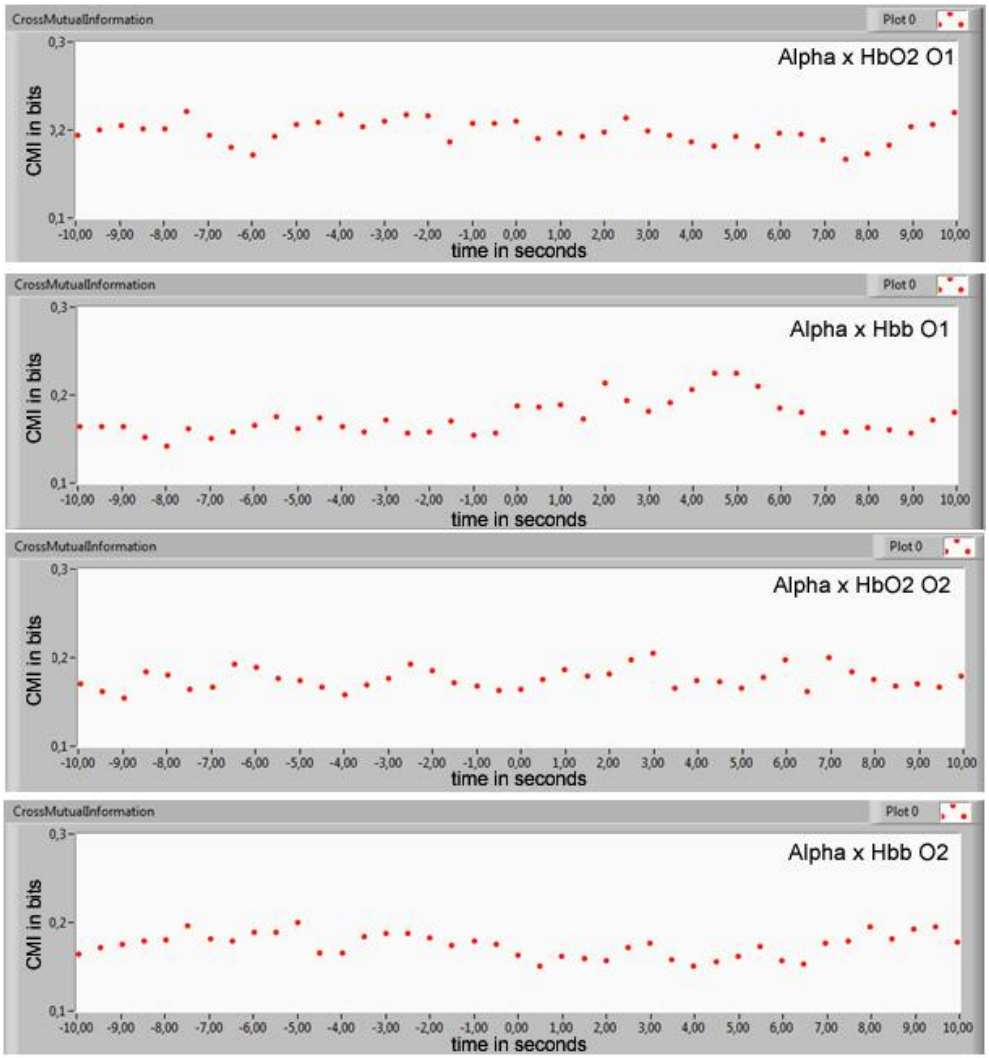

Figure 6.10 The cross mutual information (CMI) for the pairs alpha x HbO_2 and alpha x Hbb for both the O1 and O2 location. The hemodynamic signal is the signal that is lagged +10 and -10 seconds. Legend: O1= left visual cortex, O2= right visual cortex, HbO_2= oxygenated haemoglobin, Hbb= deoxygenated haemoglobin.

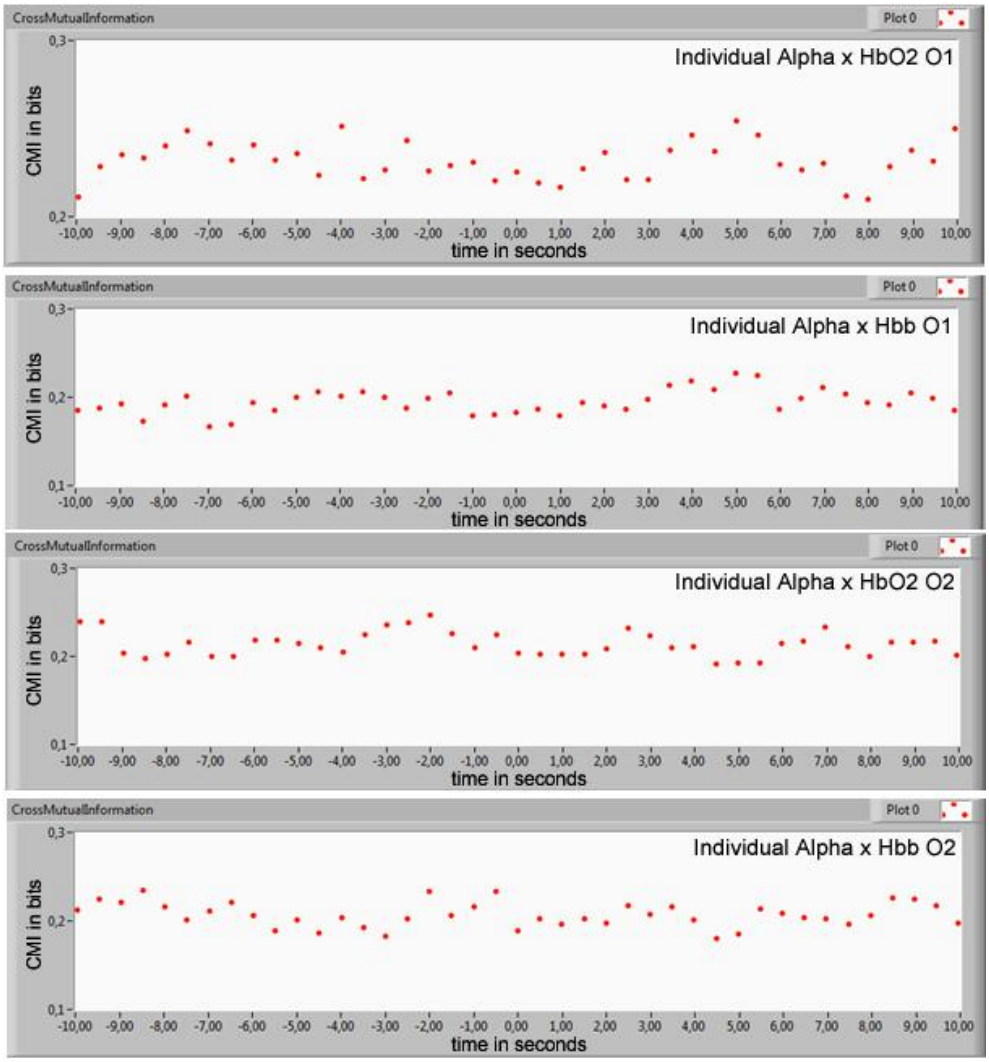

Figure 6.11 The cross mutual information (CMI) for the pairs individual alpha x HbO_2 and individual alpha x Hbb for both the O1 and O2 location. The hemodynamic signal is the signal that is lagged +10 and -10 seconds. Legend: O1= left visual cortex, O2= right visual cortex, HbO_2= oxygenated haemoglobin, Hbb= deoxygenated haemoglobin.

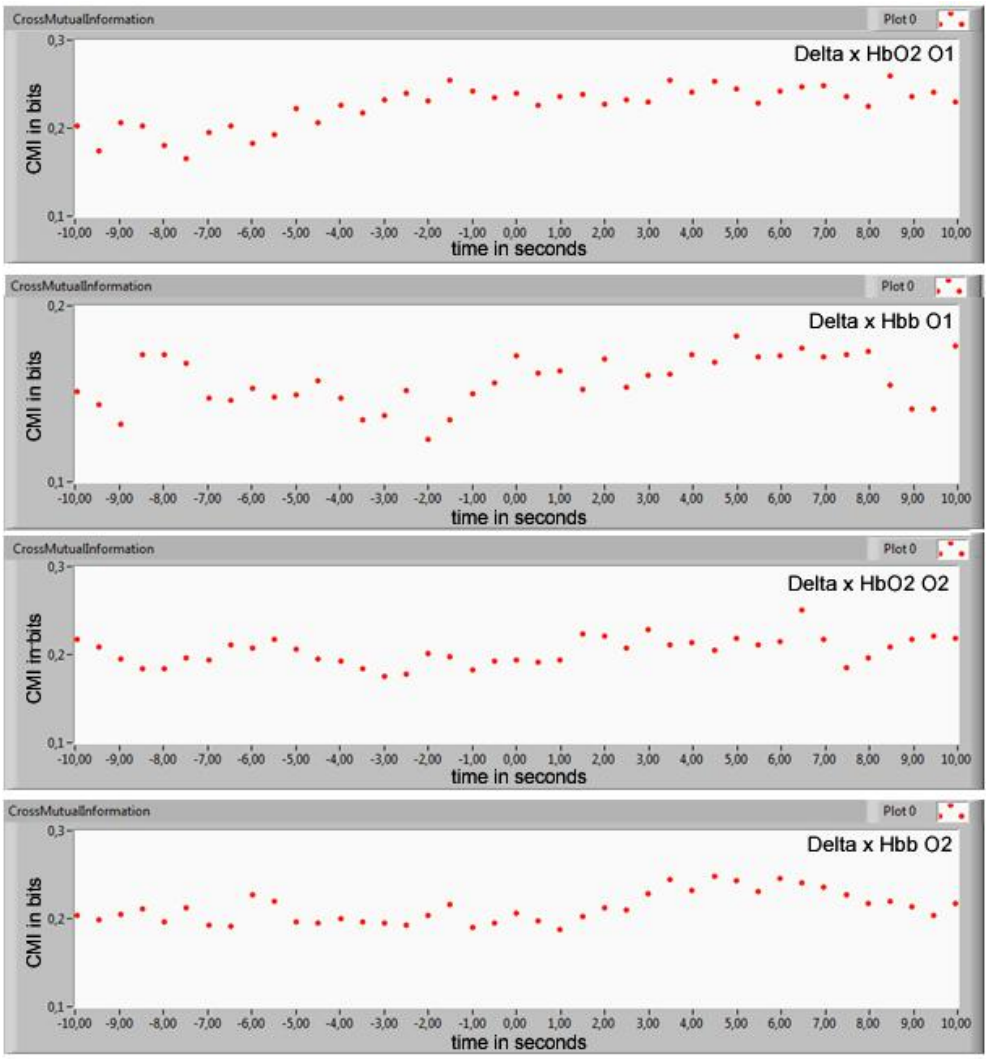

Figure 6.12 The cross mutual information (CMI) for the pairs delta x HbO_2 and delta x Hbb for both the O1 and O2 location. The hemodynamic signal is the signal that is lagged +10 and -10 seconds. Legend: O1= left visual cortex, O2= right visual cortex, HbO_2= oxygenated haemoglobin, Hbb= deoxygenated haemoglobin.

	t	df	Sig (two tailed)	Mean dif.	Tested value	Group mean
Alpha x HbO_2 O1	5.459	10	.000*	9.10432	3.7520	12.8564
Alpha x Hbb O1	5.181	9	.001*	10.81426	4.2437	15.0580
Alpha x HbO_2 O2	3.109	9	.013*	6.82382	3.494	10.3180
Alpha x Hbb O2	3.730	8	.006*	6.20758	3.2169	9.4244
Individual Alpha x HbO_2 O1	5.121	10	.000*	8.54019	4.3162	12.8564
Individual Alpha x Hbb O1	5.384	9	.000*	11.23684	3.8212	15.0580
Individual Alpha x HbO_2 O2	2.675	9	.025*	5.87120	4.4468	10.3180
Individual Alpha x Hbb O2	3.006	8	.017*	5.00295	4.4215	9.4244
Delta x HbO_2 O1	3.852	10	.003*	6.42366	6.4327	12.8564
Delta x Hbb O1	5.534	9	.000*	11.54920	3.5088	15.0580
Delta x HbO_2 O2	2.358	9	.043*	5.17480	5.1432	10.3180
Delta x Hbb O2	2.590	8	.032*	4.31044	5.1140	9.4244

Table 6.7 The difference in relative cross mutual information (CMIrel). Results from the one samples t-test testing the difference between the stroke patient and the healthy sample which has the bad quality data removed. Significant results are indicated with an asterisk. Legend: O1= left visual cortex, O2= right visual cortex, HbO_2= oxygenated haemoglobin, Hbb= deoxygenated haemoglobin.

6.4 Discussion

In this chapter the measurements that were used to investigate the brain activity of healthy individuals throughout this thesis were used to investigate possible changes in brain function in two cases of patients who had suffered a stroke. It became evident that the static analyses on the individual measures, the dynamic analyses, as well as the findings of the combined measurement modalities seemed to indicate differences between stroke and the healthy individuals.

Investigation of the combined NIRS and EEG activity never has been described before and is therefore an exciting new finding.

The cases that were described are very different in nature. Not only was there a difference in sex, there was also a difference in stroke onset (childhood vs. adulthood) and ability (no impairment vs. extreme impairment). Adults do not recover after stroke as well as children and are usually left with more deficits (Popa-Wagner et al., 2007), which was a distinction that was seen here. However, the patient in which childhood stroke had occurred had gone through a recovery period expanding over two decades. The fact that the second patient had suffered multiple strokes also indicated a more severe case. Because of this, two ends of the stroke spectrum could be investigated, the end in which patients seem to function independently after recovery and the end in which extreme impairment occurs. Both ends display differences from healthy working brains.

6.4.1 Case1

The findings in the static analysis of the EEG indicated an expected response as is reported in the literature to the opening and closing of the eyes in which an elevation in all bands during EC blocks is seen (Barry et al., 2007). In the healthy sample this was not entirely the case (possible reasons for this deviance are reported in paragraph 3.4.1). However, the differences that were found between this patient and the healthy sample were that an elevated magnitude in all bands during all blocks was seen. A higher magnitude of the QEEG bands, and therefore higher amplitude of the registered EEG could be an indication that more neurons are firing in synchrony (Bear et al., 2007).

The NIRS response did show more diversity than the EEG response and the expected response to the task was sometimes reversed. On the O1 location a lower HbO_2 concentration was registered during EO blocks. On the O2 location consistently a higher HbO_2 and lower Hbb concentration was registered compared to the healthy sample. The stroke had occurred in the right hemisphere which possibly could explain differences between hemispheres and the switches during the task. A reversed response in which an increase of Hbb concentration during a simple motor task was observed in patients 5 months post stroke has been reported before (Nakamura et al., 2010). However, in this case 22 years have gone

by and it is unknown whether this is still seen after so many years. In order to explain these findings better it would be helpful to know the exact stroke location and additionally have access to the findings of a recent cerebral angiogram which could reveal any structural changes in vasculature and cerebral blood flow. The APF at first did not show differences and was 10.5 Hz. However, in the last three minutes a drop in APF only during the EO blocks was seen. Interestingly, the O2 location showed a reversed pattern of oxygenation during these minutes in which a decrease in HbO_2 was observed. A decrease in APF has been described in stroke due to the loss of blood supply (Finnigan and van Putten, 2013). So perhaps on a smaller scale, a decrease in oxygenation can also result in a reversible drop in APF. It does not explain though why this drop occurs on both locations while the decrease in oxygenation is only structurally seen on the O2 location.

The occurrence of long temporal correlations (LRTC) was investigated and in line with the healthy sample. LRTCs could be observed in the alpha envelope of this patient. However, the slopes that were found were all significantly steeper for this patient. In chapter 4 it was explained that the steeper the slope of the power law is, the more quickly the energy evaporates from the system and the shorter the in time the correlations are (Linkenkaer-Hansen et al., 2001). In this patient, despite more synchronous oscillations of the neurons, the correlations over time were shorter than was observed in the healthy sample. The different findings in entropy for the alpha band (higher entropy) also indicate that more uncertainty and therefore less predictability is seen (Shannon, 1948). For the NIRS signals on the other hand a lower entropy was observed which in turn indicates that the oxygenation changes are more predictable then in healthy brains.

When the linear correlations between alpha and the NIRS signals were explored it was found that the highest correlations were in the opposite direction as was seen in the healthy group and that the highest correlations were found at negative time lags indicating that a change in the hemodynamic parameter preceded changes in alpha activity. When the nonlinear CMI_{rel} analysis was used it was found that all dependencies were lower than were seen in the healthy sample. However, only the dependencies on the O1 location reached a statistical significant difference. Since evidence shows that recovery depends on the involvement of areas unaffected by stroke, either proximal to the damaged areas or in contra lateral homologues (Eliassen et al., 2008) a lower dependency

between hemodynamic and electrical parameters after stroke can be expected due to this structural or functional reorganization. It would therefore be of great added value to take more measuring locations into account in order to see whether higher dependencies are found in proximal areas. When nonlinear aspects of the relationship are taken into account it appears that the timing of the maximum dependency can switch from negative to positive or become less negative. This could be due to the nonlinear aspects, but it also could be an indication that when the question of timing is posed in order to find out what signal is leading the changes another method would be more appropriate. In paragraph 5.4.2 already the Transfer Entropy (TE) and Mutual Information from mixed embedding (MIME) were suggested to hold potential in answering this question (Faes and Nollo, 2013, Kugiumtzis, 2013).

6.4.2 Case 2

The findings in the EEG for the second patient were striking mainly because hardly any reactivity was seen to the opening and closing of the eyes, except in the delta band. Jordan et al. (2004) have described that following stroke first the fast wave activity diminishes followed by a decrease of the APF and that as a last phase primarily delta activity occurs. In their review, Finnigan and Van Putten (2013) add to that that the delta band can be used to predict treatment outcome and that more delta indicates worse outcome. This seems to be true for this case, in which extensive impairment is seen.

Interestingly, the NIRS parameters did show reactivity to the task. This reactivity was, just as in case 1 sometimes as expected during activation and sometimes reversed. On the O1 location the Hbb concentration changes were larger than the HbO_2 changes and the two signals did not always follow an opposite pattern. When compared to the healthy sample usually on O1 lower HbO_2 was found with higher Hbb during both EO and EC blocks. When differences are seen on the O2 location again lower HbO_2 and higher Hbb concentrations are reported. As is mentioned above, it would help a great deal in explaining these findings when the exact stroke locations were known and data from a cerebral angiogram was available. Because of the lack of neuronal response the lower HbO_2 and higher Hbb concentrations it is hypothesized here that changes in vascular structure have

occurred that have lower perfusion as a consequence. When a lower perfusion is seen this can result in an increase of Hbb concentrations (Murata et al., 2006).

In line with the EEG changes after stroke that are described by Jordan et al. (2004) also a lower APF was registered during all blocks. This led to the creation of an additional individual alpha band. However, this individual band also was irresponsive to the paradigm. Because the delta band was the only band that was responsive this band was also analyzed in the dynamic analyses and the analyses of both measuring modalities simultaneously.

When LRTCs were investigated for the three electrical parameters it appeared that both the alpha and individual alpha showed differences from the healthy sample. However, in both parameters it occurred that the slope found in the original band was not different from its surrogate data. Surrogate data are created to have no temporal correlations (Linkenkaer-Hansen et al., 2001). When no differences are found between the recorded signal and the surrogate signals this is an indication that no temporal correlations exist in the original signal. For depression it has been reported that long-range temporal correlations of the theta band measured with MEG were absent in patients but prominent in healthy controls (Linkenkaer-Hansen et al., 2005). The magnitude of these correlations correlated with the severity of the depression. As is seen in depression the absence of LRTCs in the alpha band in stroke could be indicative for severity of pathology or neural distress. Albeit a strong hypothesis based on one case. When the LRTCs were investigated for the delta band and compared to the slopes for the healthy sample no differences were found anymore between stroke and health or between original and surrogate data.

All electrical signals indicated to have higher entropy and therefore lower predictability than was found in the healthy sample, except for the delta band on the O1 location which did not show a difference with the alpha entropy of the healthy group. For the NIRS signals only a difference was found for the O1 location in which the patient showed higher entropy as well. In the first case a lower entropy for the NIRS signals was found. This might be due to the location of the lesion but is unfortunately a question that cannot be answered now. The linear correlations between the alpha and the hemodynamic parameters were low and sometimes reversed from what was expected. A slight increase was

seen when the individual alpha band was used, and the use of the delta band even increased the maximum correlations further. When this was tested against the healthy sample the delta band was the only band that showed no differences from the healthy group in 3 out of 4 correlations. The correlation that did show a difference was caused by the reversed pattern in the delta x HbO_2 comparison.

When the delta band was analysed as if it were the alpha band the preceding analyses showed that fewer differences could be found from the healthy sample. This could be an indication that the central oscillating rhythm of this patients brain is the delta band instead of the alpha band as is usually seen. However, to test this claim the changes in delta band and correlation analyses should also have been carried out for the healthy group. Especially because it has been reported that out of 20 QEEG measures, the delta power measure has the strongest correlation with regional CBF (Tolonen and Sulg, 1981). This correlation however, was reported to be negative whereas the alpha correlation in was reported to be positive. Since in this case the delta activity seems to behave like the alpha activity this would be a very interesting parameter for future research.

When the nonlinear CMI_{rel} was used to investigate the dependencies it appeared that all were very low. Also the dependencies of the delta band and the NIRS parameters were significantly lower than seen in healthy brains. This is very interesting since for the previous measures, the use of the delta band seemed to normalize the results. This could be an indication the using the CMI_{rel} as additional parameter in investigating brain function in terms of the dependency between EEG and NIRS could contribute significantly in differentiating health from pathology. Similar to the first case, changes in timing were observed that potentially better could be investigated with other measures.

However, caution is warranted in the interpretation of the results of this subject. The fact that results were obtained during the measurements in this subject that showed differences from the healthy group may not only originate from the multiple strokes, but may also have to do with the visual impairments afterwards. After all the measurements were conducted over the O1 and O2 locations that correspond with the visual cortex (Jasper, 1958).

The study of Moosmann et al. (2003) showed that alpha activity over the occipital cortex was shown to be positively cross-correlated with the Hbb component of simultaneous NIRS measurements. This study was performed in a block design switching from eyes open to eyes closed and vice versa, while healthy subjects were sitting in a completely dark room with their eyes additionally shielded by an eye mask. This generates the believe that it is not necessarily the sight component of the eyes open eyes shut paradigm that induces the changes in brain activity that are responsible for the underlying physiological relationship between alpha activity and NIRS parameters. However, it has been reported that when this visual impairment or blindness is innate this causes remarkable plastic changes in both function and structure (Hawellek et al., 2013). For example, the visual cortex tends to be smaller, but nonetheless the metabolic demands seem heightened compared to visually able humans (De Volder et al., 1997). Furthermore a decrease in alpha wave activity over the occipital areas is also observed (Kriegseis et al., 2006). Nonetheless it has been reported that a distinctive peak can still be found in the spectrum in the alpha to beta range of innate blind people as well as this is found in healthy people (Hawellek et al., 2013). If these findings are also true in acquired blindness, as is the case with subject 2, is describe less coherently and less extensively. Findings that would apply to this particular subject are even more complicated by the fact that the visual impairments are due to the stroke, and that it was unrecorded where the lesion sites of the different strokes were. A study of Wang et al. (2012) in stroke patients with hemianopia, which affects multiple visual functions, showed during resting state EEG it is the left primary visual cortex of the stroke patients that shows diminished activity compared to healthy controls. This seems to be compensated with increased activity in the more temporal and frontally located brain regions compared to healthy controls as well as increased activity in the right associative visual cortex. If these results apply to the case under investigation remains debatable.

6.4.3 A future for multimodal imaging in stroke research

The finding that differences exist between stroke patients in both electrical and hemodynamic parameters as well as in their coupling compared to healthy subject is not surprising. As mentioned in the introduction it is known that neurovascular coupling is disrupted in stroke (Girouard and Iadecola, 2006, Blicher et al., 2012, Ayata, 2013). In focal ischemia, the greatest reduction in blood flow is seen in the

center of the affected area which is termed ischemic core. At the periphery, or the ischemic penumbra, the reduction in blood flow is less pronounced (Girouard and Iadecola, 2006). Since the ischemic penumbra has less severe hypoperfusion, impaired neuronal activity is seen but it does not necessarily lead to neuronal damage, given that therapeutic intervention is administered within the correct time window (Canazza et al., 2014). The ischemia causes vasoparalysis in the cerebral circulation which in turn impairs the reactivity to stimuli displaying itself as decreased functional activation which causes smaller increases is CBF (Girouard and Iadecola, 2006). In fMRI research it is then sometimes observed that the BOLD response is undetected. However, BOLD responses in positive direction as well as negative direction have also been described (Blicher et al., 2012). Sakatani et al. (2007) demonstrated in their combined fMRI- NIRS research that often a lack of BOLD response exists because during activation an increase in Hbb is seen, leading to false interpretations of fMRI research in stroke. However, BOLD activation patterns obtained with fMRI after stroke are closely related with aspects of impairment (Stinear and Ward, 2013).

As stated before an increase in Hbb concentration during activation is seen more often after stroke (Nakamura et al., 2010). But that is not the only finding from NIRS research. Li et al. (2010)have reported a reduction in spontaneous NIRS oscillations in the frontal cortex in stroke patients which could be due to increased stiffness in the arterial vessels. This could originate from underlying artherosclerosis, which causes ~25% of all ischemic strokes (Mustanoja et al., 2011). The accompanying changes in CBV lead to the fact that neural activity is not necessarily coupled to regional CBF and CBV changes to the same degree as in healthy subjects (Blicher et al., 2012). Given the complexity of the neurovascular coupling, the still unknown variables, and the great variability between stroke patients it therefore makes sense to investigate functional impairments with multimodal neuroimaging as proposed in this chapter. Furthermore, the shift to functional connectivity studies may provide the opportunity to investigate whether or how surviving tissue is working and what mechanisms of reorganization and recovery are used (Carter et al., 2012, Stinear and Ward, 2013).

6.5 Conclusion

The investigation of simultaneous measurements of EEG and NIRS and different ways of analysing the data throughout this thesis has mainly been a proof of principle. In this chapter the first indication is given that differences can be found between health and pathology when using the combined measurements and that potentially the CMI_{rel} can contribute in differentiating health from pathology. Therefore it is proposed that the measures that are described in this thesis are firstly explored further before they are used as markers and implemented as clinical evaluation tools. The emphasis in this research should go out to the multimodal use of EEG and NIRS as well as connectivity research.

The largest drawback in the analysis of these case studies was the lack of data on lesion sites and any additional structural scans or angiograms. These could help greatly in explaining results and differences between the two cases. Then the number of measurement locations should be expanded in order to investigate proximal areas, connections to proximal areas and to investigate differences and connectivity between hemispheres on more locations. As Finnigan and Van Putten (2013) point out in their review the brain symmetry index is one of the parameters that is found to correlate well with recovery outcome. This index too needs to be investigated with more than 2 measurement locations. Next the timing issue for the CCF and CMI_{rel} would need to be addressed in order to address the question of which parameter drives the other or whether perhaps this changes when different oscillations are investigated.

Furthermore it should be investigated whether all suggested parameters hold promise as additional parameters to standard investigation in increasing sensitivity and specificity in differentiating health and disease. Preferably a model would be developed in which the contribution of each measure in differentiating healthy brains from pathologies and pathologies from other pathologies could be analysed. In this model several aspects should be addressed: 1. Which parameters are helpful in diagnosis; 2. Which parameters are helpful in determining progress; 3. Which parameters are helpful in predicting treatment outcome; 4. Which parameters are helpful in predicting treatment response?

These questions are of major importance in clinical use and if they can be answered by an objective brain measurement it holds great promise for future healthcare.

Chapter 7: General thoughts and conclusions

The aim of this thesis was to explore the use of combined EEG and NIRS measurements in order to enlighten brain function. Hereto different forms of analysis techniques were used to investigate the modalities separately as well as their combined features in an eyes open, eyes closed paradigm. The general conclusions and thoughts that can be derived from the body of work carried out in this thesis is discussed in this final chapter. Together with pointers and directions for future research, this chapter gives an analytical summary of the work conducted so far and the potential for transfer to clinical implementation.

7.1 Summary of work

Brain measurements could provide clinicians with a lot of additional, mostly objective information about the functioning of both healthy brains and the brain during pathology. By implementing brain measurements as a standard way of care into the clinic one could find aid in the process of diagnosis of several pathologies, as well as get help in deciding treatment and evaluating treatment progress. This will benefit patients as they will be diagnosed faster and more accurately and can be offered better tailored care. Several different modalities of brain measurements are available on the market today. However, for brain measurements to be able to implemented in general lines of healthcare, outpatient clinics as well as small individual health practices the methods chosen to objectify brain functioning would benefit from being portable, low cost, and the ability to do bedside monitoring.

When investigating brain functioning by performing brain measurements two different modalities can contribute to our understanding; electrical neuronal activity, and hemodynamic activity. Both observations can provide information about brain function and dysfunction. However, a third, additional factor could increase our knowledge of pathology even further, the relationship between electrical and hemodynamic activity or its shared information content.

In chapter 1 it was pointed out that the measurement of electrical activity by (quantitative) EEG and the recording of changes in hemodynamic activity by NIRS

seem to possess qualities for clinical use. When additionally a paradigm is used which leads to minimal patient exclusion, like measuring resting state activity, or use an easy, standardized task in order to measure different brain states (like measurements with eyes open and eyes closed) the use in all layers of the clinical field is highly promising.

For this reason the aim of this thesis was to explore the use of combined EEG and NIRS measurements. Different approaches of analysing the methods separately as well as combined were investigated to see whether more information could be gained on different brain states. In order to do so, the well established paradigm of opening and closing the eyes while measuring the visual cortex was used. After the different approaches of analysis, described in chapters 3, 4 and 5 were investigated in healthy brains, chapter 6 started the exploration of these different measures in two cases of stroke. The pathology of stroke was chosen because it is known to display disturbances in the electrical brain activity, in the hemodynamic brain activity, but also in the neurovascular coupling (Girouard and Iadecola, 2006, Blicher et al., 2012, Ayata, 2013, Finnigan and van Putten, 2013). If no differences can be found between healthy brains and brains of stroke patients in the measurement parameters used, the differentiation between more subtle differences in brain functioning in other pathologies like psychopathologies will be too farfetched. This will lead broad clinical application to be put off.

Before the exploration was commenced, a pilot study on the robustness of NIRS measurements was conducted (chapter 2). EEG methods are sensitive to noise and different kinds of artefacts in EEG traces are described in every basic EEG atlas (Krauss et al., 2006). For NIRS the quality of its robustness to artefacts and therefore its ecological validity in measuring real life paradigms is often emphasized (Arenth et al., 2007). However, more published evidence becomes available of the susceptibility to artefacts in NIRS measurements (see chapter 2). Therefore the goal of the pilot study was to investigate different common movements during a paradigm in which subjects were sitting in an upright position while measuring NIRS from the frontal cortex. The frontal cortex rather than the occipital cortex was used in order to limit additional measurement issues arising from hair blocking the optodes. A suggestion of a method to remove artefacts from experimental NIRS data, the CBSI method (Cui et al., 2010) was

tested for its effectiveness towards potential artefacts and the running correlation was evaluated in its application to detect artefacts. This pilot study led to the conclusion that motion artefacts easily arise during testing, are very variable in their morphology and expression between subjects, and that they are hard to recognise especially when only automated artefact detection is used. Some artefacts need additional attention like the "slow response" artefact, which is a type of artefact that mimics a response expected during brain activation and can therefore easily be missed. Besides, motion artefacts are not the only artefacts that arise during NIRS measurements. Artefacts that arise due to physiology based systemic responses are often coupled to the research paradigm and are therefore hard to entangle from the response of interest (Gagnon et al., 2012, Kirilina et al., 2012). Furthermore, it was established that the proposed CBSI method did not improve signal quality when artefacts were induced upon brain activity measured in resting state and sometimes even led to a distortion or switch of the actual response. The findings in this chapter are quite important to researchers and clinicians using NIRS. Since the robustness of NIRS to artefacts is often emphasized in the literature, the potential threat of artefacts and incorrect ways of repressing them might be lost, leading to false interpretations. Based on this pilot, it was decided that all measurements that were conducted afterwards needed to be in an upright sitting position in which the participants were instructed to sit very still in order to register as little artefacts as possible so the only filtering options that were used were a detrending of the signal along with a band pass filter between 0.01 and 0.5 Hz.

The data from the healthy group was collected to investigate the eyes open eyes shut response on the visual cortex and was used in chapters 3, 4 and 5 in order to explore different analysis techniques. In chapter 3, first the general accepted methods of analysing static differences between blocks as well as spectral analysis were used in order to determine differences between the activity seen in blocks measured with eyes open and blocks measured with eyes closed. Differences between blocks were found and generally confirmed earlier research findings indicating a more active visual cortex during eyes open conditions visible in a repression of alpha wave activity and an increase in HbO_2 while Hbb diminished. However, when the correlation between alpha activity and NIRS concentrations was analyzed in a static way the expected positive and negative correlations could

not be confirmed. This could be due to the static nature of the analysis in this chapter. But another reason may be that still a controversy exists whether optical changes due to neuronal changes that are seen in vitro and during invasive measurements can be detected non-invasively by NIRS in human adults (Steinbrink et al., 2000, Wolf et al., 2003, Franceschini and Boas, 2004, Steinbrink et al., 2005, Medvedev et al., 2008, Gratton and Fabiani, 2010, Tse et al., 2010, Biallas et al., 2012). Where Biallas et al. (2012) emphasize the moderate ability of CW NIRS measures to detect hemodynamic changes (40 to 55.2 %) together with a low within subject reproducibility. If this is an accurate representation the use of NIRS to investigate brain activity as well as its use together with EEG in a clinical setting becomes drastically less appealing.

In chapter 4 an introduction to a dynamic way of analysing brain activity was given which potentially suits the data better since a brain behaves as a dynamical system (McKenna et al., 1994, Fox et al., 2005). A dynamic measure that could be useful in doing so is the analysis of long range temporal correlations. These were found to exist within the alpha oscillations of the participants and differed between participants with good and bad quality data. Unfortunately, the registered NIRS signal and the chosen paradigm were not appropriate for detecting LRTCs in NIRS signals. This chapter also expressed a dynamic approach to analyse the correlation between alpha wave activity and HbO_2 as well as Hbb concentration changes by means of cross correlation analysis. The results of previous research in which a positive correlation between alpha activity and Hbb concentrations and a negative correlation between alpha activity and HbO_2 concentrations was found in which a delay in response of the hemodynamic signal was seen of around 8 seconds (Moosmann et al., 2003) could only be established when all data of questionable quality as well as physiological illogical data were removed. The most important finding of this replication is that it could only be obtained by excluding a major part of the investigated population. Since inter individual differences are found to occur within the largest part of the investigated population, this emphasizes that the suggested model of an 8 second delayed hemodynamic response with respect to the electrical response might not be the “golden standard”. In some cases, perhaps it indeed is the change in electrical activity that requires an adapted hemodynamic response and causes this response to be delayed with regard to the electrical changes. However, the

opposite could be argued for as well; when an increased or restricted supply of oxygen causes the electrical activity to change. The first (Moosmann et al., 2003) as well as the latter (Pfurtscheller et al., 2012) has been proposed already in previous research.

Cross correlation analysis can only give insight in linear relationships between two signals. In order to illuminate knowledge on nonlinear relationships as well, the use of Mutual Information (MI) analysis was explored in chapter 5. The use of MI analysis has not been conducted on NIRS measurements before and therefore has never been used to analyse possible dependencies of EEG and NIRS parameters. A few challenges had to be overcome before this could be initiated, the first being the choice of appropriate bin sizes. Chapter 5 therefore provides a guideline showing how to choose an appropriate bin size, which has not been described detailed in previous research before. The second challenge was the challenge of interpreting the obtained results and comparing them between subjects. In order to make this process easier the transformation of cross mutual information (CMI) into relative CMI (CMI_{rel}) was invented and explained in this chapter as well. This chapter is therefore extremely valuable for this thesis. It provides a newly suggested method of how EEG and NIRS measurements can be analysed simultaneously creating value for both EEG and NIRS. Furthermore, it broadens use of methodology derived from information theoretical measures making it applicable to any research field that uses these measures. The transformation towards CMI_{rel} required the separate calculation of the entropy or information content of each signal. This showed that the information content of HbO_2 and Hbb signals was significantly different from each other which helps the discussion in the field of NIRS research that will enable researchers to report on both measures when reporting results and not restrict the results to the use of the Hbb parameter alone, which is often done as this is the parameter that is supposed to correlate well with fMRI findings.

As a final study, all measures that were used in chapters 3, 4 and 5 were used to analyze the data collected from the same eyes open, eyes closed paradigm as used before in two stroke patients. A pathology that is known to display changes in electrical brain activity, hemodynamic brain activity and the neurovascular coupling (Girouard and Iadecola, 2006, Blicher et al., 2012, Ayata, 2013, Finnigan

and van Putten, 2013). The cases of stroke described in chapter 6 were two cases at opposite ends of the stroke spectrum. The analysis revealed that changes in brain activity in the separate modalities as well as the combined analyses were found. Because the cases were very different from each other, the differences found in the separate measurement modalities were different as well. Caution is warranted though with the results of the second case, because due to the multiple strokes this person was left blind which might distort the results. And even though a response in brain activity from eyes open to eyes closed is seen when subjects are completely shielded from visual input (Moosmann et al., 2003), the blindness itself may have caused plastic changes in both function and structure in the visual cortex (Hawellek et al., 2013).

In the independent functioning stroke patient, similar responses in the EEG were seen as were reported in the literature, but all bands had higher magnitudes during all conditions than seen in the healthy sample. The stroke patient with large disability showed hardly a response in all EEG bands except for delta. The responses seen in hemodynamic parameters were variable, but the striking observation occurred that even though in the second patient hardly an EEG response was seen, a response was present in the NIRS signals. The differences in dynamics investigated with the LRTC and entropy showed in the first patient shorter correlations in time, while a lack of difference between the surrogate signals in the second patient even indicated no long range correlations at all. The entropy of the alpha band was found to be higher in both patients, indicating lower predictability than seen in healthy brains. For the NIRS parameters different results between both patients were obtained in which the first patient showed NIRS signals with higher predictability than the healthy participants and the second patient lower predictability when a difference was found. Also differences in the coupling of EEG and NIRS parameters were found in both patients when compared to the healthy group. Especially the difference in relative cross mutual information which was found to be significantly lower for both patients, provides the proof of principle that the analysis of the combined EEG and NIRS measures can have added clinical value. Therefore this chapter can be considered the most important chapter of the thesis. It provides the proof of concept for transfer to other pathologies as well as a transfer to the clinic.

7.2 Readiness to transfer to clinical use

As described in chapter 6 the results found in this thesis are first of all a starting point for future research and a proof of principle that the used measurements will be able to tell something about brain functioning in health and in pathology. Possible future research paths are shortly mentioned in the next paragraph while this paragraph will address the issue of transfer to the clinic.

Based on the findings within this thesis the actual transfer of multimodal brain measurements with EEG and NIRS to broad clinical use is still a long journey away. To start off with, the susceptibility of NIRS measurements to a wide variety of motion artefacts and physiological systemic artefacts is something that needs to be resolved. Especially because artefacts appear hard to be detected and proposed filtering methods produce variable results in filtering these artefacts. In determining the efficacy of filtering often the knowledge of the true form of the original (noise-free) signal lacks which is necessary to quantify improvement (Sweeney et al., 2012). Other methods use second measurement modalities like fMRI to regress artefacts out (Kirilina et al., 2012) or use a short distance channel (Zhang et al., 2009, Zhang et al., 2007a, Zhang et al., 2007b). However, Gagnon et al. (2012) showed that for every measurement channel the short distance channel cannot be further away than 1.5 cm which basically means that the number of channels which needs to be used increases drastically. The use of additional fMRI measurements or multiple additional channels just to correct for possible artefacts is not desirable in a clinical environment. Especially because in a clinical setting fast, reliable, and low-cost measurements are needed with limited setup time.

A second issue is the measurement quality of the NIRS technology. In chapter 3 it was shown that between half and two-thirds of the NIRS data that were measured in the healthy group were data of questionable quality. This is in line with the sensitivity of NIRS to actual hemodynamic changes of 40 to 55.2 % that has been reported before (Biallas et al., 2012). For a measurement to have a clinically added value it needs to be possible to get an adequate and accurate registry in nearly all patients. Currently this is not the case. Of course, use was made of just one system for this thesis and the possibility exists that systems which are capable

of delivering higher quality signals are available. However, a lot can be gained on the technical side of the measurement, both in optode positioning comfort and signal quality. In these investigations and improvements thought should be granted to the issue of hair obstructing the light, leading to bad signal quality especially in dark pigmented hair. A start already has been made in these improvements by the suggestion of the brush optode (Khan et al., 2012) as well as the collodion fixed micro-optode (Yucel et al., 2014) that were briefly mentioned in chapter 2.

Furthermore, the possibilities for the combined use of EEG and NIRS needs to be expanded. Surely the correlation or shared information content between the two measurements is not the only parameter that could be useful in investigating brain function. Other factors can be deduced and used to differentiate a healthy functioning brain from a brain during pathology and even between different pathologies. In doing so, the developments and findings in hybrid EEG and NIRS BCI research could be extremely valuable. Whereas BCI research aims at classifying ongoing brain states for communication or the control of external devices (Pfurtscheller et al., 2010), the classification of brain states to differentiate pathologies might not be all that different. Therefore, we can learn from these ongoing studies, especially the research stream that uses NIRS measurement to improve EEG classification (Pfurtscheller et al., 2010, Fazli et al., 2012). Fazli et al. (2012) showed in their research that EEG features are earlier classifiable than NIRS parameters and also have higher classification accuracy. However, when both measures are used the overall accuracy of classification improves and for subjects that showed poor EEG classification these improvements could be extensive. This is a promising result when broad clinical use is in order because when these methods are brought to the clinic it are single patients that need to be diagnosed. The averaging of group results is not of interest to a single patient that just needs to obtain the right diagnosis and the correct treatment in order to feel better soon.

Besides the technological issues, and the expanding of the parameters from dual measurements that can be considered, the proof of principle needs to be expanded to multiple measurement channels and other brain areas. Preferably, global, whole headed measurements should be possible with the ease of short

preparation and measurement time. This way the functioning of the whole brain can be evaluated from just one measurement. Short preparation time will reduce discomfort for the patient as well as it will save time for the clinician which in acute situations can be life saving. When measuring from more sites also the connectivity measures can be researched which in their turn also can contribute to a more sensitive and specific classification (Fox and Raichle, 2007, Raichle, 2010, Buckner, 2012). This will be further highlighted in paragraph 7.3.

Furthermore, an appropriate software package needs to become available in which the outcomes of a number of measures can be given to the clinician without the need for this person to be an expert on the measurement and its interpretation. However, a flag should be raised for the automation of results and the blind reliance on the analysis techniques used though. Once a algorithm is used to analyze brain activity a result will always be obtained despite the reliability of the measurement. This occurs in different techniques. For example LORETA in which a deeper lying source for the brain activity observed over the scalp is always generated despite the possibility of multiple dipole fitting solutions or local field potentials that originate strictly cortical or even the influence of noise (Buzsáki et al., 2012). These results are then erroneously coupled to tasks under investigation leading to papers arguing that different, specific brain areas are involved in the pathology or the information processing of the stimulus under investigation (Cannon, 2012). LORETA is not the only technique in which this occurs. Probably the best known example is the study in which a dead salmon is scanned in an fMRI session in which the salmon was shown pictures of human interactions in social situations. Upon analyzing the results voxels appeared active in the dead fish's brain region which could be interpreted as the active processing of the stimuli by the fish (Bennett et al., 2009). A finding that is physically impossible. The authors use this example to raise awareness for a well developed methodological and statistical sense in researchers and clinicians using these methods when inferring conclusions about obtained results. Knowledge that may lack when automated analysis is offered to a broader, less experienced scope of users and which therefore will increase the risk of wrong conclusions based on the gathered data. Nevertheless, some sort of automation of data analysis with an additional reliability check will be a prerequisite in order to transfer multimodal

brain measurements to a broad clinical field, making it accessible for the broad public.

7.3 Future research

Clearly more research and development lies ahead before the simultaneous use of EEG and NIRS measurements is ready to be transferred to the clinic. With this thesis as a starting point several suggestions are given for future research.

Especially for the NIRS community it would be helpful if a NIRS atlas was devised that illustrates, just like EEG atlases do, basic knowledge about NIRS signals. For example what aspects of the signal are normal, but that also describes:

- how to recognise different types of artefacts.
- what types of filtering exist and what the pros and cons of the different options are.
- what patterns can be expected in healthy brains during rest and due to tasks which are easy to implement, like opening and closing of eyes, cognitive tasks or simple hand movement paradigms and how these responses are known to be different in all kinds of neurological- or psychopathologies.
- analysis guidelines in the form of a Standard Operating Procedure (SOP) which would benefit this area of research very much in creating unity in the research findings.

Next to the development of guidelines for basic analysis, the use of dynamic analyses for the NIRS signals should be investigated further since this is still unexplored territory. A starting point of the analysis of dependency between electrical and hemodynamic signals is already given in this thesis along with guidelines of how to perform the analysis. Additional attention should be directed though to the part of the dependency in which is determined which signal drives the other and in what kind of situations a switch of driver and follower occurs. Once this is established in healthy functioning brains we might discover that it is the rigidity in switching from driver to follower of either modality that is an underlying cause of pathology.

This thesis illustrated the proof of principle of the added value of combined brain measurements by means of analysing the pathology of stroke. Other pathologies are at least as interesting to study and should be studied before the majority of patients can benefit from brain measurements. For instance the pathology of depression has shown to express more alpha activity over the left frontal cortex and sometimes the right parietal cortex (Debener et al., 2000). It would be extremely interesting to find out if these findings go accompanied by changes in dependency between alpha activity and NIRS parameters or whether this is only the case when late onset depression is diagnosed which seems to go accompanied by changes in cerebrovascular function (Motomura et al., 2002). Another way to study how this dependency between alpha activity and NIRS parameters changes is by introducing a substance which is known to alter both (or one of the two) signals. A good candidate for the dependency studied in this thesis would be caffeine. Caffeine has been shown to alter alpha activity (Barry et al., 2008) as well as oxygenation parameters (Liu et al., 2004). Studies on popular stimulants as caffeine could then be followed by studies investigating psychiatric drugs that are often prescribed to patients, such as methylphenidate in ADHD or SSRI's (selective serotonin reuptake inhibitors) in depression. These studies could be helpful in determining whether certain substances are wise to prescribe when a change in the dependency between electrical and hemodynamic activity is found.

As a last suggestion the investigation of resting state networks could be conducted for the combination of EEG and NIRS. The steady rise in the number of resting state functional neuroimaging studies is a serious indication that the importance of the functioning of the brain at rest is being recognised and used to explore brain function (Cole et al., 2010). Breakthroughs in this research have been the discovery of the default mode network (Raichle et al., 2001, Greicius et al., 2003), and resting state networks (Beckmann et al., 2005, Buckner, 2012). The presence of these networks has been established in PET and fMRI first (Raichle et al., 2001, Greicius et al., 2003), but can also be identified with EEG (Buzsáki and Draguhn, 2004, Mantini et al., 2007) and NIRS (Lu et al., 2010, Mesquita et al., 2010). Furthermore, differences in connectivity of these networks have been indicated in various pathologies, ranging from neurological (Vecchio et al., 2012, Diessen et al., 2013) to psychological pathologies (Karbasforoushan and

Woodward, 2012, Wang and Lagopoulos, 2012, Vargas et al., 2013). Therefore added analysis of functional resting state networks could create more insight in the brain behaviour relationship and help distinguishing different pathologies with a higher sensitivity and specificity. Additionally, the use of the resting state as measurement condition will include the broadest scope of patients since most of them are able to rest for several minutes.

In short, the path into the clinic seems a long route. And many ways can be thought of which could move the field of combined EEG and NIRS measurements forward. Nevertheless, once the these steps forward are being made the scope of clinical utility will be endless. The non-invasive objectifying of complaints can be done in all age groups, especially when a resting state measure will suffice. It will allow faster and more accurate diagnosis in neurology, but also in psychopathology an area that is currently underserved. Furthermore, it can aid in choosing the right treatment especially when pharmacological studies are included. Besides, the use of regular, multimodal brain measurements in the objective monitoring of a patients progress will allow clinicians to adjust their treatment plans in time. So to conclude, the advances in non-invasive multimodal brain measurements will benefit clinical issues and lead to exiting new findings which will benefit patients. But the quest has just begun.

Appendices

Appendix A

	t	df	Sig (two tailed)	Mean dif.	Tested value	Group mean
DeltaEO1	-2.164	38	.037*	-1.2359	14.7	13.464
Theta EO1	-25,593	38	.000*	-9.9000	21.10	11.200
AlphaEO1	-19.490	38	.000*	-10.2923	21.40	11.108
Beta1EO1	-19.137	38	.000*	-5.8077	12.20	6.392
Beta2EO1	-13.890	38	.000*	-5.9359	13.7	7.764
DeltaEC1	-11.434	31	.000*	-4.1875	14.5	10.312
Theta EC1	-20.795	31	.000*	-9.6469	20.0	10.353
AlphaEC1	-9.034	31	.000*	-21.1625	43.4	22.238
Beta1EC1	-8.838	31	.000*	-5.0344	13.7	8.666
Beta2EC1	-13.986	31	.000*	-6.8344	15.5	8.666
DeltaEO2	-1.162	33	.254	-.6176	13.8	13.182
Theta EO2	-14.357	33	.000*	-6.2529	16.9	10.647
AlphaEO2	-20.020	33	.000*	-9.5118	20.1	15.588
Beta1EO2	-14.538	33	.000*	-4.3265	10.4	6.074
Beta2EO2	-17.115	33	.000*	-5.7353	13.1	7.365
DeltaEC2	-16.577	32	.000*	-7.1515	18.1	10.948
Theta EC2	-20.490	32	.000*	-14.7152	26	11.285
AlphaEC2	-11.985	32	.000*	-32.2333	57.7	25.467
Beta1EC2	-14.811	32	.000*	-8.0455	16.9	8.855
Beta2EC2	-16.417	32	.000*	-8.0424	17.2	9.158
DeltaEO3	-6.030	38	.000*	-3.3026	16.3	12.997
Theta EO3	-24.140	38	.000*	-9.2667	20.1	10.833
AlphaEO3	-24.201	38	.000*	-13.9462	25.1	11.154
Beta1EO3	-27.244	38	.000*	-6.8923	13.1	6.308
Beta2EO3	-14.500	38	.000*	-6.2564	14.1	7.844
DeltaEC3	-3.878	35	.000*	-2.5917	14.5	11.908
Theta EC3	-19.847	35	.000*	-13.3806	24.4	11.019
AlphaEC3	-15.021	35	.000*	-35.7917	59.1	23.308
Beta1EC3	-15.741	35	.000*	-8.1250	16.8	8.675
Beta2EC3	-14.529	35	.000*	-7.2222	16.3	9.078
DeltaEO4	-3.877	38	.000*	-2.5179	15.9	13.382
Theta EO4	-21.300	38	.000*	-8.100	18.9	10.800
AlphaEO4	-19.308	38	.000*	-13.3154	25.0	11.685
Beta1EO4	-29.768	38	.000*	-8.1744	14.5	6.326
Beta2EO4	-20.770	38	.000*	-8.3923	16.0	7.608
DeltaEC4	-12.817	35	.000*	-6.7667	18.2	11.433
Theta EC4	-32.380	35	.000*	-19.7528	31.0	11.247
AlphaEC4	-11.858	35	.000*	-28.4500	53.1	24.650
Beta1EC4	-19.153	35	.000*	-10.0333	18.8	8.767
Beta2EC4	-21.905	35	.000*	-9.2722	18.2	8.928
DeltaEO5	-8.924	38	.000*	-4.8487	18.0	13.151
Theta EO5	-30.954	38	.000*	-13.1692	23.8	10.631
AlphaEO5	-33.355	38	.000*	-18.8974	29.9	11.003
Beta1EO5	-29.616	38	.000*	-7.8359	14.1	6.264

Beta2EO5	-27.568	38	.000*	-10.9385	18.4	7.462
DeltaEC5	-9.987	36	.000*	-6.5568	18.1	11.543
Theta EC5	-25.138	36	.000*	-15.5136	26.6	11.086
AlphaEC5	-13.294	36	.000*	-30.3108	54.1	23.789
Beta1EC5	-21.457	36	.000*	-10.7919	19.2	8.408
Beta2EC5	-21.512	36	.000*	-8.9568	17.9	8.943

Table A1. Results from the one sample t-tests of all frequency bands on the left occipital (O1) location for all eyes open (EO) and eyes closed (EC) blocks. Significant results are indicated with an asterisk.

	t	**df**	**Sig (two tailed)**	**Mean dif.**	**Tested value**	**Group mean**
DeltaEO1	-3.674	38	.001*	-2.0692	15.3	13.231
Theta EO1	-26.559	38	.000*	-10.9410	21.8	10.859
AlphaEO1	-25.494	38	.000*	-13.6487	24.4	10.751
Beta1EO1	-31.858	38	.000*	-7.6667	13.8	6.133
Beta2EO1	-22.986	38	.000*	-7.9615	15.3	7.338
DeltaEC1	-4.895	38	.000*	-4.4821	16.9	14.418
Theta EC1	-16.579	38	.000*	-12.4821	24.0	11.518
AlphaEC1	-10.490	38	.000*	-34.0718	61.4	27.328
Beta1EC1	-16.360	38	.000*	-8.8333	17.9	9.067
Beta2EC1	-27.465	38	.000*	-11.4231	20.1	8.677
DeltaEO2	-4.584	37	.000*	-2.4500	15.4	12.950
Theta EO2	-18.821	37	.000*	-8.4526	19.2	10.747
AlphaEO2	-18.138	37	.000*	-13.0711	24.6	11.529
Beta1EO2	-20.121	37	.000*	-5.4895	11.6	6.111
Beta2EO2	-22.450	37	.000*	-7.1895	14.6	7.411
DeltaEC2	-7.138	38	.000*	-6.8615	19.6	12.738
Theta EC2	-20.616	38	.000*	-17.2923	29.3	12.008
AlphaEC2	-13.737	38	.000*	-43.422	70.7	27.626
Beta1EC2	-20.455	38	.000*	-11-5462	20.8	9.254
Beta2EC2	-30.653	38	.000*	-11.9897	21.1	9.110
DeltaEO3	-8.105	38	.000*	-4.3615	17.30	12.938
Theta EO3	-27.519	38	.000*	-11.6051	22.2	10.595
AlphaEO3	-27.593	38	.000*	-17.0692	28.0	10.931
Beta1EO3	-37.480	38	.000*	-8.5769	14.8	6.223
Beta2EO3	-21.588	38	.000*	-7.6641	15.0	7.336
DeltaEC3	-24.386	27	.000*	-7.0750	16.9	9.825
Theta EC3	-69.093	27	.000*	-20.6893	29.6	8.911
AlphaEC3	-29.198	27	.000*	-54.1500	73.5	19.350
Beta1EC3	-22.739	27	.000*	-11.7714	19.7	7.929
Beta2EC3	-31.093	27	.000*	-13.5036	21.8	8.296
DeltaEO4	-5.802	38	.000*	-3.8308	17.1	13.269
Theta EO4	-27.624	38	.000*	-11.0564	21.6	10.544
AlphaEO4	-25.580	38	.000*	-18.1974	29.7	11.503
Beta1EO4	-37.308	38	.000*	-9.5564	15.8	6.244
Beta2EO4	-30.370	38	.000*	-9.8897	17.1	7.210
DeltaEC4	-9.658	37	.000*	-8.0789	20.3	12.221
Theta EC4	-34.246	37	.000*	-24.8132	36.6	11.787

AlphaEC4	-14.459	37	.000*	-43.9132	71.0	27.087
Beta1EC4	-21.411	37	.000*	-12.0289	21.0	8.971
Beta2EC4	-36.228	37	.000*	-14.4974	23.4	8.903
DeltaEO5	-12.563	37	.000*	-6.3816	18.9	12.518
Theta EO5	-43.158	37	.000*	-16.0289	26.2	10.171
AlphaEO5	-38.761	37	.000*	-22.3395	33.1	10.761
Beta1EO5	-41.012	37	.000*	-10.5474	16.6	6.053
Beta2EO5	-38.144	37	.000*	-12.2105	19.4	7.189
DeltaEC5	-19.797	34	.000*	-10.5886	21.1	10.511
Theta EC5	-40.674	34	.000*	-22.1743	32.6	10.426
AlphaEC5	-18.064	34	.000*	-40.7600	63.9	23.140
Beta1EC5	-29.428	34	.000*	-15.6886	24.2	8.511
Beta2EC5	-32.259	34	.000*	-13.5657	22.5	8.934

Table A2. Results from the one sample t-tests of all frequency bands on the right occipital (O2) location for all eyes open (EO) and eyes closed (EC) blocks. Significant results are indicated with an asterisk.

	t	**df**	**Sig (two tailed)**	**Mean dif.**	**Tested value**	**Group mean**
HbO_2 EO1	2.800	34	.008*	0.3105	0.0692	0.3796
Hbb EO1	-2.162	34	.038*	-.2048	0.0037	-0.2011
HbO_2 EC1	.983	34	.333	.1155	0.1086	0.2240
Hbb EC1	-.928	34	.360	-0.8437	-0.0184	-0.1028
HbO_2 EO2	3.360	34	.002*	.3893	0.0404	0.4297
Hbb EO2	-2.344	34	.025*	-.2281	0.0086	-.2196
HbO_2 EC2	.328	34	.745	.0345	0.0707	0.1052
Hbb EC2	-.769	34	.447	-.0702	-0.0029	-0.0731
HbO_2 EO3	2.744	34	.010*	.3227	0.0987	0.4214
Hbb EO3	-1.932	34	.062	-.1860	-0.0126	-0.1986
HbO_2 EC3	.378	34	.708	.0398	0.0644	.01041
Hbb EC3	-.892	34	.379	-.0831	-0.0078	-0.0909
HbO_2 EO4	2.727	34	.010*	.2846	0.1056	0.3902
Hbb EO4	-1.670	34	.104	-.1586	-0.0346	-0.1932
HbO_2 EC4	.641	34	.526	.0646	0.0295	0.0941
Hbb EC4	-1.171	34	.250	-.1033	0.0132	-0.0901
HbO_2 EO5	4.225	34	.000*	.4391	-0.029	0.4099
Hbb EO5	-2.260	34	.030*	-.2095	-0.0079	-0.2174
HbO_2 EC5	-.474	34	.638	-.0523	0.2231	0.1708
Hbb EC5	-.278	34	.783	-.0236	-0.0461	-0.0698

Table A3. Results from the one sample t-test of the oxygenated haemoglobin (HbO_2) and deoxygenated haemoglobin (Hbb) concentrations on the left occipital cortex (O1) for all eyes open (EO) and eyes closed (EC) blocks. Significant results are indicated with an asterisk.

	t	**df**	**Sig (two tailed)**	**Mean dif.**	**Tested value**	**Group mean**
HbO_2 EO1	-5.863	35	.000*	-1.1866	1.7290	.5424
Hbb EO1	4.548	35	.000*	.6163	-1.0161	-.3998
HbO_2 EC1	-5.677	35	.000*	-1.1358	1.4819	0.3461

Hbb EC1	4.926	35	.000*	.6661	-0.9595	-0.2934
HbO_2 EO2	-5.158	35	.000*	-1.0903	1.5900	0.4997
Hbb EO2	4.561	35	.000*	.6454	-1.0165	-0.3741
HbO_2 EC2	-8.207	34	.000*	-1.3978	1.5702	0.1724
Hbb EC2	6.141	34	.000*	.8152	-1.0516	-0.2364
HbO_2 EO3	-3.467	35	.001*	-.7471	1.2864	0.5393
Hbb EO3	2.650	35	.012*	.3829	-0.7889	-0.4061
HbO_2 EC3	-8.749	34	.000*	-1.3572	1.5380	0.1808
Hbb EC3	5.741	34	.000*	.7101	-0.9646	-0.2544
HbO_2 EO4	-3.870	35	.000*	-.7778	1.3693	0.5915
Hbb EO4	3.067	35	.004*	0.4401	-0.8710	-0.4309
HbO_2 EC4	-6.611	35	.000*	-1.2313	1.5053	0.2740
Hbb EC4	5.335	35	.000*	.6802	-0.9970	-0.3168
HbO_2 EO5	-3.338	35	.002*	-.7011	1.2958	0.5947
Hbb EO5	3.329	35	.002*	0.4706	-0.8986	-0.4280
HbO_2 EC5	-5.943	35	.000*	-1.1371	1.4440	0.3070
Hbb EC5	5.012	35	.000*	0.6516	-0.9285	-0.2769

Table A4. Results from the one sample t-test of the oxygenated haemoglobin (HbO_2) and deoxygenated haemoglobin (Hbb) concentrations on the right occipital cortex (O2) for all eyes open (EO) and eyes closed (EC) blocks. Significant results are indicated with an asterisk.

	t	**df**	**Sig (two tailed)**	**Mean dif.**	**Tested value**	**Group mean**
Alpha x HbO_2 O1	-11.011	37	.000*	-.4597	0.289	-.1707
Timing Alpha x HbO_2 O1	9.989	37	.000*	245.816	-176	69.82
Alpha x Hbb O1	10.281	37	.000*	.5407	-0.358	0.183
Timing Alpha x Hbb O1	9.630	37	.000*	223.421	-175	48.42
Alpha x HbO_2 O2	-6.654	37	.000*	-.2186	0.099	-.1196
Timing Alpha x HbO_2 O2	7.716	37	.000*	221.421	-209	12.42
Alpha x Hbb O2	9.523	37	.000*	.3105	-0.207	0.1035
Timing Alpha x Hbb O2	6.648	37	.000*	186.079	-188	-1.92

Table A5. Results from the one sample t-test of the cross correlation analyses for both the correlation value and the time point at which the highest correlation was found. Significant results are indicated with an asterisk. Legend: O1= left visual cortex, O2= right visual cortex, HbO_2= oxygenated haemoglobin, Hbb= deoxygenated haemoglobin.

Appendix B

	t	df	Sig (two tailed)	Mean dif.	Tested value	Group mean
DeltaEO1	1.163	38	.252	.6641	12.8	13.464
Theta EO1	-6.98	38	.000*	-2.7000	13.9	11.200
AlphaEO1	-10.022	38	.000*	-5.2923	16.4	11.108
Beta1EO1	.963	38	.342	.2923	6.10	6.392
Beta2EO1	-1.722	38	.093	-.7359	8.5	7.764
DeltaEC1	-14.984	31	.000*	-5.4875	15.8	10.312
Theta EC1	-8.508	31	.000*	-3.9469	14.3	10.353
AlphaEC1	2.108	31	.043*	4.9375	17.3	22.238
Beta1EC1	5.206	31	.000*	2.9656	5.7	8.666
Beta2EC1	.544	31	.591	.2656	8.4	8.666
DeltaEO2	2.788	33	.009*	1.4824	11.7	13.182
Theta EO2	-4.484	33	.000*	-1.9529	12.6	10.647
AlphaEO2	-8.865	33	.000*	-4.2118	14.8	15.588
Beta1EO2	-.089	33	.930	-.0265	6.1	6.074
Beta2EO2	-3.388	33	.002*	-1.1353	8.5	7.365
DeltaEC2	-2.206	32	.035*	-.9515	11.9	10.948
Theta EC2	-.717	32	.478	-.5152	11.8	11.285
AlphaEC2	4.226	32	.000*	11.3667	14.1	25.467
Beta1EC2	6.176	32	.000*	3.3545	5.5	8.855
Beta2EC2	.730	32	.471	.3576	8.8	9.158
DeltaEO3	4.012	38	.000*	2.1974	10.8	12.997
Theta EO3	-3.039	38	.004*	-1.1667	12.0	10.833
AlphaEO3	-7.195	38	.000*	-4.1462	15.3	11.154
Beta1EO3	4.774	38	.000*	1.2077	5.1	6.308
Beta2EO3	-1.058	38	.279	-.4564	8.3	7.844
DeltaEC3	-6.571	35	.000*	-4.3917	16.3	11.908
Theta EC3	-1.306	35	.200	-.8806	11.9	11.019
AlphaEC3	2.773	35	.009*	6.6083	16.7	23.308
Beta1EC3	5.957	35	.000*	3.0750	5.6	8.675
Beta2EC3	3.375	35	.002*	1.6778	7.4	9.078
DeltaEO4	5.978	38	.000*	3.8821	9.5	13.382
Theta EO4	-1.578	38	.123	-.6000	11.4	10.800
AlphaEO4	-2.197	38	.034*	-1.5154	13.2	11.685
Beta1EO4	2.278	38	.028*	.6256	5.7	6.326
Beta2EO4	-.971	38	.338	-.3923	8	7.608
DeltaEC4	-10.165	35	.000*	-5.3667	16.8	11.433
Theta EC4	-3.201	35	.003*	-1.9528	13.2	11.247
AlphaEC4	3.230	35	.003*	7.7500	16.9	24.650
Beta1EC4	6.618	35	.000*	3.4667	5.3	8.767
Beta2EC4	4.318	35	.000*	1.8278	7.1	8.928
DeltaEO5	1.935	38	.060	1.0513	12.1	13.151
Theta EO5	-3.688	38	.001*	-1.5692	12.2	10.631
AlphaEO5	-9.703	38	.000*	-5.4974	16.5	11.003
Beta1EO5	3.266	38	.002*	.8641	5.4	6.264
Beta2EO5	-.601	38	.551	-.2385	7.7	7.462

DeltaEC5	-5.821	36	.000*	-3.8568	15.4	11.543
Theta EC5	-5.045	36	.000*	-3.1135	14.2	11.086
AlphaEC5	2.495	36	.017*	5.6892	18.1	23.789
Beta1EC5	3.993	36	.000*	2.0081	6.4	8.408
Beta2EC5	-.376	36	.709	-.1568	9.1	8.943

Table B1. Results from the one sample t-tests of all frequency bands on the left occipital (O1) location for all eyes open (EO) and eyes closed (EC) blocks. Significant results are indicated with an asterisk.

	t	**df**	**Sig (two tailed)**	**Mean dif.**	**Tested value**	**Group mean**
DeltaEO1	2.896	38	.006*	1.6308	11.6	13.231
Theta EO1	-8.353	38	.000*	-3.4410	14.3	10.859
AlphaEO1	-6.255	38	.000*	-3.3487	14.1	10.751
Beta1EO1	3.463	38	.001*	.8333	5.3	6.133
Beta2EO1	-.755	38	.455	-2.615	7.6	7.338
DeltaEC1	-1.946	38	.059	-1.7821	14.2	14.418
Theta EC1	-3.297	38	.002*	-2.4821	14.0	11.518
AlphaEC1	3.734	38	.001*	12.1282	15.2	27.328
Beta1EC1	7.717	38	.000*	4.1667	4.9	9.067
Beta2EC1	3.791	38	.001*	1.5769	7.1	8.677
DeltaEO2	1.777	37	.084	.9500	12.0	12.950
Theta EO2	-8.356	37	.000*	-3.7526	14.5	10.747
AlphaEO2	-4.262	37	.000*	-3.0711	14.6	11.529
Beta1EO2	2.604	37	.013*	.7105	5.4	6.111
Beta2EO2	0.970	37	.339	.3105	7.1	7.411
DeltaEC2	.664	38	.511	.6385	12.1	12.738
Theta EC2	.725	38	.473	.6077	11.4	12.008
AlphaEC2	4.760	38	.000*	14.9256	12.7	27.626
Beta1EC2	7.713	38	.000*	4.3538	4.9	9.254
Beta2EC2	3.094	38	.004*	1.2103	7.9	9.110
DeltaEO3	5.646	38	.000*	3.0385	9.9	12.938
Theta EO3	-3.332	38	.002*	-1.4051	12.0	10.595
AlphaEO3	-3.668	38	.001*	-2.2692	13.2	10.931
Beta1EO3	7.530	38	.000*	1.7231	4.5	6.223
Beta2EO3	-1.871	38	.069	-.6641	8.0	7.336
DeltaEC3	-21.284	27	.000*	-6.1750	16.0	9.825
Theta EC3	-5.975	27	.000*	-1.7893	10.7	8.911
AlphaEC3	2.993	27	.006*	5.5500	13.8	19.350
Beta1EC3	5.464	27	.000*	2.8286	5.1	7.929
Beta2EC3	1.604	27	.120	.6964	7.6	8.296
DeltaEO4	6.315	38	.000*	4.1692	9.1	13.269
Theta EO4	-3.389	38	.002*	-1.3564	11.9	10.544
AlphaEO4	-2.808	38	.008*	-1.9974	13.5	11.503
Beta1EO4	4.074	38	.000*	1.0436	5.2	6.244
Beta2EO4	-1.197	38	.239	-.3987	7.6	7.210
DeltaEC4	-6.191	37	.000*	-5.1789	17.4	12.221
Theta EC4	-2.916	37	.006*	-2.1132	13.9	11.787
AlphaEC4	4.177	37	.000*	12.6868	14.4	27.087
Beta1EC4	7.424	37	.000*	4.1711	4.8	8.971

Beta2EC4	3.755	37	.001*	1.5026	7.4	8.903
DeltaEO5	3.580	37	.001*	1.8184	10.7	12.518
Theta EO5	-5.732	37	.000*	-2.1289	12.3	10.171
AlphaEO5	-6.141	37	.000*	-3.5395	14.3	10.761
Beta1EO5	3.704	37	.001*	.9526	5.1	6.053
Beta2EO5	-.345	37	.732	-.1105	7.3	7.189
DeltaEC5	-7.831	34	.000*	-4.1886	14.7	10.511
Theta EC5	-5.639	34	.000*	-3.0743	13.5	10.426
AlphaEC5	3.076	34	.004*	6.9400	16.2	23.140
Beta1EC5	4.336	34	.000*	2.3114	6.2	8.511
Beta2EC5	-1.821	34	.077	-.7657	9.7	8.934

Table B2. Results from the one sample t-tests of all frequency bands on the right occipital (O2) location for all eyes open (EO) and eyes closed (EC) blocks. Significant results are indicated with an asterisk.

	t	**df**	**Sig (two tailed)**	**Mean dif.**	**Tested value**	**Group mean**
HbO_2 EO1	4.894	34	.000*	.5427	-0.1631	0.3796
Hbb EO1	-9.075	34	.000*	-.8596	0.6584	-0.2011
HbO_2 EC1	2.519	34	.017*	.2960	-0.0719	0.2240
Hbb EC1	-16.405	34	.000*	-1.4923	1.389	-0.1028
HbO_2 EO2	4.915	34	.000*	.5695	-0.1398	0.4297
Hbb EO2	-11.680	34	.000*	-1.1369	0.9174	-.2196
HbO_2 EC2	.514	34	0.611	.0541	0.0511	0.1052
Hbb EC2	-11.345	34	.000*	-1.0435	0.9705	-0.0731
HbO_2 EO3	4.486	34	.000*	.5275	-0.1061	0.4214
Hbb EO3	-10.873	34	.000*	-1.0464	0.8478	-0.1986
HbO_2 EC3	1.240	34	0.223	.1305	-0.0263	.01041
Hbb EC3	-13.355	34	.000*	-1.2446	1.1537	-0.0909
HbO_2 EO4	3.983	34	.000*	.4158	-0.0255	0.3902
Hbb EO4	-9.485	34	.000*	-.9007	0.7075	-0.1932
HbO_2 EC4	2.253	34	.031*	.2270	-0.1329	0.0941
Hbb EC4	-17.646	34	.000*	-1.5566	1.4665	-0.0901
HbO_2 EO5	4.809	34	.000*	.4999	-0.0899	0.4099
Hbb EO5	-7.899	34	.000*	-.7322	0.5148	-0.2174
HbO_2 EC5	-.223	34	.825	-.0247	0.1955	0.1708
Hbb EC5	-15.954	34	.000*	-1.3575	1.2877	-0.0698

Table B3. Results from the one sample t-test of the oxygenated haemoglobin (HbO_2) and deoxygenated haemoglobin (Hbb) concentrations on the left occipital cortex (O1) for all eyes open (EO) and eyes closed (EC) blocks. Significant results are indicated with an asterisk.

	t	**df**	**Sig (two tailed)**	**Mean dif.**	**Tested value**	**Group mean**
HbO_2 EO1	4.611	35	.000*	.9331	-0.3908	.5424
Hbb EO1	-2.291	35	.028*	-.3105	-0.0893	-.3998
HbO_2 EC1	2.089	35	.044*	.4180	-0.0719	0.3461
Hbb EC1	-.816	35	.420	-.1103	-0.1831	-0.2934
HbO_2 EO2	3.765	35	.001*	.7959	-0.2961	0.4997

Hbb EO2	-1.609	35	.117	-.2277	-0.1464	-0.3741
HbO_2 EC2	1.786	34	.083	.3041	-0.1317	0.1724
Hbb EC2	-.405	34	.688	-.0538	-0.1826	-0.2364
HbO_2 EO3	3.707	35	.001*	.7987	-0.2594	0.5393
Hbb EO3	-1.553	35	.130	-.2243	-0.1818	-0.4061
HbO_2 EC3	5.123	34	.000*	.7947	-0.6139	0.1808
Hbb EC3	-2.311	34	.027*	-.2859	0.0314	-0.2544
HbO_2 EO4	3.102	35	.004*	.6233	-0.0318	0.5915
Hbb EO4	-1.209	35	.235	-.1735	-0.2574	-0.4309
HbO_2 EC4	4.667	35	.000*	.8692	-0.5952	0.2740
Hbb EC4	-1.989	35	.055	-.2536	-0.0632	-0.3168
HbO_2 EO5	4.324	35	.000*	.9080	-0.3133	0.5947
Hbb EO5	-2.462	35	.019*	-.3480	-0.0800	-0.4280
HbO_2 EC5	2.696	35	.011*	.5159	-0.2089	0.3070
Hbb EC5	.215	35	.831	-.2793	-0.3048	-0.2769

Table B4. Results from the one sample t-test of the oxygenated haemoglobin (HbO_2) and deoxygenated haemoglobin (Hbb) concentrations on the right occipital cortex (O2) for all eyes open (EO) and eyes closed (EC) blocks. Significant results are indicated with an asterisk.

	t	**df**	**Sig (two tailed)**	**Mean dif.**	**Tested value**	**Group mean**
Alpha x HbO_2 O1	-7.945	37	.000*	-.3317	0.161	-0.1707
Timing Alpha x HbO_2 O1	5.763	37	.000*	141.816	-72	69.82
Alpha x Hbb O1	5.090	37	.000*	.2677	-0.085	0.1827
Timing Alpha x Hbb O1	-2.999	37	.005*	-69.579	118	48.42
Alpha x HbO_2 O2	-.748	37	.459	-.02455	-0.095	-0.1196
Timing Alpha x HbO_2 O2	-1.135	37	.264	-32.579	45	12.42
Alpha x Hbb O2	1.119	37	.270	.0365	0.067	0.1035
Timing Alpha x Hbb O2	-1.569	37	.125	-43.921	42	-1.92
Individual Alpha x HbO_2 O1	-6.029	37	.000*	.2517	0.081	-0.1707
Timing Individual Alpha x HbO_2 O1	0196	37	.846	4.816	65	69.82
Individual Alpha x Hbb O1	1.592	37	.120	.0837	0.099	0.1827
Timing Individual Alpha x Hbb O1	-4.508	37	.000*	-104.579	153	48.42
Individual Alpha x HbO_2 O2	-.047	37	.963	-.068	-0.118	-0.1196
Timing Individual Alpha x HbO_2 O2	-2.843	37	.007*	-81.579	94	12.42
Individual Alpha x Hbb O2	.445	37	.659	.0145	0.089	0.1035

Timing Individual Alpha x Hbb O2	-3.927	37	.000*	-109.921	108	-1.92
Delta x HbO_2 O1	-6.939	37	.000*	-.28974	0.119	-0.1707
Timing Delta x HbO_2 O1	11.249	37	.000*	276.816	-207	69.82
Delta x Hbb O1	-1.584	37	.122	-.08329	0.266	0.1827
Timing Delta x Hbb O1	-1.361	37	.182	-31.579	80	48.42
Delta x HbO_2 O2	2.175	37	.036*	.07145	-0.191	-0.1196
Timing Delta x HbO_2 O2	-4.062	37	.000	-116.579	129	12.42
Delta x Hbb O2	-.782	37	.439	-.0255	0.129	0.1035
Timing Delta x Hbb O2	-4.570	37	.000*	-127,921	126	-1.92

Table B5. Results from the one sample t-test of the cross correlation analyses for both the correlation value and the time point at which the highest correlation was found. The entire healthy sample is evaluated. Significant results are indicated with an asterisk. Legend: O1= left visual cortex, O2= right visual cortex, HbO_2= oxygenated haemoglobin, Hbb= deoxygenated haemoglobin.

	t	**df**	**Sig (two tailed)**	**Mean dif.**	**Tested value**	**Group mean**
Alpha x HbO_2 O1	-5.500	10	.000*	-.43655	0.161	-.27555
Timing Alpha x HbO_2 O1	3.866	10	.003*	197.636	-72	125.64
Alpha x Hbb O1	5.678	9	.000*	.48840	-0.085	0.403
Timing Alpha x Hbb O1	.175	9	.865	7.200	118	125.20
Alpha x HbO_2 O2	-.838	9	.427	-.07400	-0.095	-0.169
Timing Alpha x HbO_2 O2	-.262	9	.799	-15.800	45	29.2
Alpha x Hbb O2	2.785	8	.024*	.18411	0.067	0.251
Timing Alpha x Hbb O2	.665	8	.524	-96.42	42	81.11
Individual Alpha x HbO_2 O1	-4.492	10	.001*	-.35655	0.081	-.27555
Timing Individual Alpha x HbO_2 O1	1.186	10	.263	60.636	65	125.64
Individual Alpha x Hbb O1	3.539	9	.006*	.30440	0.099	0.403
Timing Individual Alpha x Hbb O1	-.675	9	.517	-27.800	153	125.20
Individual Alpha x HbO_2 O2	-.574	9	.580	-.0510	-0.118	-0.169
Timing Individual Alpha x HbO_2 O2	-1.073	9	.311	-64.800	94	29.2
Individual Alpha	2.452	8	.040*	.1621	0.089	0.251

x Hbb O2						
Timing Individual Alpha x Hbb O2	-.458	8	.659	-26.889	108	81.11
Delta x HbO_2 O1	-4.971	10	.001*	-.39455	0.119	-.27555
Timing Delta x HbO_2 O1	6.506	10	.000*	332.636	-207	125.64
Delta x Hbb O1	1.597	9	.145	.13740	0.266	0.403
Timing Delta x Hbb O1	1.097	9	.301	45.200	80	125.20
Delta x HbO_2 O2	.248	9	.810	.0220	-0.191	-0.169
Timing Delta x HbO_2 O2	-1.653	9	.133	-99.800	129	29.2
Delta x Hbb O2	1.847	8	.102	.12211	0.129	0.251
Timing Delta x Hbb O2	-.764	8	.467	-44.889	126	81.11

Table B6. Results from the one sample t-test of the cross-correlation analyses for both the correlation value and the time point at which the highest correlation was found. Bad data are removed from the healthy sample. Significant results are indicated with an asterisk. Legend: O1= left visual cortex, O2= right visual cortex, HbO_2= oxygenated haemoglobin, Hbb= deoxygenated haemoglobin.

Appendix C1

The filled out Barthel Index for the patient discussed under case 1. The original research data were documented in Dutch. In order to make the given answers on the Dutch scale more insightful, the answers were projected on the English version of the scale.

Barthel Index of Activities of Daily Living

Instructions: Choose the scoring point for the statement that most closely corresponds to the patient's current level of ability for each of the following 10 items. Record actual, not potential, functioning. Information can be obtained from the patient's self-report, from a separate party who is familiar with the patient's abilities (such as a relative), or from observation. Refer to the Guidelines section on the following page for detailed information on scoring and interpretation.

The Barthel Index

Bowels
0 = incontinent (or needs to be given enemata)
1 = occasional accident (once/week)
2 = continent
Patient's Score: 2

Bladder
0 = incontinent, or catheterized and unable to manage
1 = occasional accident (max. once per 24 hours)
2 = continent (for over 7 days)
Patient's Score: 2

Grooming
0 = needs help with personal care
1 = independent face/hair/teeth/shaving (implements provided)
Patient's Score: 1

Toilet use
0 = dependent
1 = needs some help, but can do something alone
2 = independent (on and off, dressing, wiping)
Patient's Score: 2

Feeding
0 = unable
1 = needs help cutting, spreading butter, etc.
2 = independent (food provided within reach)
Patient's Score: 2

Transfer
0 = unable – no sitting balance
1 = major help (one or two people, physical), can sit
2 = minor help (verbal or physical)
3 = independent
Patient's Score: 3

Mobility
0 = immobile
1 = wheelchair independent, including corners, etc.
2 = walks with help of one person (verbal or physical)
3 = independent (but may use any aid, e.g., stick)
Patient's Score: 3

Dressing
0 = dependent
1 = needs help, but can do about half unaided
2 = independent (including buttons, zips, laces, etc.)
Patient's Score: 2

Stairs
0 = unable
1 = needs help (verbal, physical, carrying aid)
2 = independent up and down
Patient's Score: 2

Bathing
0 = dependent
1 = independent (or in shower)
Patient's Score: 1

Total Score: 20

(Collin et al., 1988)

Scoring:
Sum the patient's scores for each item. Total possible scores range from 0 – 20, with lower scores indicating increased disability. If used to measure improvement after rehabilitation, changes of more than two points in the total score reflect a probable genuine change, and change on one item from fully dependent to independent is also likely to be reliable.

Appendix C2

The filled out Barthel Index for the patient discussed under case 2. The original research data were documented in Dutch. In order to make the given answers on the Dutch scale more insightful, the answers were projected on the English version of the scale.

Barthel Index of Activities of Daily Living

Instructions: Choose the scoring point for the statement that most closely corresponds to the patient's current level of ability for each of the following 10 items. Record actual, not potential, functioning. Information can be obtained from the patient's self-report, from a separate party who is familiar with the patient's abilities (such as a relative), or from observation. Refer to the Guidelines section on the following page for detailed information on scoring and interpretation.

The Barthel Index

Bowels
0 = incontinent (or needs to be given enemata)
1 = occasional accident (once/week)
2 = continent
Patient's Score: 0

Bladder
0 = incontinent, or catheterized and unable to manage
1 = occasional accident (max. once per 24 hours)
2 = continent (for over 7 days)
Patient's Score: 0

Grooming
0 = needs help with personal care
1 = independent face/hair/teeth/shaving (implements provided)
Patient's Score: 0

Toilet use
0 = dependent
1 = needs some help, but can do something alone
2 = independent (on and off, dressing, wiping)
Patient's Score: 0

Feeding
0 = unable
1 = needs help cutting, spreading butter, etc.
2 = independent (food provided within reach)
Patient's Score: 0

Transfer
0 = unable – no sitting balance
1 = major help (one or two people, physical), can sit
2 = minor help (verbal or physical)
3 = independent
Patient's Score: 1

Mobility
0 = immobile
1 = wheelchair independent, including corners, etc.
2 = walks with help of one person (verbal or physical)
3 = independent (but may use any aid, e.g., stick)
Patient's Score: 0

Dressing
0 = dependent
1 = needs help, but can do about half unaided
2 = independent (including buttons, zips, laces, etc.)
Patient's Score: 0

Stairs
0 = unable
1 = needs help (verbal, physical, carrying aid)
2 = independent up and down
Patient's Score: 0

Bathing
0 = dependent
1 = independent (or in shower)
Patient's Score: 0

Total Score: 1

(Collin et al., 1988)

Scoring:
Sum the patient's scores for each item. Total possible scores range from 0 – 20, with lower scores indicating increased disability. If used to measure improvement after rehabilitation, changes of more than two points in the total score reflect a probable genuine change, and change on one item from fully dependent to independent is also likely to be reliable.

References

ABASOLO, D., ESCUDERO, J., HORNERO, R., GOMEZ, C. & ESPINO, P. 2008. Approximate entropy and auto mutual information analysis of the electroencephalogram in Alzheimer's disease patients. *Med Biol Eng Comput,* 46**,** 1019-28.

ABASOLO, D., HORNERO, R., ESPINO, P., ESCUDERO, J. & GOMEZ, C. 2007. Electroencephalogram background activity characterization with approximate entropy and auto mutual information in Alzheimer's disease patients. *Conf Proc IEEE Eng Med Biol Soc,* 2007**,** 6192-5.

ACHARYA, U. R., SREE, S. V., CHATTOPADHYAY, S. & SURI, J. S. 2012. Automated diagnosis of normal and alcoholic EEG signals. *Int J Neural Syst,* 22**,** 1250011.

ALONSO, J. F., MANANAS, M. A., ROMERO, S., HOYER, D., RIBA, J. & BARBANOJ, M. J. 2010. Drug effect on EEG connectivity assessed by linear and nonlinear couplings. *Hum Brain Mapp,* 31**,** 487-97.

ALONSO, J. F., MANANAS, M. A., ROMERO, S., RIBA, J., BARBANOJ, M. J. & HOYER, D. 2007. Connectivity analysis of EEG under drug therapy. *Conf Proc IEEE Eng Med Biol Soc,* 2007**,** 6188-91.

ARCA DIAZ, G., CESARON, E., ALFONSO, I., DUNOYER, C. & YAYLALI, I. 2006. Near infrared spectroscopy in the management of status epilepticus in a young infant. *Eur J Paediatr Neurol,* 10**,** 19-21.

ARENTH, P. M., RICKER, J. H. & SCHULTHEIS, M. T. 2007. Applications of functional near-infrared spectroscopy (fNIRS) to Neurorehabilitation of cognitive disabilities. *Clin Neuropsychol,* 21**,** 38-57.

ASSOCIATION, A. P. 2000. Diagnostic And Statistical Manual Of Mental Disorders DSM-IV-TR Fourth Edition (Text Revision) Author: American Psychiatr.

AYATA, C. 2013. Spreading depression and neurovascular coupling. *Stroke,* 44**,** S87-S89.

BAK, P., TANG, C. & WIESENFELD, K. 1987. Self-organized criticality: An explanation of the 1/f noise. *Phys Rev Lett,* 59**,** 381-384.

BARRY, R. J., CLARKE, A. R., JOHNSTONE, S. J., MAGEE, C. A. & RUSHBY, J. A. 2007. EEG differences between eyes-closed and eyes-open resting conditions. *Clin Neurophysiol,* 118**,** 2765-73.

BARRY, R. J., CLARKE, A. R., JOHNSTONE, S. J. & RUSHBY, J. A. 2008. Timing of caffeine's impact on autonomic and central nervous system measures: clarification of arousal effects. *Biological psychology,* 77**,** 304-316.

BAZANOVA, O. & VERNON, D. 2013. Interpreting EEG alpha activity. *Neuroscience & Biobehavioral Reviews*.

BEAR, M. F., CONNORS, B. W. & PARADISO, M. A. 2007. *Neuroscience*, Wolters Kluwer Health.

BECERRA, J., FERNANDEZ, T., HARMONY, T., CABALLERO, M., GARCIA, F., FERNANDEZ-BOUZAS, A., SANTIAGO-RODRÍGUEZ, E. & PRADO-ALCALÁ, R. 2006. Follow-up study of learning-disabled children treated with neurofeedback or placebo. *Clinical EEG and neuroscience,* 37**,** 198-203.

BECKMANN, C. F., DELUCA, M., DEVLIN, J. T. & SMITH, S. M. 2005. Investigations into resting-state connectivity using independent component analysis. *Philos Trans R Soc Lond B Biol Sci,* 360**,** 1001-13.

BENNETT, C. M., MILLER, M. & WOLFORD, G. 2009. Neural correlates of interspecies perspective taking in the post-mortem Atlantic Salmon: An argument for multiple comparisons correction. *Neuroimage,* 47**,** S125.
BERGER, H. 1929. Über das elektrenkephalogramm des menschen. *European Archives of Psychiatry and Clinical Neuroscience,* 87**,** 527-570.
BERGER, H. 1969a. On the electroencephalogram of man. *Electroencephalogr Clin Neurophysiol***,** Suppl 28:37+.
BERGER, H. 1969b. On the electroencephalogram of man. Eighth report. *Electroencephalogr Clin Neurophysiol***,** Suppl 28:209+.
BERGER, H. 1969c. On the electroencephalogram of man. Eleventh report. *Electroencephalogr Clin Neurophysiol***,** Suppl 28:255+.
BERGER, H. 1969d. On the electroencephalogram of man. Fifth report. *Electroencephalogr Clin Neurophysiol***,** Suppl 28:151+.
BERGER, H. 1969e. On the electroencephalogram of man. Fourteenth report. *Electroencephalogr Clin Neurophysiol***,** Suppl 28:299+.
BERGER, H. 1969f. On the electroencephalogram of man. Fourth report. *Electroencephalogr Clin Neurophysiol***,** Suppl 28:133+.
BERGER, H. 1969g. On the electroencephalogram of man. Ninth report. *Electroencephalogr Clin Neurophysiol***,** Suppl 28:225+.
BERGER, H. 1969h. On the electroencephalogram of man. Second report. *Electroencephalogr Clin Neurophysiol***,** Suppl 28:75+.
BERGER, H. 1969i. On the electroencephalogram of man. Seventh report. *Electroencephalogr Clin Neurophysiol***,** Suppl 28:191+.
BERGER, H. 1969j. On the electroencephalogram of man. Sixth report. *Electroencephalogr Clin Neurophysiol***,** Suppl 28:173+.
BERGER, H. 1969k. On the electroencephalogram of man. Tenth report. *Electroencephalogr Clin Neurophysiol***,** Suppl 28:243+.
BERGER, H. 1969l. On the electroencephalogram of man. Third report. *Electroencephalogr Clin Neurophysiol***,** Suppl 28:95+.
BERGER, H. 1969m. On the electroencephalogram of man. Thirteenth report. *Electroencephalogr Clin Neurophysiol***,** Suppl 28:291+.
BERGER, H. 1969n. On the electroencephalogram of man. Twelfth report. *Electroencephalogr Clin Neurophysiol***,** Suppl 28:267+.
BERSANI, F. S., MINICHINO, A., ENTICOTT, P. G., MAZZARINI, L., KHAN, N., ANTONACCI, G., RACCAH, R. N., SALVIATI, M., DELLE CHIAIE, R., BERSANI, G., FITZGERALD, P. B. & BIONDI, M. 2013. Deep transcranial magnetic stimulation as a treatment for psychiatric disorders: a comprehensive review. *Eur Psychiatry,* 28**,** 30-9.
BIALLAS, M., TRAJKOVIC, I., HAENSSE, D., MARCAR, V. & WOLF, M. 2012. Reproducibility and sensitivity of detecting brain activity by simultaneous electroencephalography and near-infrared spectroscopy. *Experimental brain research,* 222**,** 255-264.
BISWAL, B., YETKIN, F. Z., HAUGHTON, V. M. & HYDE, J. S. 1995. Functional connectivity in the motor cortex of resting human brain using echo-planar MRI. *Magn Reson Med,* 34**,** 537-41.
BLICHER, J. U., STAGG, C. J., O'SHEA, J., ØSTERGAARD, L., MACINTOSH, B. J., JOHANSEN-BERG, H., JEZZARD, P. & DONAHUE, M. J. 2012. Visualization of altered neurovascular coupling in chronic stroke patients using multimodal functional MRI. *Journal of Cerebral Blood Flow & Metabolism,* 32**,** 2044-2054.

BOAS, D. A., DALE, A. M. & FRANCESCHINI, M. A. 2004. Diffuse optical imaging of brain activation: approaches to optimizing image sensitivity, resolution, and accuracy. *Neuroimage,* 23 Suppl 1**,** S275-88.

BODIZS, R., SVERTECZKI, M. & MESZAROS, E. 2008. Wakefulness-sleep transition: emerging electroencephalographic similarities with the rapid eye movement phase. *Brain Res Bull,* 76**,** 85-9.

BODY, L. C. P. & DE ROSA, E. 2007. Cholinergic influences on feature binding. *Behavioral Neuroscience,* 121**,** 264-276.

BONNÉRY, C., LECLERC, P.-O., DESJARDINS, M., HOGE, R., BHERER, L., POULIOT, P. & LESAGE, F. 2012. Changes in diffusion path length with old age in diffuse optical tomography. *Journal of biomedical optics,* 17**,** 0560021-0560028.

BOX, G. E., JENKINS, G. M. & REINSEL, G. C. 2013. *Time series analysis: forecasting and control*, Wiley. com.

BRABOSZCZ, C. & DELORME, A. 2011. Lost in thoughts: neural markers of low alertness during mind wandering. *Neuroimage,* 54**,** 3040-7.

BRIGADOI, S., CECCHERINI, L., CUTINI, S., SCARPA, F., SCATTURIN, P., SELB, J., GAGNON, L., BOAS, D. A. & COOPER, R. J. 2014. Motion artifacts in functional near-infrared spectroscopy: A comparison of motion correction techniques applied to real cognitive data. *Neuroimage,* 85 Pt 1**,** 181-91.

BROYD, S. J., HELPS, S. K. & SONUGA-BARKE, E. J. 2011. Attention-induced deactivations in very low frequency EEG oscillations: differential localisation according to ADHD symptom status. *PLoS One,* 6**,** e17325.

BRUMMER, V., SCHNEIDER, S., VOGT, T., STRUDER, H., CARNAHAN, H., ASKEW, C. D. & CSUHAJ, R. 2011. Coherence between brain cortical function and neurocognitive performance during changed gravity conditions. *J Vis Exp*.

BUCHHEIM, K., OBRIG, H., MÜLLER, A., HEEKEREN, H., VILLRINGER, A. & MEIERKORD, H. 2004. Decrease in haemoglobin oxygenation during absence seizures in adult humans. *Neuroscience letters,* 354**,** 119-122.

BUCKHOLTZ, J. W. & MEYER-LINDENBERG, A. 2012. Psychopathology and the human connectome: toward a transdiagnostic model of risk for mental illness. *Neuron,* 74**,** 990-1004.

BUCKNER, R. L. 2012. The serendipitous discovery of the brain's default network. *Neuroimage,* 62**,** 1137-45.

BULLMORE, E., BARNES, A., BASSETT, D. S., FORNITO, A., KITZBICHLER, M., MEUNIER, D. & SUCKLING, J. 2009. Generic aspects of complexity in brain imaging data and other biological systems. *Neuroimage,* 47**,** 1125-34.

BUTTI, M., PASTORI, A., MERZAGORA, A., ZUCCA, C., BIANCHI, A., RENI, G. & CERUTTI, S. 2006. Multimodal analysis of a sustained attention protocol: continuous performance test assessed with near infrared spectroscopy and EEG. *Conf Proc IEEE Eng Med Biol Soc,* 1**,** 1040-3.

BUXTON, R. B., WONG, E. C. & FRANK, L. R. 1998. Dynamics of blood flow and oxygenation changes during brain activation: the balloon model. *Magn Reson Med,* 39**,** 855-64.

BUZSÁKI, G., ANASTASSIOU, C. A. & KOCH, C. 2012. The origin of extracellular fields and currents—EEG, ECoG, LFP and spikes. *Nature Reviews Neuroscience,* 13**,** 407-420.

BUZSÁKI, G. & DRAGUHN, A. 2004. Neuronal oscillations in cortical networks. *Science,* 304**,** 1926-1929.

CABALLERO-GAUDES, C., VAN DE VILLE, D., GROUILLER, F., LEMIEUX, L., SEECK, M., LAZEYRAS, F. & VULLIEMOZ, S. 2012. Mapping interictal epileptic discharges using mutual information between concurrent EEG and fMRI. *Neuroimage*.

CANAZZA, A., MINATI, L., BOFFANO, C., PARATI, E. & BINKS, S. 2014. Experimental models of brain ischemia: a review of techniques, magnetic resonance imaging, and investigational cell-based therapies. *Frontiers in neurology,* 5.

CANNON, R. L. 2012. *Low resolution brain electromagnetic tomography (LORETA): Basic concepts and clinical applications*, BMED Press.

CARSKADON, M. A. & DEMENT, W. C. 1994. Normal human sleep: an overview. *Principles and practice of sleep medicine,* 4**,** 13-23.

CARTER, A. R., SHULMAN, G. L. & CORBETTA, M. 2012. Why use a connectivity-based approach to study stroke and recovery of function? *Neuroimage,* 62**,** 2271-2280.

CATON, R. 1875. Electrical currents of the brain. *The Journal of Nervous and Mental Disease,* 2**,** 610.

CAULI, B. & HAMEL, E. 2010. Revisiting the role of neurons in neurovascular coupling. *Frontiers in neuroenergetics,* 2.

CHEN, C.-C., HSU, C.-Y., CHIU, H.-W., HU, C.-J. & LEE, T.-C. 2013. Frequency power and coherence of electroencephalography are correlated with the severity of Alzheimer's disease: A multicenter analysis in Taiwan. *Journal of the Formosan Medical Association*.

CHEN, S. & LI, X. 2012. Functional magnetic resonance imaging for imaging neural activity in the human brain: the annual progress. *Comput Math Methods Med,* 2012**,** 613465.

CHIALVO, D. R. 2006. The brain near the edge. *arXiv preprint q-bio/0610041*.

CLARKE, A. R., BARRY, R. J., MCCARTHY, R., SELIKOWITZ, M. & BROWN, C. R. 2002. EEG evidence for a new conceptualisation of attention deficit hyperactivity disorder. *Clinical Neurophysiology,* 113**,** 1036-1044.

COBURN, K. L., LAUTERBACH, E. C., BOUTROS, N. N., BLACK, K. J., ARCINIEGAS, D. B. & COFFEY, C. E. 2006. The value of quantitative electroencephalography in clinical psychiatry: a report by the Committee on Research of the American Neuropsychiatric Association. *J Neuropsychiatry Clin Neurosci,* 18**,** 460-500.

COLD, C. S. H. P. M. & COLD, C. S. H. H. B. 2007. *Observed brain dynamics*, Oxford University Press.

COLE, D. M., SMITH, S. M. & BECKMANN, C. F. 2010. Advances and pitfalls in the analysis and interpretation of resting-state FMRI data. *Front Syst Neurosci,* 4**,** 8.

COLZATO, L. S., VAN WOUWE, N. C. & HOMMEL, B. 2007. Feature binding and affect: emotional modulation of visuo-motor integration. *Neuropsychologia,* 45**,** 440-6.

COOLEY, J. W. & TUKEY, J. W. 1965. An algorithm for the machine calculation of complex Fourier series. *Mathematics of computation,* 19**,** 297-301.

COOPER, R. J., SELB, J., GAGNON, L., PHILLIP, D., SCHYTZ, H. W., IVERSEN, H. K., ASHINA, M. & BOAS, D. A. 2012. A systematic comparison of motion artifact correction techniques for functional near-infrared spectroscopy. *Front Neurosci,* 6**,** 147.

COPE, M. & DELPY, D. T. 1988. System for long-term measurement of cerebral blood and tissue oxygenation on newborn infants by near infra-red transillumination. *Med Biol Eng Comput,* 26**,** 289-94.

COTILLON-WILLIAMS, N. & EDELINE, J. M. 2004. Evoked oscillations in unit recordings from the thalamo-cortical auditory system: an aspect of temporal processing or the reflection of hyperpolarized brain states? *Acta Neurobiologiae Experimentalis,* 64**,** 253-270.

CUI, X., BRAY, S. & REISS, A. L. 2010. Functional near infrared spectroscopy (NIRS) signal improvement based on negative correlation between oxygenated and deoxygenated hemoglobin dynamics. *Neuroimage,* 49**,** 3039-46.
CUSPINEDA, E., MACHADO, C., GALAN, L., AUBERT, E., ALVAREZ, M., LLOPIS, F., PORTELA, L., GARCÍA, M., MANERO, J. & AVILA, Y. 2007. QEEG prognostic value in acute stroke. *Clinical EEG and neuroscience,* 38**,** 155-160.
DALY, I., NICOLAOU, N., NASUTO, S. J. & WARWICK, K. 2013. Automated Artifact Removal From the Electroencephalogram A Comparative Study. *Clinical EEG and neuroscience,* 44**,** 291-306.
DAVID, O., COSMELLI, D. & FRISTON, K. J. 2004. Evaluation of different measures of functional connectivity using a neural mass model. *Neuroimage,* 21**,** 659-73.
DAVIDSON, R. J. 1992. Emotion and affective style: Hemispheric substrates. *Psychological science,* 3**,** 39-43.
DAVIDSON, R. J. 1998. Anterior electrophysiological asymmetries, emotion, and depression: conceptual and methodological conundrums. *Psychophysiology,* 35**,** 607-14.
DE GENNARO, L., MARZANO, C., VENIERO, D., MORONI, F., FRATELLO, F., CURCIO, G., FERRARA, M., FERLAZZO, F., NOVELLI, L. & CONCETTA PELLICCIARI, M. 2007. Neurophysiological correlates of sleepiness: a combined TMS and EEG study. *Neuroimage,* 36**,** 1277-1287.
DE HAAN, R., LIMBURG, M., SCHULING, J., BROESHART, J., JONKERS, L. & VAN ZUYLEN, P. 1993. [Clinimetric evaluation of the Barthel Index, a measure of limitations in dailly activities]. *Ned Tijdschr Geneeskd,* 137**,** 917-21.
DE VOLDER, A. G., BOL, A., BLIN, J., ROBERT, A., ARNO, P., GRANDIN, C., MICHEL, C. & VERAART, C. 1997. Brain energy metabolism in early blind subjects: neural activity in the visual cortex. *Brain research,* 750**,** 235-244.
DEBENER, S., BEAUDUCEL, A., EACUTE, NESSLER, D., BROCKE, B., HEILEMANN, H., KAYSER, J. & RGEN, U. 2000. Is resting anterior EEG alpha asymmetry a trait marker for depression? *Neuropsychobiology,* 41**,** 31-37.
DELPY, D. T., COPE, M., VAN DER ZEE, P., ARRIDGE, S., WRAY, S. & WYATT, J. 1988. Estimation of optical pathlength through tissue from direct time of flight measurement. *Physics in medicine and biology,* 33**,** 1433.
DEMYTTENAERE, K., BRUFFAERTS, R., POSADA-VILLA, J., GASQUET, I., KOVESS, V., LEPINE, J., ANGERMEYER, M. C., BERNERT, S., DE GIROLAMO, G. & MOROSINI, P. 2013. Prevalence, severity, and unmet need for treatment of mental disorders in the World Health Organization World Mental Health Surveys.
DIESSEN, E., DIEDEREN, S. J., BRAUN, K. P., JANSEN, F. E. & STAM, C. J. 2013. Functional and structural brain networks in epilepsy: What have we learned? *Epilepsia,* 54**,** 1855-1865.
DIETSCH, G. 1932. Fourier-analyse von elektrencephalogrammen des menschen. *Pflüger's Archiv für die gesamte Physiologie des Menschen und der Tiere,* 230**,** 106-112.
DOMÍNGUEZ, L. G., VELÁZQUEZ, J. L. P. & GALÁN, R. F. 2013. A model of functional brain connectivity and background noise as a biomarker for cognitive phenotypes: application to autism. *PloS one,* 8**,** e61493.
DUFFY, F. H., ALBERT, M. S., MCANULTY, G. & GARVEY, A. J. 1984. Age-related differences in brain electrical activity of healthy subjects. *Annals of neurology,* 16**,** 430-438.
DUNCAN, A., MEEK, J. H., CLEMENCE, M., ELWELL, C. E., FALLON, P., TYSZCZUK, L., COPE, M. & DELPY, D. T. 1996. Measurement of cranial optical path length

as a function of age using phase resolved near infrared spectroscopy. *Pediatr Res,* 39**,** 889-94.

EGNER, T., ZECH, T. F. & GRUZELIER, J. H. 2004. The effects of neurofeedback training on the spectral topography of the electroencephalogram. *Clin Neurophysiol,* 115**,** 2452-60.

EHLIS, A. C., RINGEL, T. M., PLICHTA, M. M., RICHTER, M. M., HERRMANN, M. J. & FALLGATTER, A. J. 2009. Cortical correlates of auditory sensory gating: a simultaneous near-infrared spectroscopy event-related potential study. *Neuroscience,* 159**,** 1032-43.

ELIASSEN, J. C., BOESPFLUG, E. L., LAMY, M., ALLENDORFER, J., CHU, W.-J. & SZAFLARSKI, J. P. 2008. Brain-mapping techniques for evaluating poststroke recovery and rehabilitation: a review. *Topics in stroke rehabilitation,* 15**,** 427-450.

ENGEL, A. K. & FRIES, P. 2010. Beta-band oscillations--signalling the status quo? *Curr Opin Neurobiol,* 20**,** 156-65.

ESCUDERO, J., HORNERO, R. & ABASOLO, D. 2009. Interpretation of the auto-mutual information rate of decrease in the context of biomedical signal analysis. Application to electroencephalogram recordings. *Physiol Meas,* 30**,** 187-99.

ESCUDERO, J., HORNERO, R., ABASOLO, D. & LOPEZ, M. 2008. On the application of the auto mutual information rate of decrease to biomedical signals. *Conf Proc IEEE Eng Med Biol Soc,* 2008**,** 2137-40.

FAES, L. & NOLLO, G. 2013. Decomposing the transfer entropy to quantify lag-specific Granger causality in cardiovascular variability. *Conf Proc IEEE Eng Med Biol Soc,* 2013**,** 5049-52.

FAZEKAS, F., NIEDERKORN, K., EBNER, F. & DIEZ-TEJEDOR, E. 2009. Relevance of neuroimaging in the evaluation of cerebral ischemia. *Cerebrovasc Dis,* 27 Suppl 1**,** 1-8.

FAZLI, S., MEHNERT, J., STEINBRINK, J., CURIO, G., VILLRINGER, A., MÜLLER, K.-R. & BLANKERTZ, B. 2012. Enhanced performance by a hybrid NIRS–EEG brain computer interface. *Neuroimage,* 59**,** 519-529.

FERRARI, M., MOTTOLA, L. & QUARESIMA, V. 2004. Principles, techniques, and limitations of near infrared spectroscopy. *Can J Appl Physiol,* 29**,** 463-87.

FERRARI, M. & QUARESIMA, V. 2012. A brief review on the history of human functional near-infrared spectroscopy (fNIRS) development and fields of application. *Neuroimage,* 63**,** 921-35.

FINNIGAN, S. & VAN PUTTEN, M. J. 2013. EEG in ischaemic stroke: quantitative EEG can uniquely inform (sub-)acute prognoses and clinical management. *Clin Neurophysiol,* 124**,** 10-9.

FINNIGAN, S. P., ROSE, S. E., WALSH, M., GRIFFIN, M., JANKE, A. L., MCMAHON, K. L., GILLIES, R., STRUDWICK, M. W., PETTIGREW, C. M., SEMPLE, J., BROWN, J., BROWN, P. & CHALK, J. B. 2004. Correlation of quantitative EEG in acute ischemic stroke with 30-day NIHSS score: comparison with diffusion and perfusion MRI. *Stroke,* 35**,** 899-903.

FOX, M. D. & RAICHLE, M. E. 2007. Spontaneous fluctuations in brain activity observed with functional magnetic resonance imaging. *Nat Rev Neurosci,* 8**,** 700-11.

FOX, M. D., SNYDER, A. Z., VINCENT, J. L., CORBETTA, M., VAN ESSEN, D. C. & RAICHLE, M. E. 2005. The human brain is intrinsically organized into dynamic, anticorrelated functional networks. *Proc Natl Acad Sci U S A,* 102**,** 9673-8.

FRANCESCHINI, M. A. & BOAS, D. A. 2004. Noninvasive measurement of neuronal activity with near-infrared optical imaging. *Neuroimage,* 21**,** 372-386.
FRASER, A. M. & SWINNEY, H. L. 1986. Independent coordinates for strange attractors from mutual information. *Phys Rev A,* 33**,** 1134-1140.
FRIES, P. 2009. Neuronal gamma-band synchronization as a fundamental process in cortical computation. *Annu Rev Neurosci,* 32**,** 209-24.
FRISTON, K. 2010. The free-energy principle: a unified brain theory? *Nature Reviews Neuroscience,* 11**,** 127-138.
FUHRMANN ALPERT, G., HEIN, G., TSAI, N., NAUMER, M. J. & KNIGHT, R. T. 2008. Temporal characteristics of audiovisual information processing. *J Neurosci,* 28**,** 5344-9.
GAGNON, L., COOPER, R. J., YÜCEL, M. A., PERDUE, K. L., GREVE, D. N. & BOAS, D. A. 2012. Short separation channel location impacts the performance of short channel regression in NIRS. *Neuroimage,* 59**,** 2518-2528.
GAO, J. & HU, J. 2013. Fast monitoring of epileptic seizures using recurrence time statistics of electroencephalography. *Front Comput Neurosci,* 7**,** 122.
GAZZANIGA, M. S., IVRY, R. B. & MANGUN, G. R. 2002. Cognitive Neuroscience.
GHOSH, A., ELWELL, C. & SMITH, M. 2012. Review article: cerebral near-infrared spectroscopy in adults: a work in progress. *Anesth Analg,* 115**,** 1373-83.
GIROUARD, H. & IADECOLA, C. 2006. Neurovascular coupling in the normal brain and in hypertension, stroke, and Alzheimer disease. *Journal of Applied Physiology,* 100**,** 328-335.
GÓMEZ-VERDEJO, V., MARTÍNEZ-RAMÓN, M., FLORENSA-VILA, J. & OLIVIERO, A. 2012. Analysis of fmri time series with mutual information. *Medical Image Analysis,* 16**,** 451-458.
GRANDY, T. H., WERKLE-BERGNER, M., CHICHERIO, C., LOVDEN, M., SCHMIEDEK, F. & LINDENBERGER, U. 2013a. Individual alpha peak frequency is related to latent factors of general cognitive abilities. *Neuroimage,* 79**,** 10-8.
GRANDY, T. H., WERKLE-BERGNER, M., CHICHERIO, C., SCHMIEDEK, F., LOVDEN, M. & LINDENBERGER, U. 2013b. Peak individual alpha frequency qualifies as a stable neurophysiological trait marker in healthy younger and older adults. *Psychophysiology,* 50**,** 570-82.
GRATTON, G. & FABIANI, M. 2010. Fast optical imaging of human brain function. *Frontiers in human neuroscience,* 4.
GREICIUS, M. D., KRASNOW, B., REISS, A. L. & MENON, V. 2003. Functional connectivity in the resting brain: a network analysis of the default mode hypothesis. *Proc Natl Acad Sci U S A,* 100**,** 253-8.
GUDMUNDSSON, S., RUNARSSON, T. P., SIGURDSSON, S., EIRIKSDOTTIR, G. & JOHNSEN, K. 2007. Reliability of quantitative EEG features. *Clinical Neurophysiology,* 118**,** 2162-2171.
HAIMOVICI, A., TAGLIAZUCCHI, E., BALENZUELA, P. & CHIALVO, D. R. 2013. Brain organization into resting state networks emerges at criticality on a model of the human connectome. *Physical review letters,* 110**,** 178101.
HANDWERKER, D. A., OLLINGER, J. M. & D'ESPOSITO, M. 2004. Variation of BOLD hemodynamic responses across subjects and brain regions and their effects on statistical analyses. *Neuroimage,* 21**,** 1639-51.
HANSLMAYR, S., SAUSENG, P., DOPPELMAYR, M., SCHABUS, M. & KLIMESCH, W. 2005. Increasing individual upper alpha power by neurofeedback improves cognitive performance in human subjects. *Applied psychophysiology and biofeedback,* 30**,** 1-10.

HARI, R. & SALMELIN, R. 2012. Magnetoencephalography: From SQUIDs to neuroscience. Neuroimage 20th anniversary special edition. *Neuroimage,* 61**,** 386-96.

HARMONY, T., MAROSI, E., BECKER, J., RODRÍGUEZ, M., REYES, A., FERNÁNDEZ, T., SILVA, J. & BERNAL, J. 1995. Longitudinal quantitative EEG study of children with different performances on a reading-writing test. *Electroencephalography and clinical neurophysiology,* 95**,** 426-433.

HARRISON, L. M., DUGGINS, A. & FRISTON, K. J. 2006. Encoding uncertainty in the hippocampus. *Neural Netw,* 19**,** 535-46.

HAWELLEK, D. J., SCHEPERS, I. M., ROEDER, B., ENGEL, A. K., SIEGEL, M. & HIPP, J. F. 2013. Altered intrinsic neuronal interactions in the visual cortex of the blind. *The Journal of Neuroscience,* 33**,** 17072-17080.

HERFF, C., PUTZE, F., HEGER, D., GUAN, C. & SCHULTZ, T. 2012. Speaking mode recognition from functional Near Infrared Spectroscopy. *Conf Proc IEEE Eng Med Biol Soc,* 2012**,** 1715-8.

HINRICHS, H., HEINZE, H. J. & SCHOENFELD, M. A. 2006. Causal visual interactions as revealed by an information theoretic measure and fMRI. *Neuroimage,* 31**,** 1051-60.

HORNERO, R., ABASOLO, D., ESCUDERO, J. & GOMEZ, C. 2009. Nonlinear analysis of electroencephalogram and magnetoencephalogram recordings in patients with Alzheimer's disease. *Philos Trans A Math Phys Eng Sci,* 367**,** 317-36.

HOWARTH, C. 2014. The contribution of astrocytes to the regulation of cerebral blood flow. *Frontiers in neuroscience,* 8.

HOWELL, D. C. 2011. *Statistical methods for psychology*, Cengage Learning.

HOWLAND, R. H., SHUTT, L. S., BERMAN, S. R., SPOTTS, C. R. & DENKO, T. 2011. The emerging use of technology for the treatment of depression and other neuropsychiatric disorders. *Ann Clin Psychiatry,* 23**,** 48-62.

HUPPERT, T. J., DIAMOND, S. G., FRANCESCHINI, M. A. & BOAS, D. A. 2009. HomER: a review of time-series analysis methods for near-infrared spectroscopy of the brain. *Appl Opt,* 48**,** D280-98.

IBER, C. 2007. *The AASM manual for the scoring of sleep and associated events: rules, terminology and technical specifications*, American Academy of Sleep Medicine.

IRANI, F., PLATEK, S. M., BUNCE, S., RUOCCO, A. C. & CHUTE, D. 2007. Functional near infrared spectroscopy (fNIRS): an emerging neuroimaging technology with important applications for the study of brain disorders. *Clin Neuropsychol,* 21**,** 9-37.

IRIARTE, J., URRESTARAZU, E., VALENCIA, M., ALEGRE, M., MALANDA, A., VITERI, C. & ARTIEDA, J. 2003. Independent component analysis as a tool to eliminate artifacts in EEG: a quantitative study. *Journal of clinical neurophysiology,* 20**,** 249-257.

ISHII, Y., OGATA, H., TAKANO, H., OHNISHI, H., MUKAI, T. & YAGI, T. 2008. Study on mental stress using near-infrared spectroscopy, electroencephalography, and peripheral arterial tonometry. *Conf Proc IEEE Eng Med Biol Soc,* 2008**,** 4992-5.

IVERSEN, J. R., REPP, B. H. & PATEL, A. D. 2009. Top-down control of rhythm perception modulates early auditory responses. *Ann N Y Acad Sci,* 1169**,** 58-73.

IZZETOGLU, M., CHITRAPU, P., BUNCE, S. & ONARAL, B. 2010. Motion artifact cancellation in NIR spectroscopy using discrete Kalman filtering. *Biomed Eng Online,* 9**,** 16.

IZZETOGLU, M., DEVARAJ, A., BUNCE, S. & ONARAL, B. 2005. Motion artifact cancellation in NIR spectroscopy using Wiener filtering. *IEEE Trans Biomed Eng,* 52**,** 934-8.

JASPER, H. H. 1958. The ten twenty electrode system of the international federation. *Electroencephalography and clinical neurophysiology,* 10**,** 371-375.

JEONG, J., GORE, J. C. & PETERSON, B. S. 2001. Mutual information analysis of the EEG in patients with Alzheimer's disease. *Clin Neurophysiol,* 112**,** 827-35.

JIN, S. H., KWON, Y. J., JEONG, J. S., KWON, S. W. & SHIN, D. H. 2006. Increased information transmission during scientific hypothesis generation: mutual information analysis of multichannel EEG. *Int J Psychophysiol,* 62**,** 337-44.

JIN, S. H., LIN, P. & HALLETT, M. 2010. Linear and nonlinear information flow based on time-delayed mutual information method and its application to corticomuscular interaction. *Clin Neurophysiol,* 121**,** 392-401.

JOBSIS, F. F. 1977. Noninvasive, infrared monitoring of cerebral and myocardial oxygen sufficiency and circulatory parameters. *Science,* 198**,** 1264-7.

JORDAN, K. G. 2004. Emergency EEG and continuous EEG monitoring in acute ischemic stroke. *J Clin Neurophysiol,* 21**,** 341-52.

KAISER, D. A. 2005. Basic principles of quantitative EEG. *Journal of Adult Development,* 12**,** 99-104.

KARBASFOROUSHAN, H. & WOODWARD, N. 2012. Resting-state networks in schizophrenia. *Current topics in medicinal chemistry,* 12**,** 2404-2414.

KATO, H., IZUMIYAMA, M., KOIZUMI, H., TAKAHASHI, A. & ITOYAMA, Y. 2002. Near-infrared spectroscopic topography as a tool to monitor motor reorganization after hemiparetic stroke: a comparison with functional MRI. *Stroke,* 33**,** 2032-6.

KHAMSI, R. 2012. Diagnosis by default. *Nat Med,* 18**,** 338-40.

KHAN, B., WILDEY, C., FRANCIS, R., TIAN, F., DELGADO, M. R., LIU, H., MACFARLANE, D. & ALEXANDRAKIS, G. 2012. Improving optical contact for functional nearinfrared brain spectroscopy and imaging with brush optodes. *Biomed Opt Express,* 3**,** 878-98.

KHAN, M. J., HONG, M. J. & HONG, K.-S. 2014. Decoding of four movement directions using hybrid NIRS-EEG brain-computer interface. *Frontiers in human neuroscience,* 8.

KIM, B., BOES, J. L., BLAND, P. H., CHENEVERT, T. L. & MEYER, C. R. 1999. Motion correction in fMRI via registration of individual slices into an anatomical volume. *Magn Reson Med,* 41**,** 964-72.

KIRILINA, E., JELZOW, A., HEINE, A., NIESSING, M., WABNITZ, H., BRÜHL, R., ITTERMANN, B., JACOBS, A. M. & TACHTSIDIS, I. 2012. The physiological origin of task-evoked systemic artefacts in functional near infrared spectroscopy. *Neuroimage,* 61**,** 70-81.

KLIMESCH, W. 1999. EEG alpha and theta oscillations reflect cognitive and memory performance: a review and analysis. *Brain research reviews,* 29**,** 169-195.

KLIMESCH, W., DOPPELMAYR, M., SCHIMKE, H. & PACHINGER, T. 1996. Alpha frequency, reaction time, and the speed of processing information. *Journal of clinical neurophysiology,* 13**,** 511-518.

KLIMESCH, W., SAUSENG, P. & GERLOFF, C. 2003. Enhancing cognitive performance with repetitive transcranial magnetic stimulation at human individual alpha frequency. *European Journal of Neuroscience,* 17**,** 1129-1133.

KLIMESCH, W., SAUSENG, P. & HANSLMAYR, S. 2007. EEG alpha oscillations: the inhibition-timing hypothesis. *Brain Res Rev,* 53**,** 63-88.
KLIMESCH, W., SCHIMKE, H. & PFURTSCHELLER, G. 1993. Alpha frequency, cognitive load and memory performance. *Brain topography,* 5**,** 241-251.
KLOPPEL, S., ABDULKADIR, A., JACK, C. R., JR., KOUTSOULERIS, N., MOURAO-MIRANDA, J. & VEMURI, P. 2012. Diagnostic neuroimaging across diseases. *Neuroimage,* 61**,** 457-63.
KOBAYASHI, K., YOSHINAGA, H., OHTSUKA, Y. & GOTMAN, J. 2005. Dipole modeling of epileptic spikes can be accurate or misleading. *Epilepsia,* 46**,** 397-408.
KOCH, S. P., KOENDGEN, S., BOURAYOU, R., STEINBRINK, J. & OBRIG, H. 2008. Individual alpha-frequency correlates with amplitude of visual evoked potential and hemodynamic response. *Neuroimage,* 41**,** 233-42.
KOCH, S. P., STEINBRINK, J., VILLRINGER, A. & OBRIG, H. 2006. Synchronization between background activity and visually evoked potential is not mirrored by focal hyperoxygenation: implications for the interpretation of vascular brain imaging. *J Neurosci,* 26**,** 4940-8.
KOCH, S. P., WERNER, P., STEINBRINK, J., FRIES, P. & OBRIG, H. 2009. Stimulus-induced and state-dependent sustained gamma activity is tightly coupled to the hemodynamic response in humans. *J Neurosci,* 29**,** 13962-70.
KONDACS, A. & SZABO, M. 1999. Long-term intra-individual variability of the background EEG in normals. *Clin Neurophysiol,* 110**,** 1708-16.
KOO, B., LEE, H.-G., NAM, Y., KANG, H., KOH, C. S., SHIN, H.-C. & CHOI, S. 2014. A hybrid NIRS-EEG system for self-paced brain computer interface with online motor imagery. *Journal of neuroscience methods*.
KOPRUNER, V., PFURTSCHELLER, G. & AUER, L. M. 1984. Quantitative EEG in normals and in patients with cerebral ischemia. *Prog Brain Res,* 62**,** 29-50.
KRAUSS, G. L., FISHER, R. S. & KAPLAN, P. W. 2006. *The Johns Hopkins atlas of digital EEG: an interactive training guide*, Johns Hopkins University Press.
KRIEGSEIS, A., HENNIGHAUSEN, E., RÖSLER, F. & RÖDER, B. 2006. Reduced EEG alpha activity over parieto-occipital brain areas in congenitally blind adults. *Clinical neurophysiology,* 117**,** 1560-1573.
KUGIUMTZIS, D. 2013. Direct-coupling information measure from nonuniform embedding. *Phys Rev E Stat Nonlin Soft Matter Phys,* 87**,** 062918.
LANSBERGEN, M. M., ARNS, M., VAN DONGEN-BOOMSMA, M., SPRONK, D. & BUITELAAR, J. K. 2011. The increase in theta/beta ratio on resting-state EEG in boys with attention-deficit/hyperactivity disorder is mediated by slow alpha peak frequency. *Prog Neuropsychopharmacol Biol Psychiatry,* 35**,** 47-52.
LEE, T. W., YU, Y. W., HONG, C. J., TSAI, S. J., WU, H. C. & CHEN, T. J. 2011. The effects of catechol-O-methyl-transferase polymorphism Val158Met on functional connectivity in healthy young females: a resting EEG study. *Brain Res,* 1377**,** 21-31.
LEISTEDT, S., DUMONT, M., LANQUART, J. P., JURYSTA, F. & LINKOWSKI, P. 2007. Characterization of the sleep EEG in acutely depressed men using detrended fluctuation analysis. *Clin Neurophysiol,* 118**,** 940-50.
LENNE, B., BLANC, J. L., NANDRINO, J. L., GALLOIS, P., HAUTECAEUR, P. & PEZARD, L. 2013. Decrease of mutual information in brain electrical activity of patients with relapsing-remitting multiple sclerosis. *Behav Neurol,* 27**,** 201-12.
LEON-CARRION, J., MARTIN-RODRIGUEZ, J. F., DAMAS-LOPEZ, J., BARROSO Y MARTIN, J. M. & DOMINGUEZ-MORALES, M. R. 2009. Delta–alpha ratio

correlates with level of recovery after neurorehabilitation in patients with acquired brain injury. *Clinical Neurophysiology,* 120**,** 1039-1045.
LI, Z., WANG, Y., LI, Y., WANG, Y., LI, J. & ZHANG, L. 2010. Wavelet analysis of cerebral oxygenation signal measured by near infrared spectroscopy in subjects with cerebral infarction. *Microvascular research,* 80**,** 142-147.
LINDSLEY, D. B. 1939. A longitudinal study of the occipital alpha rhythm in normal children: Frequency and amplitude standards. *The Pedagogical Seminary and Journal of Genetic Psychology,* 55**,** 197-213.
LINKENKAER-HANSEN, K., MONTO, S., RYTSÄLÄ, H., SUOMINEN, K., ISOMETSÄ, E. & KÄHKÖNEN, S. 2005. Breakdown of long-range temporal correlations in theta oscillations in patients with major depressive disorder. *The Journal of Neuroscience,* 25**,** 10131-10137.
LINKENKAER-HANSEN, K., NIKOULINE, V. V., PALVA, J. M. & ILMONIEMI, R. J. 2001. Long-range temporal correlations and scaling behavior in human brain oscillations. *J Neurosci,* 21**,** 1370-7.
LIU, T. T., BEHZADI, Y., RESTOM, K., ULUDAG, K., LU, K., BURACAS, G. T., DUBOWITZ, D. J. & BUXTON, R. B. 2004. Caffeine alters the temporal dynamics of the visual BOLD response. *Neuroimage,* 23**,** 1402-1413.
LU, C. F., TENG, S., HUNG, C. I., TSENG, P. J., LIN, L. T., LEE, P. L. & WU, Y. T. 2011. Reorganization of functional connectivity during the motor task using EEG time-frequency cross mutual information analysis. *Clin Neurophysiol,* 122**,** 1569-79.
LU, C. M., ZHANG, Y. J., BISWAL, B. B., ZANG, Y. F., PENG, D. L. & ZHU, C. Z. 2010. Use of fNIRS to assess resting state functional connectivity. *J Neurosci Methods,* 186**,** 242-9.
LUO, A. & SAJDA, P. 2009. Comparing neural correlates of visual target detection in serial visual presentations having different temporal correlations. *Front Hum Neurosci,* 3**,** 5.
MACHADO, A., LINA, J. M., TREMBLAY, J., LASSONDE, M., NGUYEN, D. K., LESAGE, F. & GROVA, C. 2011. Detection of hemodynamic responses to epileptic activity using simultaneous Electro-EncephaloGraphy (EEG)/Near Infra Red Spectroscopy (NIRS) acquisitions. *Neuroimage,* 56**,** 114-25.
MACHLEIDT, W. & GUTJAHR, L. 1984. Ultradian periodicity, diurnal and circannual rhythms in the electroencephalogram]. *Fortschritte der Neurologie-Psychiatrie,* 52**,** 135.
MALLIANI, A., PAGANI, M., LOMBARDI, F. & CERUTTI, S. 1991. Cardiovascular neural regulation explored in the frequency domain. *Circulation,* 84**,** 482-492.
MANDELL, D. M., HAN, J. S., POUBLANC, J., CRAWLEY, A. P., STAINSBY, J. A., FISHER, J. A. & MIKULIS, D. J. 2008. Mapping cerebrovascular reactivity using blood oxygen level-dependent MRI in patients with arterial steno-occlusive disease comparison with arterial spin labeling MRI. *Stroke,* 39**,** 2021-2028.
MANTINI, D., PERRUCCI, M. G., DEL GRATTA, C., ROMANI, G. L. & CORBETTA, M. 2007. Electrophysiological signatures of resting state networks in the human brain. *Proceedings of the National Academy of Sciences,* 104**,** 13170-13175.
MCCORMICK, D. A., WANG, Z. & HUGUENARD, J. 1993. Neurotransmitter control of neocortical neuronal activity and excitability. *Cerebral Cortex,* 3**,** 387-398.
MCKENNA, T. M., MCMULLEN, T. A. & SHLESINGER, M. F. 1994. The brain as a dynamic physical system. *Neuroscience,* 60**,** 587-605.

MEDVEDEV, A. V., KAINERSTORFER, J., BORISOV, S. V., BARBOUR, R. L. & VANMETER, J. 2008. Event-related fast optical signal in a rapid object recognition task: improving detection by the independent component analysis. *Brain research,* 1236**,** 145-158.

MEINZER, M., ELBERT, T., WIENBRUCH, C., DJUNDJA, D., BARTHEL, G. & ROCKSTROH, B. 2004. Intensive language training enhances brain plasticity in chronic aphasia. *BMC Biol,* 2**,** 20.

MERKER, B. 2013. Cortical gamma oscillations: the functional key is activation, not cognition. *Neurosci Biobehav Rev,* 37**,** 401-17.

MESQUITA, R. C., FRANCESCHINI, M. A. & BOAS, D. A. 2010. Resting state functional connectivity of the whole head with near-infrared spectroscopy. *Biomed Opt Express,* 1**,** 324-336.

MICHEL, C. M. & MURRAY, M. M. 2012. Towards the utilization of EEG as a brain imaging tool. *Neuroimage,* 61**,** 371-385.

MIGUEL-HIDALGO, J. J. 2013. Brain structural and functional changes in adolescents with psychiatric disorders. *International journal of adolescent medicine and health,* 25**,** 245-256.

MIN, B. C., JIN, S. H., KANG, I. H., LEE, D. H., KANG, J. K., LEE, S. T. & SAKAMOTO, K. 2003. Analysis of mutual information content for EEG responses to odor stimulation for subjects classified by occupation. *Chem Senses,* 28**,** 741-9.

MIYAI, I., YAGURA, H., HATAKENAKA, M., ODA, I., KONISHI, I. & KUBOTA, K. 2003. Longitudinal optical imaging study for locomotor recovery after stroke. *Stroke,* 34**,** 2866-70.

MONASTRA, V. J., LUBAR, J. F., LINDEN, M., VANDEUSEN, P., GREEN, G., WING, W., PHILLIPS, A. & FENGER, T. N. 1999. Assessing attention deficit hyperactivity disorder via quantitative electroencephalography: an initial validation study. *Neuropsychology,* 13**,** 424-33.

MONTEZ, T., POIL, S.-S., JONES, B. F., MANSHANDEN, I., VERBUNT, J. P., VAN DIJK, B. W., BRUSSAARD, A. B., VAN OOYEN, A., STAM, C. J. & SCHELTENS, P. 2009. Altered temporal correlations in parietal alpha and prefrontal theta oscillations in early-stage Alzheimer disease. *Proceedings of the National Academy of Sciences,* 106**,** 1614-1619.

MOORE, D. S., MCCABE, G. P. & CRAIG, B. A. 2012. *Introduction to the Practice of Statistics*, WH Freeman.

MOOSMANN, M., RITTER, P., KRASTEL, I., BRINK, A., THEES, S., BLANKENBURG, F., TASKIN, B., OBRIG, H. & VILLRINGER, A. 2003. Correlates of alpha rhythm in functional magnetic resonance imaging and near infrared spectroscopy. *Neuroimage,* 20**,** 145-158.

MORETTI, D. V., BABILONI, C., BINETTI, G., CASSETTA, E., DAL FORNO, G., FERRERIC, F., FERRI, R., LANUZZA, B., MINIUSSI, C. & NOBILI, F. 2004. Individual analysis of EEG frequency and band power in mild Alzheimer's disease. *Clinical Neurophysiology,* 115**,** 299-308.

MORITZ, S., KASPRZAK, P., ARLT, M., TAEGER, K. & METZ, C. 2007. Accuracy of cerebral monitoring in detecting cerebral ischemia during carotid endarterectomy: a comparison of transcranial Doppler sonography, near-infrared spectroscopy, stump pressure, and somatosensory evoked potentials. *Anesthesiology,* 107**,** 563-9.

MOTOMURA, E., INUI, K., NAKASE, S., HAMANAKA, K. & OKAZAKI, Y. 2002. Late-onset depression: can EEG abnormalities help in clinical sub-typing? *Journal of affective disorders,* 68**,** 73-79.

MURATA, Y., SAKATANI, K., HOSHINO, T., FUJIWARA, N., KANO, T., NAKAMURA, S. & KATAYAMA, Y. 2006. Effects of cerebral ischemia on evoked cerebral

blood oxygenation responses and BOLD contrast functional MRI in stroke patients. *Stroke,* 37**,** 2514-20.
MUSTANOJA, S., MERETOJA, A., PUTAALA, J., VIITANEN, V., CURTZE, S., ATULA, S., ARTTO, V., HÄPPÖLÄ, O. & KASTE, M. 2011. Outcome by stroke etiology in patients receiving thrombolytic treatment descriptive subtype analysis. *Stroke,* 42**,** 102-106.
NA, S. H., JIN, S. H. & KIM, S. Y. 2006. The effects of total sleep deprivation on brain functional organization: mutual information analysis of waking human EEG. *Int J Psychophysiol,* 62**,** 238-42.
NA, S. H., JIN, S. H., KIM, S. Y. & HAM, B. J. 2002. EEG in schizophrenic patients: mutual information analysis. *Clin Neurophysiol,* 113**,** 1954-60.
NAKAMURA, S., SAKATANI, K., KANO, T., HOSHINO, T., FUJIWARA, N., MURATA, Y. & KATAYAMA, Y. 2010. Effects of revascularisation on evoked cerebral blood oxygenation responses in stroke patients. *Adv Exp Med Biol,* 662**,** 525-30.
NIKULIN, V. V., JONSSON, E. G. & BRISMAR, T. 2012. Attenuation of long-range temporal correlations in the amplitude dynamics of alpha and beta neuronal oscillations in patients with schizophrenia. *Neuroimage,* 61**,** 162-9.
NOLTE, C., KOHL, M., SCHOLZ, U., WEIH, M. & VILLRINGER, A. 1998. Characterization of the pulse signal over the human head by near infrared spectroscopy. *Adv Exp Med Biol,* 454**,** 115-23.
OBRIG, H. 2013. NIRS in clinical neurology - a 'promising' tool? *Neuroimage*.
OBRIG, H. & STEINBRINK, J. 2011. Non-invasive optical imaging of stroke. *Philos Trans A Math Phys Eng Sci,* 369**,** 4470-94.
OBRIG, H. & VILLRINGER, A. 2003. Beyond the visible--imaging the human brain with light. *J Cereb Blood Flow Metab,* 23**,** 1-18.
OKAZAKI, M., KANEKO, Y., YUMOTO, M. & ARIMA, K. 2008. Perceptual change in response to a bistable picture increases neuromagnetic beta-band activities. *Neurosci Res,* 61**,** 319-28.
ORGANIZATION, W. H. 2000. International Consortium in Psychiatric Epidemiology. Cross-national comparisons of the prevalences and correlates of mental disorders. *Bull World Health Organ,* 78**,** 413-426.
OSTWALD, D., PORCARO, C. & BAGSHAW, A. P. 2010. An information theoretic approach to EEG-fMRI integration of visually evoked responses. *Neuroimage,* 49**,** 498-516.
OSTWALD, D., PORCARO, C. & BAGSHAW, A. P. 2011. Voxel-wise information theoretic EEG-fMRI feature integration. *Neuroimage,* 55**,** 1270-86.
OSTWALD, D., PORCARO, C., MAYHEW, S. D. & BAGSHAW, A. P. 2012. EEG-fMRI Based Information Theoretic Characterization of the Human Perceptual Decision System. *PLoS One,* 7**,** e33896.
PALANCA, B. J. A. & DEANGELIS, G. C. 2005. Does neuronal synchrony underlie visual feature grouping? *Neuron,* 46**,** 333-346.
PALMER, S. J., LEE, P. W., WANG, Z. J., AU, W. L. & MCKEOWN, M. J. 2010. theta, beta But not alpha-band EEG connectivity has implications for dual task performance in Parkinson's disease. *Parkinsonism Relat Disord,* 16**,** 393-7.
PARZEN, E. 1962. On estimation of a probability density function and mode. *The annals of mathematical statistics,* 33**,** 1065-1076.
PASCUAL-MARQUI, R. D., ESSLEN, M., KOCHI, K. & LEHMANN, D. 2002. Functional imaging with low-resolution brain electromagnetic tomography (LORETA): a review. *Methods Find Exp Clin Pharmacol,* 24 Suppl C**,** 91-5.

PASCUAL-MARQUI, R. D., MICHEL, C. M. & LEHMANN, D. 1994. Low resolution electromagnetic tomography: a new method for localizing electrical activity in the brain. *Int J Psychophysiol,* 18**,** 49-65.
PFURTSCHELLER, G. 1992. Event-related synchronization (ERS): an electrophysiological correlate of cortical areas at rest. *Electroencephalogr Clin Neurophysiol,* 83**,** 62-9.
PFURTSCHELLER, G., ALLISON, B. Z., BRUNNER, C., BAUERNFEIND, G., SOLIS-ESCALANTE, T., SCHERER, R., ZANDER, T. O., MUELLER-PUTZ, G., NEUPER, C. & BIRBAUMER, N. 2010. The hybrid BCI. *Frontiers in neuroscience,* 4.
PFURTSCHELLER, G., DALY, I., BAUERNFEIND, G. & MULLER-PUTZ, G. R. 2012. Coupling between intrinsic prefrontal HbO2 and central EEG beta power oscillations in the resting brain. *PLoS One,* 7**,** e43640.
PFURTSCHELLER, G., NEUPER, C. & MOHL, W. 1994. Event-related desynchronization (ERD) during visual processing. *Int J Psychophysiol,* 16**,** 147-53.
PHAN, T. G. & BULLEN, A. 2010. Practical intravital two-photon microscopy for immunological research: faster, brighter, deeper. *Immunol Cell Biol,* 88**,** 438-44.
PIEVANI, M., DE HAAN, W., WU, T., SEELEY, W. W. & FRISONI, G. B. 2011. Functional network disruption in the degenerative dementias. *Lancet Neurol,* 10**,** 829-43.
PINEL, J. 2003. Biopsychology. 5th. Allyn and Bacon Boston, MA:.
POPA-WAGNER, A., CARMICHAEL, S. T., KOKAIA, Z., KESSLER, C. & WALKER, L. C. 2007. The response of the aged brain to stroke: too much, too soon? *Curr Neurovasc Res,* 4**,** 216-27.
PORTNOW, L. H., VAILLANCOURT, D. E. & OKUN, M. S. 2013. The history of cerebral PET scanning: from physiology to cutting-edge technology. *Neurology,* 80**,** 952-6.
PUTNAM, K. M. & MCSWEENEY, L. B. 2008. Depressive symptoms and baseline prefrontal EEG alpha activity: a study utilizing Ecological Momentary Assessment. *Biol Psychol,* 77**,** 237-40.
R CHIALVO, D. 2004. Critical brain networks. *Physica A: Statistical Mechanics and its Applications,* 340**,** 756-765.
RAICHLE, M. E. 2010. The brain's dark energy. *Sci Am,* 302**,** 44-9.
RAICHLE, M. E., MACLEOD, A. M., SNYDER, A. Z., POWERS, W. J., GUSNARD, D. A. & SHULMAN, G. L. 2001. A default mode of brain function. *Proc Natl Acad Sci U S A,* 98**,** 676-82.
RAKIC, P. 2009. Evolution of the neocortex: a perspective from developmental biology. *Nature Reviews Neuroscience,* 10**,** 724-735.
RAMANAND, P., BRUCE, M. C. & BRUCE, E. N. 2010. Mutual information analysis of EEG signals indicates age-related changes in cortical interdependence during sleep in middle-aged versus elderly women. *J Clin Neurophysiol,* 27**,** 274-84.
RAUSCHENBERGER, R. & YANTIS, S. 2006. Perceptual encoding efficiency in visual search. *Journal of Experimental Psychology-General,* 135**,** 116-131.
RAZ, N. & RODRIGUE, K. M. 2006. Differential aging of the brain: patterns, cognitive correlates and modifiers. *Neurosci Biobehav Rev,* 30**,** 730-48.
RICHARD CLARK, C., VELTMEYER, M. D., HAMILTON, R. J., SIMMS, E., PAUL, R., HERMENS, D. & GORDON, E. 2004. Spontaneous alpha peak frequency predicts working memory performance across the age span. *International Journal of Psychophysiology,* 53**,** 1-9.

ROCHE-LABARBE, N., WALLOIS, F., PONCHEL, E., KONGOLO, G. & GREBE, R. 2007. Coupled oxygenation oscillation measured by NIRS and intermittent cerebral activation on EEG in premature infants. *Neuroimage,* 36**,** 718-27.

ROCHE-LABARBE, N., ZAAIMI, B., BERQUIN, P., NEHLIG, A., GREBE, R. & WALLOIS, F. 2008. NIRS-measured oxy- and deoxyhemoglobin changes associated with EEG spike-and-wave discharges in children. *Epilepsia,* 49**,** 1871-80.

ROCHE-LABARBE, N., ZAAIMI, B., MAHMOUDZADEH, M., OSHARINA, V., WALLOIS, A., NEHLIG, A., GREBE, R. & WALLOIS, F. 2010. NIRS-measured oxy- and deoxyhemoglobin changes associated with EEG spike-and-wave discharges in a genetic model of absence epilepsy: the GAERS. *Epilepsia,* 51**,** 1374-84.

ROLLS, E. T. & DECO, G. 2006. Attention in natural scenes: Neurophysiological and computational bases. *Neural Networks,* 19**,** 1383-1394.

SAKATANI, K., MURATA, Y., KATAYAMA, Y., FUJIWARA, N., HOSHINO, T., NAKAMURA, S. & KANO, T. 2007. Comparison of blood-oxygen-level–dependent functional magnetic resonance imaging and near-infrared spectroscopy recording during functional brain activation in patients with stroke and brain tumors. *Journal of biomedical optics,* 12**,** 062110-062110-8.

SAKKALIS, V., GIANNAKAKIS, G., FARMAKI, C., MOUSAS, A., PEDIADITIS, M., VORGIA, P. & TSIKNAKIS, M. 2013. Absence seizure epilepsy detection using linear and nonlinear eeg analysis methods. *Conf Proc IEEE Eng Med Biol Soc,* 2013**,** 6333-6.

SALETU, B., ANDERER, P. & SALETU-ZYHLARZ, G. M. 2010. EEG topography and tomography (LORETA) in diagnosis and pharmacotherapy of depression. *Clin EEG Neurosci,* 41**,** 203-10.

SALINSKY, M. C., OKEN, B. S. & MOREHEAD, L. 1991. Test-retest reliability in EEG frequency analysis. *Electroencephalogr Clin Neurophysiol,* 79**,** 382-92.

SALVADOR, R., MARTINEZ, A., POMAROL-CLOTET, E., SARRO, S., SUCKLING, J. & BULLMORE, E. 2007. Frequency based mutual information measures between clusters of brain regions in functional magnetic resonance imaging. *Neuroimage,* 35**,** 83-8.

SASAI, S., HOMAE, F., WATANABE, H., SASAKI, A. T., TANABE, H. C., SADATO, N. & TAGA, G. 2012. A NIRS-fMRI study of resting state network. *Neuroimage,* 63**,** 179-93.

SASAI, S., HOMAE, F., WATANABE, H. & TAGA, G. 2011. Frequency-specific functional connectivity in the brain during resting state revealed by NIRS. *Neuroimage,* 56**,** 252-7.

SCHOLKMANN, F., SPICHTIG, S., MUEHLEMANN, T. & WOLF, M. 2010. How to detect and reduce movement artifacts in near-infrared imaging using moving standard deviation and spline interpolation. *Physiol Meas,* 31**,** 649-62.

SCHREIBER, T. 2000. Measuring information transfer. *Phys Rev Lett,* 85**,** 461-4.

SCHWILDEN, H. 2006. Concepts of EEG processing: from power spectrum to bispectrum, fractals, entropies and all that. *Best Pract Res Clin Anaesthesiol,* 20**,** 31-48.

SELVAM, V. S. & SHENBAGADEVI, S. 2011. Brain tumor detection using scalp eeg with modified Wavelet-ICA and multi layer feed forward neural network. *Conf Proc IEEE Eng Med Biol Soc,* 2011**,** 6104-9.

SHANNON, C. E. 1948. A mathematical theory of communication. *Bell System Technical Journal,* 27**,** 379-423.

SHE, H. C., JUNG, T. P., CHOU, W. C., HUANG, L. Y., WANG, C. Y. & LIN, G. Y. 2012. EEG dynamics reflect the distinct cognitive process of optic problem solving. *PLoS One,* 7**,** e40731.

SMITH, C., GOSWAMI, N., ROBINSON, R., VON DER WIESCHE, M. & SCHNEIDER, S. 2013. The relationship between brain cortical activity and brain oxygenation in the prefrontal cortex during hypergravity exposure. *J Appl Physiol (1985),* 114**,** 905-10.

SMITH, J. R. 1938. The electroencephalogram during normal infancy and childhood: II. The nature of the growth of the alpha waves. *The Pedagogical Seminary and Journal of Genetic Psychology,* 53**,** 455-469.

SMITH, S. M., FOX, P. T., MILLER, K. L., GLAHN, D. C., FOX, P. M., MACKAY, C. E., FILIPPINI, N., WATKINS, K. E., TORO, R., LAIRD, A. R. & BECKMANN, C. F. 2009. Correspondence of the brain's functional architecture during activation and rest. *Proc Natl Acad Sci U S A,* 106**,** 13040-5.

STEINBRINK, J., KEMPF, F. C., VILLRINGER, A. & OBRIG, H. 2005. The fast optical signal—robust or elusive when non-invasively measured in the human adult? *Neuroimage,* 26**,** 996-1008.

STEINBRINK, J., KOHL, M., OBRIG, H., CURIO, G., SYRE, F., THOMAS, F., WABNITZ, H., RINNEBERG, H. & VILLRINGER, A. 2000. Somatosensory evoked fast optical intensity changes detected non-invasively in the adult human head. *Neuroscience Letters,* 291**,** 105-108.

STERN, R. M. 2001. *Brain: Electroncephalography and Imaging,* Oxford, Oxford University Press.

STINEAR, C. M. & WARD, N. S. 2013. How useful is imaging in predicting outcomes in stroke rehabilitation? *International Journal of Stroke,* 8**,** 33-37.

STRANGMAN, G., BOAS, D. A. & SUTTON, J. P. 2002. Non-invasive neuroimaging using near-infrared light. *Biol Psychiatry,* 52**,** 679-93.

STRANGMAN, G., FRANCESCHINI, M. A. & BOAS, D. A. 2003. Factors affecting the accuracy of near-infrared spectroscopy concentration calculations for focal changes in oxygenation parameters. *Neuroimage,* 18**,** 865-79.

STRENS, L. H., ASSELMAN, P., POGOSYAN, A., LOUKAS, C., THOMPSON, A. J. & BROWN, P. 2004. Corticocortical coupling in chronic stroke: its relevance to recovery. *Neurology,* 63**,** 475-84.

SWEENEY, K. T., AYAZ, H., WARD, T. E., IZZETOGLU, M., MCLOONE, S. F. & ONARAL, B. 2012. A methodology for validating artifact removal techniques for physiological signals. *Information Technology in Biomedicine, IEEE Transactions on,* 16**,** 918-926.

TAKAHASHI, T., CHO, R. Y., MIZUNO, T., KIKUCHI, M., MURATA, T., TAKAHASHI, K. & WADA, Y. 2010. Antipsychotics reverse abnormal EEG complexity in drug-naive schizophrenia: a multiscale entropy analysis. *Neuroimage,* 51**,** 173-82.

TAKEDA, K., GOMI, Y., IMAI, I., SHIMODA, N., HIWATARI, M. & KATO, H. 2007. Shift of motor activation areas during recovery from hemiparesis after cerebral infarction: a longitudinal study with near-infrared spectroscopy. *Neurosci Res,* 59**,** 136-44.

TEPLAN, M. 2002. Fundamentals of EEG measurement. *Measurement science review,* 2**,** 1-11.

TEPLAN, M., KRAKOVSKA, A. & STOLC, S. 2006. EEG responses to long-term audio-visual stimulation. *Int J Psychophysiol,* 59**,** 81-90.

THAKOR, N. V. & TONG, S. 2004. Advances in quantitative electroencephalogram analysis methods. *Annu Rev Biomed Eng,* 6**,** 453-95.

TOET, M. C., FLINTERMAN, A., LAAR, I., VRIES, J. W., BENNINK, G. B., UITERWAAL, C. S. & BEL, F. 2005. Cerebral oxygen saturation and electrical brain activity before, during, and up to 36 hours after arterial switch procedure in neonates without pre-existing brain damage: its relationship to neurodevelopmental outcome. *Exp Brain Res,* 165**,** 343-50.

TOET, M. C. & LEMMERS, P. M. 2009. Brain monitoring in neonates. *Early Hum Dev,* 85**,** 77-84.

TOLONEN, U. & SULG, I. A. 1981. Comparison of quantitative EEG parameters from four different analysis techniques in evaluation of relationships between EEG and CBF in brain infarction. *Electroencephalogr Clin Neurophysiol,* 51**,** 177-85.

TOMITA, Y., VIALATTE, F.-B., DREYFUS, G., MITSUKURA, Y., BAKARDJIAN, H. & CICHOCKI, A. 2014. Bimodal BCI using simultaneously NIRS and EEG.

TONG, Y. & FREDERICK, B. D. 2010. Time lag dependent multimodal processing of concurrent fMRI and near-infrared spectroscopy (NIRS) data suggests a global circulatory origin for low-frequency oscillation signals in human brain. *Neuroimage,* 53**,** 553-64.

TONG, Y., HOCKE, L. M., NICKERSON, L. D., LICATA, S. C. & LINDSEY, K. P. 2013. Evaluating the effects of systemic low frequency oscillations measured in the periphery on the independent component analysis results of resting state networks. *Neuroimage,* 76**,** 202-215.

TORONOV, V. Y., ZHANG, X. & WEBB, A. G. 2007. A spatial and temporal comparison of hemodynamic signals measured using optical and functional magnetic resonance imaging during activation in the human primary visual cortex. *Neuroimage,* 34**,** 1136-1148.

TREGELLAS, J. R., SMUCNY, J., HARRIS, J. G., OLINCY, A., MAHARAJH, K., KRONBERG, E., EICHMAN, L. C., LYONS, E. & FREEDMAN, R. 2014. Intrinsic hippocampal activity as a biomarker for cognition and symptoms in schizophrenia. *American Journal of Psychiatry,* 171**,** 549-556.

TSE, C.-Y., GORDON, B. A., FABIANI, M. & GRATTON, G. 2010. Frequency analysis of the visual steady-state response measured with the fast optical signal in younger and older adults. *Biological psychology,* 85**,** 79-89.

TZOVARA, A., MURRAY, M. M., MICHEL, C. M. & DE LUCIA, M. 2012. A tutorial review of electrical neuroimaging from group-average to single-trial event-related potentials. *Dev Neuropsychol,* 37**,** 518-44.

ULUDAG, K., DUBOWITZ, D. J., YODER, E. J., RESTOM, K., LIU, T. T. & BUXTON, R. B. 2004a. Coupling of cerebral blood flow and oxygen consumption during physiological activation and deactivation measured with fMRI. *Neuroimage,* 23**,** 148-55.

ULUDAG, K., STEINBRINK, J., VILLRINGER, A. & OBRIG, H. 2004b. Separability and cross talk: optimizing dual wavelength combinations for near-infrared spectroscopy of the adult head. *Neuroimage,* 22**,** 583-9.

UMEYAMA, S. & YAMADA, T. 2009. New cross-talk measure of near-infrared spectroscopy and its application to wavelength combination optimization. *J Biomed Opt,* 14**,** 034017.

VARGAS, C., LÓPEZ-JARAMILLO, C. & VIETA, E. 2013. A systematic literature review of resting state network—functional MRI in bipolar disorder. *Journal of affective disorders,* 150**,** 727-735.

VECCHIO, F., BABILONI, C., LIZIO, R., FALLANI, F. V., BLINOWSKA, K., VERRIENTI, G., FRISONI, G. & ROSSINI, P. 2012. Resting state cortical EEG rhythms in Alzheimer's disease: toward EEG markers for clinical applications: a review. *Supplements to Clinical neurophysiology,* 62**,** 223-236.

WALTERS-WILLIAMS J., L. Y. 2009. Estimation of Mutual Information: A Survey. *In:* WEN P., L. Y., POLKOWSKI L., YAO Y., TSUMOTO S, WANG G (ed.) *Rough Sets and Knowledge Technology.* Berlin: Springer Berlin Heidelberg.

WANG, L., GUO, X., SUN, J., JIN, Z. & TONG, S. Year. Cortical networks of hemianopia stroke patients: A graph theoretical analysis of EEG signals at resting state. *In:* Engineering in Medicine and Biology Society (EMBC), 2012 Annual International Conference of the IEEE, 2012. IEEE, 49-52.

WANG, L. & LAGOPOULOS, J. 2012. A systematic review of resting-state functional-MRI studies in major depression. *Journal of affective disorders,* 142**,** 6-12.

WANG, Z. J., LEE, P. W. & MCKEOWN, M. J. 2009. A novel segmentation, mutual information network framework for EEG analysis of motor tasks. *Biomed Eng Online,* 8**,** 9.

WARD, T. E. 2013. Hybrid Optical–Electrical Brain Computer Interfaces, Practices and Possibilities. *Towards Practical Brain-Computer Interfaces.* Springer.

WARWICK, J. M. 2004. Imaging of brain function using SPECT. *Metabolic brain disease,* 19**,** 113-123.

WASCHER, E., RASCH, B., SANGER, J., HOFFMANN, S., SCHNEIDER, D., RINKENAUER, G., HEUER, H. & GUTBERLET, I. 2013. Frontal theta activity reflects distinct aspects of mental fatigue. *Biol Psychol*.

WHITE, B. R., SNYDER, A. Z., COHEN, A. L., PETERSEN, S. E., RAICHLE, M. E., SCHLAGGAR, B. L. & CULVER, J. P. 2009. Resting-state functional connectivity in the human brain revealed with diffuse optical tomography. *Neuroimage,* 47**,** 148-56.

WHITFIELD-GABRIELI, S. & FORD, J. M. 2012. Default mode network activity and connectivity in psychopathology. *Annual review of clinical psychology,* 8**,** 49-76.

WHO. Available: http://www.who.int/healthinfo/statistics/bod_cerebrovasculardiseasestroke.pdf [Accessed 02-12-2013 2013].

WOLF, M., WOLF, U., CHOI, J. H., TORONOV, V., ADELINA PAUNESCU, L., MICHALOS, A. & GRATTON, E. 2003. Fast cerebral functional signal in the 100-ms range detected in the visual cortex by frequency-domain near-infrared spectrophotometry. *Psychophysiology,* 40**,** 521-528.

XU, J., LIU, Z.-R., LIU, R. & YANG, Q.-F. 1997. Information transmission in human cerebral cortex. *Physica D: Nonlinear Phenomena,* 106**,** 363-374.

YENER, G. G. & BAŞAR, E. 2012. Biomarkers in Alzheimer's disease with a special emphasis on event-related oscillatory responses. *Supplements to Clinical neurophysiology,* 62**,** 237-273.

YUCEL, M. A., SELB, J., BOAS, D. A., CASH, S. S. & COOPER, R. J. 2014. Reducing motion artifacts for long-term clinical NIRS monitoring using collodion-fixed prism-based optical fibers. *Neuroimage,* 85 Pt 1**,** 192-201.

ZHANG, H., ZHANG, Y. J., LU, C. M., MA, S. Y., ZANG, Y. F. & ZHU, C. Z. 2010. Functional connectivity as revealed by independent component analysis of resting-state fNIRS measurements. *Neuroimage,* 51**,** 1150-61.

ZHANG, Q., BROWN, E. N. & STRANGMAN, G. E. 2007a. Adaptive filtering for global interference cancellation and real-time recovery of evoked brain activity: a Monte Carlo simulation study. *Journal of biomedical optics,* 12**,** 044014-044014-12.

ZHANG, Q., BROWN, E. N. & STRANGMAN, G. E. 2007b. Adaptive filtering to reduce global interference in evoked brain activity detection: a human subject case study. *Journal of biomedical optics,* 12**,** 064009-064009-12.

ZHANG, Q., STRANGMAN, G. E. & GANIS, G. 2009. Adaptive filtering to reduce global interference in non-invasive NIRS measures of brain activation: How well and when does it work? *Neuroimage,* 45**,** 788-794.
ZHANG, Y., BROOKS, D. H., FRANCESCHINI, M. A. & BOAS, D. A. 2005. Eigenvector-based spatial filtering for reduction of physiological interference in diffuse optical imaging. *Journal of biomedical optics,* 10**,** 011014-01101411.